General Disclaimer

One or more of the Following Statements may affect this Document

- This document has been reproduced from the best copy furnished by the organizational source. It is being released in the interest of making available as much information as possible.

- This document may contain data, which exceeds the sheet parameters. It was furnished in this condition by the organizational source and is the best copy available.

- This document may contain tone-on-tone or color graphs, charts and/or pictures, which have been reproduced in black and white.

- This document is paginated as submitted by the original source.

- Portions of this document are not fully legible due to the historical nature of some of the material. However, it is the best reproduction available from the original submission.

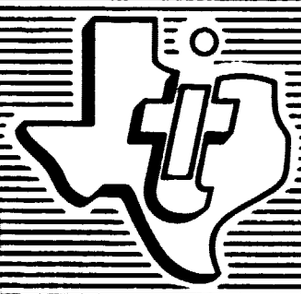

TEXAS INSTRUMENTS
INCORPORATED

STUDY OF SOLID-STATE INTEGRATED MICROWAVE CIRCUITS

Scientific Report No. 6

U33-811500-33

1 December 1967

Prepared for

NATIONAL AERONAUTICS AND SPACE ADMINISTRATION
Electronics Research Center
Cambridge, Massachusetts

Work Performed Under
Contract No. NAS-12+75
Control No. ERC/R&D 65-45

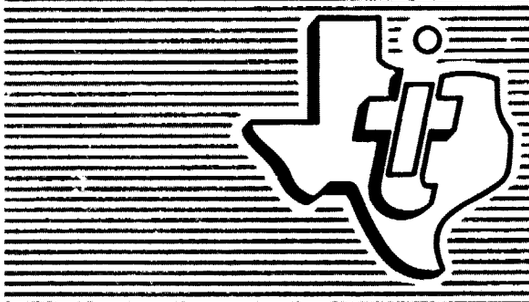

TEXAS INSTRUMENTS
INCORPORATED

ABSTRACT

This report discusses a study undertaken to develop a low-noise microwave PCM/FM receiver and the ceramic-circuit development of a transmitter development program. The package design of the transmitter also is reported. The receiver study report is a major portion of this report. The study seeks to determine a system that best meets a low-noise high-information capacity requirement with integrated circuit techniques. The study first examines the fundamental considerations which must be given to developing a PCM/FM receiver, then a final receiver model is selected by performing a trade study. The final receiver configuration uses a balanced mixer as the first stage and phase-lock demodulation. The design of the thin-film circuits necessary to achieve the desired receiver performance is discussed.

The transfer of the transmitter VCO/Modulator circuit and the power amplifier matching network to ceramic substrates is reported, the performance of the VCO ceramic circuit is given, and the final ceramic design is illustrated. A computer printout of the program used to realize the values of the matching network is included.

PREFACE

A study of solid-state integrated microwave circuits under the sponsorship of the Electronics Research Center of the National Aeronautics and Space Administration, is being performed by Texas Instruments Incorporated under Contract NAS 12-75. The object of this contract is to design and develop two each thin-film, hybrid, breadboard telemetry transmitters and receivers. The models will not necessarily be integrated in a single substrate, but may be several chips interconnected by conventional techniques.

This report presents the results of work performed under the seventh, eighth, and tenth items of the work statement. The period covered is 17 June 1967 to 1 November 1967. The seventh task is concerned with the fabrication of two breadboard models of the specified integrated telemetry transmitter subsystem, exclusive of AFC circuitry, and based on the results of item five. The eighth task is concerned with the test and evaluation of the integrated telemetry breadboard developed in item seven. Item ten concerns the design of the integrated telemetry receiver subsystem.

Separate sections of the report present descriptions of the systems, detailed circuit design, analysis of individual blocks and laboratory work. The appendix includes an analysis of mixer design.

TABLE OF CONTENTS

TABLE OF CONTENTS (Continued)

LIST OF ILLUSTRATIONS

LIST OF ILLUSTRATIONS (Continued)

LIST OF ILLUSTRATIONS (Continued)

LIST OF TABLES

SECTION I

INTRODUCTION

In the next few years, all telemetry links designated for space applications will operate within the 2200- to 2300-MHz frequency band. The shift to these higher frequencies brings a need for low-noise microwave receivers so that maximum operating range between a ground station and space vehicle may be obtained. Concurrently, the need for a receiver which has a high information-handling capacity exists. However, the two requirements are incompatible as larger information bandwidth restricts the sensitivity which a receiver may achieve.

The best compromise between information capacity or bandwidth requirements and sensitivity is obtained with a PCM/FM telemetry system. This method of transmitting information provides a higher communication efficiency than other FM systems. This report analyzes a performance specification for a PCM/FM receiver intended for use in the 2200- to 2300-MHz frequency region.

In Section III a trade study of various processes common to communication such as amplification, frequency conversion, and demodulation is performed in an effort to develop a receiver system that meets the specified performance requirements. The prime requirement for the receiver is low-noise figure. The trade study examines each process in order to develop a total receiver configuration which meets the low-noise requirement. In addition, the receiver configuration is developed to accommodate the maximum possible information that may be achieved in a specified 2.0-MHz predetection bandwidth. The resulting receiver system is examined to determine the possibility of its implementation with present state-of-the-art high-frequency components. The design of the receiver is aimed at achieving micro-miniaturization through the use of microstrip and thin-film hybrid circuits. The circuits described in this report are untried. They represent an attempt to determine the feasibility of building a compact reliable receiver with low-noise characteristics utilizing integrated techniques.

The receiver configuration is implemented in microelectronics using microstrip techniques in the fabrication of the balanced mixer which serves as the first stage in the receiver. The remaining intermediate stages operate at 100 MHz and thin-film hybrid techniques are used in their construction. The fixed-tuning requirement is satisfied with a 107.5-MHz crystal oscillator and 2200- to 2300-MHz preselector at the receiver input terminals. Selection of any other frequency is accomplished by crystal replacement. The 107.5-MHz local oscillator frequency is multiplied by twenty to obtain a frequency of 2150 MHz, which, when combined in the mixer with the 2250 MHz received signal, produces the IF.

This report demonstrates that microelectronics can feasibly be used in the mechanization of a low-noise microwave receiver with the capability of recovering a modulating NRZ code transmitted at a bit rate of 1.2 megabits/second.

The ceramic fabrication of the S-Band Transmitter was partially completed during the reporting period. The voltage-controlled oscillator circuit occupies an area of 341 by 280 mils and delivers an output power of 102 to 124 mW across the 100 MHz band (2200 to 2300 MHz), corresponding to an attenuation of 0.85 dB. The oscillator is tunable over a 440 MHz (1922 to 2362 MHz) bandwidth with a power output of 5 and 80 mW at the end points.

The final modulator circuit contains five elements, four resistors and one capacitor. For a constant 1V rms input, the output varies from 15.2 to 16.1 mV over the modulation frequency range, 2 kHz to 1 MHz. The size of the modulator circuit is 206 by 230 mils. The combined oscillator and modulator occupy an area of 625 by 286 mils.

The power amplifier was scaled from Teflon-fiberglass to ceramic with a corresponding reduction in area of 83 percent. A further reduction of 25 percent over the scaled version was realized when new matching networks were designed which limited the characteristic impedance range of the elements from 50 to 100 ohms. The power amplifier circuitry occupies an area 1.600 by 0.720 inches.

Two ceramic networks, the buffer amplifier output matching network and the power divider/combiner, were cut from a main power amplifier substrate and tested in order to check the results against the design. In both cases, the data indicated that the realized circuitry was close to the design values.

A buffer amplifier was fabricated and tested. The amplifier had 4.8 dB of gain for a 245 mW output at 2.25 GHz. When the buffer amplifier and oscillator were mated, the gain was 3.6 dB for a 205 mW output at 2.25 GHz. The reduction in gain indicates that modifications to the matching networks are necessary to achieve an optimum match. The output power varies from 197 to 213 mW across the 100 MHz band corresponding to an inband loss of 0.84 dB.

A package design was initiated and completed. The transmitter package will consist of a gold plated Kovar housing with a gold plated sheet metal cover. The package will measure approximately 2.000 by 1.000 by 0.250 inches.

SECTION II

SUMMARY OF RESULTS

The receiver system and its design were developed from a list of performance requirements that specified low-noise recovery of PCM/FM modulation. Before designing a receiver system that would meet the specified performance, the limitations placed upon selecting and designing PCM/FM receivers were defined. Considerations of these restraints clarified the performance requirements which had to be met. These fundamental considerations defined the modulation to be the recovery of NRZ code from a transmitter employing premodulation filtering and utilizing a deviation ratio of 0.7. The receiver was developed on the basis that the maximum bit rate of the system would not exceed 1.2 megabits/second. The effects of noise and bandwidths in determining the receiver's input and output signal-to-noise ratios, and the effects these ratios have in establishing the system error rate were also outlined. The considerations, which must be given to the rejection of spurious signals produced by mixing, were also reviewed.

Based upon these considerations, a receiver configuration is developed by using a trade-study analysis of possible operations which may occur in a receiver. Such operations as amplification, frequency conversion, and demodulation are considered in light of meeting the performance requirements at various stages in the receiver. Examination of these operations at the receiver input terminals and intermediate stages resulted in a single conversion receiver utilizing a phase-lock discriminator to achieve demodulation. The overall noise figure of the receiver is less than 5 dB, and for a 600-kHz information bandwidth, a sensitivity greater than −100 dBm is achieved.

During the same reporting period, the circuit development of the transmitter configuration selected in earlier phases of this contract was continued. In Section IV of this report, the transfer of the VCO/modulator circuits and power amplifier circuits to a ceramic substrate material is discussed. The packaging design for the completed transmitter system is reported, and demonstrates that the final transmitter will occupy approximately 0.5 in.^{3} and its weight will not exceed two ounces.

SECTION III

RECEIVER

A. GENERAL

The high-frequency and low-noise performance of semiconductor devices as well as thin-film techniques and microstrip characteristics were reviewed in Scientific Report No. 4. These devices, techniques and related microwave components were examined with regard to their application in a low-noise, solid-state microwave receiver. Undoubtedly, a receiver which combined the low-noise performance of state-of-the-art high-frequency devices with the miniaturization offered by thin-film techniques would result in a tremendous reduction in size and weight. If the performance of such a receiver is not worse than a conventional solid-state receiver operating within the 2200- to 2400-MHz frequency region, then such a receiver would certainly be beneficial in spacecraft communication systems where size and weight is of paramount importance. In this section of the report, the feasibility of implementing a telemetry receiver designated to operate within the 2200- to 2300-MHz frequency band allocated for near space applications is analyzed. The feasibility analysis of a receiver using integrated circuit techniques and state-of-the-art high frequency components was conducted to determine whether specific performance requirements could be realized. Two aspects of the problem were studied. First, given a well-defined list of performance specifications, what is the optimum set of individual building blocks that will accomplish the desired requirements? Second, with the new integrated circuit technology and microwave techniques, how can the necessary electronic circuitry making up the receiver system configuration be realized? The results of the study of these problems are summarized in the following paragraphs.

B. SYSTEM REQUIREMENTS

A list of performance requirements that may be expected from a modern microwave receiver intended for use as part of a space-earth communication system is shown in Table 1. The requirements listed in the table typically exemplify several conflicting demands required in modern receivers intended for space applications. The foremost conflict being that between bandwidth and sensitivity. The microwave carrier frequency makes possible wider system bandwidths which result in increased information handling capability. However, large system bandwidths increase the inherent noise power of the receiver thereby reducing sensitivity. Thus, usable signal levels between the spacecraft and a ground station can only be obtained at the expense of increased transmitter power. If the conservation of transmitter power is a prime requisite, then sensitivity can be achieved at the expense of bandwidth and information capacity. Unfortunately, large bandwidths and desirable sensitivity

do not go hand in hand. A second factor influencing sensitivity is noise figure. Present day S-band receivers have overall noise figures in excess of 9.0 dB unless parametric amplifiers or cryogenic techniques are used. The requirements listed in Table 1 for the receiver in this study specify a 4 to 6 dB noise figure.

Table 1. S-Band Telemetry Receiver Specifications

Modulation	PCM/FM
Operating frequency	2200 to 2300 MHz
Sensitivity	−110 dBm
Bandwidth	2 to 3 MHz minimum
Noise figure	4 to 6 dB
Dynamic range	50 dB
Image rejection	60 dB
Spurious response	50 dB
Frequency stability	± 0.002 percent
Tuning	Semifixed
Power input	4 watts, −24 Vdc
Temperature range	−28°C to 71°C
Size	144 in.^{3}
Weight	1 kG

The performance specifications of Table 1 should be defined to establish a framework for the following analysis and to clarify assumptions which necessarily must be made.

1. Modulation

The final receiving system must provide for the recovery of a PCM data format. The PCM format is assumed to frequency modulate an S-band carrier with a deviation ratio of 0.7, which is the deviation normally employed in PCM transmission. Upon being extracted from the carrier, the PCM data will be available to the video or telemetry (TLM) output terminals of the receiver.

2. Operating Frequency

The operating frequency selected is 2250 MHz which is the center of the 2200- to 2300-MHz frequency spectrum allocated for near space communication networks. This permits compatibility with the transmitter developed under this contract and discussed in Section IV of this report. The selection of this frequency defines the frequency modulated RF carrier that is to be received.

3. Sensitivity

The sensitivity requirement shown in Table 1 defines the minimum detectable power level of the incoming signal which will still provide a usable baseband signal at the output terminals of the receiver. The minimum usable output signal implies a baseband signal-to-noise ratio which permits an acceptable bit error rate.

4. Bandwidth

The specified bandwidth (shown in Table 1) which the receiver must exhibit defines the predetection 3 dB passband characteristic of the receiving system. The chosen bandwidth must be wide enough to accommodate the highest expected frequency of the baseband signal spectrum and anticipated system instabilities. Normally, this bandwidth is defined as being two-sided, that is, ideally it is at least twice as wide as the spectrum of the modulating signal. On this basis, the information capacity of the receiver is equal to one-half the predetection bandwidth.

5. Noise Figure

The noise figure specified limits the amount of noise that the receiver may add to the received signal as compared to an ideal receiver which contributes only thermal noise. Thermal noise of an ideal receiver matched to fifty ohms is -174 dBm. This is derived from the thermal noise expression, KTB watts/Hz, where K is Boltzmann constant (1.38×10^{-23} joules/erg), T is the ambient temperature (290°K) and B is a one Hz bandwidth. The noise figure defines the noise performance of the linear portion of the receiver from the first stage of signal reception at the receiver input terminals to the stage of detection.

6. Dynamic Range

The receiver dynamic range defines the amount that the incoming signal level may increase above its defined minimum detectable level before overloading in the amplifier stages occurs. Overloading then places a limit upon the maximum acceptable incoming signal level. This limit is defined as the signal level at which the resulting distortion products equal the noise level.

7. Image Rejection

The image rejection of the receiver is a measure of its ability to reject the image frequency. The specified image rejection in Table 1 defines the receiver response to a signal at the image frequency as compared to its response to the desired carrier signal of the same amplitude. Thus, the receiver response to the image frequency should be at least 60 dB below its response to the RF carrier.

8. Spurious Responses

Spurious responses are defined as the receiver response to an undesirable signal. Spurious responses result when the sum or difference of the various harmonics of two separate input signals will yield the receiver tuned frequency. The equation for this relationship is

$$f_o = mf_a \pm mf_b$$

where

f_o is the tuned frequency of the receiver

f_a is the frequency of the interfering frequency source nearest to f_o

m is an integer

f_b is the interfering source of the second frequency

n is an integer

Only second order sums and differences, third order differences, and fifth order differences are normally considered (Order = n + m). The third order difference products are potentially the most serious, as signals are produced which fall in the RF passband.

The receiver response to spurious responses must be at least 50 dB below the response to the desired signal.

9. Frequency Stability

In receivers wherein the received carrier frequency is translated either upward or downward by frequency conversion, frequency stability defines the tolerance that the local oscillator frequency can vary about its nominal value. This variation about its designed nominal value is taken to imply long-term stability. If a local oscillator is not used, stability is defined as the tolerance that the center frequency of the receiver can vary about its designed value.

10. Tuning

The requirement for semifixed tuning defines a receiver that is fixed-tuned to a desired operating frequency, and retuning is accomplished by physically altering the network elements that determine the receiver fixed operating frequency. The final receiver will be designed to operate at the selected 2250 MHz frequency with provisions for arbitrarily selecting a different channel within the 2200- to 2300-MHz frequency range.

11. Temperature

The temperature range shown in Table 1 defines the ambient temperature extremes for which the receiver performance will remain within acceptable limits.

C. FUNDAMENTAL CONSIDERATIONS

The recovery of modulating signal spectrums from RF carriers masked in noise is essentially a demodulation process. In order for the process to be successful so that the detected baseband signal presented to the receiver output is useful, a quantitative measure of the effectiveness of demodulation is required. Two commonly used measures or figures of merit used to evaluate signal detection techniques are signal-to-noise ratio (SNR) and mean-squared error existing between the actual detected output and desired output. In the case of data systems such as Pulse Code Modulation/Frequency Modulation (PCM/FM), the bit error rate is used as a measure of demodulation effectiveness. Before these concepts can be applied to determine bandwidth requirements and to establish system gain requirements, the modulating spectrum and the properties of noise must be known. Attention is also required to the manner in which spurious signals may degrade desired performance. Fundamental considerations of these concepts are outlined below. These considerations define the framework of the problem of signal processing in the presence of noise, a problem which the optimum receiver system and associated individual integrated circuits must meet and overcome.

1. Modulation

PCM/FM in which pulse encoded information frequency modulates an RF carrier has been used extensively in space communication systems. This modulation scheme is frequently classified as frequency-shift-keying (FSK). However, a distinction between FSK and PCM does exist. Both types of modulation effectively transmit binary data but conventional PCM can be thought of as frequency modulating a single oscillator. On the other hand, FSK may be considered as "switched" PCM in which two oscillators at different frequencies are switched in accordance with the modulation. The primary difference is seen to be that FSK has a constant shift in carrier frequency from the unmodulated frequency regardless of the frequency of the

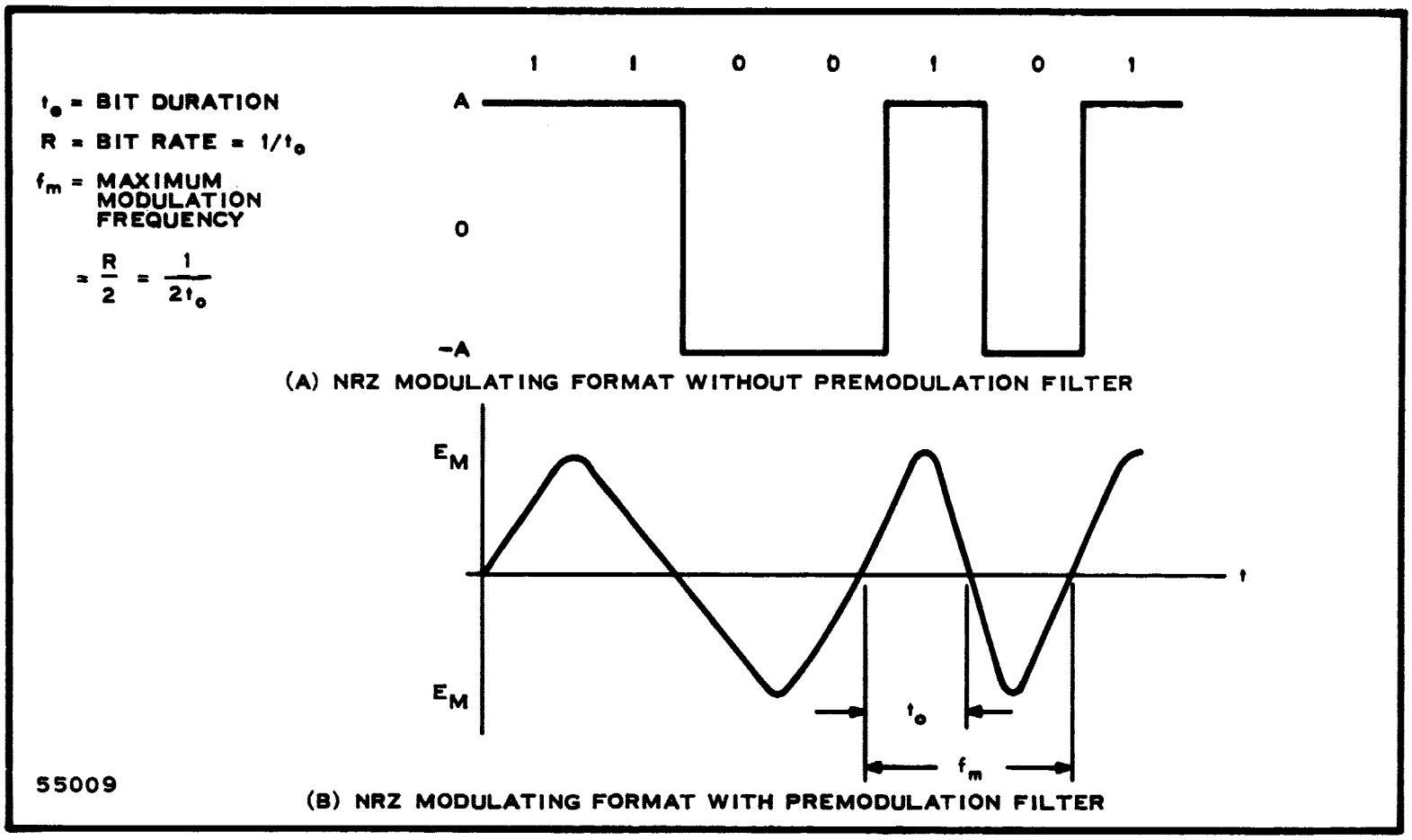

Figure 1. NRZ Modulating Format

modulating signal. In the case of conventional PCM, the carrier frequency varies about its center value in accordance with the frequency of the modulating signal. The deviation ratio, defined as the ratio of the peak-to-peak shift in carrier frequency to the highest modulating frequency is usually higher in FSK modulation than in the case of PCM. Usually, the minimum deviation ratio for PCM is 0.7 as compared to values of 5 normally used for FSK.

The modulating or baseband signal in PCM/FM systems is generally an NRZ format, as shown in Figure 1. This figure illustrates that the format changes level when there is a change in binary representation. The change between the two possible levels occurs randomly and the resulting RF power spectrum of the FM carrier can only be expressed in a statistical manner. Nevertheless, for either FSK or conventional PCM/FM, knowledge of the maximum modulating frequency can be determined from the bit rate.[1] If it is assumed that a premodulation filter precedes the transmitter modulator, the modulating signal may be said to be sinusoidal.[2] This is a valid assumption, as modulating a carrier with essentially a square wave and its associated high harmonic content does not fall within good engineering practice.

Each bit in an encoded PCM message may assume either one of two possible bits, a zero or a one, which may occur with equal probability during

a given bit period or duration. The speed at which these bits may occur is defined as the bit rate, which is the reciprocal of the bit period. The highest modulating frequency that can be anticipated equals one-half the bit rate. This is illustrated in Figure 1, where it is seen that the maximum modulating frequency occurs for successive alternating levels corresponding to successive unlike bits.

2. Bandwidth

a. Predetection Bandwidth

The most critical parameters to be selected in receiver design are proper bandwidths. This is especially important in FM reception where theoretically an infinite number of sidebands exist and any attempt to band-limit the received RF spectrum does not allow exact recovery of the original modulating signal. Whatever predetection bandwidth is selected must be wide enough to accommodate an acceptable portion of the RF power spectrum without causing an intolerable amount of distortion. Yet, the bandwidth should be narrow enough to limit the amount of receiver noise power in order to obtain acceptable receiver sensitivity. The video bandwidth, on the other hand, needs only to be wide enough to pass the highest modulating frequency.

The video bandwidth determines the available amount of noise power existing at the receiver output terminals just as the predetection bandwidth determines the total noise power at the input. Then, unquestionably, both bandwidths will determine the signal-to-noise ratios existing in the receiver.

That the RF spectrum resulting from a carrier frequency modulated by a sinusoid is in terms of Bessel functions and that p-order sidebands exist which are displaced from the carrier by integer values of the modulating frequency are well known. Theoretical investigations by many researchers to establish a usable criteria for FM bandwidth have been inconclusive. In the case of digital transmission, a rule that the predetection bandwidth should equal the bit rate is sometimes used. However, this leads to a very restrictive bandwidth and the output pulse train will be distorted by comparison with the original modulating data.[3]

A commonly used method to establish bandwidths in FM systems is

$$BW_{IF} = 2(f_d + f_m) \qquad (1)$$

where f_d is the peak frequency deviation and f_m is the maximum expected modulating frequency. The maximum modulating frequency for the system, as mentioned previously, can be considered equal to one-half the bit rate. The maximum bit rate recommended to be used in the 2200- to 2300-MHz frequency bands allocated for space application is 1.2×10^6 bits/second.

The highest bit rate allowed under IRIG standards gives a maximum modulating frequency of 600 kHz. Rearranging equation (1),

$$BW_{IF} = 2f_m\left(\frac{f_d}{f_m} + 1\right) \tag{2}$$

$$BW_{IF} = 2f_m\,(D + 1) \tag{3}$$

and using a deviation ratio of 0.7 which has been stated in the literature as optimum for PCM/FM[1, 5] results in a bandwidth of

$$BW_{IF} = 3.4\,f_m \tag{4}$$

$$= 3.4\,(600\text{ kHz}) = 2.04\text{ MHz}. \tag{5}$$

This bandwidth is sufficient to recover a 1.2×10^6 bit rate that frequency modulates an RF carrier. It also satisfies the minimum bandwidth specification.

In Figure 2, the ratio, (B) of the predetection bandwidth to peak frequency deviation is plotted as a function of the deviation ratio (D) for the expression

$$J_p(D) = \gamma. \tag{6}$$

The quantity, γ, defines an arbitrary fraction of sideband amplitude to the amplitude of the unmodulated carrier, and J_p is the p^{th} order Bessel function. This curve allows the selection of the ratio (B) needed to pass unattenuated all sidebands that are greater in amplitude than any chosen fraction γ, for any deviation. For a 600-kHz maximum modulating frequency and 0.7 deviation ratio, the carrier deviation is 420 kHz. The ratio (B) for a 204 MHz predetection bandwidth is

$$B = \frac{BW_{IF}}{f_d} = \frac{2.04}{0.42} = \frac{204}{42} \approx 4.9. \tag{7}$$

All sidebands with amplitudes greater than ten percent of the unmodulated carrier are passed unattenuated.

The RF power spectrum contained within the passband may be easily examined by considering the expression for a frequency modulated carrier. Assuming the use of a premodulation filter at the transmitter,

$$E(t) = A \sin\left(\omega_C + \frac{2\pi f_d}{\omega_m} \sin \omega_m\right)t \tag{8}$$

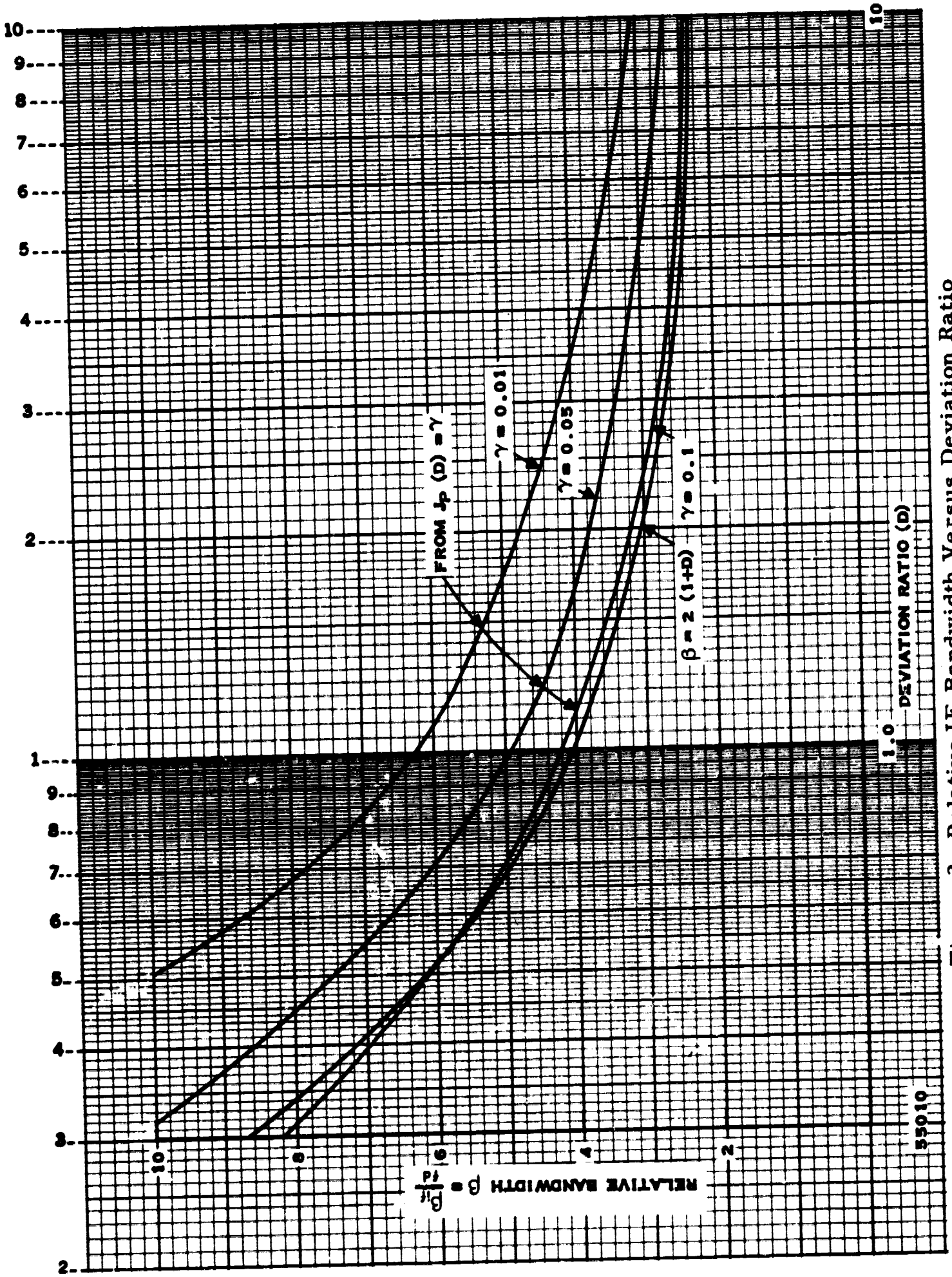

Figure 2. Relative IF Bandwidth Versus Deviation Ratio

where f_d is the peak frequency deviation, and the quantity $2\pi f_d/\omega_m$ defines the deviation ratio, D. Using the power series identity for the Bessel functions,

$$\cos (X \sin Y) = 1 - \frac{X^2 \sin^2 Y}{2!} + \frac{X^4 \sin^4 Y}{4!} + \ldots \tag{9}$$

$$\sin (X \sin Y) = X \sin Y - \frac{(X \sin Y)^3}{3!} + \frac{(X \sin Y)^5}{5!} + \ldots \tag{10}$$

where X = D and for PCM/FM X < 1, only the first few terms need to be considered. Hence,

$$\cos (X \sin Y) = 1 - \frac{X^2 \sin^2 Y}{2!} \tag{11}$$

$$\sin (X \sin Y) = X \sin Y. \tag{12}$$

Expanding Equation (8) and substituting Equations (11) and (12) where X = D and $Y = \omega_m t$,

$$E(t) = A \left[\sin \omega_c t \cos (D \sin \omega_m t) + \cos \omega_c t \sin (D \sin \omega_m t)\right] \tag{13}$$

$$= A \left\{\sin \omega_c t \left[1 - D^2 \frac{\sin^2 \omega_m t}{2!} + \cos \omega_c t (D \sin \omega_m t)\right]\right\} \tag{14}$$

$$= A \left[\sin \omega_c t - \frac{D^2}{2!} \sin \omega_c t \sin^2 \omega_m t + D \cos \omega_c t \sin \omega_m t\right] \tag{15}$$

$$= A \left\{\sin \omega_c t - \frac{D^2}{2!} \sin \omega_c t \left[\frac{1}{2}(1 - \cos 2\omega_m t)\right]\right\} \tag{16}$$

$$+ \frac{D}{2} \sin (\omega_c t + \omega_m t) + \frac{D}{2} \sin (\omega_c t - \omega_m t)\Big]$$

$$= A \left[\sin \omega_c t - \frac{D^2}{4} \sin \omega_c t + \frac{D^2}{4} \sin \omega_c t \cos 2\omega_m t \right. \tag{17}$$

$$\left. + \frac{D}{2} \sin (\omega_c t + \omega_m t) + \frac{D}{2} \sin (\omega_c t - \omega_m t)\right]$$

$$= A\left[\left(1-\frac{D^2}{4}\right)\sin\omega_c t + \frac{D}{2}\sin(\omega_c t - \omega_m t) + \frac{D}{2}\sin(\omega_c t - \omega_m t)\right. \quad (18)$$

$$\left. + \frac{D^2}{8}\sin(\omega_c t + 2\omega_m t) + \frac{D^2}{8}\sin(\omega_c t - 2\omega_m t)\right] .$$

Equation (18) illustrates that two sets of sidebands result which are displaced from the carrier by $\omega_c \pm \omega_m$ and $\omega_c \pm 2\omega_m$. Considering the modulating signal to be periodic and ω_m to be the maximum radian modulating frequency, the power spectrum may be written, without resorting to a statistical analysis, as

$$G(\omega) = A_c{}^2\left\{|J_o(D)|^2\,\delta(\omega-\omega_c)^2\right. \quad (19)$$

$$+ |J_1(D)|^2\,\delta[\omega-(\omega_c \pm \omega_m)]$$

$$\left. + |J_2(D)|^2\,\delta[\omega-(\omega_c \pm 2\omega_m)]\right\}$$

This equation is plotted in Figure 3 as a one-sided spectrum for various deviation ratios, and it is seen that for D = 0.7, 95 percent of the power spectrum lies within a bandwidth equal to 1.5 times the bit rate. Equation (19) compares favorably with the results obtained by Pelchant who analyzed the PCM/FM RF spectrum for random modulation.[6]

Obviously, the 2.0- to 3.0-MHz bandwidth in Table 1 is not compatible with the transmitter with the presently defined modulation parameters. If the receiver is designed for a 2.0-MHz 3-dB bandwidth, it will not pass 1.5 MHz carrier deviations unattenuated unless the modulating frequency is considerably less than 1.0 MHz. Under the reduced modulating frequency condition PCM/FM could be transmitted and recovered, as PCM's with peak deviations of 1.5 MHz are feasible where multiplexing is employed.

b. Postdetection bandwidth

The postdetection bandwidth necessary to recover the baseband signal is determined by the cutoff frequency of the video filter. This filter establishes the amount of noise appearing at the output of the receiver. In the following paragraph, the noise output of the demodulator is shown to vary as the cube root of the IF bandwidth.

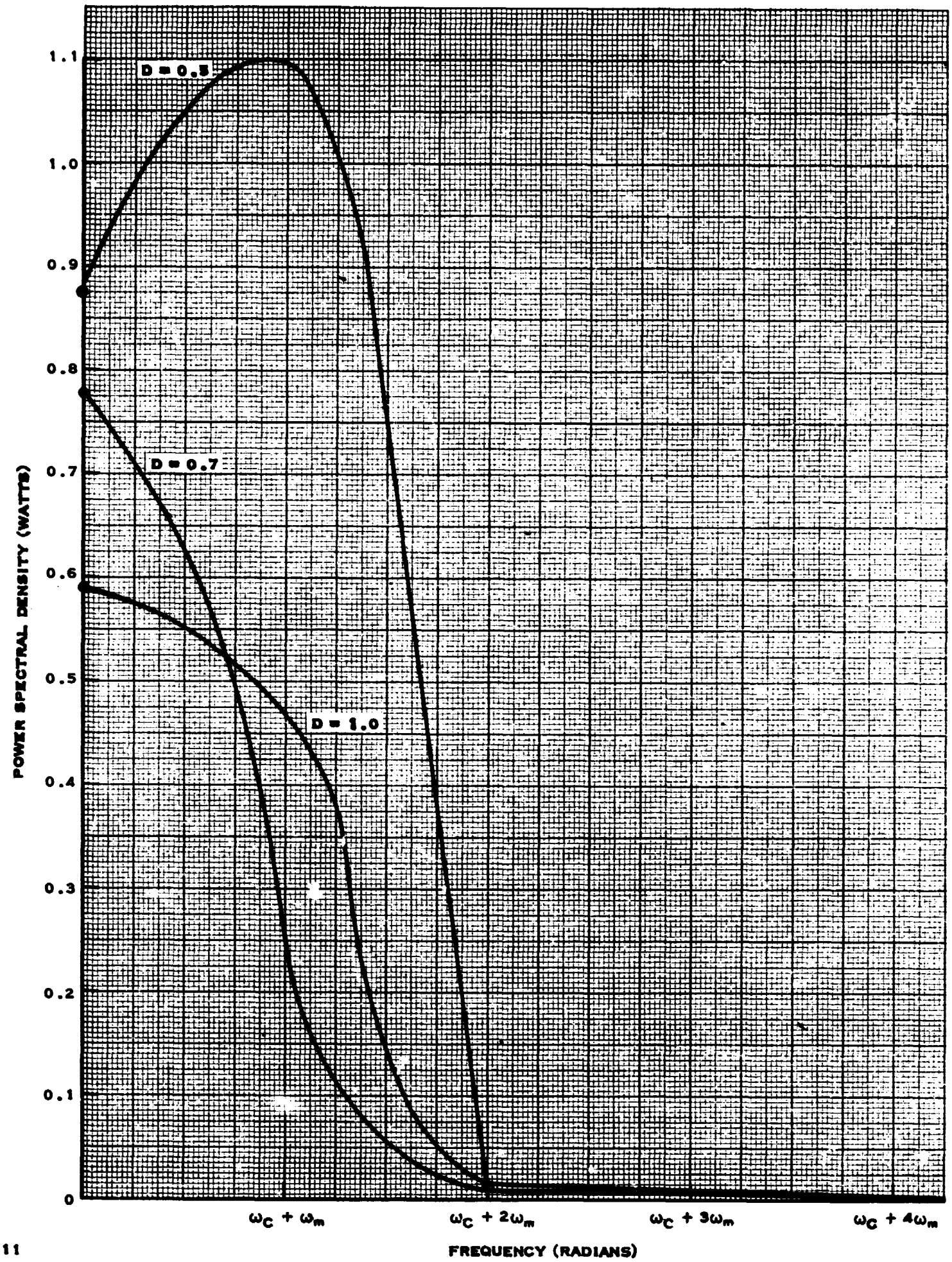

55011

Figure 3. Power Spectrum of PCM/FM of Periodic NRZ Baseband With Deviation Ratio As Parameter

The ratio of the predetection bandwidth to the baseband bandwidth, BW_{IF}/B_m establishes the output signal-to-noise ratio of the receiver for a prescribed deviation ratio. This is shown by

$$(S/N)_o = 3D^2\left(\frac{BW_{IF}}{2B_m}\right)(S/N)_{in}$$

where the quantity, S/N, defines the power ratios existing in the receiver. The above relation demonstrates that the output signal-to-noise ratio is improved over the input signal-to-noise ratio by the factor, $3D^2(B_{IF}/2B_m)$.

In the case of a video filter with an ideal rectangular bandwidth, the cutoff (3dB bandwidth) necessary to recover a NRZ modulating code equals one-half the bit rate. This bandwidth also establishes the video or output noise bandwidth. For an anticipated 1.2×10^6 bit rate, the cutoff frequency of the baseband filter is 600 kHz. Therefore, the ratio of predetection bandwidth to postdetection is

$$\frac{BW_{IF}}{2B_m} = \frac{2.04 \times 10^6}{1.2 \times 10^6} = 1.7$$

and the improvement over the input signal-to-noise ratio for a 0.7 deviation is

$$3(0.49)(1.7) = 2.49$$

Therefore, when the input signal-to-noise ratio exceeds a threshold value $(CNR)_T$, the output signal-to-noise ratio of the receiver is

$$(S/N)_o = 10 \log (2.49) + (S/N)_{in} = 3.94 + (S/N)_{in} .$$

3. Noise

One of the prime factors concerning the effectiveness of communication systems is noise. System noise behavior establishes a lower limit on receiver performance by determining the minimum detectable signal level feasible. Although signals buried in noise can be detected, a limit is placed on detectable signal level by noise figure and the amount of noise existing in the passband response of the receiver.

The fluctuation voltages existing in the input passband of a receiver are commonly referred to as noise. The instantaneous amplitudes of noise voltage components measured in a given interval of time may be any finite value. Thus, noise voltage is described as a random process and as such its properties require definition in terms of the mathematics of probability. That the properties of noise are described in terms of the Gaussian probability function has been shown, [4]

$$P\{X < x\} = \int_{-\infty}^{X} \frac{1}{\sqrt{2\pi\sigma}} \epsilon^{\frac{-X^2}{2\sigma 2}} \, dt \qquad (20)$$

which states the probability that the amplitude of noise voltage does not exceed an arbitrary value, (X), in some time interval. The parameter σ is the standard deviation and it signifies the rms amplitude of noise voltage. It follows then that σ^2 is a quantitative measure of noise power corresponding to the instantaneous fluctuation voltages contained in the band-limited response of the receiver. To be more explicit

$$\sigma^2 = \overline{\frac{1}{2} V^2(t)} \qquad (21)$$

where V(t) represents the peak Gaussian noise voltage and the bar denotes the average value of peak voltage over a large interval of time.

The power spectrum due to the fluctuation noise voltages contained within the passband of the receiver may be found from the spectral density of noise, G(f), which is a constant in the case of fluctuation or white noise.

$$G(f) = k^2 \text{ (watts/Hz)} \qquad (22)$$

Integrating over the passband defines the band-limited noise power contained in the receiver response

$$\sigma^2 = \int_{-B}^{B} G(f)df \qquad (23)$$

$$\sigma^2 = 2\int_{o}^{B} G(f)df \qquad (24)$$

where B represents one-half of a rectangular bandwidth response. Assuming an ideal rectangular response, the resulting noise power after integration is

$$\sigma^2 = 2\ k^2\ B \tag{25}$$

and a flat or uniform noise power spectrum is seen to exist in the receiver passband. The constant k^2 is the noise spectral density of the receiver, consisting of the familiar KT product of thermal noise that relates Boltzmann constant and ambient temperature and fluctuation noise given by the receiver noise figure (NF). Expressing k^2 in decibels for a 50-ohm system,

$$k^2 = -174\ \text{dBm} + \text{NF} \tag{26}$$

and the noise power contained within the receiver response may be conveniently written in decibels as

$$P_N = 10 \log \sigma^2 + \text{NF} \tag{27}$$

$$P_N = -174\ \text{dBm} + 10 \log B + \text{NF}\ . \tag{28}$$

The total receiver noise power assuming a rectangular predetection bandwidth,

$$P_N = -174\ \text{dBm} + 10 \log [2.04 \times 10^6] + \text{NF}$$

$$= -110.9 + \text{NF dBm}\ . \tag{29}$$

Many texts[3,5,6] treat the case of an unmodulated carrier in the presence of narrowband noise. The resulting relationship indicates the manner in which the carrier and noise components combine. To briefly review the procedure as given by Downing,[3] consider the expression for a sinusoidal carrier and random noise combined at the receiver input

$$E(t) = A \sin \omega_c t + n(t) \tag{30}$$

The noise can be considered as appearing in a narrowband as the passband is normally small compared to the carrier frequency. Thus,

$$n(t) = X_c(t) \cos \omega_c t - X_s(t) \sin \omega_c t \tag{31}$$

where $X_c(t)$ and $X_s(t)$ are also Gaussian random variables denoting the amplitude of the quadrature carrier terms. Thus,

$$E(t) = A \sin \omega_c t + X_c(t) \cos \omega_c t - X_s(t) \sin \omega_c t \tag{32}$$

$$= A(t) \sin (\omega_c t + \theta) \tag{33}$$

where

$$\theta = \tan^{-1} \frac{X_c(t)}{A - X_s(t)} \tag{34}$$

and before limiting

$$A(t) = \sqrt{[A - X_s(t)]^2 + [X_c(t)]^2} \tag{35}$$

The phase angle of Equation (36) is time variant due to the quadrature noise component. Therefore, the instantaneous frequency of the carrier, $\omega_c t + \phi$, is seen to vary about its nominal value in accordance with the noise component, $X_c(t)$.

This perturbation has the same effect as modulation and generates a finite amount of demodulated noise at the output of the frequency detector.

The instantaneous radian frequency resulting from noise modulation is defined as the time rate of change of the phase angle, ϕ.

$$\omega_i = \frac{d\phi}{dt} = \frac{d}{dt} (\omega_c t + \theta) \tag{36}$$

The output of the detector is proportional to the instantaneous phase angle,

$$E_o(t) = K_d \frac{d\phi}{dt} . \tag{37}$$

Substituting Equation (34)

$$E_o(t) = K_d \frac{d}{dt} \left\{ \frac{\tan^{-1} X_c(t)}{A - X_s(t)} \right\} \tag{38}$$

$$E_o(t) = K_d \left\{ \frac{[A - X_s(t)]\, X_c'(t) + X_c(t)\, X_s'(t)}{[A - X_s(t)]^2 + X_c^2(t)} \right\} \tag{39}$$

where the primes denote differentiation with respect to time and K_d is the detector sensitivity constant in volts per radian. If the receiver utilizes a limiter, the noise component, $X_s(t)$, in-phase with the carrier is eliminated. Thus,

$$E_o(t) = K_d \left\{ \frac{X_c'(t)}{A + X^2(t)} \right\} \tag{40}$$

and for high input signal-to-noise ratios,

$$E_o(t) = K_d \frac{X_c'(t)}{A} \tag{41}$$

Thus, although limiting is used, the noise modulation on the carrier gives rise to a detected noise output which is inversely proportional to signal strength. Obviously, without limiting, the detected output noise would be higher. Note that the output noise is also Gaussian since the derivative of a Gaussian process is also Gaussian.

The total amount of noise power appearing in the postdetection bandwidth at the receiver output is obtained from

$$P_o = \int_o G_x(f)\,df \tag{42}$$

where $G_x(f)$ is the noise power spectral density due to $K X_c'(t)/A$. Rice[7] and others have shown that $G_x(f)$ has a quadratic dependence upon positive frequencies up to one-half the predetection bandwidth 3 dB cutoff frequency.

$$G_x(f) = \frac{2k^2 f^2}{A^2} \qquad o \leq f < B \tag{43}$$

$$= o \qquad f > B \tag{44}$$

Carrying out the integration in Equation (44), the noise power at the receiver output is defined:

$$P_o = \frac{2k^2 f_m^3}{3A^2} \tag{45}$$

The output noise power given above was defined for high input signal-to-noise ratios. As the input signal to noise ratio is decreased, a secondary noise phenomenon occurs in which randomly occurring impulses or noise spikes of both positive and negative polarity are present at the output of the frequency detector. These impulses, or "clicks" as they are commonly referred to, may seriously impair detection of digital information due to the smoothing effect of the video filter. The filter integrates the "clicks" into recognizable pulses which may be mistaken for a one or zero by the decoding process performed on the receiver output. This erroneous decoding contributes to bit error. Detectors which reduce this error and bit error probability concerning the presence of these noise spikes have recently appeared in the literature.[5, 8] A complete treatment of the theory of noise "clicks" has been published by Rice.[7]

Rice has investigated the number of clicks occurring in a given time interval as a function of signal-to-noise ratio and the noise spectrum resulting when these noise spikes are combined with the output noise power previously obtained. His investigations revealed that the noise power generated by these noise spikes is

$$P_i = 16\pi^2 N_+ f_m \tag{46}$$

where N_+ is the number of clicks or spikes appearing each second. Combining this expression with the noise power in Equation (45) yields a total output noise given by

$$P_o = \frac{2k^2 f_m^3}{3A^2} + 16\pi^2 N_+ f_m \ . \tag{47}$$

Fluctuation noise resulting from the physical components making up the detection and amplification processes involved in recovery of the base-band signal is within control of the designer. A measure of this control is noise figure, which is a quantitative way of expressing the noise contributions of the receiver physical components to the noise present at the receiver input. The available noise power at the input terminals, generated by the signal source, is given by

$$N_i = KTB \tag{48}$$

where $K = 1.374 \times 10^{-23}$ joules/°K

$T = 290°K$

B = Bandwidth.

In a practical system, N_i appears at the receiver input terminals as a result of a voltage equivalent to the thermal noise generated in the radiation resistance of the antenna. Therefore, even if the receiver produced no internal noise, noise with which an incoming weak signal would have to compete would still be introduced into the system.

In terms of input and output signal-to-noise ratio, noise figure is expressed

$$NF = 10 \log\left(\frac{S_i/N_i}{S_o/N_o}\right) \tag{49}$$

where S_i is the available power from the input signal source, S_o is the available output power and N_o is the total amount of available output noise consisting of the amplified input noise and internal noise contributed by the system. The input noise, N_i, is the available noise power due to the signal source.

Each functional stage or network of the receiver has a noise figure relationship that denotes the amount of noise each network adds to the input signal which it is amplifying. This stage noise figure may be expressed in terms of the stage power gain

$$NF = 10 \log\left(\frac{S_i/N_i}{S_o/N_o}\right) \tag{50}$$

$$NF = 10 \log\left(\frac{N_o}{N_i S_o/S_i}\right) \tag{51}$$

$$NF = 10 \log\left(\frac{N_o}{N_i G}\right) \tag{52}$$

where

$G = S_o/S_i$ defines the network power gain.

Therefore, the output noise, expressed in decibels, for a given network is

$$N_o(dB) = NF(dB) + 10 \log N_i G \tag{53}$$

and since $N_i = KTB$,

$$N_o(dB) = NF(dB) + 10 \log KTBG \tag{54}$$

and it is seen that the output noise power of a network is given by the noise figure of the network and the amplified input noise. The noise figure characteristic of the network is given by its internal parameters. The noise figure characteristics of transistors, FET's, and diodes in terms of their physical properties were evaluated in Scientific Report No. 4 of this program.

When cascaded stages are considered, the overall noise figure for the complete system is given by the expression

$$NF_o(dB) = 10 \log \left[F_1 + \frac{F_2 - 1}{G_1} + \frac{F_3 - 1}{G_1 G_2} + \ldots \right] \tag{55}$$

where F_n and G_n denote the noise factors and power gains of the individual stages, respectively. The noise factor of the various stages are pure numbers defined as the antilog of the corresponding stage noise figure. With this connotation we may replace F_1, by the antilogarithm of Equation (52), and write

$$NF_o(dB) = 10 \log \left[F_1 + \frac{F_2 - 1}{G_1} + \frac{F_3 - 1}{G_1 G_2} + \ldots \right] \tag{56}$$

$$= 10 \log \left[\left(\frac{N_o}{N_i G_1} \right) + \frac{F_2 - 1}{G_1} + \frac{F_3 - 1}{G_1 G_2} + \ldots \right]$$

In microwave systems the first stage is normally a bandpass filter which does not add or reduce noise, thus $N_o = N_i$ and defining $G_1 = 1/L_1$, where L_1 is the insertion loss of the filter.

$$NF_o\,(dB) = 10 \log \left[L_1 + L_1 (F_2 - 1) + \frac{L_1 (F_3 - 1)}{G_2} \right] \qquad (57)$$

where L is the insertion gain, then

$$NF_o\,(dB) = 10 \log L_1 + 10 \log \left[F_2 + \frac{F_3 - 1}{G_2} \right] \qquad (58)$$

and it is noted that the insertion loss in dB adds directly to the overall noise figure expression, thereby degrading system noise performance. Equation (58) also demonstrates that the system noise figure is mainly determined by the noise figure of the first few stages as subsequent noise figures are diminished rapidly by the product of network gains.

4. Spurious Signals

It is the prevailing practice in modern receivers to translate the incoming signal to a new location in the frequency domain. This translation is a nonlinear process referred to as conversion, or more commonly as "mixing." The process requires a secondary frequency source within the receiver that is conventionally provided by a local oscillator. Converting the incoming signal to a lower frequency provides the advantage of achieving power gains more efficiently, but drawbacks exist in this practice in that frequency conversion, being a nonlinear process, also creates undesirable frequencies. The difference frequency between the incoming signal and the local oscillator is the desired frequency; however, many undesirable or spurious signals are created in addition to the difference frequency. These spurious signals are a source of interference, which when combined with the desired signal, may degrade performance.

Probably the most significant undesirable signal which must be discriminated against by the receiver response is the image frequency. The image frequency is separated from the desired input signal by twice the difference or intermediate frequency, and may fall either above or below the input signal frequency depending on the choice of local oscillator frequency. This is illustrated in Figure 4 for a difference frequency of 100 MHz. The troublesome effect of the image frequency is best explained by considering that for a prescribed difference and local oscillator (LO) frequency (f_{IF} and f_{LO}) the receiver may respond to either of two possible input frequencies (f). That is,

$$f = f_{IF} \pm f_{LO} \tag{59}$$

where depending upon the choice of LO frequency, one frequency constitutes the desired signal frequency (f_S); the other is termed the image frequency (f_i). In the case of a LO frequency lower than the input signal frequency, the desired and image frequencies are given

$$f_S = f_{IF} + f_{LO} \tag{60}$$

$$f_i = f_{LO} - f_{IF} \tag{61}$$

Substituting, $f_{LO} = f_i + f_{IF}$ from Equation (61) into Equation (60) results in

$$f_S = f_{IF} + (f_i + f_{IF}) \tag{62}$$

$$f_S = f_i + 2f_{IF} \tag{63}$$

and the image frequency is defined

$$f_i = f_S - 2f_{IF} \tag{64}$$

which is illustrated in Figure 4a.

Reducing the receiver's response to the image frequency is usually accomplished by the rf selectivity preceding the mixer. If such filtering requirements are severe or impractical to achieve, double or triple conversion within the receiver lessens the restrictions of shaping of the RF passband.

For the semi-fixed tuning requirements specified in Table 1, meeting the 60-dB attenuation, required to be presented to the image over the entire 2200- to 2300-MHz frequency band, would be ideal. Such an accomplishment would allow interchange of the receiver frequency determining networks without the need to alter the RF filter providing the selectivity. To examine the feasibility of broadband selectivity and of meeting the 60 dB image rejection requirement, consider a semi-fixed tuned receiver with a 100 MHz if. and its center frequency altered for operation at 2300 MHz. Utilizing Equation (64), the image frequency is 200 MHz less than the center frequency or 2100 MHz. For the chosen 100-MHz difference, the image is 100 MHz below the lowest operating frequency of the UHF telemetry band, 2200 MHz. Assuming an RF selectivity with a 150-MHz passband, the image frequency is 75 MHz below the lowest cutoff frequency of the RF filter and 60 dB attenuation to the image is required in this portion of the out-of-passband response. This is illustrated in Figure 5. As shown in the figure, the image rejection required for an image signal of 2050 MHz when the receiver is tuned to 2250 MHz must exceed the 60-dB requirement. The needed skirt steepness, required for broadband selectivity, can be achieved using a Tchebyscheff response.

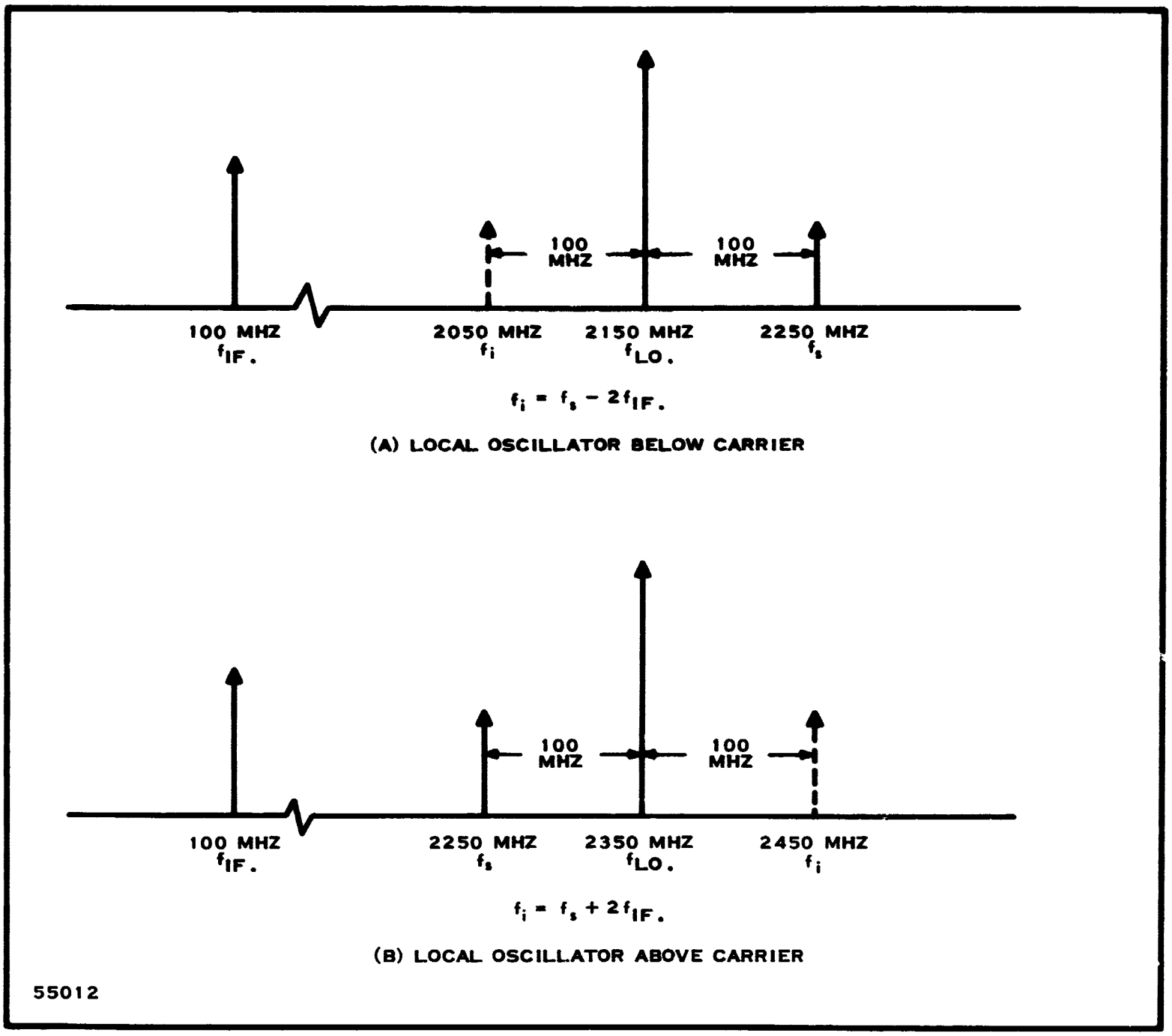

Figure 4. Image Frequency Location In Relation To Desired Signal

As seen above, the selection of the difference frequency is a major consideration in determining selectivity requirements with respect to the image signal. In addition, the difference frequency must also be selected with attention given to the intermodulation products (IM) that may fall within the if. passband. The intermodulation products which appear for three various mixer configurations; single diode, balanced and double-balanced mixers are given in Table 2. For the most part, careful design and proper if. response may minimize the effects of these products. However, one intermodulation product is very difficult to eliminate or reduce by filtering. This IM product is the result of second order nonlinearity characteristics of the mixer and is defined.

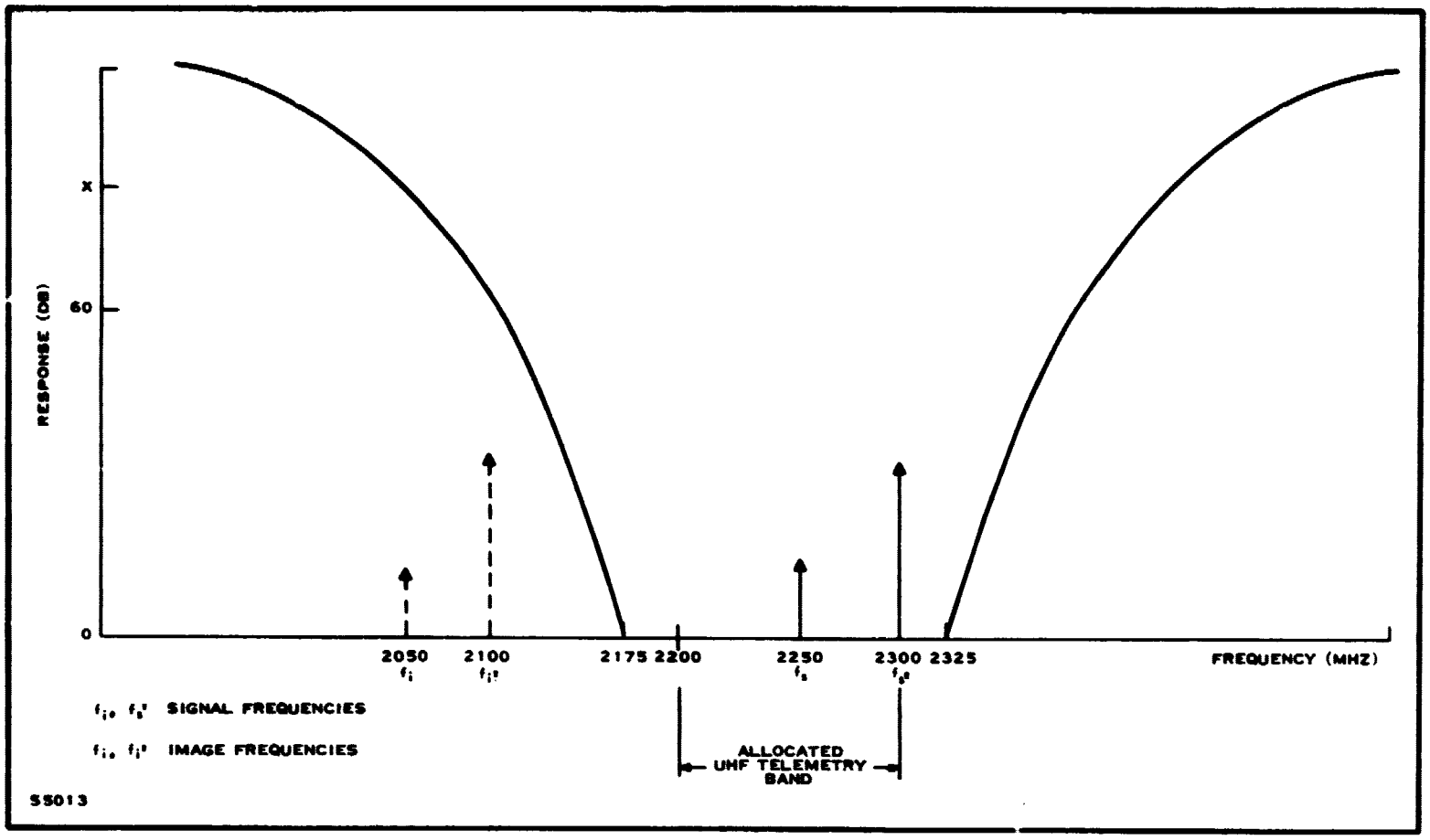

Figure 5. Selectivity Requirements For Semi-Fixed Tuning

$$f_X = f_S + \frac{f_{IF}}{2} \tag{65}$$

The seriousness of this product develops when its second harmonic combines with the second harmonic of the signal, and the difference frequency is produced. This is demonstrated as follows:

$$\begin{aligned} f &= 2f_X \pm 2f_S \\ &= 2\left[f_S + \frac{f_{IF}}{2}\right] \pm 2f_S \\ &= 2f_S + f_{IF} \pm 2f_S \end{aligned} \tag{66}$$

$$f = \begin{cases} 4f_S + f_{IF} \text{ (filtered)} \\ \\ f_{IF} \end{cases}$$

The higher frequency, $4f_S + f_{IF}$, can be neglected as it falls outside the if. passband.

Table 2. Intermodulation Products

f_S = signal frequency

f_o = local oscillator signal

Single Diode	Balanced Mixer	Double Balanced Mixer
f_S	f_S	
$2f_S$		
$3f_S$	$3f_S$	
$5f_S$	$5f_S$	
$6f_S$		
f_o		
$f_o \pm f_S$	$f_o \pm f_S$	$f_o \pm f_S$
$f_o \pm 2f_S$		
$f_o \pm 3f_S$	$f_o \pm 3f_S$	$f_o \pm 3f_S$
$f_o \pm 4f_S$		
$f_o \pm 5f_S$	$f_o \pm 5f_S$	$f_o \pm 5f_S$
$2f_o$		
$2f_o \pm f_S$	$2f_o \pm f_S$	
$2f_o \pm 3f_S$	$2f_o \pm 3f_S$	
$2f_o \pm 4f_S$		
$3f_o$		
$3f_o \pm f_S$	$3f_o \pm f_S$	$3f_o \pm f_S$
$3f_o \pm 2f_S$		
$3f_o \pm 3f_S$	$3f_o \pm 3f_S$	$3f_o \pm 3f_S$
$4f_o$		
$4f_o \pm f_S$	$4f_o \pm f_S$	
$4f_o \pm 2f_S$		
$5f_o$		
$5f_o \pm f_S$	$5f_o \pm f_S$	$5f_o \pm f_S$
$6f_o$		

5. Receiver Threshold

All FM receivers exhibit a threshold property, which has been extensively analyzed.[9] This threshold effect is not sharp and is dependent on the deviation ratio and the type of demodulator used. PCM/FM receivers are complicated in that two threshold conditions exist which must be satisfied. The first threshold establishes the value of the carrier-to-noise ratio required so that the output signal-to-noise ratio of the demodulator is improved over the input signal-to-noise ratio. The second threshold requirement determines the necessary or minimum output video signal to allow low error decoding of the recovered PCM wave train.

The improvement characteristic establishing the first threshold necessary for carrier detection results from the nonlinear property of the demodulator which exhibits a captive phenomenon in which the weakest of two signals is suppressed. Therefore, for large input carrier levels, noise is suppressed and the signal-to-noise ratio at the output of the demodulator, as compared to the input carrier-to-noise ratio, is improved.

When the input signal is decreased to a value such that impulsive character of noise is evident at the receiver output, the detector no longer exhibits a quieting effect and this improvement no longer exists. This occurs at the threshold value of carrier-to-noise ratio, $(CNR)_T$, which defines the ultimate receiver sensitivity. This is shown by

$$P_S\,(\text{dBm}) = P_N + (CNR)_T \tag{67}$$

where P_N is the noise power at the demodulator input terminals, and P_S is the necessary carrier level above the noise level to establish the carrier-to-noise ratio. The noise power at the detector terminals is

$$P_N = P_i + NF \tag{68}$$

where P_i, the receiver input noise, is defined as

$$P_i = -174\ \text{dBm} + 10 \log BW_{IF} \tag{69}$$

and NF is the receiver noise figure. Thus, the ultimate receiver sensitivity is given by

$$P_S\,(\text{dBm}) = -174\ \text{dBm} + 10 \log BW_{IF} + NF + (CNR)_T \tag{70}$$

The second threshold existing in PCM/FM receivers occurs after demodulation of the carrier. The resulting detected PCM modulation is applied to a decoder which recovers the analog signal by sampling the receiver output and deciding whether the baseband signal is a "0" digit or a "1" digit. As a consequence of noise in the receiver output, the decoder may decide incorrectly

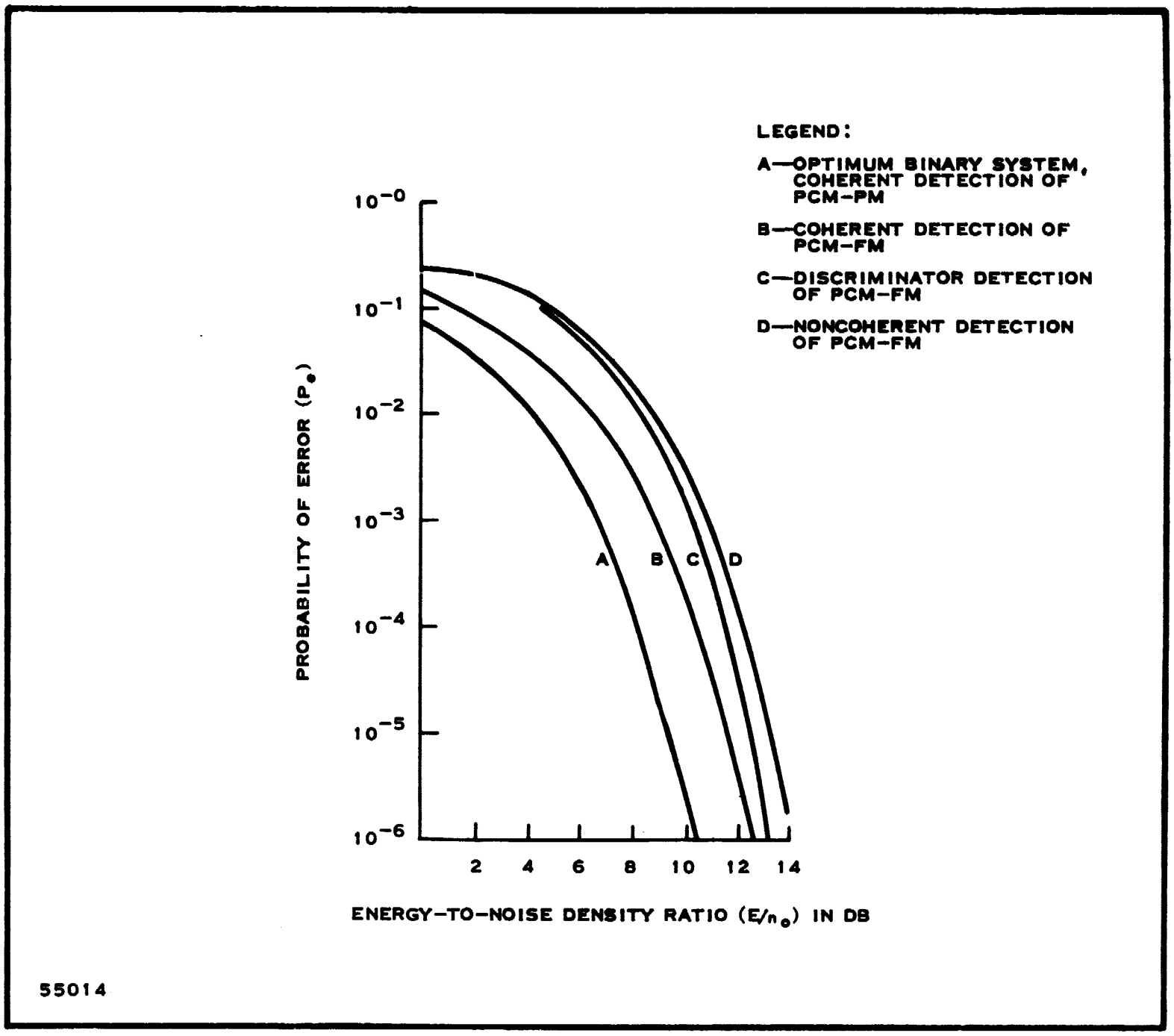

Figure 6. Probability Of Error

that a "0" digit or a "1" digit is present in the demodulated signal. In order to ensure a low probability that these errors occur, the demodulated signal must be sufficiently above the noise level in the receiver output. Thus, the minimum useful output signal after detection is one that satisfies this relation for any arbitrary error rate.

The error rate in various PCM/FM reception systems is shown in Figure 6. The error probability is plotted as a function of energy-to-noise density rather than signal-to-noise ratio to remove the bandwidth factor. However, these two parameters are the same when the predetection bandwidth equals the bit rate. Approximately one dB difference exists between PCM/FM detection using a conventional discriminator as compared to the error probability given for orthogonal binary signaling (PSK/FM).

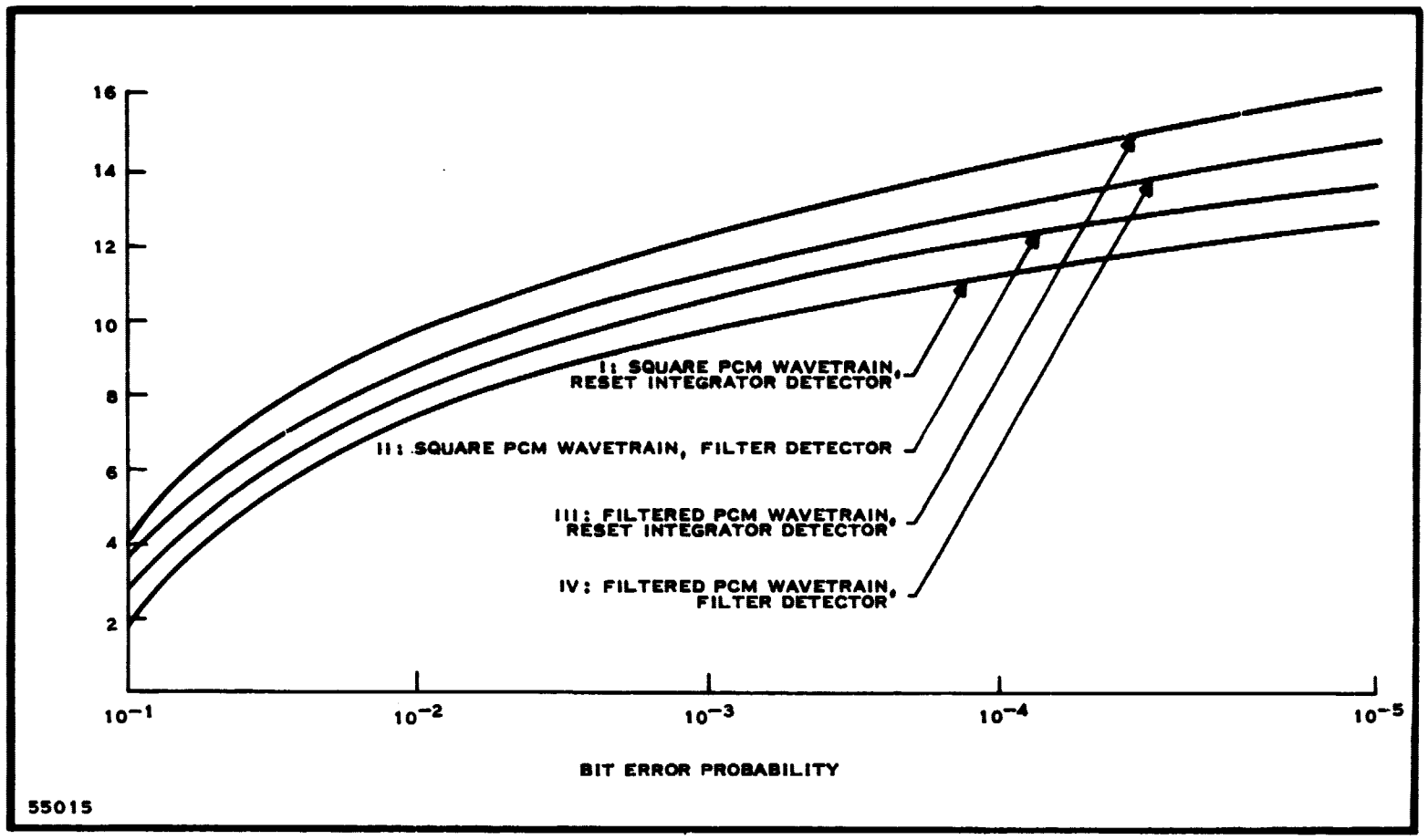

Figure 7. Bit Error Probability

If the signal level out of the PCM demodulator is not sufficiently higher than the noise level in the receiver output, the reconstructed analog signal will contain errors. The performance of this signal processing is usually specified by error rate as a function of the signal-to-noise ratio out of the PCM detector. A family of these curves is given in Figure 7 for various decoding techniques, and PCM waveform shapes.[10] The ordinate is peak signal voltage to rms noise voltage and must be corrected by subtracting 3 dB to obtain the rms signal-to-rms noise voltage at the demodulator output.

The plots given in Figure 7 are for Gaussian output noise and no dc offset in the detected PCM wavetrain and random modulating NRZ code. Curve I is for a matched filter, or reset integrator detector which has a noise bandwidth equal to one-half the bit rate. Curve II is shown for the case where the detected PCM waveform is a square waveform and a detector with a filtered response which has a 3 dB frequency equal to one-half the bit rate, and a noise bandwidth of 1.05/2 times the bit rate. Curve IV is for the same detector, but a premodulation filter is assumed with a 3 dB frequency at 0.75 times the bit rate. Curve III is the same as Curve I, but an identical premodulation filter identical to the above is assumed. Assume that the receiver output will be applied to a reset-integrator. Curve III specifies

the demodulator performance desired. Hence, for a 10^{-4} assumed bit error rate a 15 dB signal-to-noise ratio out of the detector is required as shown by Curve III. Correcting for an rms signal, this corresponds to a signal-to-noise ratio of 12 dB.

6. Summary

The system performance specifications were earlier defined in Section I and in this section the basic considerations that must be given to selecting and designing a system to satisfy these requirements were outlined. The requirements that a receiver configuration must meet to provide the desired performance listed in Table 1 under the constraints mentioned in this section are summarized in Table 3.

Table 3. Receiver Performance Requirements

Selectivity	2200 to 2300 MHz
Operating frequency	2250 MHz
Output signal	NRZ
Sensitivity	−110 dBm
Bandwidth: Predetection	2.04 MHz
Postdetection	600 kHz
Noise figure	5 dB
Dynamic range	50 dB
Image rejection	> 60 dB
Spurious rejection	50 dB
Output signal-to-noise ratio	12 dB
Threshold bit error rate	1×10^{-4}

D. SYSTEM DEVELOPMENT

In the preceding sections, the performance requirements for a UHF telemetry receiver were defined and some basic considerations which these requirements imply were briefly reviewed. The task now at hand is the development of a configuration of black boxes that best meet the implementation needs and the determination of whether or not the defined specifications can be met. The performance requirements will be determined to be either satisfiable or unsatisfiable; and if they can be satisfied, in what manner.

Before any approach to this problem is undertaken, what is implied as best needs clarification. In the following system development, the best system is defined as a system built with high reliability using current

state-of-the-art components and without undue complexity. With this definition of the best receiver configuration, the implementation of a system is best analyzed in terms of individual functional stages required to satisfy the amplification and detection requirements of the total system. One analytical approach to determine the necessary individual "black boxes" is with a trade study.

1. Introduction to Trade Study Analysis

The trade study technique used in developing a receiver system to meet the parameters listed in Table 2 need some introduction. This technique was believed to be the most appropriate analytical tool to develop a receiver which could satisfy the demanded performance. By contrast, an approach that singly weighs the advantages and disadvantages of all presently known receiver configurations would only result in a comparative analysis of the systems.

A trade study analysis begins by first grouping likely devices capable of achieving amplification, detection and frequency conversion at the receiver input and then compares each device separately with its ability to meet the performance requirements. Then based on the constraints and limitations imposed on each process by the performance requirements, each device is either deleted or retained for further examination. The process is repeated with a second group of devices that are combined with the devices remaining after the first round evaluation. Finally, one or more probable systems may result in the final evaluation which satisfies the total system needs. This method is illustrated in the following subparagraphs.

2. Trade Study of RF Stages

Three possible processes may occur at the receiver input to enhance detection of the PCM baseband signal—amplification, demodulation, and frequency conversion. Each process and the individual functional black boxes which could be performed is shown in Figure 8. The ability of each process to meet the system parameters outlined in Table 2 is considered in the following analysis.

a. Amplification

Four basic devices used in modern communication receivers to achieve low-noise microwave amplification are:

State-of-the-art high frequency transistors

Tunnel diode amplifiers

Parametric amplifiers

TWT amplifiers.

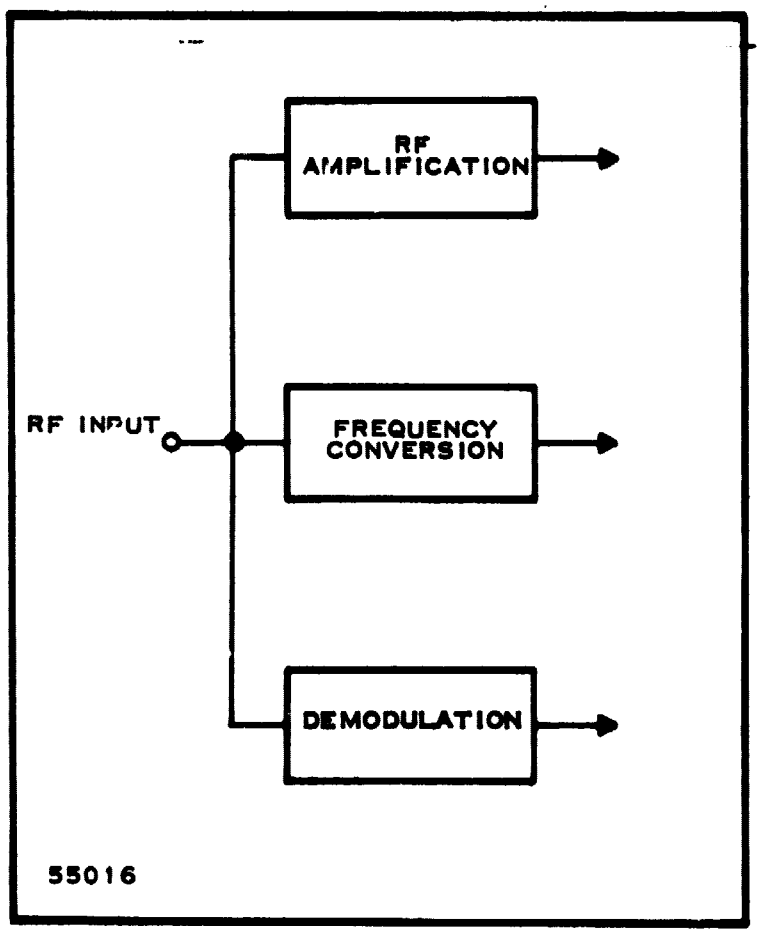

Figure 8. Possible Receiver Operations

The size and weight of TWT amplifiers are not compatible with the system packaging and power requirements and may be eliminated from further consideration. The remaining three amplifiers need further investigation of their ability to satisfy the system 4- to 6-dB noise-figure requirement and dynamic range in addition to the feasibility of their use in a totally-integrated circuit receiver.

(1) Microwave Transistor RF Amplifiers

The low-noise properties of microwave transistors were reported in Scientific Report No. 4. It was shown that current state-of-the-art transistors have typical noise figures ranging from 4.5 to 5.0 dB at 2.0 GHz and maximum power gains of 9.0 dB for germanium devices (TIMX105) to 20 dB for silicon (L-83). In Section III-C it was shown that the noise figure of a receiver is determined primarily by its first few stages and that a low-noise figure can be achieved with low-noise devices exhibiting large gain. The L-83 device is a reasonable choice to satisfy the need of an RF amplifier in a low-noise receiver.

Designing the first stage for its best noise figure would require transforming the 50-ohm source impedance to an optimum noise resistance. Assuming a minimum insertion loss of 0.5 dB for this network, the first-stage noise figure is given

$$NF = 10 \log \left[L + L (F_2 - 1) \right] \tag{71}$$

where L is the insertion loss of the matching network, and F_2 is the noise factor of the transistor. Assuming production transistors with a maximum noise figure of 5.0 dB (noise factor 3.162), the resulting noise figure is

$$NF = 10 \log \left[1.122 + 1.122 (3.162 - 1) \right] \tag{72}$$

$$NF = 5.5 \text{ dB} \tag{73}$$

This noise figure is within the requirements, assuming the losses in the matching network over the 2200- to 2300-MHz frequency band do not exceed 0.5 dB. The transistor input stage could satisfy the 50-dB dynamic range required of the receiver by the use of AGC in the final design analysis, if it is shown to be needed.

(2) Tunnel Diode RF Amplifier

Microwave tunnel-diode amplifiers generally have noise figures in the 3- to 5-dB range and power gains of about 15 dB. The dynamic range of these amplifiers is normally less than 70 dB, but this is sufficient to meet the needs of the receiver.

The microwave tunnel diode is a reflection amplifier whose gain is dependent on the reflection coefficient it sees. At high gain, a small change in reflection coefficient results in an unfavorable impedance being presented to the tunnel diode and causes it to go into oscillation. Therefore, stability is of major concern and methods of stabilization must necessarily be considered in the design of a tunnel-diode preamplifier. In practical tunnel-diode microwave amplifiers, matching the tunnel diode to its source and load is normally accomplished by the use of ferrite circulators. Three-port or Y-junction microstrip circulators have been reported in Scientific Report No. 4, and recently an article on an integrated microwave tunnel-diode amplifier was published.[11] Thus, construction of an integrated preamplifier to meet the noise performance and size requirements of the desired receiver system is feasible. However, the circulator requires an external magnet whose weight and power requirements could offset the advantages of light weight, compactness, and low noise.

(3) Parametric Amplifiers

Uncooled parametric amplifiers offer another source of microwave amplification with low-noise performance excelling that of tunnel-diode amplifiers. However, a secondary frequency source is required to supply the "pump" frequency necessary for operation of the amplifier. The pump frequency is usually greater than twice the frequency of the input signal, and as in the tunnel-diode amplifier, ferrite circulator-coupling is required.

The tunnel-diode preamplifiers and parametric amplifiers best meet the low-noise receiver requirement as compared to microwave transistors. The use of tunnel-diode and parametric amplifiers has been the common practice for achieving low-noise systems. However, these amplifiers are complicated by their need for circulators and therefore, are not ideally suited for integrated systems. The requirements of compactness and unneeded complexity which define the best system are not met by the tunnel-diode amplifier and parametric amplifiers. Therefore, even though the transistor has a 5.5 dB noise figure compared to a 3 to 5 dB noise figure available with other amplifiers, it is the best choice as the first stage in an integrated receiver.

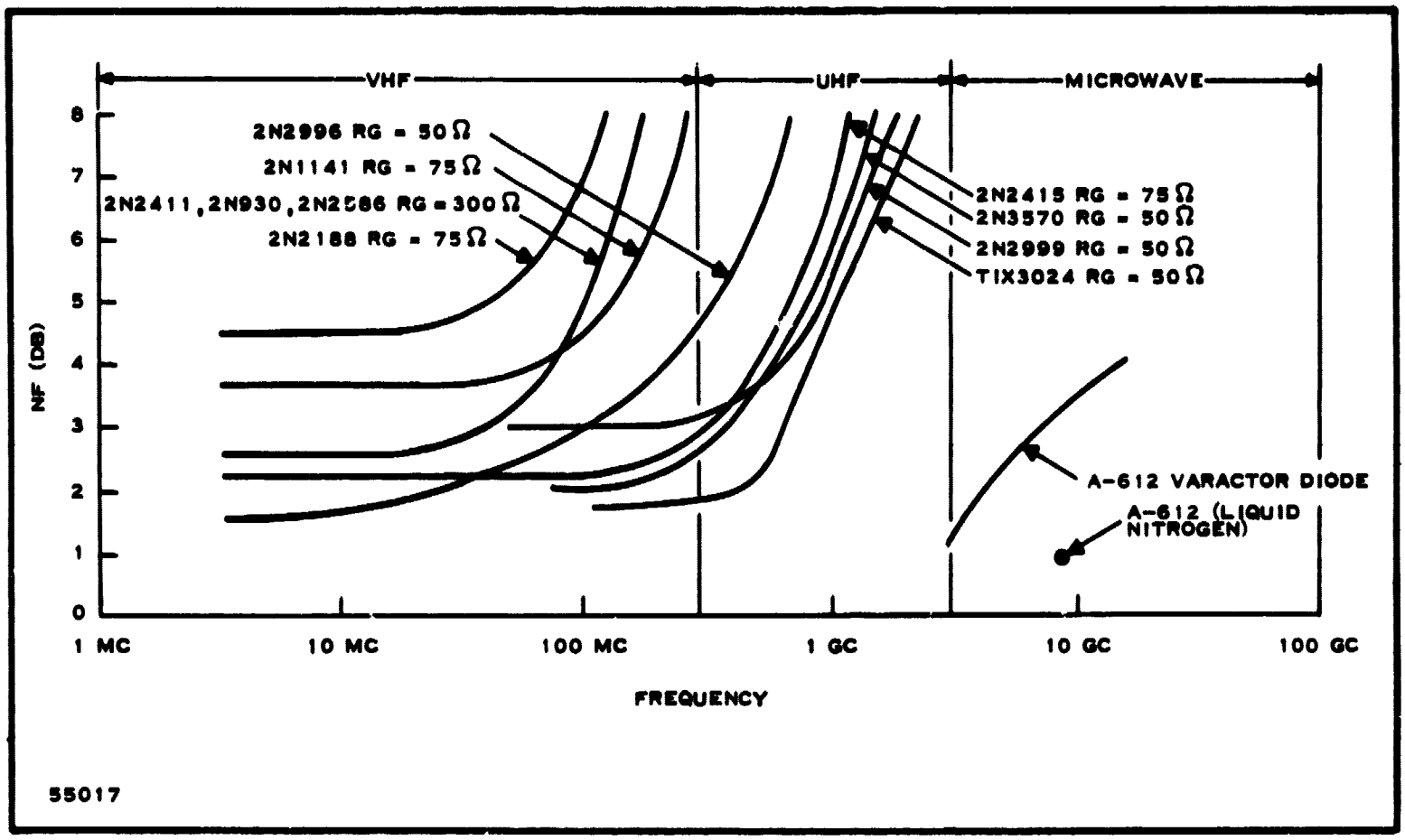

Figure 9. Transistor Noise Performance

b. Frequency Conversion

Frequency conversion is shown in Figure 8 as a possible operation that may be performed on the input signal. It offers the advantage that subsequent amplification or detection may be carried out at lower frequencies where gains and component performance are markedly better. Several types of devices offer conversion from microwave frequencies to desirable difference frequencies. Among these devices, are Schottky-barrier mixer diodes, and parametric converters utilizing tunnel diodes and varactor diodes.

The use of a frequency conversion process as the first stage will result in translating the received signal frequency to a lower frequency. In the past, low-sensitivity requirements in telemetry receivers were satisfied by converting the input signal to 30 to 60 MHz when devices with low-noise characteristics were available. As may be seen in Figure 9, currently available devices have 1.5- to 2.0-dB noise figures extending to several hundred megahertz. Typical noise figures of germanium VHF transistors do not exceed 2.0 dB; therefore, mixing the input signal to obtain a 100-MHz difference frequency is not unreasonable in modern, low-noise telemetry receivers.

If a 100-MHz intermediate frequency is assumed for the system, the effects of spurious signals may be investigated. The use of

frequency conversion in a receiver has the disadvantage that the receiver will respond to signal frequencies other than those desired. The nonlinear property of the mixer which is essential to accomplishing frequency conversion causes harmonics of the input signal and local oscillator to produce spurious intermodulation products. The receiver will respond to these products when the following equation is satisfied;

$$f_S = \frac{mf_{LO} \pm f_{IF}}{n} \tag{74}$$

where m, n are harmonic integers,

and f_{LO} = frequency of local oscillator

f_{IF} = intermediate frequency

f_S = frequency of incoming signal.

When m and n are one, the above equation defines the desired signal and the image frequency. The image frequency may be rejected by the mixer, and the selectivity provided by the preselector preceding the mixer. In balanced mixers, intermodulation products defined by other values of m and n may be reduced to 70 dB or more. In addition, this configuration also cancels local oscillator noise and prevents increasing the noise power within the receiver passband.

The most troublesome spurious signal involves that separated from the local oscillator frequency by submultiples of the if. This interfering signal is given by

$$f = f_{LO} \pm \frac{f_{IF}}{P} \tag{75}$$

The strongest response of this type is separated from the desired signal by one-half the intermediate frequency,

$$f = f_S \pm \frac{f_{IF}}{2} \tag{76}$$

In the case of a receiver employing a 100-MHz i.f., this interference signal is separated ± 50 MHz from the carrier. For a receiver operating at 2250 MHz employing a broad RF passband from 2200 to 2300 MHz, this interference occurs at 2300 MHz and passes unattenuated to the first stage.

The spurious signals produced at the output of the frequency converter when these two signals are present are

$$f_{LO} \pm (2f_1 - f_2) \qquad (77)$$

$$f_{LO} \pm (3f_1 - 2f_2)$$

$$f_{LO} \pm (2f_2 - f_1) \qquad (78)$$

$$f_{LO} \pm (3f_2 - 2f_1)$$

The resulting frequencies which fall near an if. passband centered at 100 MHz are 50 MHz, 200 MHz and 250 MHz.

If a frequency converter or mixer is to be used as the first stage in a microwave receiver, it must have low-noise performance. The noise figure of a mixer is given by

$$NF = 10 \log L_m [t_m + (F_{IF} - 1)] \qquad (79)$$

where L_m = effective mixer conversion loss

t_m = effective mixer noise temperature

F_{IF} = noise factor of IF amplifier.

The effective conversion loss of L_m of a mixer is an influencing factor in achieving low-noise figures. This loss is a function of the design of the mixer. The lowest conversion loss is obtained when the mixer is designed so that the image frequency is terminated into an open circuit. Theoretically, in this case, with an ideal diode, the conversion loss is 0 dB.

The conversion loss for an open-image terminated mixer was defined by Strum as;

$$L = \frac{(1 - \gamma_n^2)(1 + \gamma_{2n})}{\gamma_n^2 (1 - \gamma_{2n})} \left\{ \left[1 + \sqrt{\frac{1 - \gamma_n^2 (1 - \gamma_{2n})^2}{(1 - \gamma_n^2)(1 - \gamma_{2n})}} \right]^2 \right\} \qquad (80)$$

where γ_n and γ_{2n} is a mathematical relation of the diode static characteristics as given by

$$\gamma_n = \frac{\left[\frac{X-1}{2} ! \right]^2}{\frac{X}{2} ! \; \frac{X-2}{2} ! + \gamma_b} \qquad (81)$$

and

$$\gamma_{2n} \frac{\left[\frac{X-1}{2}!\right]}{\frac{X+1}{2}! \; \frac{X+3}{2}!} + \gamma_b, \tag{82}$$

where γ_b = relates the reverse bias effects, and in a proper design equals zero

X = the slope of the diode log-log static characteristics.

The solutions to the above equations are given in the appendix for a typical gallium-arsenide (GaAs) diode with the static characteristics shown in Figure 10. For an IF amplifier with a 1.5 dB noise figure and the static characteristics shown, the conversion loss is 1.75. The noise temperature of an open-image terminated mixer is given by

$$t_m = \frac{1}{L_m} \left[t_d (L_m - 1) + 1 \right] \tag{83}$$

where t_d is the diode noise temperature, which is approximately 0.5 for a Schottky-Barrier diode. Thus, the noise figure of a mixer is

$$NF = 3.2 \text{ dB} \tag{84}$$

Therefore, the possibility of achieving low-noise performance in a mixer is seen, and the feasibility of using a mixer as the first stage of a microwave receiver on the basis of achieving a low overall receiver-noise figure is realized. This concept is verified by Barber,[13] who has shown that high frequency gallium-arsenide diodes with open-image termination may have 3 dB noise figures and by Rafuse,[11] who has reported construction of balanced mixers at S-band with 2.0 dB noise figures.

c. Demodulation

Ideally, immediate detection of the received signal would be desirable from the standpoint of receiver mechanization. This would result in circuit simplicity and undoubtedly a very compact receiver.

In Scientific Report No. 3, construction of an S-band discriminator using a phase-interference principle was shown to be possible. In addition, feedback demodulators, operating at microwave frequencies, in which an oscillator can be made to track the input signal, can also be built.

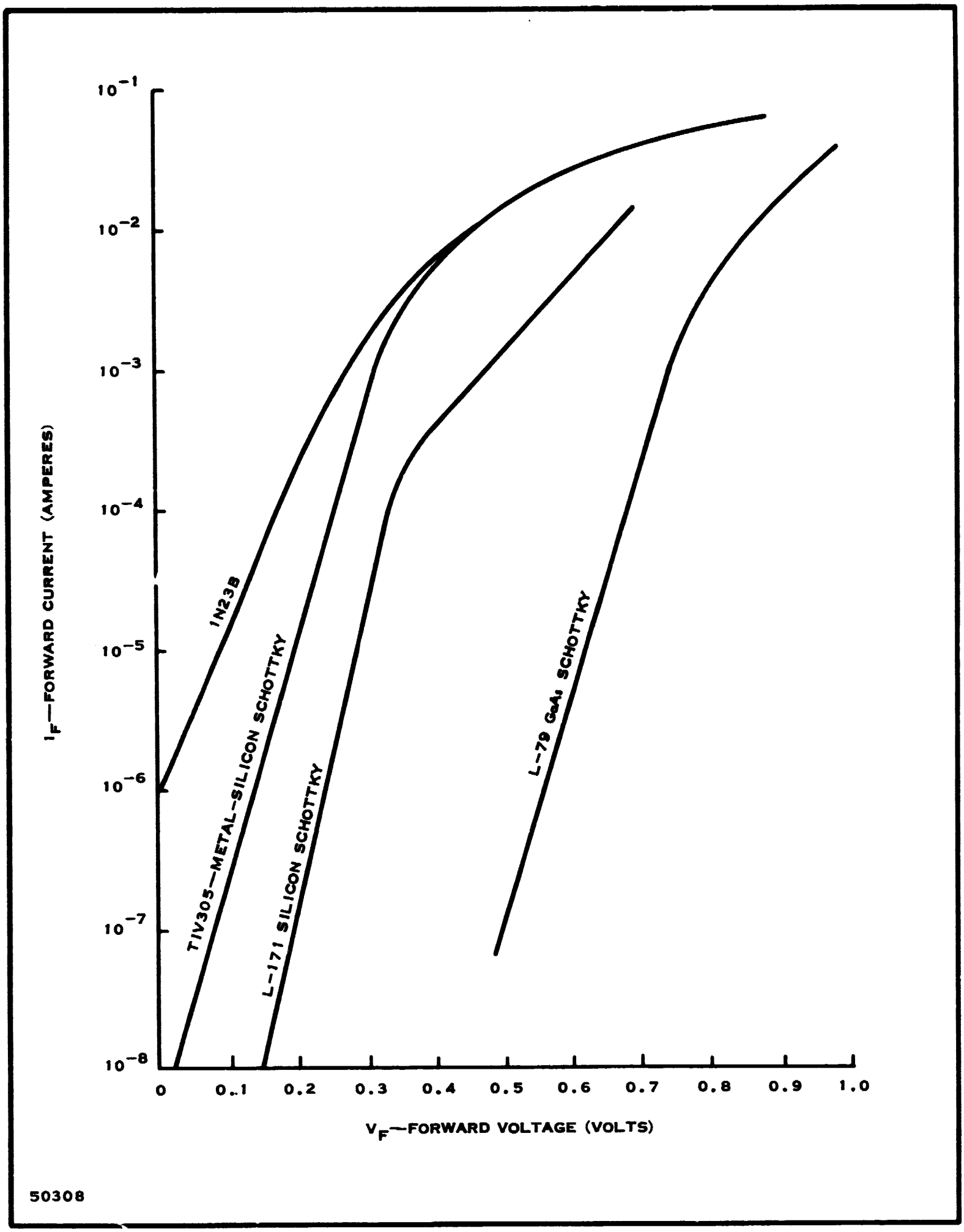

Figure 10. Forward Response of Mixer Diodes

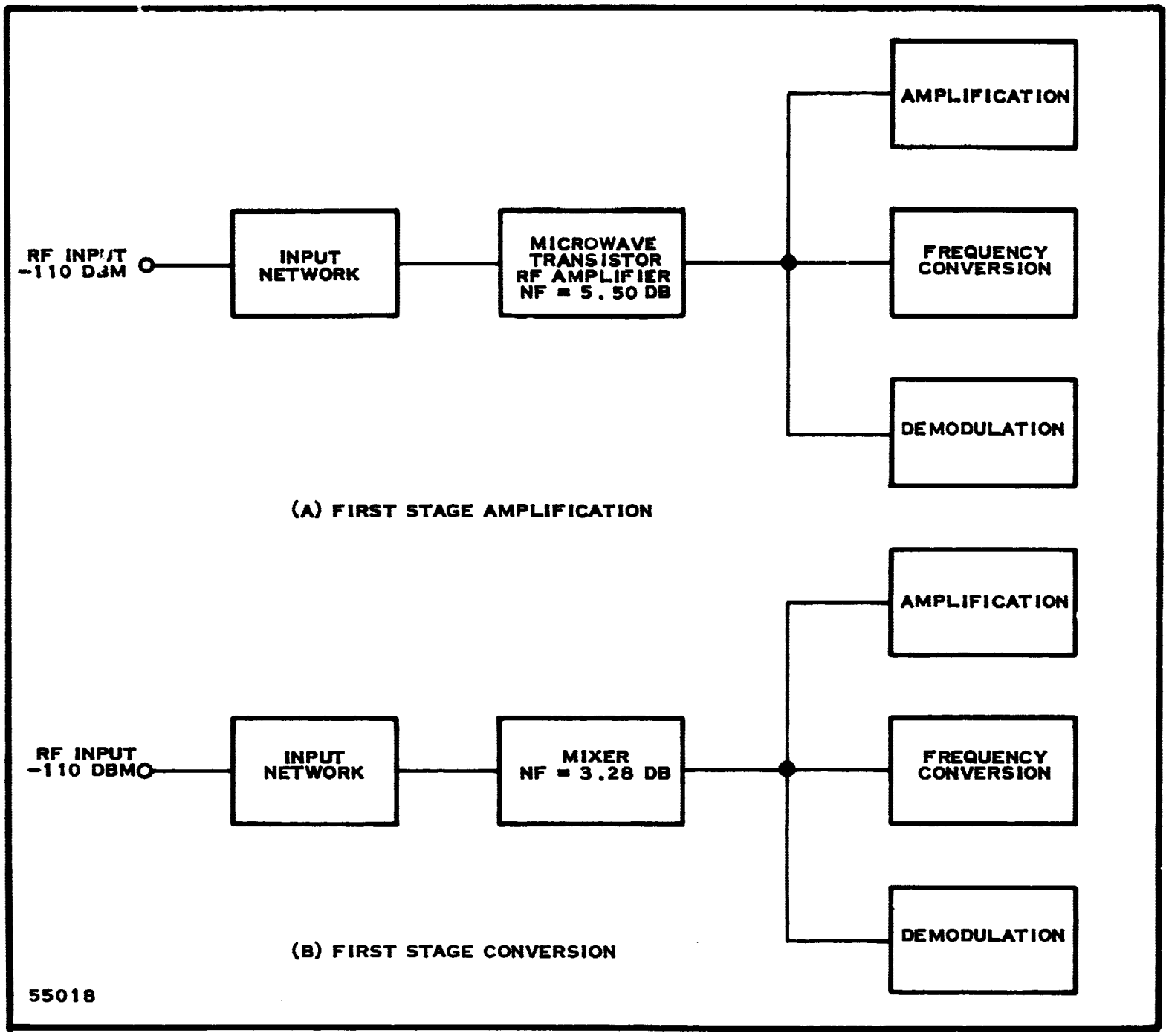

Figure 11. Possible Receiver RF Stages

However, both types of demodulators require RF filtering preceding their input terminals to shape the system noise to an acceptable level. The bandwidth required for the particular system studied is 2.04 MHz. Therefore, the use of either demodulator requires that the first input stage of the receiver be an RF filter with a 2.04-MHz passband. This configuration is not compatible with fixed-tuning operation as the demodulator would need redesign for each frequency within the 2200- to 2300-MHz operating range.

d. Results of Tradeoff Analysis of RF Stages

The above evaluation of three possible operations—amplification, frequency conversion and demodulation—which can be performed at the receiver input indicates that amplification or conversion is feasible. Either of these

processes, shown in Figure 11, satisfies the system noise-figure requirements and permits integrated fabrication. Intermediate stages to incorporate either of these input operations into a final receiver configuration capable of meeting the requirements of Table 3 remain to be determined.

3. Trade Study of Intermediate Stages

In the preceding paragraph it was shown that either a frequency converter or RF amplifier could be used as the first stage in a low-noise microwave receiver. Feasible intermediate stages following either input stage that meet the desired receiver performance are evaluated in the following subparagraphs.

a. Intermediate Processes Following the RF Amplifier

Figure 11 shows that frequency conversion, demodulation, or amplification can follow the first stage amplifier. To determine the feasibility of employing any one of these techniques in a receiver configuration, the following must be considered.

(1) Amplification

Several stages of RF gain may be required to satisfy the signal level demanded by subsequent stages. For such a case, the resulting noise figure for cascading two RF amplifiers is given by

$$NF = 10 \log \left[L + L(F_1 - 1) + \frac{L(F_2 - 1)}{G_1} \right] \qquad (85)$$

where L is the insertion loss of the input network, F_1 and F_2 are the noise factors of the respective amplifiers, and G_1 is the power gain of the first stage. The best compromise between gain and low noise is a low-noise germanium transistor, such as the TIMX106, followed by a silicon device (L-83). Using these devices the amplifier parameters are

$$L = 0.5 \text{ dB } (1.122)$$
$$F_1 = 4.5 \text{ dB } (2.82)$$
$$G_1 = 5.0 \text{ dB } (3.162)$$
$$F_2 = 5.0 \text{ dB } (3.162)$$
$$G_2 = 20 \text{ dB}$$

$$NF = 10 \log \left[1.122 + 1.122\ (1.82) + \frac{1.122\ (2.162)}{3.162} \right] \qquad (86)$$

$$NF = 5.94\ dB\ . \tag{87}$$

The resulting power gain is:

$$G = G_1 + G_2$$

$$G = 25\ dB \tag{88}$$

Thus, cascading RF stages provide 25 dB of power gain, but if higher losses occur in the input network of if the noise property of the following device degrades the above noise figure by 0.1 dB, the noise figure will not meet the system requirement of a 6.0 dB noise figure.

(2) Frequency Conversion

The use of a mixer after the first stage amplifier permits conversion to a lower frequency prior to demodulation. Thus, making it much easier to obtain the predetection bandwidth without the use of highly selective microwave circuits. In addition, necessary receiver gain is more attainable.

The noise figure of a cascaded high gain RF amplifier and mixer is given by Equation (85). Assuming that an L-83 silicon transistor is used in the first stage amplifier, and F_2 is the noise factor of the mixer, using a 3-dB noise figure for the mixer ($F_2 = 1.995$) and a transducer gain of 10 dB for the first stage would yield the following noise figure

$$NF = 10 \log \left[1.122 + \frac{(3.162-1)}{0.8913} + \frac{(1.995-1)}{(0.891)(10)} \right] \tag{89}$$

$$= 10 \log \left[3.65 \right]$$

$$NF = 5.62\ dB.$$

If a germanium device, which has a 4.5-dB noise figure and a power gain of 5.0 dB, was used as the first stage amplifier, the noise figure for the cascaded configuration is

$$NF = 10 \log \left[1.122 + \frac{1.82}{0.8913} + \frac{(0.995)}{(0.891)\,3.162} \right] \tag{90}$$

$$NF = 5.49 dB$$

As can be expected, the lowest noise figure for the front-end is achieved with an RF amplifier using a germanium transistor, although the RF gain is much less.

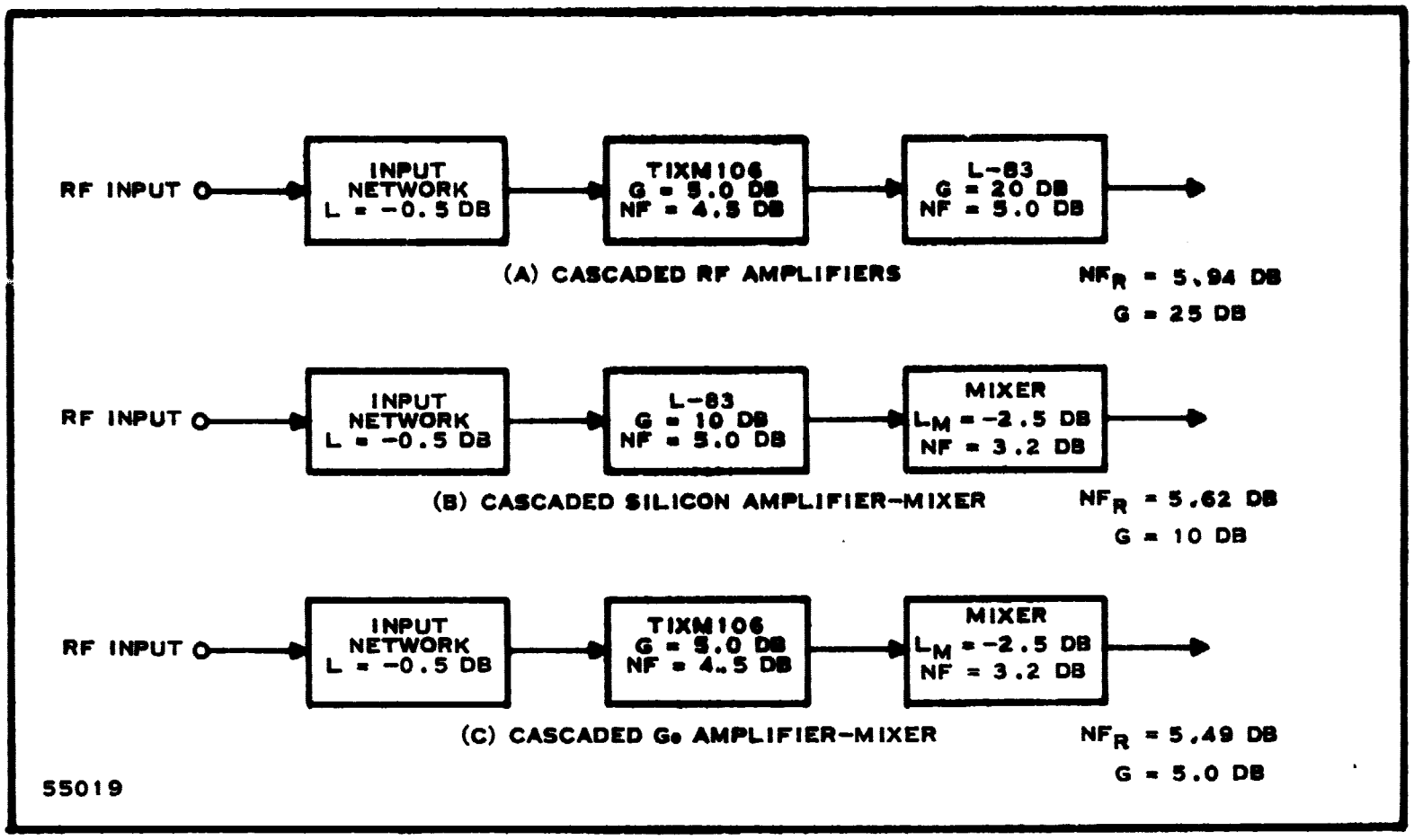

Figure 12. RF Amplifier Intermediate Stages

The gain and noise characteristics of the three configurations discussed above are summarized in Figure 12 where a 2.5-dB conversion loss is implied by the use of a 3-dB mixer.

(3) Demodulation

The efficiency with which any demodulation process may be carried out is primarily determined by the signal-to-noise ratio presented to the input of the demodulator. The amount of noise combining with the input signal to establish this ratio is determined by the bandwidth of the receiver passband response. The minimum allowable passband of this response is determined by the bandwidth required to recover the transmitted information without distortion. This is defined as the receiver predetection-bandwidth requirement. In Table 2, this requirement was listed as 2.04 MHz. Thus, giving consideration to band-limiting,the internal receiver noise requires that the demodulator must be preceded by a 2.04-MHz passband filter to achieve a favorable input signal-to-noise ratio for detection. Provision for a 2.04-MHz bandwidth centered at 2250 MHz requires the use of extremely high Q circuits. The value of Q required may be approximated by

$$Q = \frac{f_o}{\Delta f} \qquad (91)$$

where f_o is the received frequency (2250 MHz) and Δf is the 3-dB predetection bandwidth. Hence

$$Q = \frac{2250 \text{ MHz}}{2.04 \text{ MHz}}$$

$$Q \sim 1125 \tag{92}$$

Obtaining such a magnitude of Q at S-band would require the use of a cavity. The size and weight of an S-band cavity are prohibitive for a receiver where compactness is desirable.

b. Intermediate Processes Following the Input Mixer

In Figure 11, only frequency conversion or demodulation may occur after the first-stage mixer. Amplification may be omitted from consideration since the use of a low-noise mixer implies that the following stage is an amplifier. Conventionally, this is the intermediate amplifier, and the noise figure obtained for the mixer is related to the noise performance of this stage. This is seen by recalling that the mixer noise figure was defined as:

$$NF = 10 \log L_m \left[t_m + (F_{IF} - 1) \right] \tag{93}$$

where F_{IF} is the noise factor of the amplifier following the mixer.

(1) Frequency Conversion

Following the first mixer with a second frequency conversion will result in double conversion with the disadvantage that additional spurious signals are introduced. The major advantage gained by this configuration is that spurious signals present at the receiver input are more easily isolated from the predetection passband.

Double conversion also permits demodulation to take place at lower frequencies. This is not an advantage since at lower frequencies capacitors and inductors become larger and compact circuitry is difficult to achieve. Current transistors and FET's offer satisfactory high-frequency performance and overshadow the need of utilizing lower frequencies with the corresponding additional spurious signals.

(2) Demodulation

The local oscillator frequency applied to the first-stage mixer (Figure 11) can be selected so that an intermediate frequency results which permits the predetection bandwidth to be achieved without

the use of excessive Q's. Therefore, demodulation can be readily accomplished after the first-stage mixer. Before the constraints that the system parameters place on demodulation can be considered, various reception techniques need review. This review is in the following paragraph in order that the threshold requirements of various demodulators may be investigated to determine whether the system sensitivity and requirement can be met.

c. Reception Techniques

Demodulation must provide the recovery of the PCM format while simultaneously satisfying the system noise and sensitivity requirements. These requirements must be met for a system whose information bandwidth is 600 kHz. To determine applicable demodulators that may meet the above requirements, the following detection devices are considered.

(1) Discriminators

A conventional discriminator such as a pulse-counting, Foster-Seely, or Travis design closely approaches the characteristics of an ideal frequency detector and gives an output voltage proportional to the instantaneous input frequency. When any frequency demodulator is operating well above its threshold, the output signal-to-noise ratio $(SNR)_o$ is linearly related to the input signal-to-noise ratio. This is shown by

$$(S/N)_o = \frac{3}{2}\left(\frac{f_d}{f_m}\right)^2 \frac{BW_{IF}}{f_m} \frac{C}{N} \qquad (94)$$

where f_d is the peak frequency deviation

f_m is the maximum baseband frequency

BW_{IF} is the 3 dB predetection bandwidth

C/N is the input carrier-to-noise power ratio.

The output signal-to-noise ratio of a frequency discriminator is improved over the input signal-to-noise ratio in proportion to the carrier deviation and ratio of predetection to baseband bandwidths. The term,

$$\frac{3}{2}\left(\frac{f_d}{f_m}\right)^2 \frac{BW_{IF}}{f_m}$$

is commonly referred to as the wideband improvement factor. However, as the input signal-to-noise ratio at the discriminator input is decreased, it eventually reaches a value at which improvement over the input signal-to-noise is nonexistent. This level of input signal-to-noise ratio defines the

threshold, $(CNR)_T$ which is customarily defined to occur when the average carrier power is equal to four times the rms noise power at the demodulator input terminals. Thus

$$(CNR)_T = \frac{A^2}{2\sigma^2} = 4 \tag{95}$$

or

$$(CNR)_T = 9.0 \text{ dB.}$$

In most cases of FM reception, a bandpass limiter precedes the discriminator. Thus, the input signal is clipped in amplitude which results in spreading the spectrum of the received signal about its harmonic frequencies. The noise spectrum in the predetection passband is similarly spread in the frequency domain, and the recovered signal and noise within the limiter passband is related differently at the output as compared to its signal-to-noise ratio at the input. Davenport has analyzed the signal and noise relationship of bandpass limiters and reports suppression of the weakest of the two signals will occur. This suppression is demonstrated in Figure 13 which plots the relation

$$\left(\frac{S_o}{N_o}\right) = k \frac{A^2}{N_{in}} \tag{96}$$

where S_o is the power in the output signal component, N_o is the remaining amount of output noise and k is a constant defined in the interval $\pi/4 < k < 0.2$. The lower limit being approached for very low input signal-to-noise ratios, the upper limit is approached for very high ratios.

(2) Frequency Locked Demodulator

The technique of reducing the signal deviation is one of the design objectives in the frequency-lock demodulator or frequency modulation feedback demodulator (FMFB). The block diagram of the FMFB is shown in Figure 14, where the modulated signal is shown to be tracked with a replica of the actual modulation. If tracking is reasonably close, the result is an FM signal with reduced deviation. The if. signal can now be processed by an FM demodulator that is preceded by a much narrower bandwidth than originally required. The FMFB demodulator then exhibits a threshold reduction over the original demodulator in proportion to the reduction in noise bandwidths between the closed loop predetection passband and the open loop predetection passband.

A limitation to achieving threshold reduction with this technique, recognized by early investigators is that in the presence of input noise, the tracking signal contains a noise component that leads to a second threshold mechanism. This second threshold is distinct from the

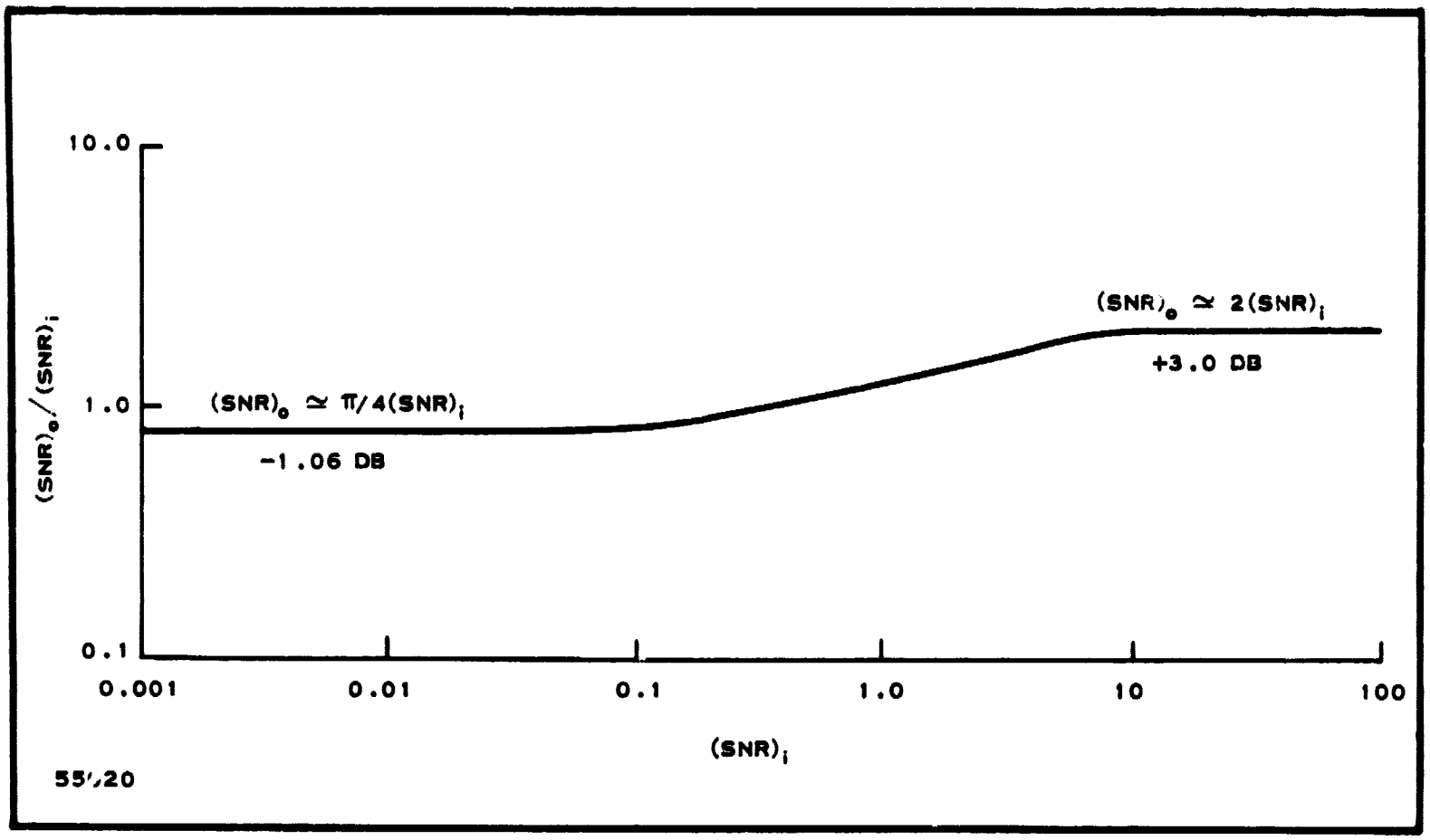

Figure 13. SNR Performance Of An Ideal Bandpass Limiter

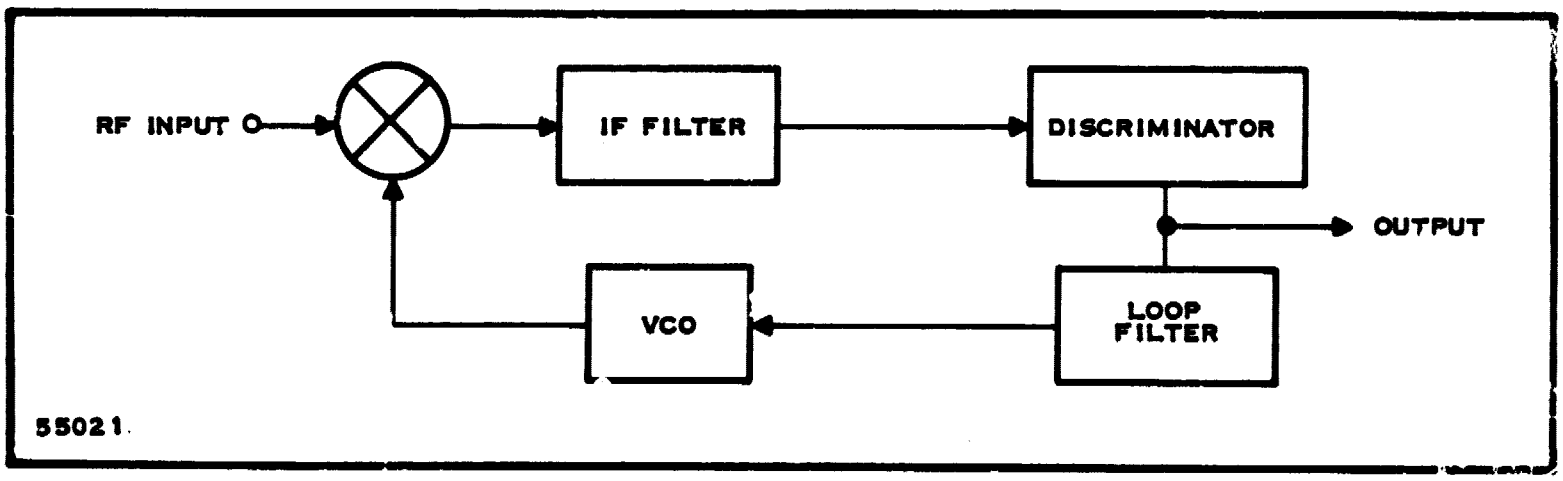

Figure 14. Block Diagram of FMFB Demodulator

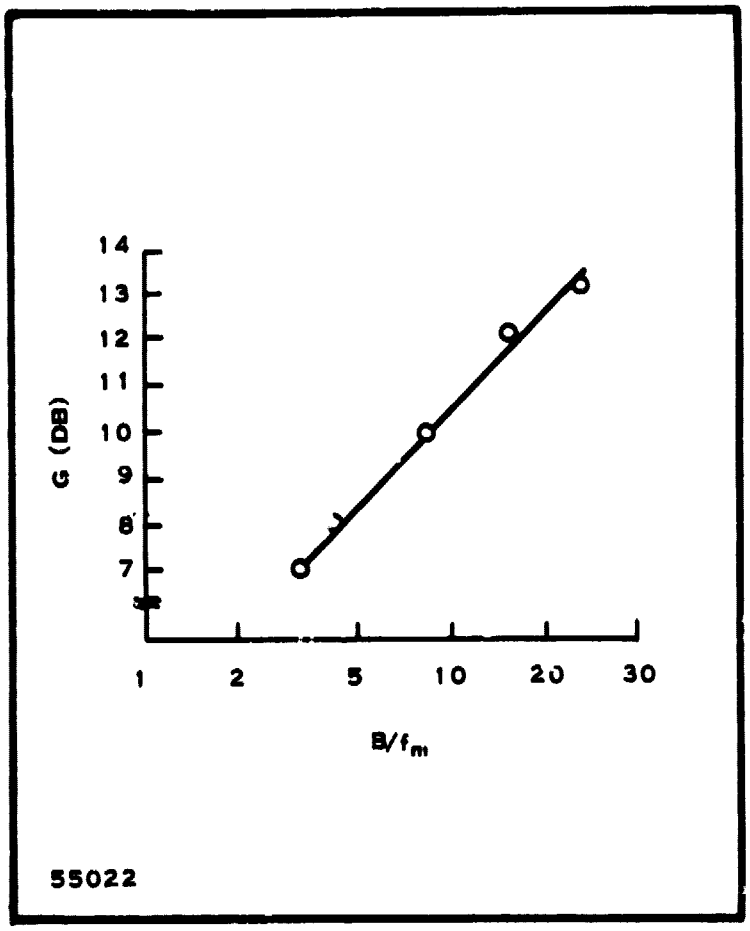

Figure 15. Variation of G With Bandwidth Ratio

threshold requirements of the discriminator used as the detector, and leads to a lower output SNR than predicated for the closed loop demodulator. Designing the demodulator for threshold reduction requires that both threshold mechanisms coincide at the same level of input carrier power. This is accomplished by controlling closed-loop response of the demodulator thus controlling the amount of noise fed back to the VCO.

The closed-loop bandwidth of the FMFB demodulator is given by

$$B = 2\left[f_m + \frac{f_d}{1 + G}\right] \qquad (97)$$

where

f_m = highest baseband modulating frequency

f_d = peak frequency deviation of carrier

$1 + G$ = feedback factor.

The feedback factor, 1 + G, plotted against the ratio of predetection-noise bandwidth to baseband-filter cutout frequency given by Hertzman[14] is shown in Figure 15. This bandwidth ratio for the system being studied is B/f_m = 2.04 MHz/600 kHz = 3.4. Then, using this curve, the feedback factor is roughly 7 dB (5.0) and the closed-loop bandwidth is

$$B = 2\left[600\ \text{kHz} + \frac{420}{5}\ \text{kHz}\right] \qquad (98)$$

$$B \sim 1.37\ \text{MHz}.$$

It has been shown by Spilker[16] that for deviation ratios less than unity that the FMFB demodulator does not provide a threshold reduction over that of conventional discriminators. His results are shown in Figure 16, where it is seen that only for deviation ratios greater than unity is threshold signal-to-noise ratio $(CNR)_T$ decreased.

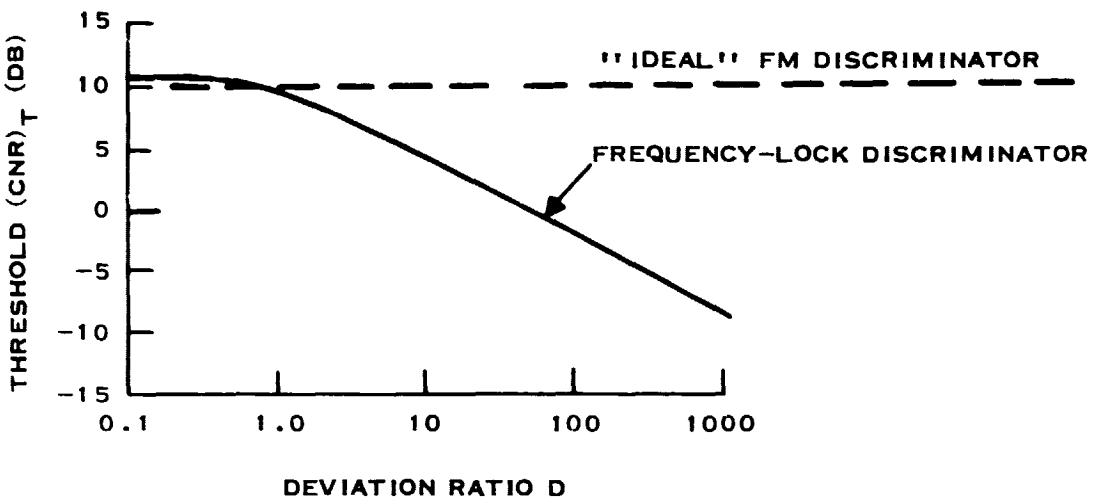

Figure 16. Threshold $(CNR)_T$ As A Function Of Deviation Ratio For The Frequency-Lock Discriminator

The overall system sensitivity employing a FMFB is limited only by its noise figure as shown by use of the following equation,

$$P_S = -174 \text{ dBm} + 10 \log B + (CNR)_T + NF$$

$$P_S = -174 \text{ dBm} + 10 \log (1.37 \times 10^6) + 9.0 \text{ dB} + NF$$

$$P_S = -103.62 \text{ dBm} + NF \qquad (99)$$

where the 9.0 dB threshold CNR of a conventional discriminator is used since the FMFB does not reduce the input CNR for the 0.7 deviation ratio assumed.

(3) The Second-Order Phase-Lock Loop As An FM Demodulator

The phase-locked loop shown in Figure 17 provides a bandpass filter action around the received signal that is sufficiently wide to contain the modulation spectrum. The filter is centered at the receiver intermediate frequency and has the loop-noise bandwidth (B_L) on each side of the center frequency for a total equivalent input noise bandwidth of $2B_L$.

Modulation on the carrier is not tracked as the loop tracks the average carrier frequency but appears at the phase detector output as an instantaneous phase error, $\theta_e(t)$. The phase error for a sinusoidal frequency modulation is given[15]

$$\theta_e(t) = M \frac{\Delta\omega}{\omega_m} \cos(\omega_m t + \phi) \tag{100}$$

where

$\frac{\Delta\omega}{\omega_m}$ = the peak radian frequency deviation

$\phi = \frac{\pi}{2} + \tan^{-1} \frac{\omega_m K_o K_d}{\omega_n^2} - \frac{\tan^{-1} 2\xi\omega_n\omega_m}{\omega_n^2 - \omega_m^2}$

M = magnitude of the error response

whenever $\theta_e(t)$ exceeds 90 degrees, the loop is said to lose lock.

The loop is essentially a servosystem and the parameters defining the loop behavior are given in terms of servo terminology. The relationship between the parameters that define the natural resonant frequency of the loop, ω_n, and the damping factor, ξ, is given

$$\omega_n \leq \frac{\pi B_i}{D+i} \left[1 - 2\xi^2 + \sqrt{(1 - 2\xi^2)^2 + 1 + \frac{4D^2}{\pi^2}} \right]^{1/2} \tag{101}$$

where

D = deviation ratio

B_i = predetection bandwidth.

The loop noise bandwidth, B_L, is defined in terms of the loop's natural frequencies as shown by

$$B_L = \frac{\omega_n}{2} \left(\xi + \frac{1}{4\xi} \right) \tag{102}$$

This bandwidth is in hertz, although the loop natural frequencies are expressed in radians/second. This bandwidth relationship is plotted in Figure 18. For optimum noise immunity, with regard to losing lock, the loop should be critically damped. Thus, assuming a damping ratio of 1.0, the ratio of modulating frequency ω_m to natural loop frequency ω_n can be found for a second-order loop from Figure 19. For a 600-kHz modulating frequency, the 3-dB loop bandwidth is determined from the figure to be

$$\omega_n = 1.52 \times 10^6 \text{ rad/sec} \tag{103}$$

$$\omega_m = 3.77 \times 10^6 \text{ rad/sec} \tag{104}$$

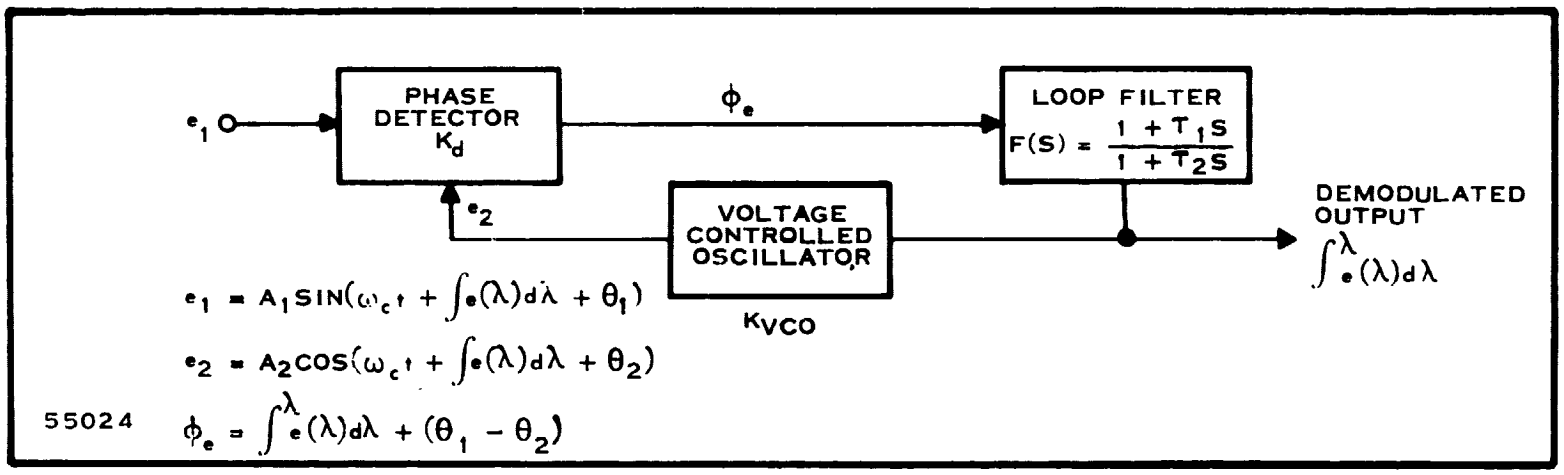

Figure 17. Phase-Locked Discriminator

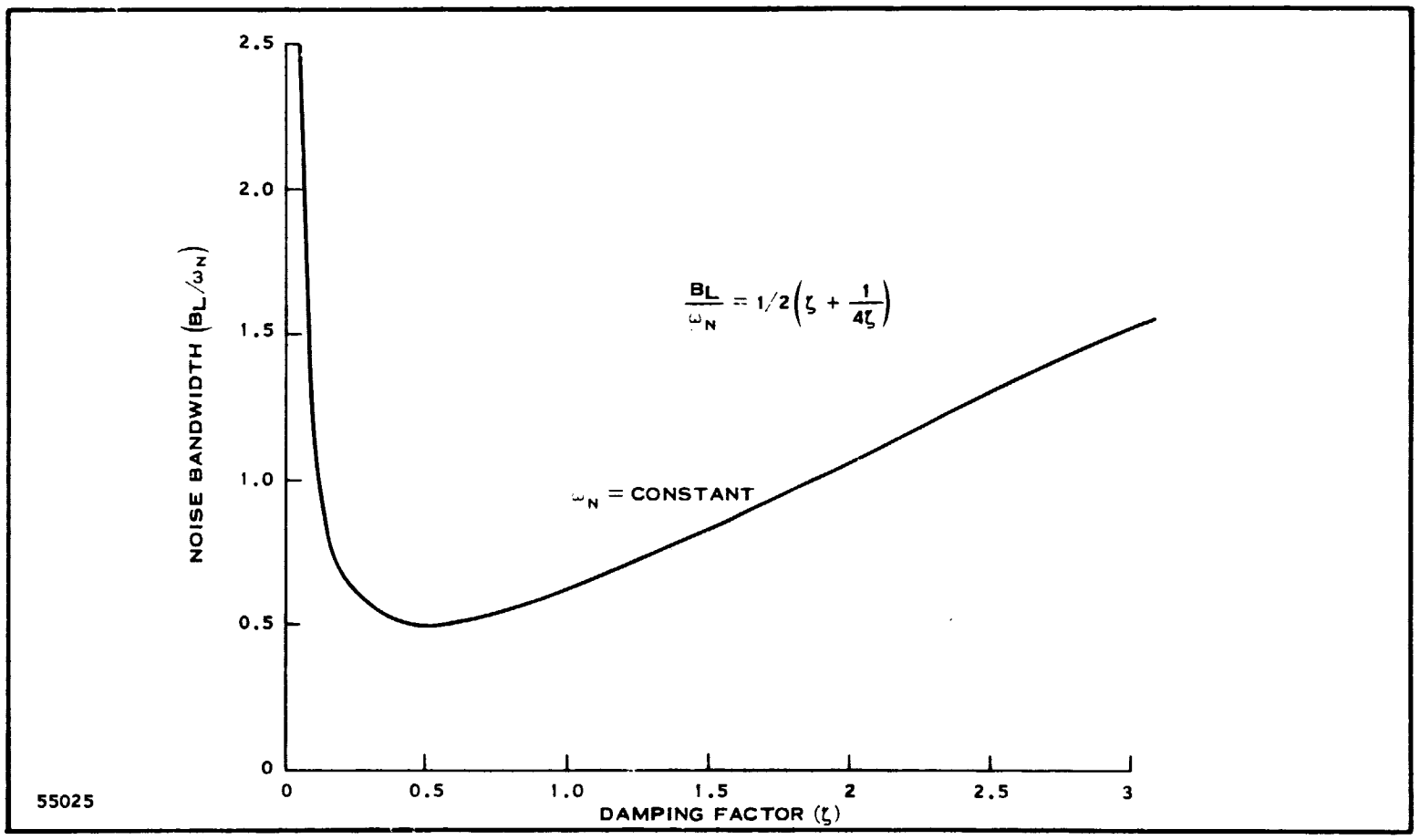

Figure 18. Loop Noise Bandwidth (For High-Gain, Second-Order Loop)

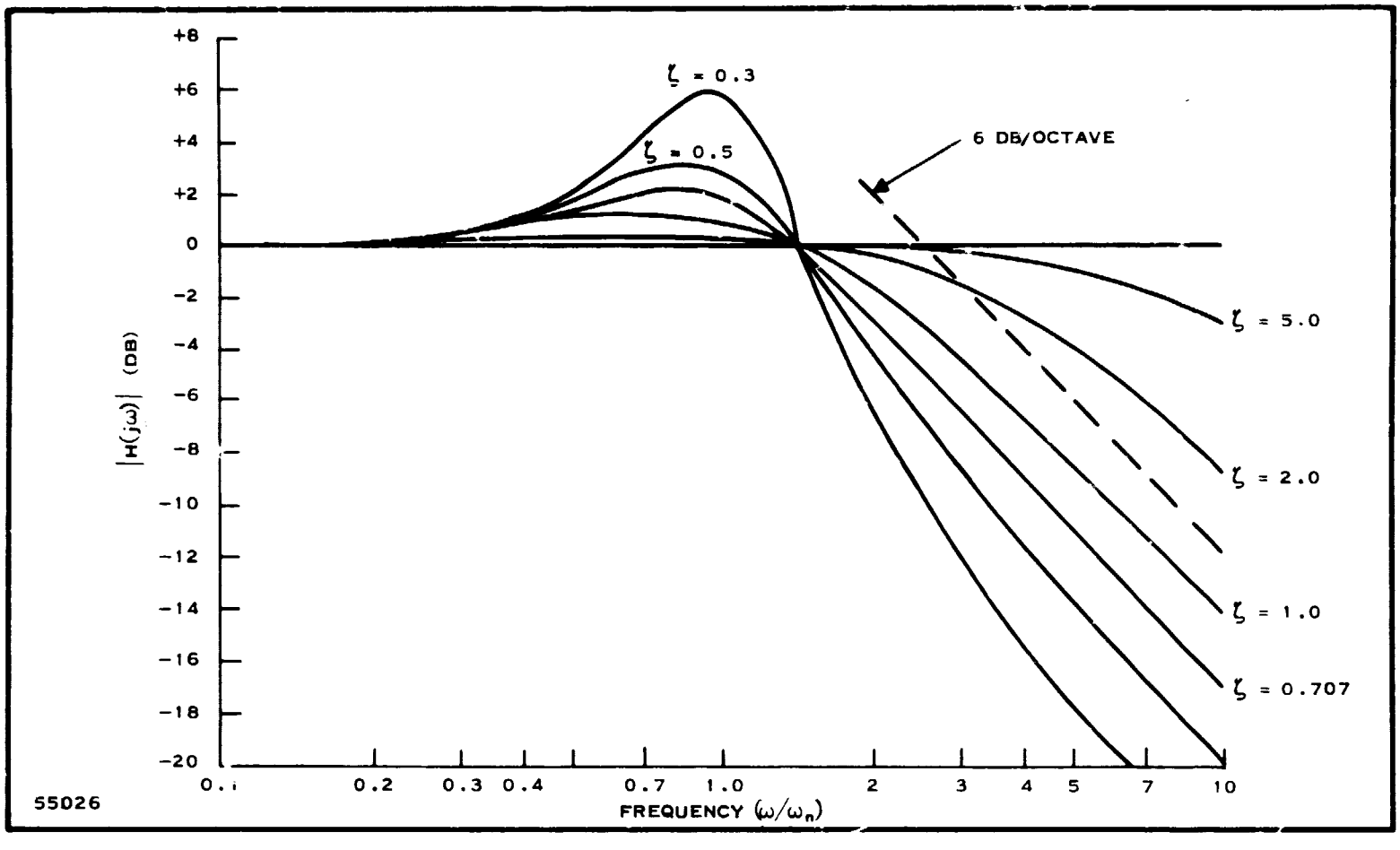

Figure 19. Frequency Response; High-Gain, Second-Order Loop

and the effective receiver input noise bandwidth $2B_L$, as given by Equation (102) is 1.9 MHz.

The phase comparator or detector compares the phase of the received signal with the reference phase of an auxiliary oscillator and provides an output voltage proportional to the phase error between the two signals. However, the phase detector has a limited range of operation; if the phase error between the two signals exceeds this range, the loop will drop out of lock. When the phase-lock loop drops out of lock an appreciable fraction of the time, the loop is customarily said to have reached its threshold. When the phase-lock demodulator uses a conventional phase detector with a sinusoidal characteristic, the loop loses lock when the closed-loop phase jitter exceeds 90 degrees. This is considered to occur when the mean-square phase error due to both modulation and noise exceeds 1 radian^2. The probability of losing lock as a function of the ratio of strong signal-to-noise to threshold signal-to-noise as derived by Spilker[16] is shown in Figure 20.

There is always some probability that the phase detector limits will be exceeded, and this probability is increased as noise increases. Martin[17] reports that lock cannot be held below 0 dB signal-to-noise ratio in the loop, and acquiring lock is very nearly impossible if the loop signal-to-noise ratio $(SNR)_L = 0$ dB. In general, a $(CNR)_T$ of 6 dB is

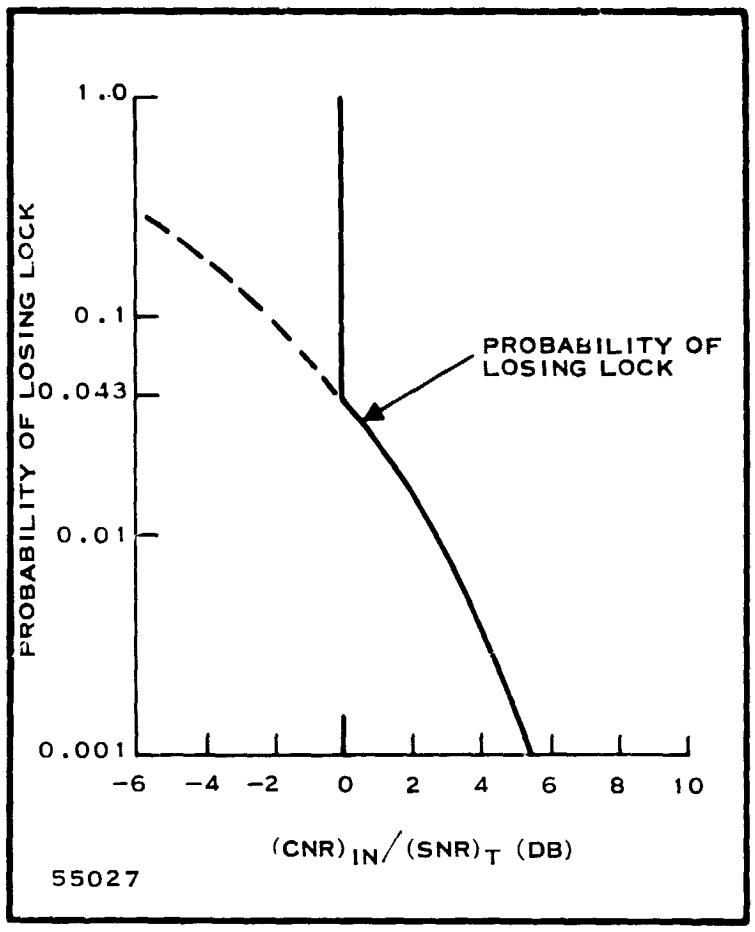

Figure 20. Probability of Losing Lock For The Phase-Lock Loop

needed for acquisition. However, if the frequency of the incoming signal is well-known, it has been indicated that a $(SNR)_L$ of 3 dB is acceptable. In comparing the threshold characteristics of various FM detectors, Spilker[16] has indicated that for deviation ratio of 0.7, the threshold requirement for a phase-lock demodulator is 5 dB. This is a 4-dB improvement over the 9.0 dB required for a conventional discriminator, and a 5-dB loop signal-to-noise threshold will be accepted in this study as the requirement to be met.

The reduction in threshold requirements as compared to a conventional discriminator for the FMFB and phase-lock demodulator is shown in Figure 21. This figure shows that for low deviation ratios, the phase-lock demodulator has a lower value of threshold than the other detectors. A 5 dB signal-to-noise ratio is shown to be required.

Spilker defined discriminator threshold to occur at 10 dB compared to 9.0 dB assumed in his study.[16] It may be seen that the threshold requirement of a FMFB is the same as that required for a discriminator. Thus, the threshold requirement for both detectors for a 0.7 deviation ratio will be taken as 9.0 dB.

d. Results of Trade Study Analysis of Intermediate Steps

In Figure 12, the results of using a mixer and further amplification after a transistor microwave amplifier are shown. Figure 12 also shows that cascading two transistor amplifiers results in a noise figure which may be easily degraded by following stages so that the performance requirement is not met. Thus, following the first RF amplifier with further amplification may be disregarded for the system under study.

In Figures 12b and c, lower noise figures are shown to be achieved in the case where the input RF amplifier is followed by a frequency conversion operation. The lowest noise figure (5.49 dB) is accomplished when a germanium transistor is used in the first amplifier. Therefore, using a mixer as an intermediate stage after a germanium microwave transistor is a feasible RF front-end for the system.

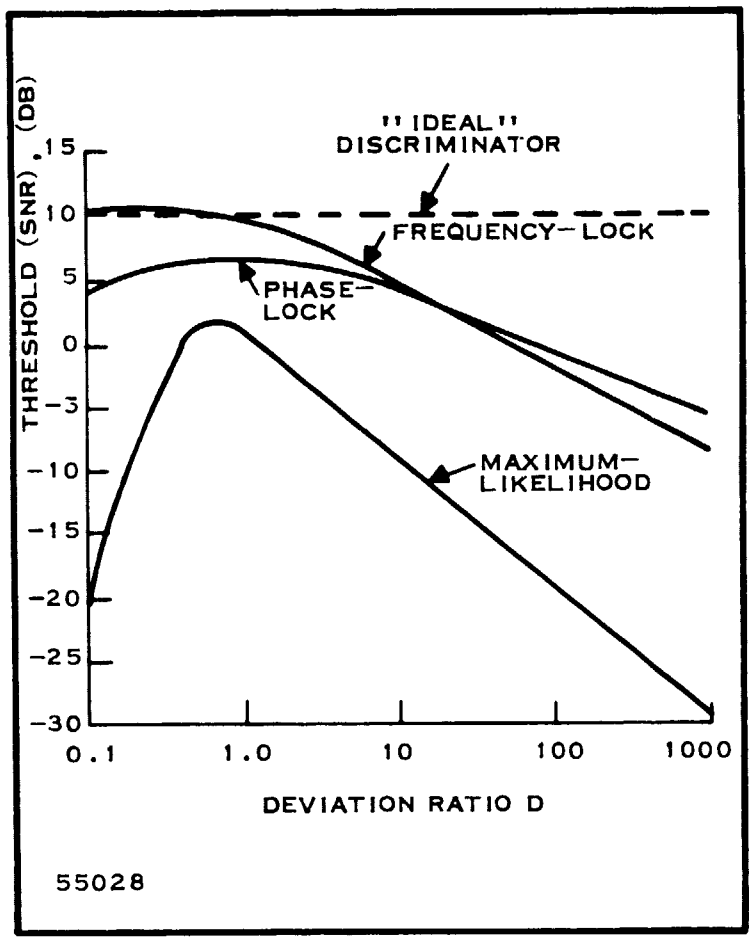

Figure 21. Comparison of The Threshold Input SNR For The Discriminators As A Function of the Deviation Ratio

The possibility of demodulation after the first stage was ruled out due to the circuit selectivity required. The resulting system in which amplification is the first operation performed at the receiver input is shown in Figure 22a.

In the case where frequency conversion is the first operation performed, intermediate amplification and further frequency conversion after the input mixer was shown to be valid. The only possible operation is demodulation. This is illustrated in Figure 22b. Therefore, in the final analysis the systems shown in Figure 22 are evaluated by the effect demodulation has on receiver sensitivity.

The threshold and bandwidth reduction characteristics of the demodulators discussed permit the sensitivity of either system shown in Figure 22 to be determined. In the system shown in Figure 22a, an RF amplifier and mixer precedes the demodulation operation. The sensitivity of this system may be calculated from

$$P_S = -174 \text{ dBm} + 10 \log B + NF + (CNR)_T \qquad (105)$$

It has previously been shown that the lowest noise figure for this system is achieved if the RF amplifier uses a germanium device. From Figure 12c, the noise figure resulting from use of an amplifier and a mixer with a 3.0-dB noise figure is 5.49 dB. Then, in the case of using a discriminator preceded by a 2.04-MHz if. passband, the sensitivity is given from the above equation as

$$P_S = -174 \text{ dBm} + 10 \log (2.04 \times 10^6) + 5.49 \text{ dB} + 9.0 \text{ dB} \qquad (106)$$

$$P_S = -97 \text{ dBm}$$

where a 9.0-dB threshold requirement is used. For the same system using a frequency-lock demodulator (FMFB) which also has a 9.0-dB threshold requirement but reduces the bandwidth to 1.3 MHz, the sensitivity is

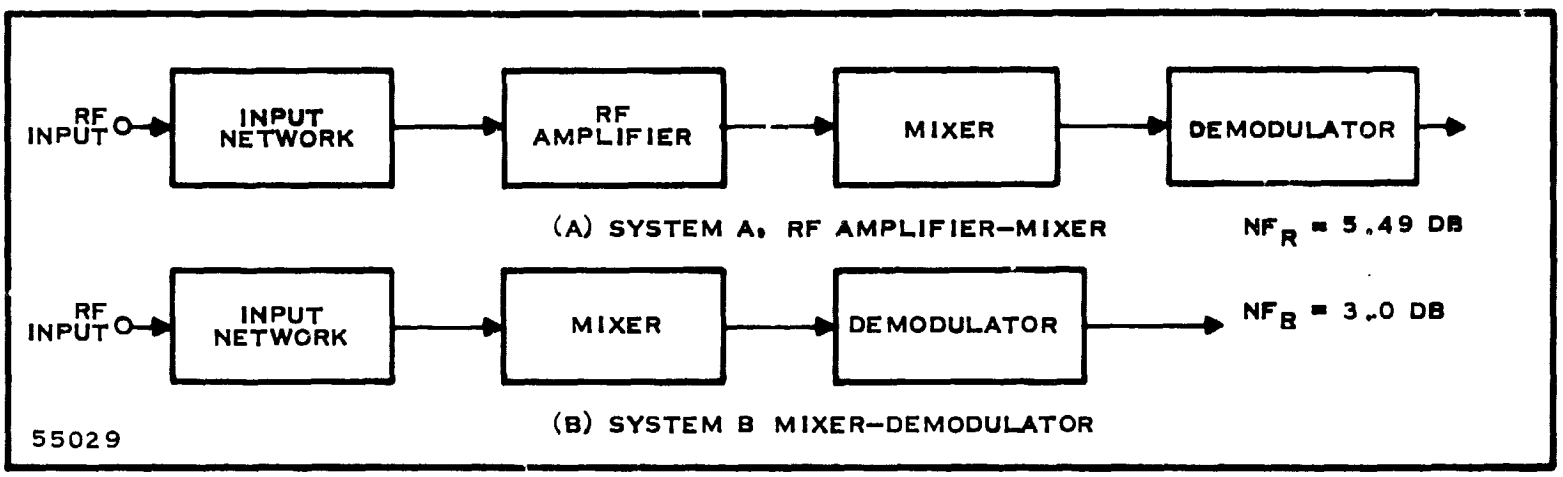

Figure 22. Possible Receiver Intermediate Stages

$$P_s = -174 \text{ dBm} + 10 \log (1.3 \times 10^6) + 5.16 \text{ dB} + 9.0 \text{ dB} \qquad (107)$$

$$P_s = -99 \text{ dBm} .$$

The use of a phase-lock demodulator reduces the threshold requirement to 5.0 dB. Employing this type of detector reduces the effective bandwidth of the receiver from 2.04 MHz to 1.95 MHz, and the resulting sensitivity required to establish a 5-dB input signal-to-noise ratio is

$$P_s = -174 \text{ dBm} + 10 \log (1.95 \times 10^6) + 5.16 + 5.0 \qquad (108)$$

$$P_s = -101 \text{ dBm} .$$

In a similar manner, the system shown in Figure 22b in which a 3.0-dB mixer is used as the input stage of the receiver can be evaluated. As shown in Figure 12, the overall noise figure is 3.0 dB, and the required signal level to establish the threshold requirements for the three demodulators can be determined. First, examining the system when a discriminator is used and when a 2.04-MHz intermediate-frequency pass-band precedes the detector results in a sensitivity of

$$P_s = -174 \text{ dBm} + 10 \log (2.04 \times 10^6) + 3.0 \text{ dB} + 9.0 \text{ dB} \qquad (109)$$

$$P_s = -99 \text{ dBm} .$$

The signal level required to establish a 9.0-dB threshold signal-to-noise ratio if an FMFB demodulator is used is

$$P_s = -174 \text{ dBm} + 10 \log (1.34 \times 10^6) + 3.0 \text{ dB} + 9.0 \text{ dB} \qquad (110)$$

$$P_s = -101 \text{ dBm} .$$

where, as above, the 2.04-MHz bandwidth is reduced to 1.3 MHz.

Finally, using a phase-locked demodulator which permits a significant decrease in the required threshold signal-to-noise ratio, the sensitivity is seen to be

$$P_s = -174 \text{ dBm} + 10 \log (1.34 \times 10^6) + 3.0 \text{ dB} + 5.0 \text{ dB} \qquad (111)$$

$$P_s = -102 \text{ dBm} .$$

The predetection bandwidth of 2.04 kHz specified in Table 2 provides the receiver with the capability of receiving a 1.2-megabits/sec data rate, but the sensitivity requirement of −110 dBm, as shown above, cannot be met with a bit rate of 1.2 megabits/sec. The best sensitivity that can be achieved is with the system utilizing a 3-dB system noise figure and a phase-locked detector with a 5-dB threshold requirement. In this system, the sensitivity and predetection bandwidth requirement can be met if the data rate is reduced. This would permit a reduction in the loop-noise bandwidth, and the effective receiver bandwidth of $2B_L$ could then offer significant reduction to permit achievement of a −110-dBm sensitivity.

e. Final Receiver Configuration

The system shown in Figure 23 best meets the performance requirements given in Table 2. The overall noise figure, using a low noise-figure mixer and intermediate-frequency amplifier, was assumed to be 3.0 dB. In the above sensitivity calculations, the phase-locked demodulator was demonstrated to be the most superior detector to use. It was shown previously that the noise figure could be achieved using an intermediate frequency of 100 MHz, and the use of double conversion was shown to be disadvantageous. Therefore, implementation of the system in Figure 23 requires that demodulation occur at a frequency of 100 MHz. This can be achieved with field effect transistors (FET's) which presently function well at frequencies extending to several hundred megahertz. Therefore, using FET's as synchronous detectors to accomplish phase detection of the intermediate-frequency signal is a plausible approach to demodulation at 100 MHz. However, this requires that sufficient gain be achieved at the intermediate frequency to meet the sensitivity requirements of the phase detector.

In Table 2, the relative advantage of using a balanced mixer as opposed to a single-ended mixer is readily seen. In addition, a balanced configuration suppresses noise on the local-oscillator signal. Rafuse reports that the attainment of balanced mixers with 2.0-dB noise figures is possible.[11] The receiver developed in this program will attempt to achieve a low noise figure using microelectronic techniques and 3.0 dB will be the design goal.

In the above calculations, a 2.04-MHz rectangular intermediate-frequency bandpass response was assumed. In practice, this requires a skirt selectivity impossible to realize. The ideal rectangular response can be approximated with a crystal filter or with the use of filters with five or

more poles. In integrated circuits, the fabrication of the inductors required at 100 MHz to construct such a response would make the intermediate-frequency circuitry excessively large. The intermediate frequency amplifier design will be guided toward the smallest amplifier design possible; thus, the selectivity will be accomplished with RC networks.

The preselector shall have a 150-MHz bandwidth, centered at 2250 MHz in order to allow fixed-tuning operation without the need to replace the filter when the receiver operates at any frequency in the 2200- to 2300-MHz band. The bandpass characteristic of this filter shall provide greater than 60-dB rejection to any frequency more than 200 MHz outside the passband.

To minimize the amount of noise appearing in the output, the bandwidth of the post-detection filter must be as small as possible. At the same time, the filter bandwidth must be sufficiently wide to prevent smearing of adjacent pulses which would result in crosstalk.

Time relationship between data pulses is preserved so that smearing is minimized with filters displaying good transient characteristics. Good transient response is exhibited with filters possessing fast settling time so that the filter does not have an oscillatory nature when the input is excited by a pulse input.

High-quality transient characteristics are related to a filter group delay. This requires a filter with linearity of its phase shift as a function of input frequency, such as a very flat delay filter. Ideally, this requires a filter with a Gaussian response, which is impossible to construct in practice, but it may be closely approximated by a Bessel filter. The Gaussian response has no overshoot and a 3-fc slope at the slicing level. Slicing level is taken to be equal to one-half the height of the output data pulse, and defines the threshold of the decision device following the filter. Above the slicing level, the decision device rules a "one" has been received; below this level, the device defines a "zero" is received.

Downing[3] defines the noise bandwidth of a Bessel filter which approximates the Gaussian response as given by

$$Bn = 1.317\ fc \tag{112}$$

where

fc = cutoff frequency of filter.

In order to recover the fundamental of the modulating NRZ code, the filter cutoff frequency is selected to be 600 kHz. Thus, the output noise bandwidth of the receiver is

$$Bn = 1.317\ (600\ kHz) \tag{113}$$

$$= 790\ kHz.$$

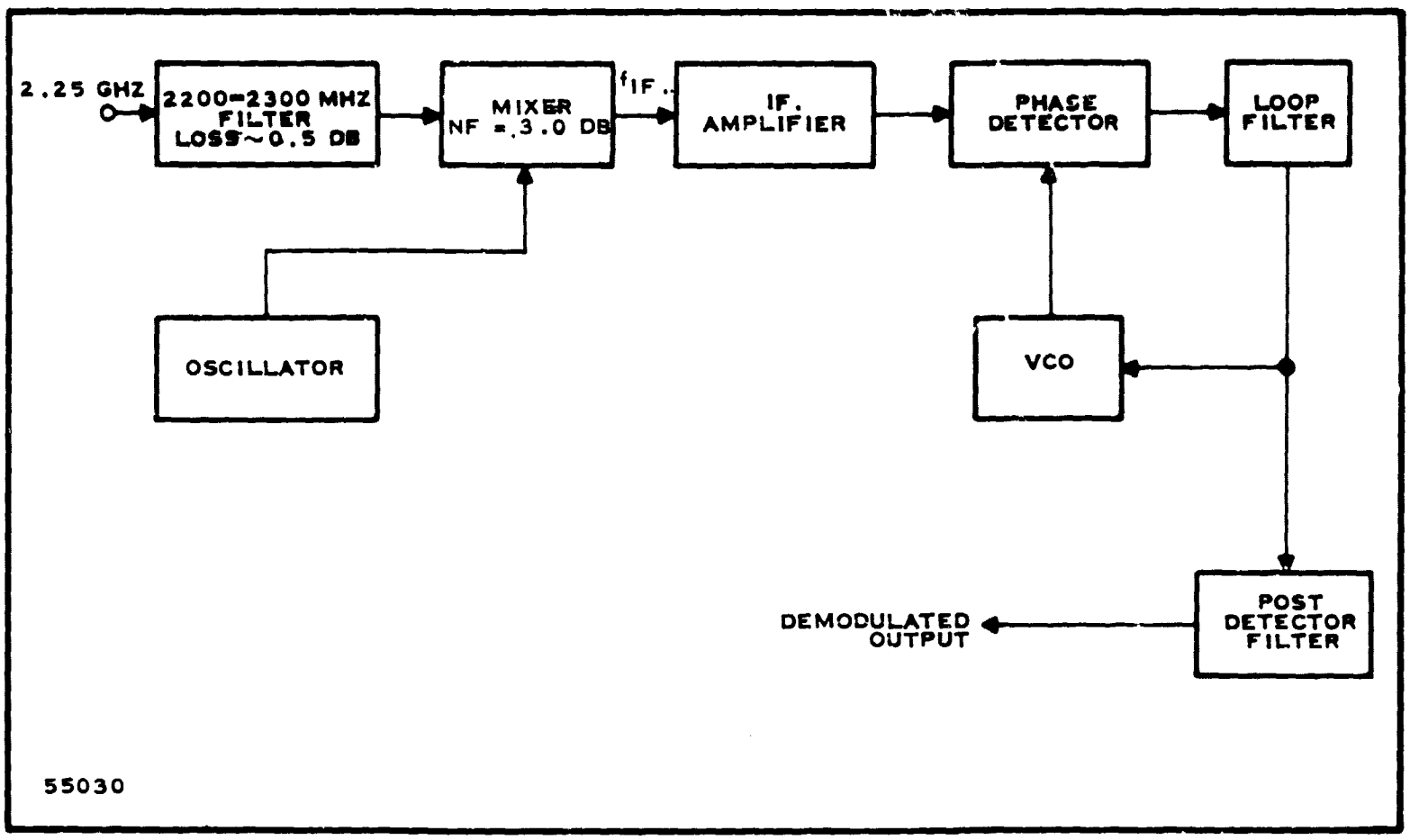

Figure 23. Final Receiver Configuration

The output signal-to-noise ratio of 15 dB which establishes the 1×10^{-4} error rate is defined within the above bandwidth.

E. CIRCUIT DESIGN AND ANALYSIS

1. Microwave Integrated Circuit Techniques

In recent years, microstrip characteristics have been extensively studied and empirical relationships between characteristic impedance, conductor line widths for various ceramic substrates, and thickness have been established. The typical variation of these parameters as well as the slowing factor for 20 mil glazed Al_2O_3 are shown in Figure 24. This ceramic was used in designing the balanced mixer, and the thin-film layouts of the intermediate circuits are designed to use the same substrate.

The resistance of the anodized tantalum resistors is given by this formula.

$$R = \frac{\ell}{w} \rho \text{ ohms} \tag{114}$$

where

R is the resistance value in ohms

ℓ is the resistor length in mils

w is the resistor width in mils

ρ is the resistivity of the anodized tantalum in ohms per square mil.

In all the following circuit designs, ρ is equal to 100 ohms per square. The minimum width (w) used is 4 mils; therefore, the minimum length for a 15,000-ohm resistor is 600 mils. As a rule of thumb for low value resistors, the width must be great enough to cause the length to be at least 10 mils. The maximum allowable power dissipation is 0.2 mW per square mil, so there is often a tradeoff between length, width, and area.

The value of the thin-film capacitors is given by the equation

$$C = 0.75 \text{ pF/mil}^2 \times \text{area} \quad \text{picofarads} \tag{115}$$

or the area required for a given capacitor is

$$\text{Area} = \frac{C}{0.75} \text{ mils}^2 \ . \tag{116}$$

Applying a minimum and maximum dimension of 10 mils and 40 mils, respectively, gives capacitance range of 75 to 1200 pF (less than 75 pF). Capacitance values between 75 pF and 40 pF can be realized by placing two capacitors in series. For values below 40 pF, discrete capacitors must be used. Beam lead capacitors are available in values from less than 1.0 pF

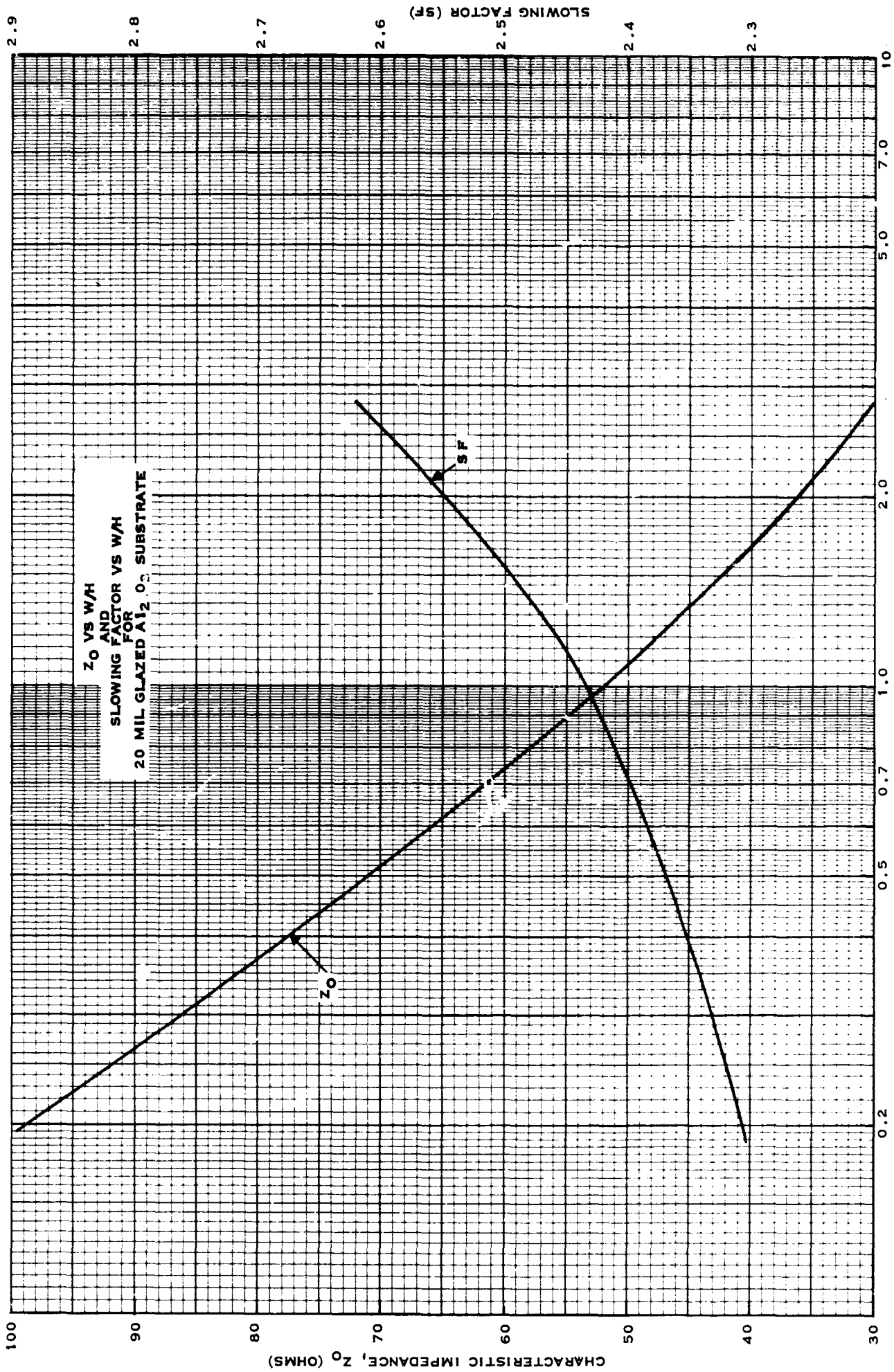

Figure 24. W/h Versus Slowing Factor and Characteristic Impedance for 20 Mil Glazed Ceramic

to 100 pF. The largest physical size for high capacitance beam lead capacitors is 20 × 35 mils; low capacitance values are somewhat smaller.

Thin-film inductors are made in square spiral geometry by using a gold conductor. The size is determined by the following formula:

$$L = 2.16 \times 10^{-2}\, DN^{5/3} \text{ nanohenries} \tag{117}$$

where

D is the side of the square in mils

N is the number of turns.

The conductor width forming the spiral is given,

$$w = \frac{D}{4N} \text{ mils} \tag{118}$$

where

w is the width of the conductor.

The spacing between the conductors also equals w.

Active devices such as chip transistors and diodes are mounted on gold pads. The substrate is made to be the collector; so the collector circuit connects to the gold pad. Transistor emitter and base connections are made by ball-bonded wires from the transistor to a gold conductor. Diode chips are mounted in similar fashion.

Integrated circuit chips and chip capacitors are also mounted on gold pads with ball-bonded wires being used to complete circuit connections.

2. RF Front End

The receiver system developed in the preceding section, utilizing a broadband preselector and low noise mixer in the input stages, offered an improvement in overall receiver noise figure. In the following paragraphs, an analytical design of the mixer is given to determine whether a 3.0-dB noise figure is feasible and to demonstrate the considerations required in constructing the mixer in microstrip.

a. 2200- to 2300-MHz Preselector

An optimum semifixed-tuned receiver was shown previously to require only that the frequency determining networks in the local oscillator be changed to change operating frequency. Therefore, a broadband preselector with a 2200- to 2300-MHz bandpass should be used at the receiver input. A microstrip design of such a preselector may be of several configurations such

as parallel coupled, interdigitated or series coupled. A lumped constant, thin-film configuration could also be employed.

The microstrip approach seems more feasible for this application; however, the design was not completed during this report period and will be completed at a later time. Computer optimization techniques will be employed when feasible during the preselector design phase.

b. Balanced Mixer

In the theory of mixer operation, the mixer is represented by a passive, linear network having terminals at signal, image and intermediate frequency only. The linear network presentation of a mixer is derived from its time varying conductance given by the Fourier series,

$$g = g_0 + \sum_{n=1}^{\infty} g_n \cos n\omega_o t \tag{119}$$

where

g is the instantaneous slope of the diode's static characteristics

g_n is the amplitude of the n^{th} harmonic component of the periodic conductance

g_0 is the time average of g.

These harmonic conductance coefficients are related to the diode forward voltage-current characteristic as shown by the Gamma functions

$$g_0 = \frac{x\, K\, \Gamma\left(\frac{x}{2}\right)}{\sqrt{\pi}\ \Gamma\left(\frac{x+1}{2}\right)} \tag{120}$$

$$g_1 = \frac{x}{\sqrt{\pi}}\ K\ \frac{\Gamma\left(\frac{x+1}{2}\right)}{\Gamma\left(\frac{x+1}{2}\right)} \tag{121}$$

$$g_2 = \frac{x}{\sqrt{\pi}}\ K \left[\frac{2\Gamma\left(\frac{x+1}{2}\right)}{\Gamma\left(\frac{x+3}{2}\right)} - \frac{\Gamma\left(\frac{x}{2}\right)}{\Gamma\left(\frac{x+1}{2}\right)} \right] \tag{122}$$

where x and K are constant for a particular diode.

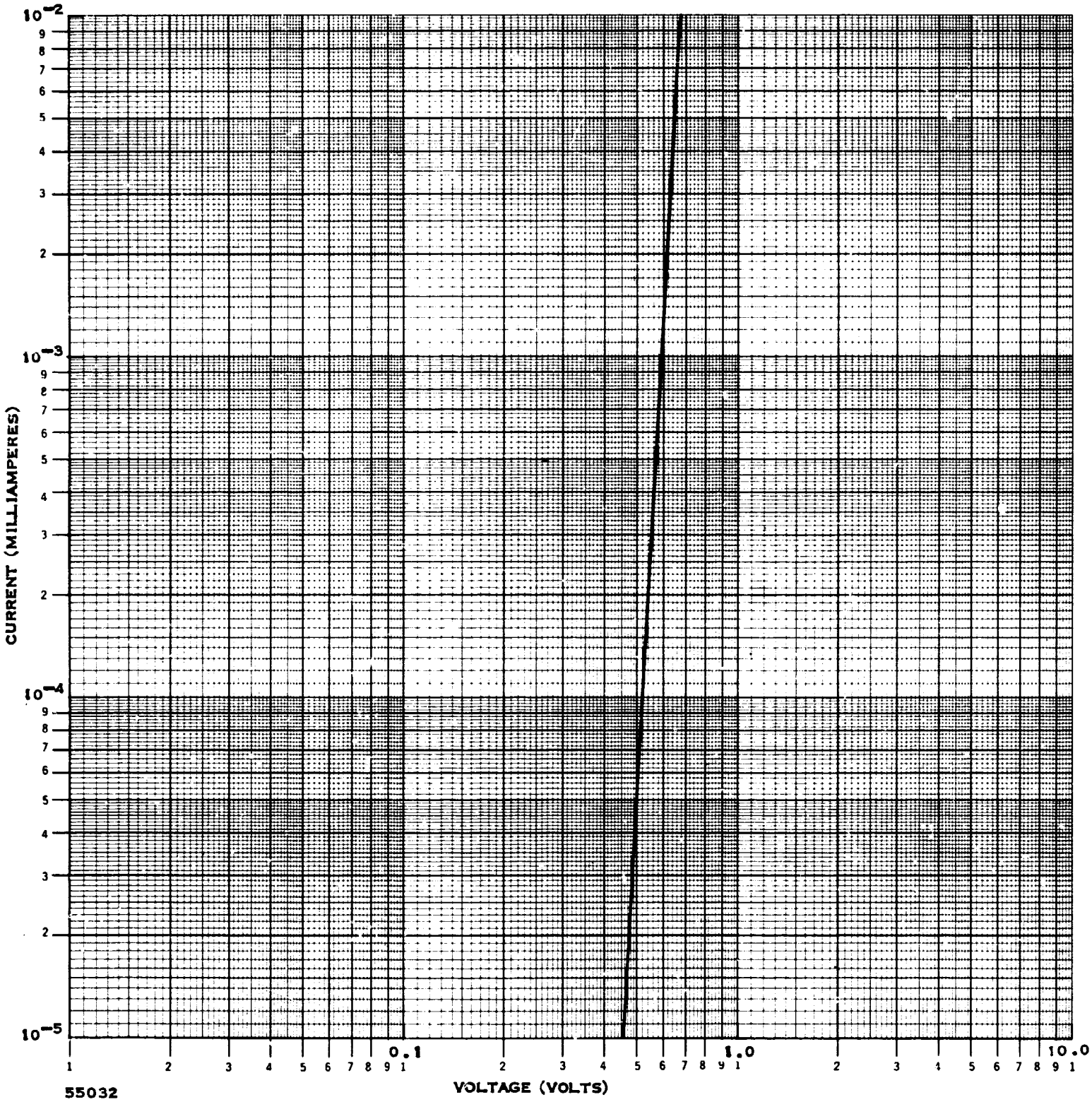

Figure 25. Typical Log-Log Characteristic for a Typical GaAs Mixer Diode

Normalizing, the g_n coefficients with respect to g_0 results in the expression,

$$\gamma_n = \frac{\left(\frac{x-1}{2}!\right)^2}{\left(\frac{x+n-1}{2}!\ \frac{x-n-1}{2}!\right)+\gamma_b} \tag{123}$$

where n takes on values between 1 and 2.

Sturm[12] has shown that the conversion loss of a diode when an open-circuit image termination is employed, is given by its normalized conductance coefficients,

$$L_c = \left[1 + \frac{\sqrt{1+\gamma_{2n}-2\gamma_n^2}}{\left(1-\gamma_n^2\right)\left(1+\gamma_{2n}\right)}\right]^2 \cdot \left[\frac{\left(1-\gamma_n^2\right)\left(1+\gamma_{2n}\right)}{\gamma_n^2\left(1-\gamma_{2n}\right)}\right] . \tag{124}$$

The diode conductance, as shown by Equations 120, 121, and 122, defining the diode conversion loss, depends primarily on the diode static voltage-current (V-I) characteristic. This characteristic for a typical Gallium Arsenide diode is shown plotted on log-log coordinates in Figure 25. The slope of a log-log plot of the diode V-I characteristics is given by

$$x = \frac{\log i_2/i_1}{\log v_2/v_1} \tag{125}$$

where $i_2 > i_1$, and $v_2 > v_1$. The value of x for the characteristics given in Figure 25 as determined by this relation is

$$x = \left[\frac{1.0-0.01}{0.68-0.604}\right] \tag{126}$$

$$x = 13 .$$

When the image frequency is terminated into an open circuit, the conversion loss of the diode calculated from Equation 124, for $x = 13$, is shown in the Appendix to be

$$L_c = 1.75 \tag{127}$$

or

$$L_c = 2.45 \text{ dB.}$$

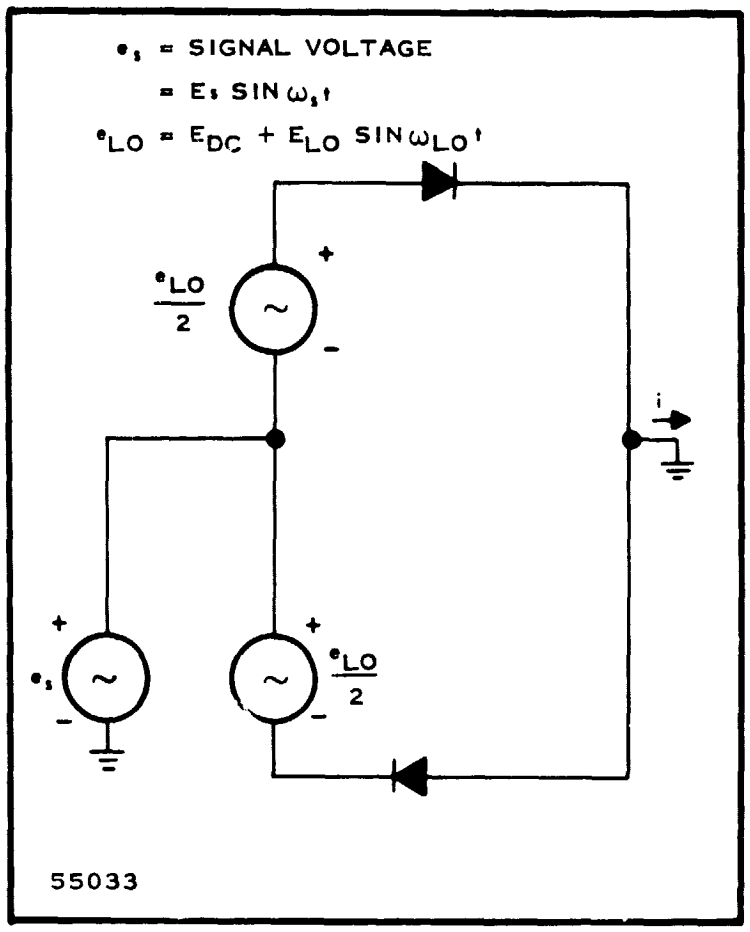

Figure 26. Equivalent Circuit of Balanced-Mixer

Terminating the image frequency into an open circuit results in the image signal being reflected back to the diode and undergoing further conversion to the intermediate frequency. Therefore, there is a decrease in conversion loss as power contained in the image signal is not dissipated. In broadband receivers, terminating the image signal properly over a wide frequency range is a difficult task. The best matching network to accomplish the optimum mismatch is most accurately determined with the aid of a computer. A computer solution to the problem of maintaining a proper image-frequency mismatch was not attempted in this phase of the study contract. Nevertheless, the final mixer designed for this contract will require a computer-aided design in an attempt to maintain a mixer noise figure of 3 dB ±0.5 dB over the operating frequency range of 2200 to 2300 MHz.

A balanced or hybrid mixer is shown in Figure 26. Its operation was discussed in Scientific Report No. 4. This report mentioned that the lowest noise figure is achieved when the local-oscillator drive, diode biasing, rf and if. impedances are improved so that conversion loss is lessened. The effects these parameters play in prescribing noise figure are seen by the following equation:

$$NF = 10 \log L_m \left[t_m + (F_{IF} - 1) \right] \tag{128}$$

where

L_m is the effective mixer conversion loss

t_m is the effective mixer noise temperature

F_{IF} is the noise factor of the if. amplifier.

The terms L_m and t_m are characteristics of the mixer configuration. The mixer noise temperature for the image terminated case is given

$$t_m = \frac{1}{L_m} \left[t_d (L_m - 1) + 1 \right] \tag{129}$$

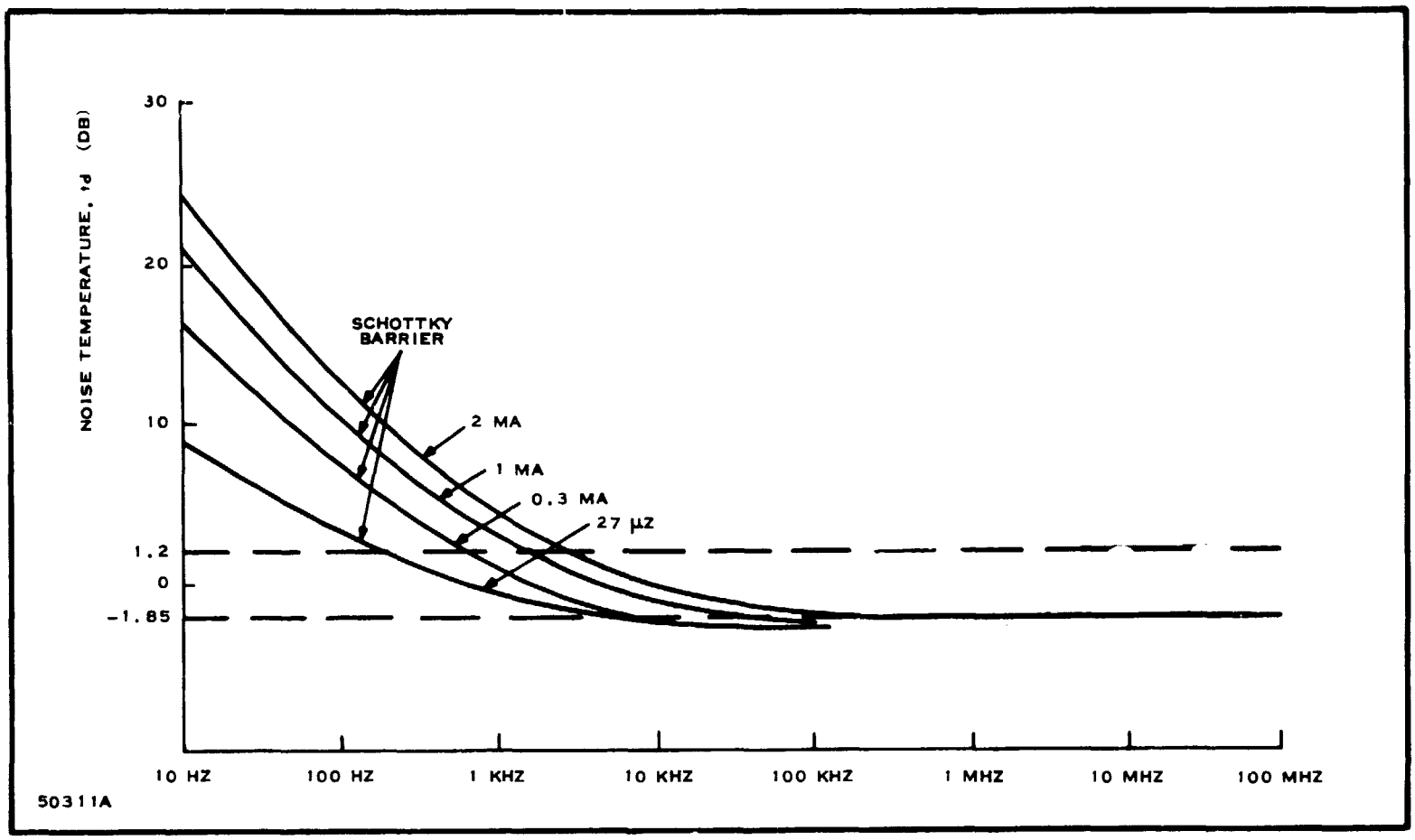

Figure 27. Noise Temperature Versus Intermediate Frequency

where t_d is the intrinsic noise temperature of the diode. As shown in Figure 27, present Schottky-barrier diodes approach a diode noise temperature of −1.85 dB when higher intermediate frequencies are used.

The effective mixer conversion loss L_m is the sum of three losses: the loss at the diode junction, diode conversion loss and circuit losses. Diode conversion loss is due to a portion of the rf signal being lost due to the presence of a finite series resistance (R_s) and the junction capacitance (C_j) of the actual diode. This loss is expressed as the ratio of the input rf signal power to the power delivered to the junction resistance (R_j) and is given

$$L_1 = 10 \log \frac{P_s}{P_j} \tag{130}$$

$$= 10 \log \left(1 + \frac{R_s}{R_j} + \omega^2 C_j^2 R_s R_j\right) .$$

This loss is reduced by adjusting the local oscillator drive so that the junction resistance equals the $1/\omega C_j$ term. The local oscillator drive required for gallium arsenide diodes to minimize this loss is approximately 7 to 10 mW. Then, the minimum junction loss due to a finite series resistance is given

$$L_1(\text{min}) = 10 \log (1 + 2\omega C_j R_s) . \tag{131}$$

For gallium-arsenide chip diodes, generally

$$C_j = 0.18 \text{ pF}$$
$$R_s = 2 \text{ ohms}$$

then

$$L_1(\text{min}) = 10 \log \left[1 + 2(6.28)(2250 \text{ MHz}) \cdot (0.18 \text{ pF})(2 \text{ ohms})\right] \quad (132)$$

$$L_1 = 10 \log (1.010)$$

$$= 0.05 \text{ dB.}$$

The circuit loss L_2 is dependent on the degree of match obtained at the rf and if. ports. Any departure from a good match at either port results in a loss of the rf signal and a loss of available intermediate frequency signal delivered to the intermediate frequency amplifier. This loss can be expressed as

$$L_2 = 10 \log \frac{(\rho_1 + 1)^2}{4\rho_1} + 10 \log \frac{(\rho_2 + 1)^2}{4\rho_2} \quad (133)$$

where ρ_1 is the VSWR at the rf port and ρ_2 is the VSWR at the if. port. The mixer diode is matched to the rf source to obtain minimum diode conversion loss, rather than maximum power transfer, the optimum source conductance required for this mismatch is given by[13]

$$\left(\frac{g_{source}}{g_0}\right)^2 = \frac{(1 - \gamma_{2n})^2}{1 - \gamma_n} (1 + \gamma_{2n}) \left[1 - 2(\gamma_n)^2 + \gamma_{2n}\right] \quad (134)$$

In the Appendix, it is shown that

$$\gamma_n = 0.96$$

$$\gamma_{2n} = 0.855$$

and

$$g_0 = 4.27 \times 10^{-2} \text{ mhos}$$

when the self-bias of the diode is 4 milliamperes. Then

$$\left(\frac{g_{source}}{g_0}\right)^2 = \frac{(1-0.855)^2}{1-0.96}(1+0.855)\left[1-2(0.922)+0.855\right] \quad (135)$$

$$g_{source} = g_0\sqrt{0.1055}$$

$$g_{source} = 13.9 \text{ millimhos}$$

$$R_{source} = \frac{1}{g_{source}} \quad (136)$$

$$R_{source} = 72 \text{ ohms.}$$

The rf VSWR is defined

$$\rho_1 = \frac{R_d}{R_g} \quad (137)$$

where

R_d = diode resistance

R_g = generator resistance.

The diode rf impedance may be found from Figure 28 where it is shown normalized to 50 ohms, for various self-bias currents, and at 4 milliamperes and a frequency of 2.2 GHz,

$$Z_d = 74.0 - j\,24.0 \ . \quad (138)$$

Matching the diode to a 72-ohm rf source results in an rf VSWR, ρ_1, of

$$\rho_1 = \frac{R_d}{R_g} = \frac{74}{72} = 1.03 \ . \quad (139)$$

If the output of the mixer is perfectly matched, the VSWR at the if. port may be neglected; therefore, the rf circuit loss is

$$L_2 \cong 10 \log \frac{(\rho_1+1)^2}{4\rho_1} \quad (140)$$

$$\cong 10 \log \frac{(1.03+1)^2}{4.12}$$

$$L_2 \cong 0 \text{ dB} \ .$$

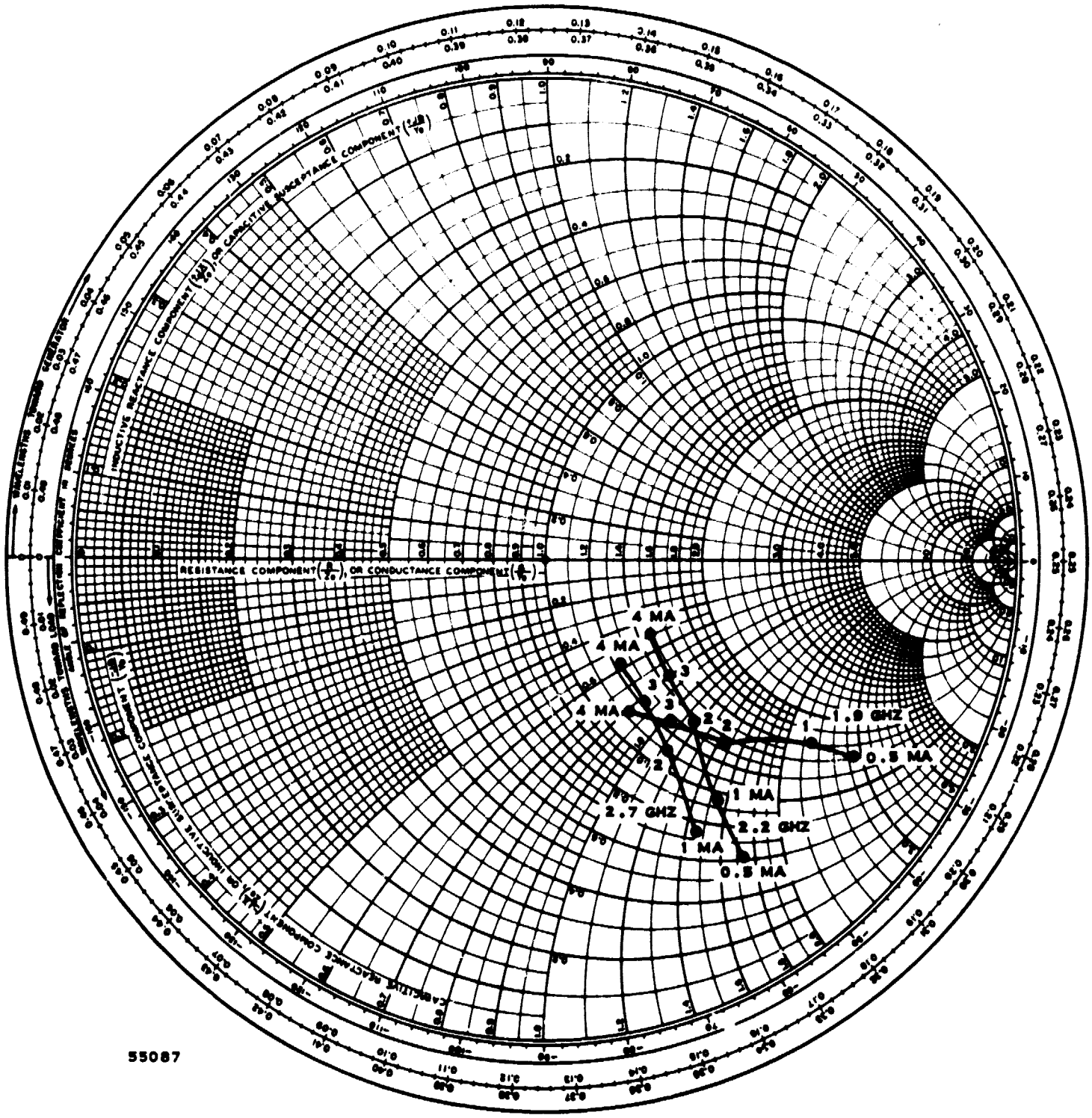

Figure 28. RF Impedance of GaAs Schottky Barrier Diode for Self-Bias

The total effective mixer loss, L_m is then the sum of losses due to the diode conversion loss, L_{c_g}, and junction loss, L_1. In Equation 127, the conversion loss was shown to be 2.45 dB. Therefore, the effective mixer loss is

$$L_m = L_c + L_1 + L_2 \tag{141}$$

$$= 2.45 \text{ dB} + 0.05 \text{ dB} + 0 \text{ dB}$$

$$L_m = 2.5 \text{ dB}.$$

The effective mixer noise temperature may now be determined, as the 2.5-dB conversion loss is a ratio of 1.75, and the noise temperature of a Schottky barrier diode, t_d, is 0.5

$$t_m = \frac{1}{L_m}\left[t_d(L_m - 1) + 1\right] \tag{142}$$

$$= \frac{1}{1.75}\left[0.5(1.75 - 1) + 1\right]$$

$$t_m = 0.783 .$$

The mixer noise figure when a 1.5-dB intermediate frequency amplifier follows the mixer is then,

$$NF = 10 \log (1.75)\left[0.783 + (1.41 - 1)\right] \tag{143}$$

$$NF = 3.28 \text{ dB}.$$

The image frequency may be terminated into an open circuit by employing a $\lambda/4$ shorted stub, which reflects an open circuit to the rf terminals of each diode. The open circuit may be accomplished by extending the transmission line connecting the diodes to the rf source by one-fourth of a wavelength beyond the diode terminals. This is shown in Figure 29. The stub length is a quarter wavelength at the image frequency which is 2050 MHz when the receiver is operating at 2250 MHz with a 100-MHz intermediate frequency. The free space wavelength of the 2050-MHz image frequency and 2250-MHz signal frequency are

$$\lambda_i = 5.75 \text{ inches}$$

$$\lambda_s = 5.25 \text{ inches}.$$

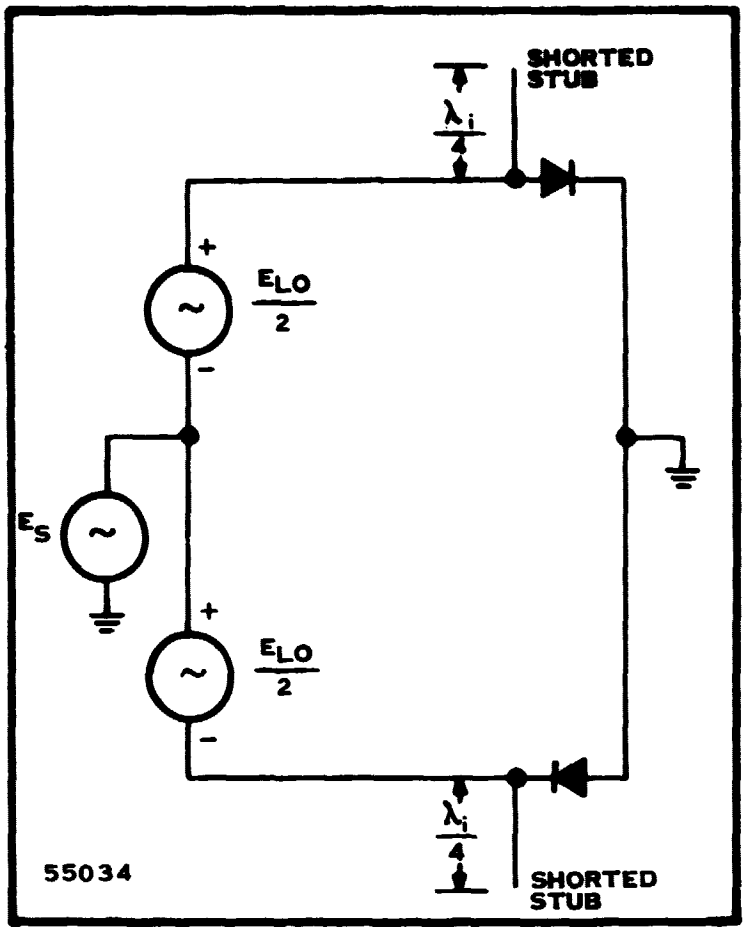

Figure 29. Image-Terminated Mixer

The input impedance of the stub is defined

$$Z_{sc} = j\, Zo \tan \beta l$$

where Zo is the characteristic impedance of the stub, and βl is its electrical line length. At the image frequency, the stub is a 90-degree line; however, at the signal frequency, the stub length is extended to

$$\beta l = \frac{2\pi}{\lambda_s} \times \frac{\lambda_i}{4} \times \frac{\lambda_s}{5.25} \times \frac{180°}{\pi} \qquad (144)$$

$$= 2\pi \times \frac{5.75}{4(5.25)} \times \frac{180°}{\pi}$$

βl = 98 degrees.

From Equation 136, it was seen that the required rf source impedance for the best mismatch was 72 ohms; therefore, using a stub with a characteristic impedance identical to that of the connecting transmission line

$$Z_{sc} = j\, 72 \tan 98° \qquad (145)$$

$$Z_{sc} = -j\, 512\ .$$

The admittance of the stub shunts the diode admittance and the stub admittance is given

$$Y_{sc} = j\, 1.95 \text{ millimhos.} \qquad (146)$$

The rf impedance of a typical GaAs diode was shown in Figure 28 to be

$$Z_d = 74 - j\, 24.0 \qquad (147)$$

for 4 milliamperes of self bias. Converting this impedance to an admittance gives

$$Y_d = 12.2 + j\, 3.96 \text{ millimhos.} \qquad (148)$$

The total admittance at the terminal and of the transmission line that connects the rf source and diode is the sum of the diode admittance and the admittance presented to the diode terminals by the shorting stub at the signal frequency.

$$Y_L = Y_d + Y_{sc} \tag{149}$$

$$Y_L = 12.2 + j\,5.91 \text{ millimhos.}$$

In order to remove the susceptance term and present a real conductance to the transmission line, the load is located on a Smith chart and rotated toward the generator until the susceptance term is zero. This is illustrated in Figure 30. Normalizing with respect to a 72-ohm transmission line (13.9 millimhos)

$$y_l = \frac{Y_L}{13.9 \times 10^{-3} \text{ mhos}} \tag{150}$$

$$y_l = 0.878 + j\,0.425$$

upon rotating

$$g_l = 0.63 + j0. \tag{151}$$

The length of line required at the signal frequency is

$$l_x = 0.123\,\lambda_s \tag{152}$$

and the resulting load conductance seen by the rf source

$$G_L = G_0\, g_l$$

$$G_L = (13.9 \times 10^{-3} \text{ mhos})(0.63) \tag{153}$$

$$G_L = 8.75 \times 10^{-3} \text{ mhos} \tag{154}$$

or the terminal impedance seen by the transmission line is

$$R_L = \frac{1}{G_L} \tag{155}$$

$$R_L = 114 \text{ ohms.}$$

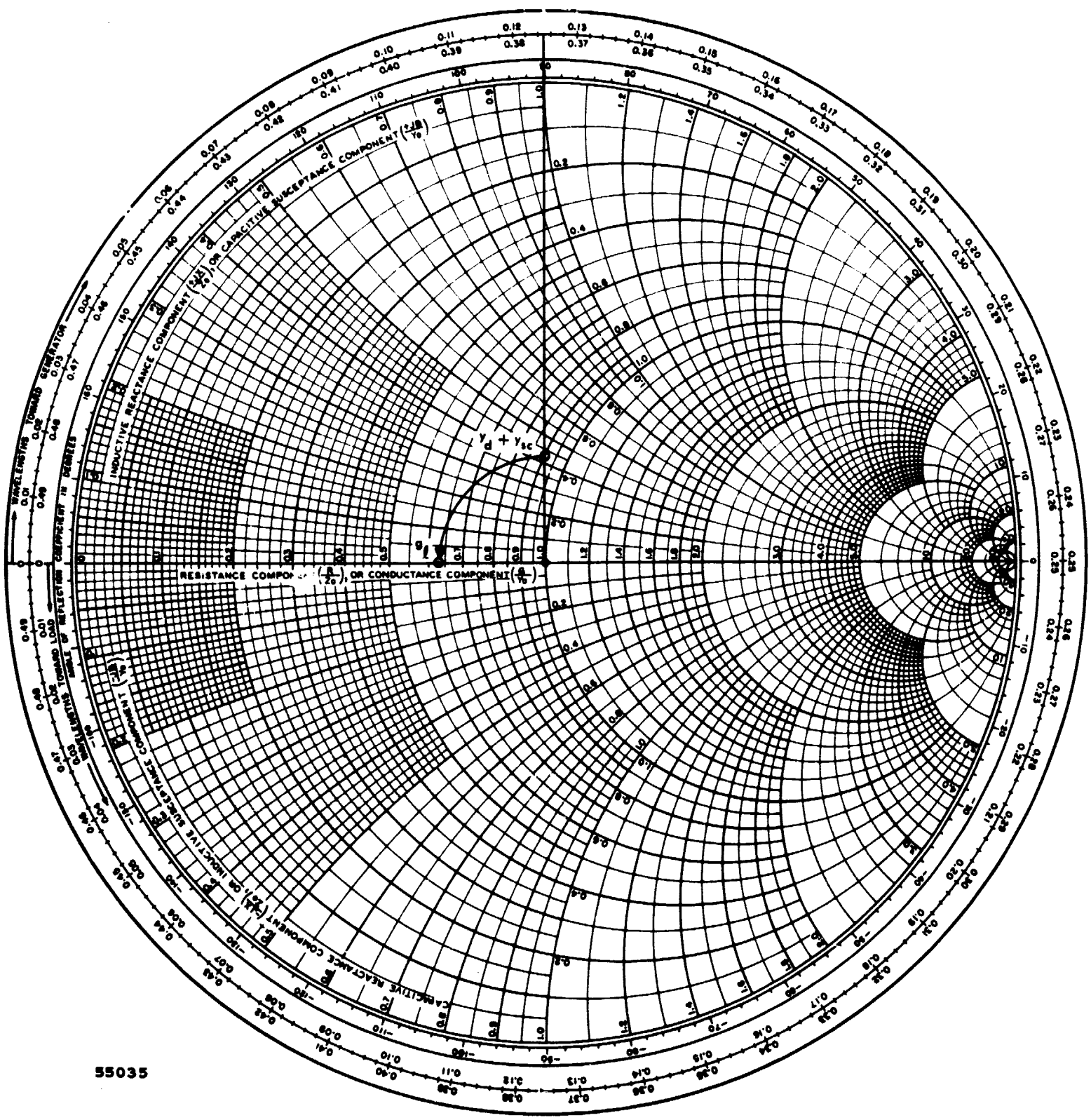

Figure 30. Load Admittance of Image Terminated Mixer at 2250 MHz

This impedance may be matched to a 50-ohm rf source by use of a $\lambda/4$ transformer with a characteristic impedance given by,

$$Z_o = \sqrt{R_L R_g} \tag{156}$$

$$= \sqrt{114 \times 50}$$

$$Z_o = 75.5 \text{ ohms.}$$

The mixer is fabricated on 20-mil glazed Al_2O_3 substrate using a hybrid branch line coupler to combine the rf signal and LO signal at the diode rf terminals. The width-to-height (w/h) ratios for this ceramic and corresponding slowing factors are determined from Figure 24 and, for a 75-ohm line,

$$\frac{w}{h} = 0.45 \tag{157}$$

$$S_f = 2.36 \tag{158}$$

for a 72-ohm line

$$\frac{w}{h} = 0.5 \tag{159}$$

$$S_f = 2.37 \ . \tag{160}$$

Hence, the width of the 75-ohm transmission line connecting the rf source and the diodes as determined by Equation 157 for $h = 20$ mils is

$$w = 9 \text{ mils} \tag{161}$$

and the free space wavelength at the signal frequency, 5.25 inches, is reduced by the slowing factor to,

$$\lambda_s' = \frac{\lambda_s}{\sqrt{S_f}} = \frac{5.25 \text{ inches}}{2.36} \tag{162}$$

$$\lambda_s' = 2.22 \text{ inches.}$$

Since the transmission line is a quarter-wave transformer, the length of the line is

$$l = \frac{\lambda_s'}{4} = \frac{2.22}{4} \tag{163}$$

$$l = 0.555 \text{ inch.}$$

The length of transmission line that locates the diode so that it appears as a real load to the rf source has a 72-ohm characteristic impedance to properly mismatch the diode for minimum conversion loss. The width of this line on glazed ceramic is given by Equation 159 as

$$w = 10 \text{ mils.} \tag{164}$$

The slowing factor for this impedance is given by Equation 160 as 2.37, and the 5.25-inch signal wavelength is reduced to

$$\lambda_s' = \frac{5.25 \text{ inches}}{2.37} \tag{165}$$

$$\lambda_s' = 2.21 \text{ inches.}$$

Therefore, the line length on the ceramic substrate from Equation 152 is

$$l_x = 0.122\,(2.21) \tag{166}$$

$$l_x = 0.275 \text{ inch.}$$

The characteristic impedance of the image terminating stub is also 72 ohms and a 10-mil line width is required. In order to have an equivalent quarter wavelength at the image frequency, the stub length on ceramic must be

$$\frac{\lambda_i}{4} = \frac{5.75}{4(2.37)} \tag{167}$$

$$\frac{\lambda_i}{4} = 0.605 \text{ inch.}$$

The intermediate frequency terminals of the diodes are bonded to a 93-ohm line, which closely matches the mixer intermediate frequency output impedance of 100 ohms. The width-to-height ratio for a 90-ohm line is

$$\frac{w}{h} = 0.28\,. \tag{168}$$

The resulting line width is

$$w = 5.6 \text{ mils.} \tag{169}$$

The intermediate frequency terminals are bypassed with a capacitor consisting of an open stub that is a quarter wavelength at the signal frequency. The characteristic impedance of this stub is 50 ohms; thus,

$$\frac{w}{h} = 1.15 \tag{170}$$

$$w = 1.15(20) = 23 \text{ mils}$$

and the slowing factor, S_f, for a 50-ohm impedance on 20-mil glazed ceramic is

$$S_f = 2.44 . \tag{171}$$

The length of the open-stub is a quarter wavelength at the signal frequency, its length in ceramic is then

$$l_s = \frac{\lambda_s}{4\sqrt{S_f}} \tag{172}$$

$$l_s = \frac{5.25}{4(2.44)}$$

$$l_s = 0.537 \text{ inch.}$$

Design of the 3-dB branch coupler was accomplished with the tables given in work done by Matthasi, Young, and Jones.[18] The series impedance, Z_1, of a two-branch line coupler to match the diode load to the signal source was given as 35 ohms; the necessary shunt impedance Z_2 was listed as 49 ohms. The width-to-height ratio and slowing factor (S_f) of these impedances are

$$Z_1 = 35 \text{ ohms} \tag{173}$$

$$\frac{w}{h} = 2.15 \tag{174}$$

$$S_f = 2.56 \tag{175}$$

$$\frac{\lambda_s'}{4} = \frac{5.25}{4(2.56)} = 0.513 \text{ inch.} \tag{176}$$

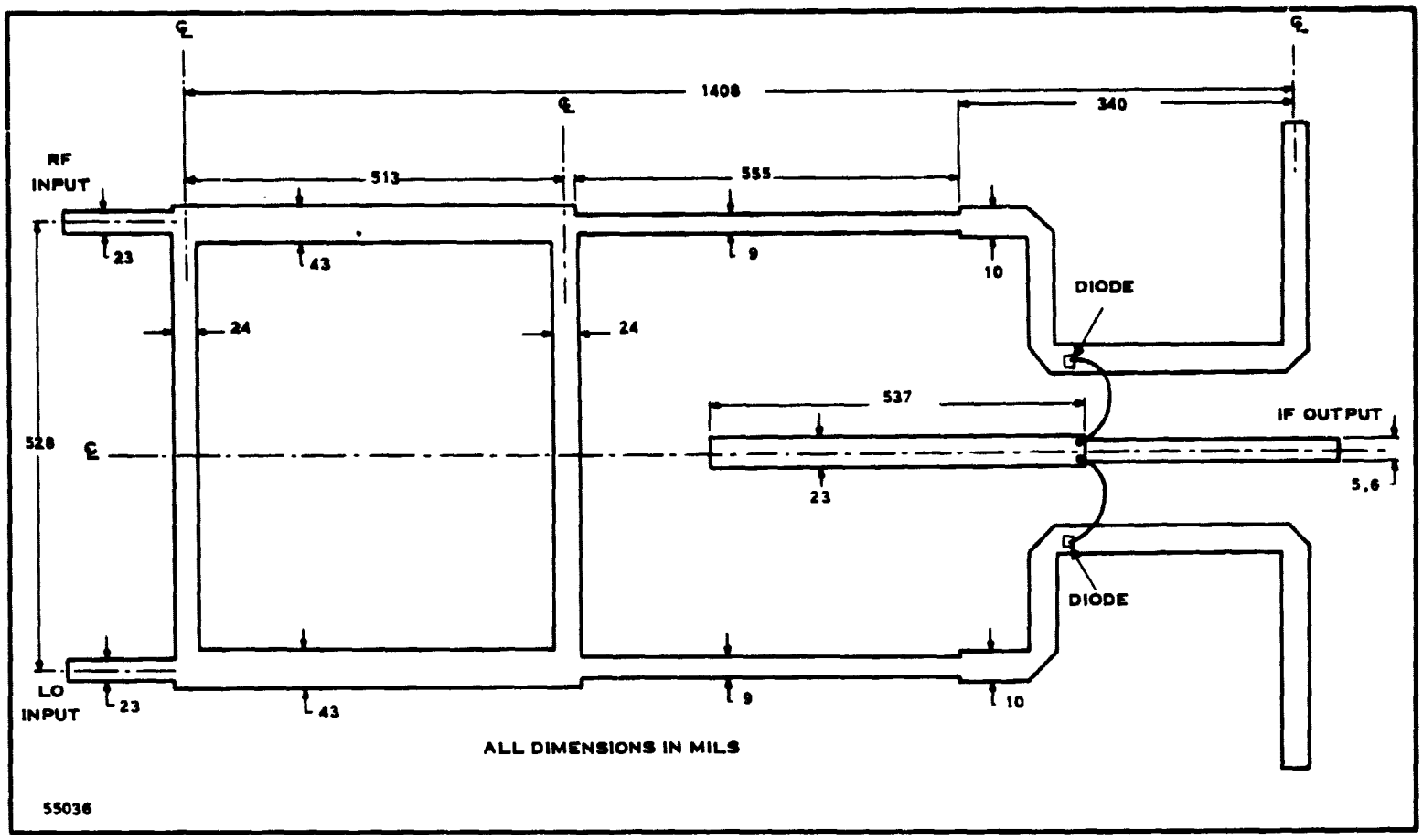

Figure 31. S-Band Balanced Mixer, Ceramic Layout

The line width of the 35-ohm line is

$$w = 2.15(20) = 43.0 \text{ mils} \tag{177}$$

$$Z_2 = 49 \text{ ohms} \tag{178}$$

$$\frac{w}{h} = 1.2 \tag{179}$$

$$S_f = 2.49 \tag{180}$$

$$\frac{\lambda_s'}{4} = \frac{5.25}{4(2.49)} \tag{181}$$

$$\frac{\lambda_s}{4} = 0.528 \text{ inch}$$

and for the 49-ohm shunt branch line

$$w = 1.2(20) = 24 \text{ mils.} \tag{182}$$

The final ceramic layout is shown in Figure 31. The mixer employs two gallium-arsenide diodes and the overall dimensions of the circuit are approximately 0.55 inch by 1.40 inches.

3. Local Oscillator

The local oscillator frequency is derived from a crystal-controlled oscillator operating at 107.5 MHz. A step recovery diode multiplier converts the output to 2150 MHz. A broadband amplifier between the oscillator and the multiplier supplies enough gain to drive the mixer with 20 mW of LO power. The design of the local oscillator and multiplier circuitry is discussed below.

a. Local Oscillator

The local oscillator frequency is derived from a crystal-controlled 107.5-MHz oscillator of a Butler configuration. The Butler oscillator uses two transistors, as shown in Figure 32. One transistor (Q1) operates as a common base amplifier with a tuned tank collector circuit. Transistor Q2 is a common emitter amplifier from which the output is taken. The crystal connects directly between the emitters of the two transistors.

The Butler oscillator as defined so far has a tendency to overdrive low power crystals (1 mW or less). Its frequency stability is also somewhat dependent on transistor characteristics. Therefore, a rectifier circuit of C7, CR1, and CR2 is added, which rectifies a small sample of the rf output and applies it to the base of Q1. The net effect of this dc feedback is to keep the gain of Q1 constant in spite of changing transistor characteristics. The result is that the crystal drive remains constant and the frequency of operation is dependent only on the crystal.

The dc biasing of the circuit is established for an emitter current of 3 mA and a static forward current gain (h_{FE}) of 25. The load of transistor Q_1 is the tuned network consisting of L_1, C_4, and C_5. Arbitrarily, selecting an inductance of 20 nH which is compatible with small geometry thin-film inductors, the total capacitance needed for resonance at 107.5 MHz is 109.5 pF.

The schematic diagram (Figure 32) shows that the series capacitance C_5 and C_6 are in parallel with C_4; neglecting stray capacitances and the device capacitances of Q_1 and Q_2, the total capacitance required for resonance is given

$$C_T = C_4 + \frac{C_5 C_6}{C_5 + C_6} = 109.5 \text{ pF}. \tag{183}$$

Then, letting $C_4 = 80$ pF

$$\frac{C_5 C_6}{C_5 + C_6} = 109.5 - 80 \text{ pF} \tag{184}$$

$$\frac{C_5 C_6}{C_5 + C_6} = 29.5 \text{ pF}.$$

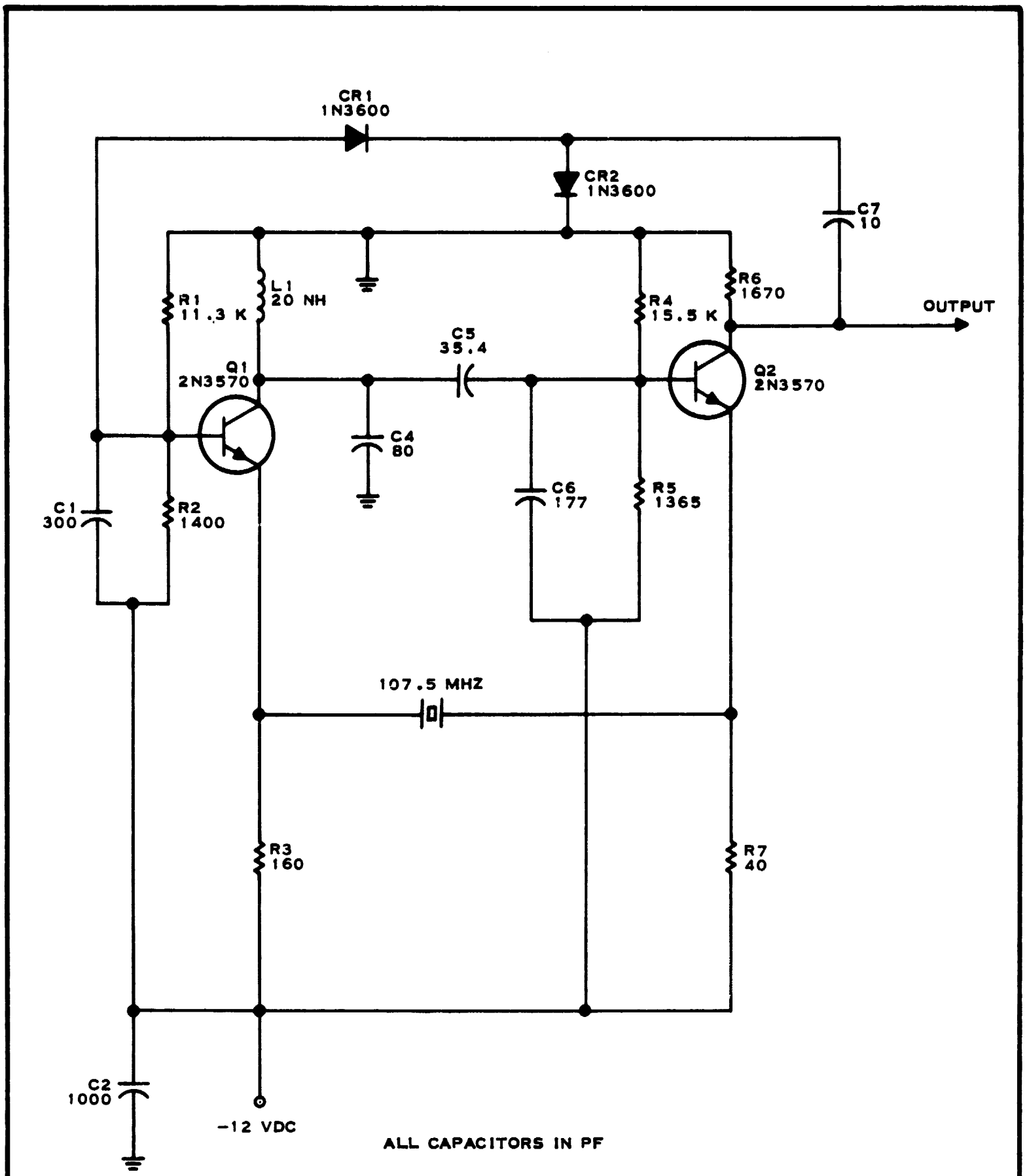

Figure 32. Crystal-Controlled Local Oscillator, Schematic Diagram

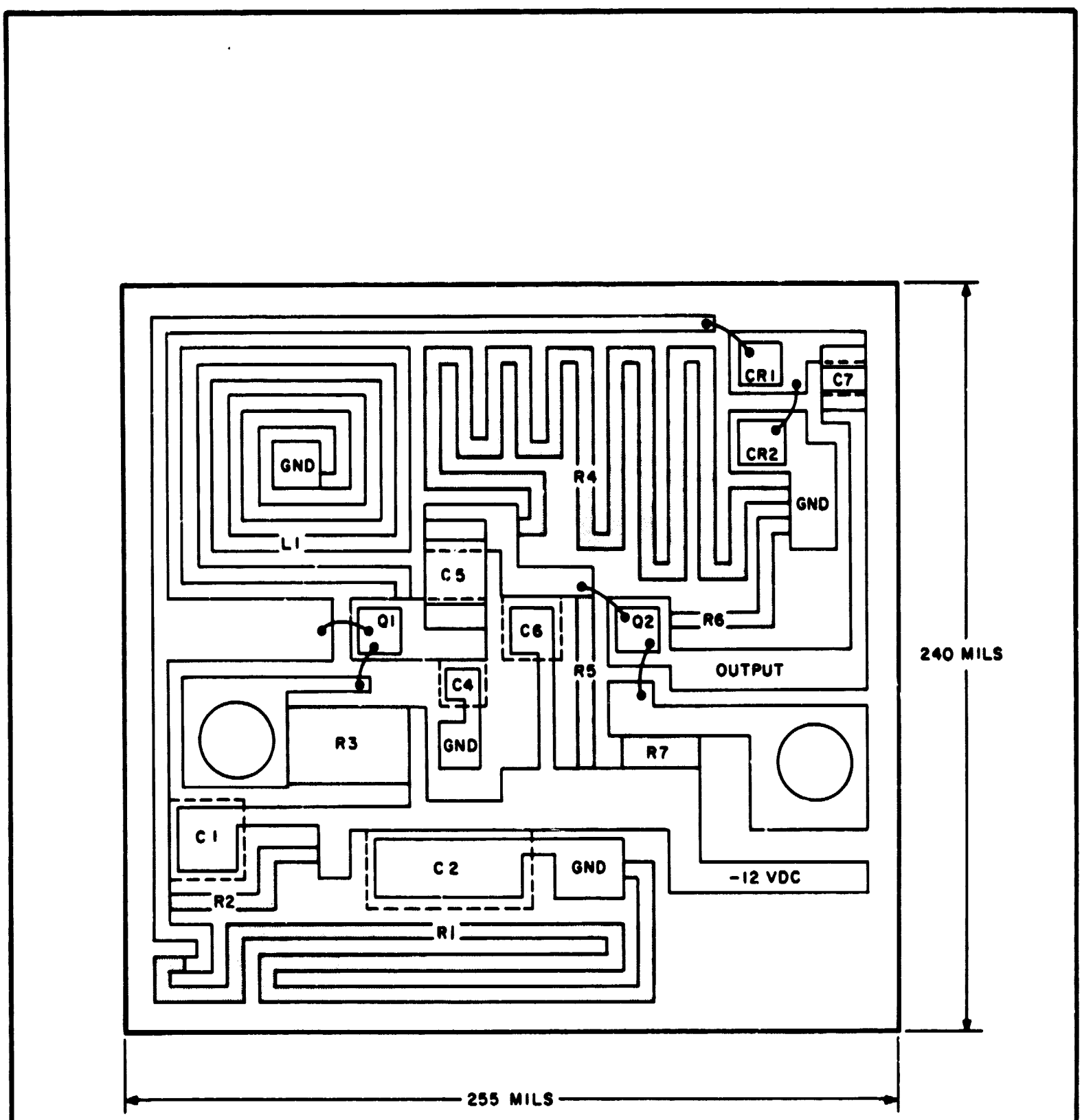

Figure 33. Receiver Crystal-Controlled Local Oscillator, Ceramic Layout

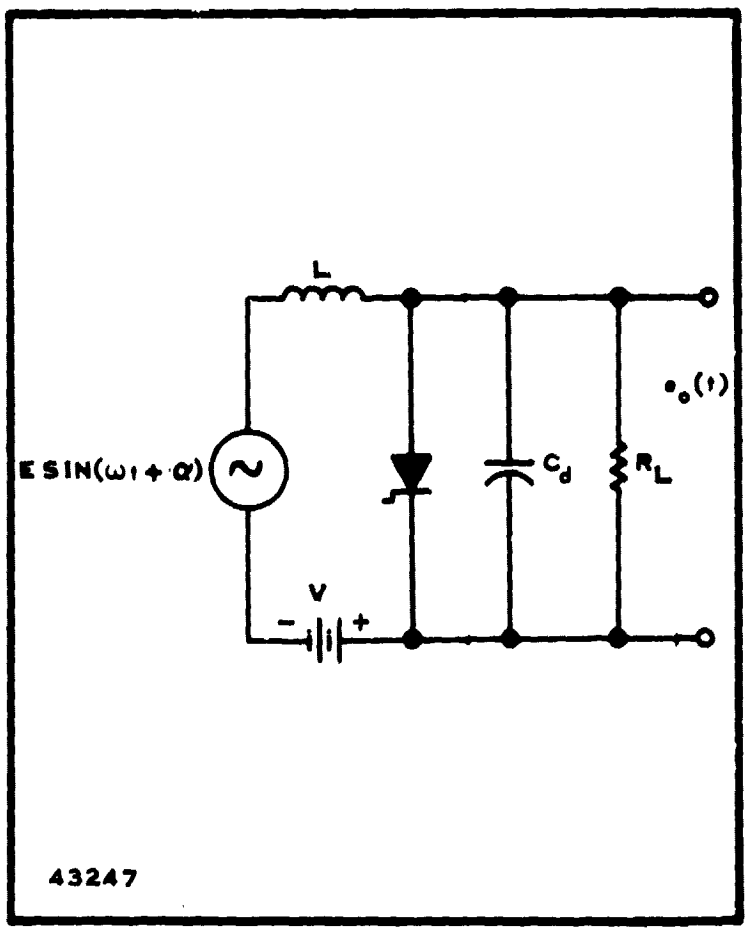

Figure 34. Step-Recovery Diode Equivalent Circuits

A satisfactory ratio of C_6 to C_5 to prevent the second transistor from loading the frequency resonant network is five. Therefore,

$$C_6 = 5\,C_5 \tag{185}$$

$$\frac{5\,C_5}{6} = 29.5\ \text{pF} \tag{186}$$

$$C_5 = 35\ \text{pF} \tag{187}$$

and from Equation 185

$$C_6 = 177\ \text{pF}. \tag{188}$$

The thin-film layout of the oscillator is shown in Figure 33.

b. The Multiplier

The LO frequency is derived by multiplying the output of the crystal oscillator. In this case, the 107.5-MHz oscillator frequency is multiplied by 20 to give 2150 MHz. This is achieved with a step-recovery diode. Figure 34 is the impulse generator circuit for this diode.

The step-recovery-diode characteristic allows it to change from a small resistance to a constant capacitance. The sudden insertion of a capacitor into the circuit causes an impulse-like function of very short duration. The impulse is very rich in harmonic content. The desired frequency is obtained by tuning the output to the desired harmonic. The efficiency is typically 1/n and may be improved to 2/n at higher orders of multiplication by proper matching. The efficiency of the ×20 multiplier is from 1/10 to 1/20 (−10 to −13 dB) dependent on the matching.

The output power of the local oscillator must be 20 mW or +13 dBm to ensure sufficient drive for the gallium-arsenide diodes used in the mixer. The output power of the crystal oscillator is approximately −8 dBm. If 13 dB is lost in the multiplier, the amplifier between the crystal oscillator and the multiplier must supply a power gain of 34 dB to provide +13 dBm drive to the mixer. The gain is supplied by the wideband amplifier (transistors Q_1 − Q_5) shown in Figure 35.

The step recovery diode provides a rich supply of harmonics. The task is to recover the 20th harmonic, however when properly biased, the diode is essentially a short circuit except during the short impulse cycle. The problem is one of sustaining an output when a short circuit exists. At least two methods are possible. First, consider a transmission line between CR3 and the load. The impulse will travel down the line to the load. If the load is not matched to the line, it will be partially reflected back. By the time it reaches the diode again, it will see a short circuit. It will then be inverted and travel back down the line. If the line length is one-quarter wavelength, the signal on the line will be a damped sinusoidal. The decay rate of this sinusoidal signal will be determined by the impedance of the output filter. The object is to make the decay rate fast enough that some oscillation is present during the entire period of the input frequency. When the output waveform is like that shown in Figure 36, the input to the load filter is always of constant frequency but varying amplitude, and the damped waveform decays to zero in one input period. Thus, the impulse energy is delivered to the load in one input period rather than one pulsewidth. The same power reaches the load, but the spectral distribution is changed so that the greatest portion of the energy is contained in the 20th harmonic. The damped waveform may now be filtered conventionally to obtain an output at nf_1.

The design of the multiplier is shown in Figure 35. The value of the drive inductor (L_2) is determined by the formula

$$L_2 = \frac{23.1}{C_{-10} f_o^2} \text{ nH} \qquad (189)$$

where f_o is the output frequency in GHz

C_{-10} is the capacitance in pF of the diode with 10 volts reverse bias.

Using an HPA 0300 step-recovery diode

$$L_2 = \frac{23.1}{4(2.15)^2} = 1.25 \text{ nH} \qquad (190)$$

In addition to making the input to the impulse generator purely resistive, capacitor (C_{10}) acts as a short to the output frequency and prevents its return to the input section. This capacitance is determined by

$$C_{10} = \frac{12.65}{L_2 (f_{in})^2} \text{ pF} \qquad (191)$$

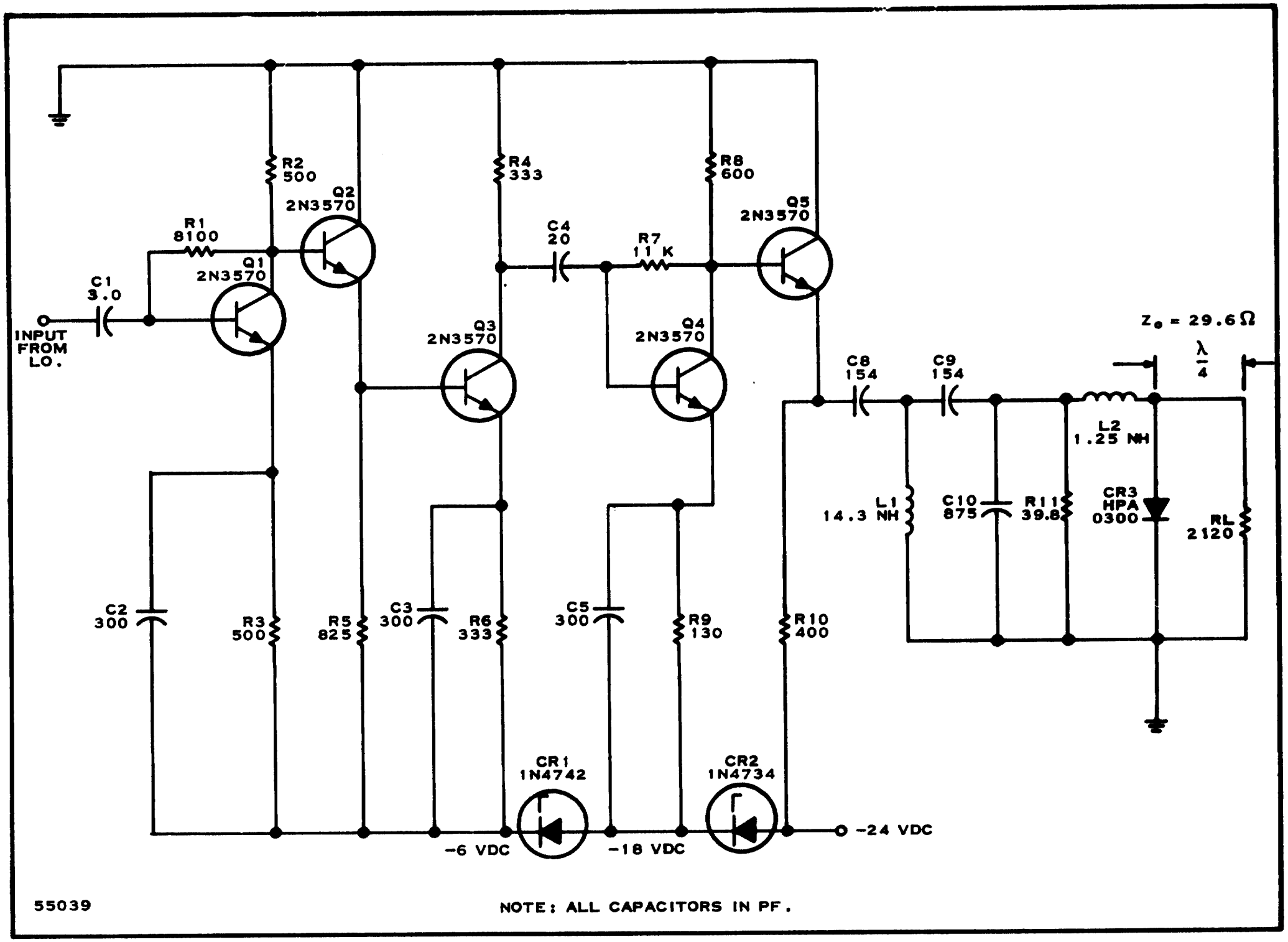

Figure 35. Receiver Local Oscillator Amplifier-Multiplier, Schematic Diagram

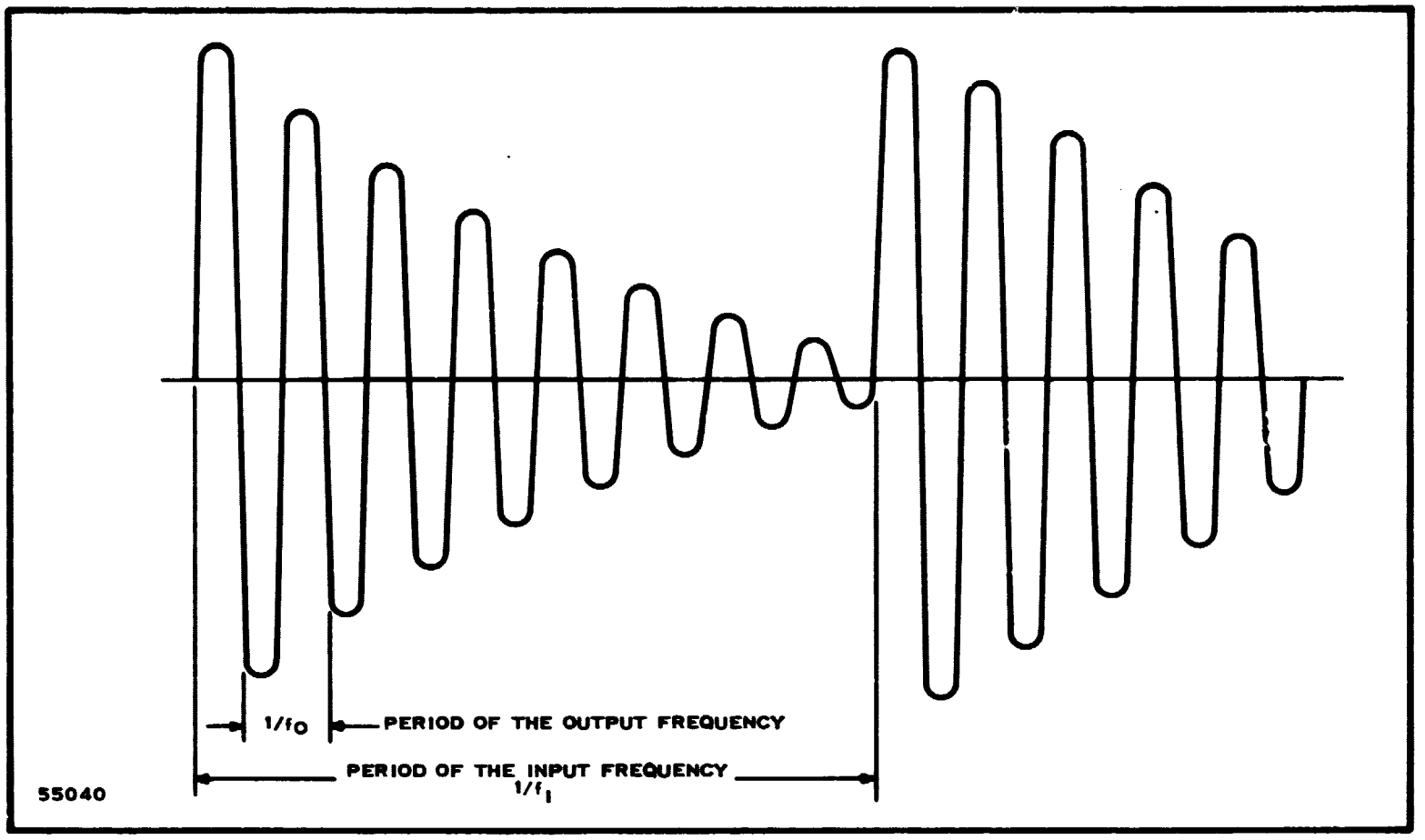

Figure 36. Output Waveform

where

L_2 is the value of the drive inductance in nH

f_{in} is the input frequency in GHz

and
$$C_{10} = \frac{12.65}{1.25\ (0.1075)^2} = 875 \times 10^{-12}\ \text{pF}. \qquad (192)$$

The input impedance to the impulse generator, consisting of C_{10}, L_2 and the step-recovery diode (CR3) is

$$Z_{in} = R_{in} = \frac{1}{2\pi N f_o\ C_{-10}}\ \text{ohms} \qquad (193)$$

where N is the order of multiplication

f_o is the output frequency

C_{-10} is the diode reverse capacitance at −10 volts

Substituting the above quantities

$$R_{in} = \frac{1}{2\pi(20)\ (2.15 \times 10^9)\ \ (4 \times 10^{-12})} = 0.925\ \text{ohms} \qquad (194)$$

The output impedance of transistor stage Q_5 is approximately 100 ohms so an impedance transformation ratio of 100 to 1 will be required. This is accomplished with C8, C9, and L_1.

Calculation of the values proceeds as follows

$$C_8 = C_9 = \frac{1}{2\pi f_{in}\sqrt{Z_1 Z_2}} \tag{195}$$

and

$$L_1 = \frac{\sqrt{Z_1 Z_2}}{2\pi f_{in}} \tag{196}$$

where

Z_1 is the input impedance of the impulse generator

Z_2 is the output impedance of transistor stage Q_5.

Thus,

$$C_8 = C_9 = 154 \text{ pF} \tag{197}$$

$$L_1 = 14.3 \text{ nH} \tag{198}$$

The diode is self-biased by the proper choice of resistor R_{11}, given by

$$R_{11} = \left(\frac{2}{\pi N^2 C_{-10}} \right) \tau \tag{199}$$

where τ is the effective minority carrier lifetime.

Thus, $$R_{11} = \left[\frac{2}{\pi (20)^2 \ 4 \times 10^{-12}} \right] 100 \times 10^{-9} = 39.8 \text{ ohms} \tag{200}$$

If the wave damps out before being reenergized, efficiency is decreased and harmonic and spurious emissions put more strenuous requirements on the output filter.

For proper matching between the step-recovery diode and the output filter, the characteristic impedance of the quarter-wavelength line must be,[19]

$$Z_o = 52.8 \sqrt{\frac{L_2}{C_{-10}}} \text{ ohms} \tag{201}$$

where

L_2 = drive inductance in nH

C_{-10} = diode reverse capacitance at −10 volts in pF

$$Z_o = 52.8\sqrt{\frac{1.25}{4}} = 29.6 \text{ ohms} \quad . \tag{202}$$

The input impedance to the filter must be

$$R_L = \frac{4NZ_o^2}{\pi Z_o - 3N} = \frac{4(20)\,(29.6)^2}{29.6\pi - 3(20)} = 2120 \text{ ohms} \, . \tag{203}$$

Another method for achieving the same result is to place a series-resonant circuit across the diode and tap off between the capacitor and the inductor. The diode impedance is less than 1 ohm after the impulse has been injected. The requirements for this circuit are the same as for the quarter-wave length line. It must have high enough Q to sustain oscillation for an input frequency period. Furthermore, the dissipation in L_1 and C_1 due to losses must be small compared to the dissipation in R_L.

The ceramic layout of the multiplier is shown in Figure 37.

4. Intermediate Stages

The intermediate stages following the mixer consist of the intermediate frequency amplifier and limiter. The intermediate frequency amplifier consists of a low noise input stage using a germanium VHF transistor followed by the broadband, untuned silicon stages. Intermediate frequency selectivity is obtained by a two-stage feedback bandpass amplifier that follows the three silicon-device amplifiers. The power gain of the first amplifier is 12 dB, the overall gain of the three silicon stages is 56.1 dB and the closed-loop gain of the bandpass amplifier is 38 dB. The total receiver gain from the input terminals to the limiter is calculated to be 106 dB.

For a signal level of −100 dBm applied to the input terminals of the receiver, the signal level applied to the limiter is +6 dB. The limiter has a power gain of 18 dB and a signal level of approximately +24 dBm is applied to the demodulator.

a. Intermediate Frequency Amplifier

The intermediate frequency amplifier must provide a 100-dB power gain and a 2.04-MHz bandwidth centered at the intermediate frequency. The schematic diagram of the amplifier is given in Figure 38 and the ceramic layout is illustrated in Figure 39.

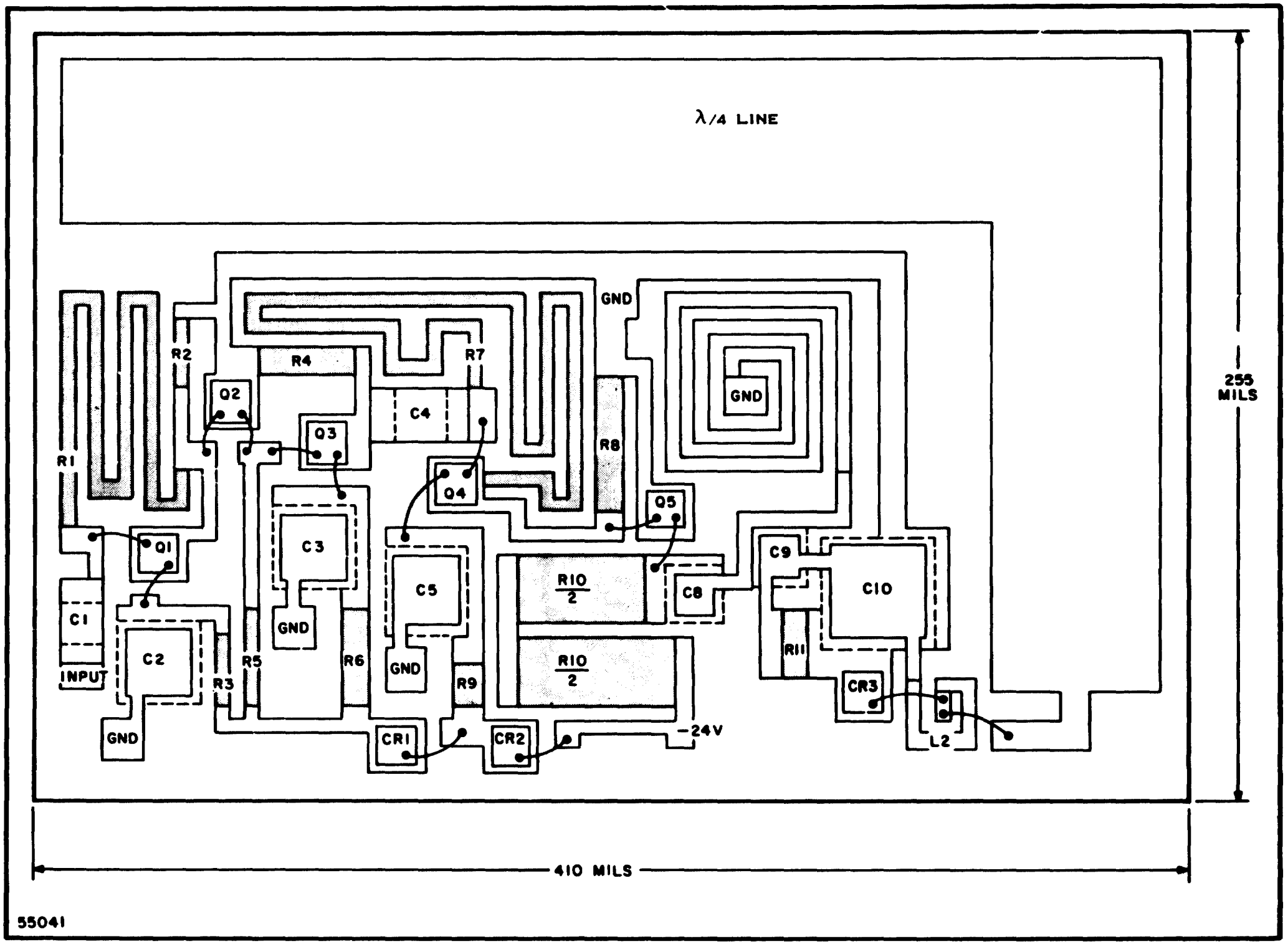

Figure 37. Receiver Local Oscillator/Amplifier-Multiplier, Ceramic Layout

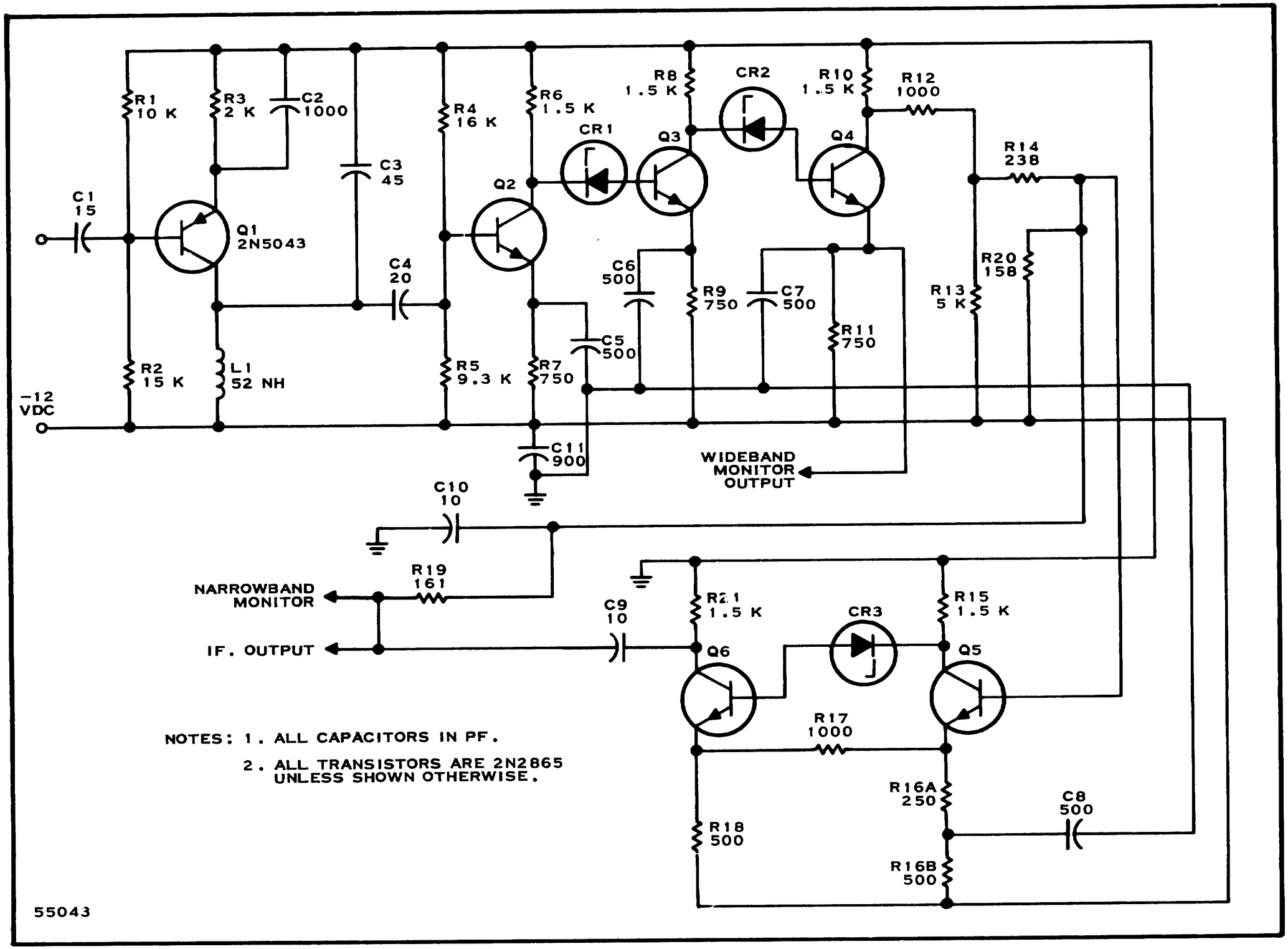

Figure 38. Receiver IF Strip, Schematic Diagram

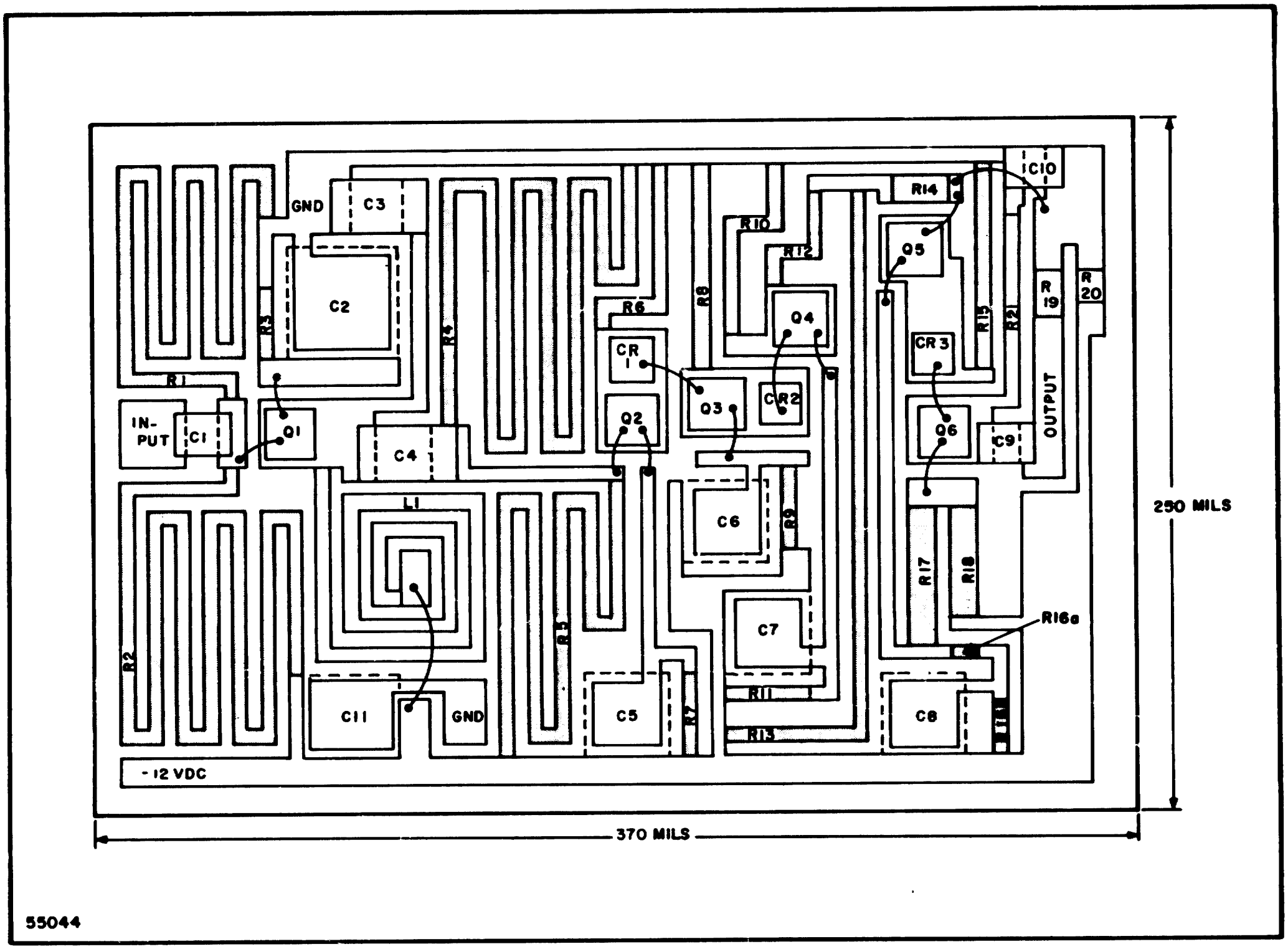

Figure 39. Receiver IF Strip, Ceramic Layout

(1) First Stage (Q_1)

The low noise requirement and high gain performance demanded of the first stage may be satisfied with a germanium VHF transistor, such as the 2N5043. The S-parameters of this transistor are given in Figure 40. The best noise performance of this transistor is obtained at 100 MHz. Therefore, the receiver intermediate frequency is selected to be 100 MHz. Selection of this frequency does not create spurious signals any closer than 50 MHz to the intermediate frequency and the image frequency is sufficiently removed from the operating range of the 2200- to 2300-MHz frequencies.

The lowest noise figure for the transistor may be obtained by mismatching the source impedance and transistor input impedance to obtain the optimum noise source resistance for the device. The optimum source resistance for a transistor may be written

$$R_{opt} = \left[(r_e + r_b')^2 + \frac{\alpha_o r_e (2r_b' + r_e)}{1/h_{FE}}\right]^{1/2} \qquad (204)$$

where r_e = emitter resistance (26 mV/I_e) ohms; I_e = emitter current in mA

r_b' = intrinsic base resistance, ohms

α_o = low frequency current ratio approximately equal to one

h_{FE} = static forward current gain.

For an emitter current of 3 milliamperes r_e is 8.6 ohms. Typical values of the remaining parameters are h_{FE} = 30, r_b' = 15 ohms. The resulting value of R_{opt} is

$$R_{opt} = \left[(23.6)^2 + \frac{8.6\ (30 + 8.6)}{1/30}\right]^{1/2} \qquad (205)$$

$$R_{opt} = 103 \text{ ohms}$$

The source resistance (R_s), which is the output impedance of the balanced mixer, is given

$$R_s = \frac{Z_{IF}}{2} \qquad (206)$$

where Z_{IF} is the intermediate frequency impedance of a single mixer diode. For Schottky barrier diodes, Z_{IF} ranges from 180 to 220 ohms, dependent on LO drive and rf source impedance. Normally, Z_{IF} is approximately 200 ohms which results in a source resistance,

$$R_s \sim 100 \text{ ohms}. \qquad (207)$$

TYPES 2N5043, 2N5044
P-N-P EPITAXIAL PLANAR GERMANIUM TRANSISTORS

[redacted]

$V_{CE} = -5$ V, $I_C = -3$ mA, $Z_G = Z_L = 50$ ohms + j0, $T_A = 25°C$

INPUT IMPEDANCE and
INPUT REFLECTION COEFFICIENT, S_{11e}

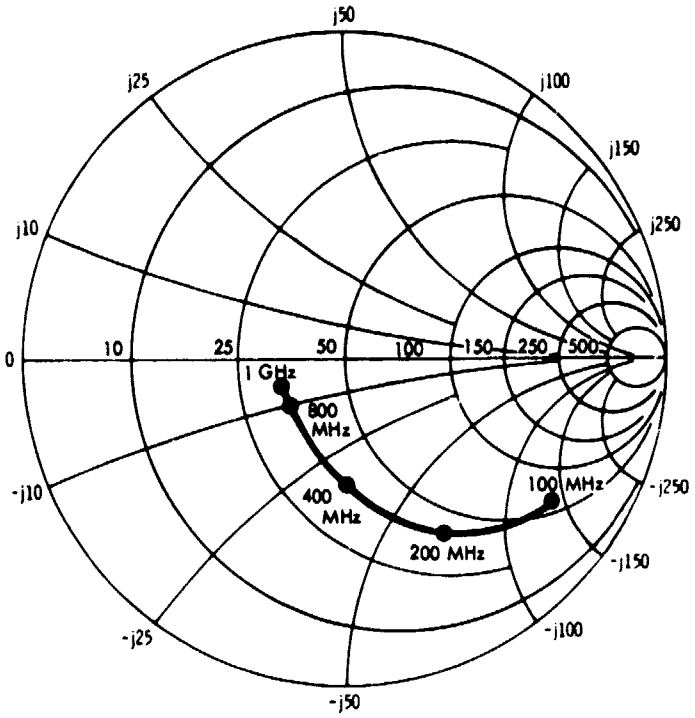

Coordinates in ohms

A

OUTPUT IMPEDANCE and
OUTPUT REFLECTION COEFFICIENT, S_{22e}

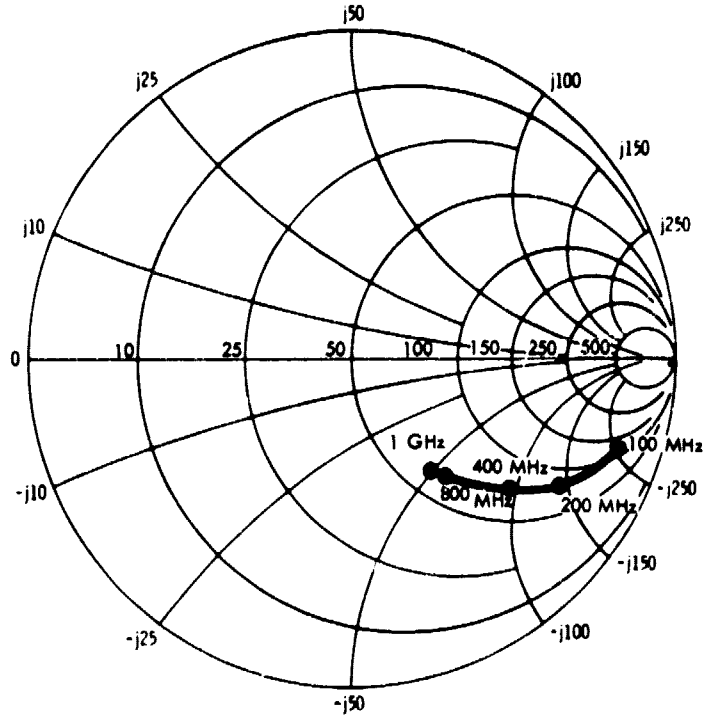

Coordinates in ohms

B

FORWARD TRANSFER COEFFICIENT, S_{21e}

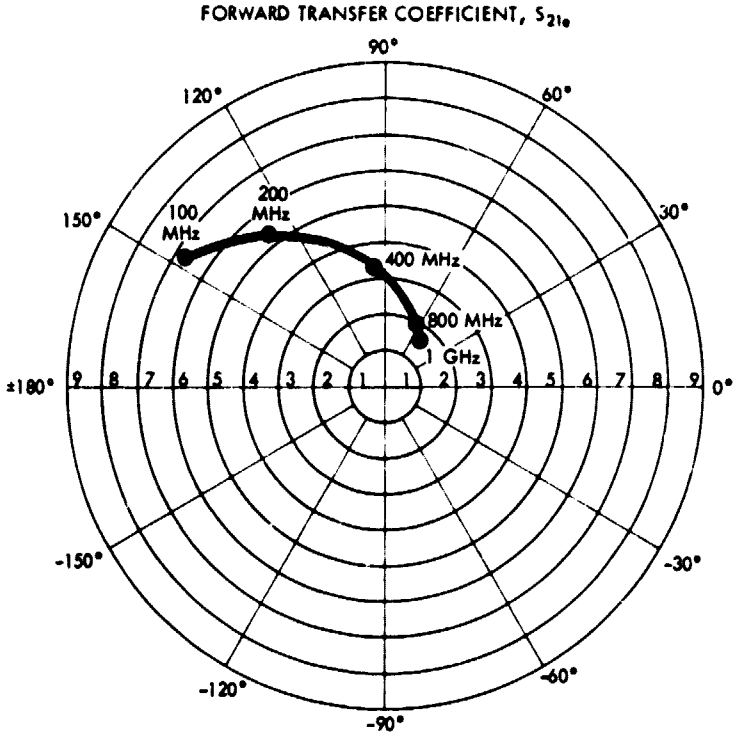

C

REVERSE TRANSFER COEFFICIENT, S_{12e}

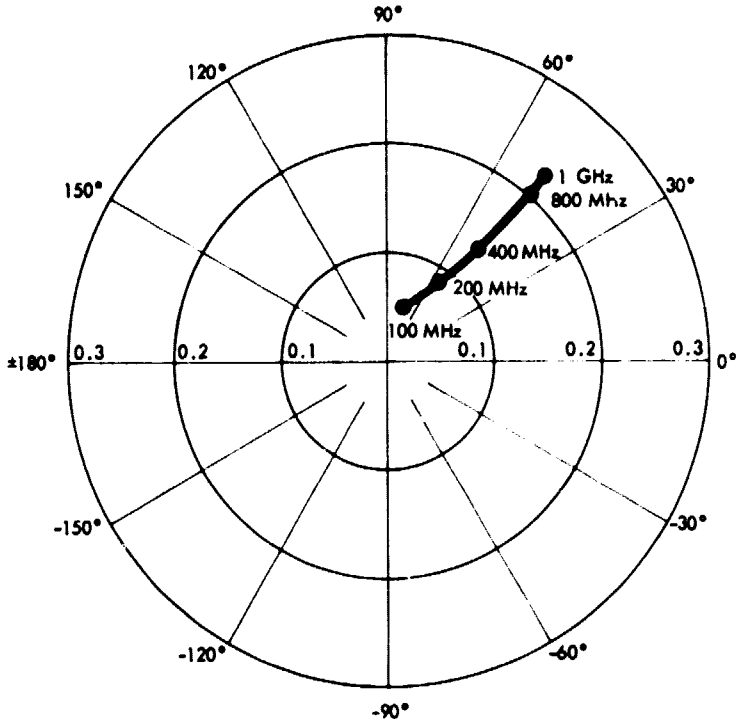

D

55042

Figure 40. 2N5043 Small-Signal Common-Emitter S-Parameters

This resistance is sufficiently close to the desired value that a matching network is not warranted.

The first stage transistor (Q_1) will be unconditionally stable at 100 MHz if the inherent stability factor (K) of the transistor is greater than unity and is positive at this frequency. The stability factor (K) in terms of the device S-parameters, is given

$$K = \frac{1 + |\Delta|^2 - |S_{11}|^2 - |S_{22}|^2}{2|S_{21}S_{12}|} \tag{208}$$

where $\Delta = S_{11}S_{22} - S_{12}S_{21}$.

At 100 MHz, the magnitude of above S-parameters is

$$|S_{11}| = 0.802$$

$$|S_{22}| = 0.881$$

$$|S_{21}| = -6.7$$

$$|S_{12}| = 0.25$$

The delta function is then

$$\Delta = S_{11}S_{22} - S_{12}S_{21} = (0.802)(0.881) - (0.25)(-6.7) = 2.73 \tag{209}$$

and

$$\Delta^2 = 5.63 \tag{210}$$

Substituting in the stability expression

$$K = \frac{1 + 5.63 - (0.802)^2 - (0.881)^2}{2|(-6.7)(0.25)|} = 1.57 \tag{211}$$

and the device is unconditionally stable for all possible values of loads. Maximum power gain is achieved when the device is conjugately matched at its input and output terminals. However, the mismatch at the input terminals to achieve optimum noise performance results in a power gain lower than the maximum gain which may be achieved.

The maximum available power gain of the device, expressed in terms of S-parameters, is the sum of three separate gain factors, given by

$$G_{max} = G_0 + G_1 + G_2 \text{ dB} \tag{212}$$

where G_0 is the power gain of the device when the input and output terminals are matched to 50 ohms. In this case, G_1, and G_2 are 0 dB, and G_0 is given

$$G_0 = 10 \log |S_{12}|^2 \tag{213}$$

At 100 MHz, S_{12} is 0.25 and the power gain (G_0), with the input and output terminals matched to 50 ohms, is

$$G_0 = 16.5 \text{ dB} \tag{214}$$

When the device is conjugately matched to its load, the power gain G_2 is defined

$$G_2 = 10 \log \left[\frac{1}{1 - |S_{22}|^2}\right] \tag{215}$$

and at 100 MHz, S_{22} is 0.881. Thus

$$G_2 = 10 \log \left[\frac{1}{1 - |0.881|^2}\right] = 6.5 \text{ dB} . \tag{216}$$

The input of the device is mismatched for best noise performance, which results in an input reflection coefficient of

$$\Gamma_1 = \frac{Z_{in} - R_{opt}}{Z_{in} + R_{opt}} \tag{217}$$

The power gain (G) is defined in terms of this reflection coefficient as

$$G_1 = 10 \log \frac{1 - |\Gamma_1|^2}{|1 - \Gamma_1 S_{11}|^2} \tag{218}$$

In Figure 40 the input impedance of the device at 100 MHz is given

$$Z_{in} = 62 - j\,140 \tag{219}$$

and the reflection coefficient resulting from mismatching this impedance to R_{opt} of 100 ohms is

$$\Gamma_1 = \frac{62 - 100 - j\,140}{62 - j\,140 + 100} = 0.679 \tag{220}$$

$$\Gamma_1 = 0.679$$

The power gain, G_1, then is given

$$G_1 = 10 \log \frac{1 - |0.679|^2}{\left[1 - (0.679)(0.802)\right]^2} = 4.14 \text{ dB} \qquad (221)$$

The total available power gain of the device at 100 MHz is found by summing the separate power gains. Therefore, the gain of the first transistor is given

$$G_{max} = G_0 + G_1 + G_2$$

$$= 16.5 + 4.14 \text{ dB} + 6.5 \text{ dB} \qquad (222)$$

$$G_{max} = 27.1 \text{ dB}$$

At least four stages with similar power gains are necessary to achieve the required overall power gain of 100 dB. In order to provide the 2.04 MHz bandwidth, each stage would ordinarily be tuned, with the bandwidth of each stage sufficiently wider than 2.04 MHz to allow for bandwidth shrinkage that results from cascading tuned networks. In microelectronics, thin-film inductors are conventionally of a spiral geometry which demands considerable area. Compact design results if the number of inductors is limited, making possible reduced dimensions in the final designed intermediate frequency amplifier. The inductors may be eliminated by using a RC notch filter as a feedback network around an amplifier to obtain intermediate frequency selectivity.

However, it still remains desirable to bandpass the mixer output spectrum in the first stage in order to filter intermodulation products before further amplification. Filtering the load of the first transistor with a simple single-tuned circuit provides a response that decreases beyond the 3 dB half-power points at the rate of 6 dB/octave. This rolloff does not provide sharp intermediate frequency selectivity and additional selectivity is provided by the feedback amplifier.

Design of the load and components required to determine the bandwidth are easily found by converting the output load, S_{22}^* to its parallel equivalent admittance. This is accomplished by rotating the point (G_2), shown on the Smith chart in Figure 41, 180 degrees.

$$Y_L = 20 (0.95 - j\, 0.14) = 19.0 - j\, 2.8 \text{ millimhos} \qquad (223)$$

The equivalent output capacitance of the device is given by the conjugate susceptance term of the load, b = j 2.8 millimhos.

$$C_0 = \frac{j\, 2.8 \times 10}{\omega_0} = \frac{j\, 2.8 \times 10^{-3}}{6.28\,(100)} = 4.4 \text{ pF} \qquad (224)$$

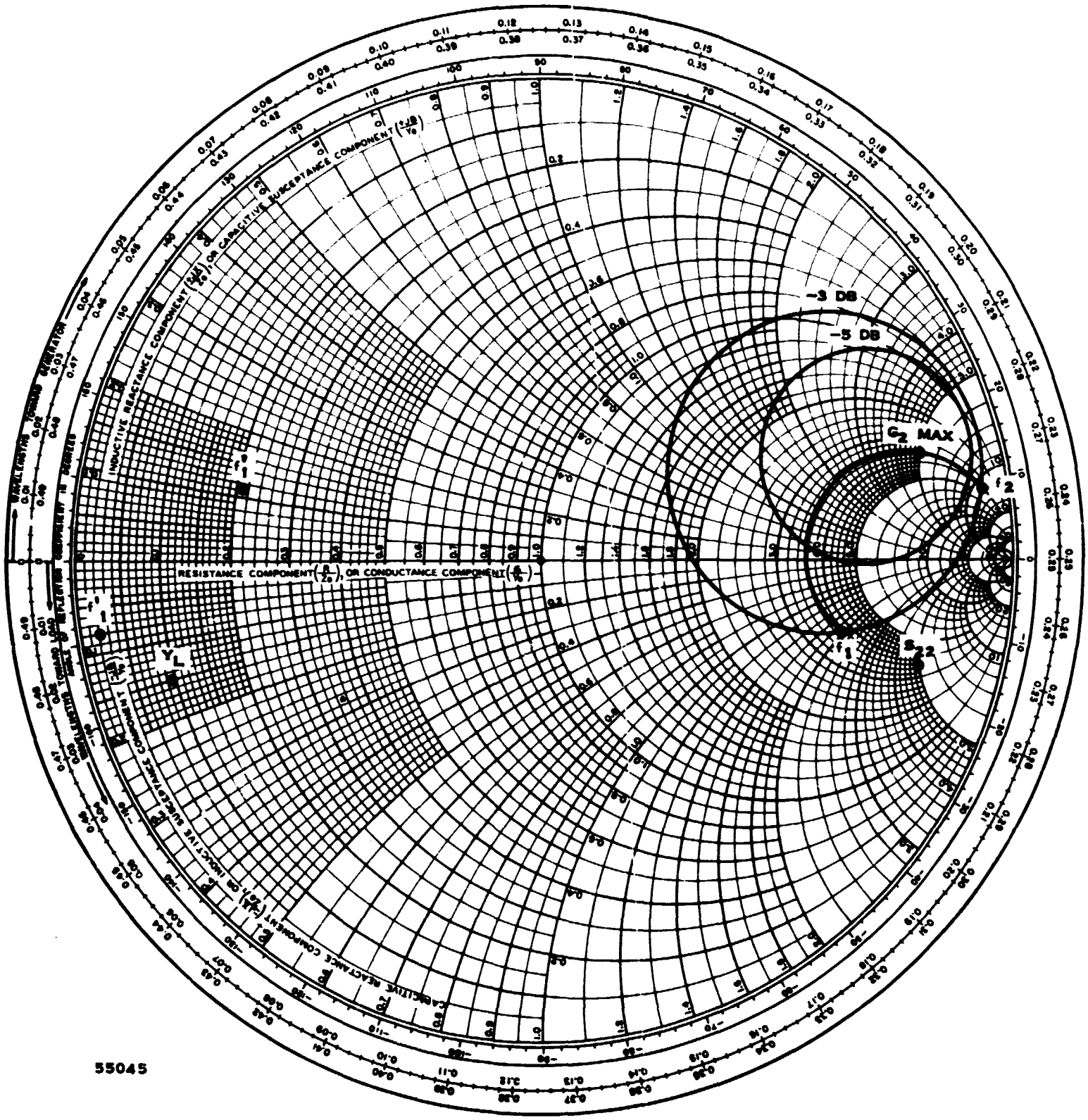

Figure 41. Smith Design for First IF-Stage Load

The external tank capacitance required to establish a 2.04-MHz bandwidth is given

$$C_e = C_T - C_0 \tag{225}$$

where C_T is the total capacitance indicated on the Smith chart as that required to determine the necessary bandwidth. The capacitance (C_T) is given

$$C_T = \frac{\Delta B}{2\omega_o} \tag{226}$$

where ω_o is the radian frequency (2π 100 MHz), and ΔB is the total change in load susceptance for the power gain (G_2) to be diminished 3 dB. In Figure 41, following the constant conductance circle passing through G_2 to its intercepts on the −3 dB power contour determines the total change in reactance. Rotating these intercepts 180 degrees, the equivalent change in susceptance is from j 0.12 to −j 0.08 millimhos. The total change is susceptance, ΔB is j −0.20 millimhos. Therefore,

$$C_T = \frac{0.20 \times 10^{-3}}{2\ (2.04\ \text{MHz})} = 49\ \text{pF}\ . \tag{227}$$

From Equation (225) the capacitance required to establish a 3-dB, 2.04-MHz bandwidth is

$$C_e = (49 - 4.4) = 45\ \text{pF}$$
$$C_e = 45\ \text{pF} \tag{228}$$

The required load inductance is found from the susceptance term in Equation (223), as

$$-2.8 \quad -2.8\ \text{millimhos} = \omega C_e - \frac{1}{\omega L} \tag{229}$$

from which

$$L = 51.5\ \text{nH} \tag{230}$$

(2) Untuned Stages (Q_2, Q_3, Q_4)

In the second and subsequent stages, silicon devices are used because they provide more stable performance with variations in temperature. These stages utilize 2N2865 silicon planar transistors which provide low-noise and high-gain performance at VHF. The y-parameters of

this transistor at 100 MHz are

$$y_{11} = 7 + j\,10 \text{ millimhos} \tag{231}$$

$$y_{22} = 0.1 + j\,1.5 \text{ millimhos} \tag{232}$$

$$y_{21} = 80 - j\,52 \text{ millimhos} \tag{233}$$

$$y_{12} = 0 - j\,6.0 \text{ millimhos} \tag{234}$$

when the device is biased at 4 mA and with $V_{CE} = 10V$. As previously mentioned, the use of inductors will be reduced by use of a feedback amplifier. Therefore, a bandpass two-stage amplifier will provide the necessary passband, in the last stages. Thus, the untuned amplifier is a broadband amplifier with a power gain determined by the resistive loading in the collector circuits. The emitter resistor of the second stage for a 4-mA biasing current is

$$R_E = \frac{V_{BB} - v_{be}}{I_e} = \frac{2.9 - 0.7}{4 \times 10^{-3}} = 550 \text{ ohms} \tag{235}$$

The collector resistor required for $V_c = 6$ volts is given

$$R_c = \frac{V_{cc} - V_{ce} - I_e R_E}{I_c} = \frac{12.0 - 3 - 3}{4 \times 10^{-3}} = 1500 \text{ ohms} \tag{236}$$

The mismatch between the load of the first transistor (Q) and the input impedance of the second transistor (Q2) results in an insertion loss (L),

$$L = 20 \log\left(\frac{I_2}{I_1}\right) \tag{237}$$

where I_2 is the current flowing into the second transistor and I_1 is the current supplied by the first transistor. In terms of load and second stage impedances, the insertion loss is

$$L = 20 \log\left[\frac{R_1}{R_1 + R_2}\right] \tag{238}$$

where R_1 is the real part of the second-stage input impedance

$$R_1 = R_e\left[\frac{1}{7 + j\,10}\right] = 47 \text{ ohms} \tag{239}$$

and R_2 is the real part of the load. From equation

$$R_2 = R_e \left[\frac{1}{1.9 - j\,2.8} \right] = 167 \text{ ohms} \tag{240}$$

The interstage-coupling insertion loss is

$$L = 20 \log \left[\frac{47}{160 + 47} \right] = -14 \text{ dB} \tag{241}$$

The first-stage power gain is then

$$G_{1st} = G_2 \text{ dB} - L = 27 - 14 = 13 \text{ dB} \tag{242}$$

The power gain of the transistor Q_2 is given

$$G_p = \frac{|y_{21}|^2 R_e Y_L}{|Y_L + y_{22}|^2 R_e \left(y_{11} - \frac{y_{12}y_{21}}{y_{22} + y_6} \right)} \tag{243}$$

The load presented to this transistor is the parallel combination of the collector resistor (R_6) and the input resistance of Q_3.

Interstage coupling between the second and third transistors is accomplished by a zener diode. For a +12-Vdc supply voltage, a 9.0-volt diode establishes 2.0 volts on the base of the second stage.

The Q_3 amplifier is identical to the Q_2 and the y-parameters given in Equations 231 to 233 define the input admittance of the third stage as

$$y_{in} = y_{11} = 0.1 + j\,10 \text{ millimhos} \tag{244}$$

The collector admittance of Q_2 is

$$y_c = \frac{1}{R_c} = \frac{1}{1.5 \text{ k}\Omega} = 0.66 \text{ millimhos} \tag{245}$$

and the load admittance of Q_2 is

$$Y_L = y_{22} + y_c + y_{11} = (0.1 + j\,1.5 + 0.66 + 7) \text{ millimhos} \tag{246}$$

$$Y_L = 7.76 + j\,1.5 \text{ millimhos} \tag{247}$$

Then the power gain of the second transistor driving a similar amplifier is

$$G_p = \frac{\left|\left(80 - j52\right) \times 10^{-3}\right|^2 \left(7.66 \times 10^{-3}\right)}{\left|7.76 + j\,1.5\right|^2 \mathrm{Re}\left[7.76 + j10 - \frac{(80 - j52)(6.0)}{7.76 + j1.5}\right]}$$

$$G_p = \frac{(9.1 \times 10^{+3})\,(7.66 \times 10^{-3})}{(193)\,(48.3) \times 10^{-3}} = 75.3 \qquad (248)$$

$$G_p = 75.3$$

The power gain in decibels is given

$$G = 10 \log G_p = 10 \log 75.3 = 18.7 \text{ dB} \qquad (249)$$

The noise figure of the second transistor (Q_2) is typically 2.0 dB, then the noise figure of the first two stages of the intermediate frequency amplifier is

$$NF = 10 \log \left[F_1 + \frac{F_2 - 1}{G_1}\right] \qquad (250)$$

where F_1 is the first stage noise factor (1.413) and F_2 is the corresponding noise factor of the second stage (1.585). The power gain of the first stage is 14 dB, and the noise figure is

$$NF = 10 \log \left[1.413 + 0.585\right] = 1.56 \text{ dB} \qquad (251)$$

This noise figure may be improved by ideally matching the output of the first stage to Q_2. This would provide maximum gain from the first stage, which would reduce the noise factor of Q_2. This would require enlarging the present intermediate frequency layout to accommodate an L-section impedance-matching network. However, it is more reasonable to first attempt to seek a lower noise figure in Q_1 by varying its emitter current.

(3) Feedback Amplifier

The last two stages of the intermediate frequency assembly form a feedback bandpass amplifier. The closed-loop gain of this network with two cascaded amplifiers with voltage gains A_5 and A_6 is given

$$G_{CL} = \frac{A_5 A_6}{1 - A_5 A_6 \beta} \qquad (252)$$

where β is the voltage-feedback ratio of the configuration. The schematic diagram of the feedback amplifier (Figure 42) shows that this feedback ratio is determined by resistor R_{20} which couples the voltage of R_{19} back to the input of Q_5. The feedback ratio is

$$\beta = \frac{R_{20}}{R_{19} + R_{20}} \tag{253}$$

The feedback is accomplished with a Wien-bridge network, and, if C_9 is made to equal C_{10}, the feedback ratio becomes

$$\beta = \frac{R_{20}}{R_{19} + 2R_{20} + j\omega_1 R_{19} C - j \frac{1}{\omega R_{20} C}} \tag{254}$$

$$\beta = \frac{1}{\frac{R_{19} + 2R_{20}}{R_{20}} + j \frac{\omega}{\omega_1} - j \frac{\omega_2}{\omega}} \tag{255}$$

where $C = C_9 = C_{10}$

$$\omega_1 = \frac{1}{R_{19} C} \tag{256}$$

$$\omega_2 = \frac{1}{R_{20} C} \tag{257}$$

and the closed-loop gain is

$$G_{CL} = \frac{A_5 A_6}{1 - A_5 A_6 \left[\frac{1}{\frac{R19 + 2R20}{R_{20}} + j \frac{\omega}{\omega_1} - j \frac{\omega 2}{\omega}} \right]} \tag{258}$$

With $C_9 = C_{10} = 10$ pF, the lower 3-dB frequency determines the R_{19} resistor in the Wien bridge

$$R_{19} = \frac{1}{\omega_1 C_1} = 161 \text{ ohms} \tag{259}$$

and the upper 3-dB frequency determines R_{20}

$$R_{20} = \frac{1}{2C} = 158 \text{ ohms} \tag{260}$$

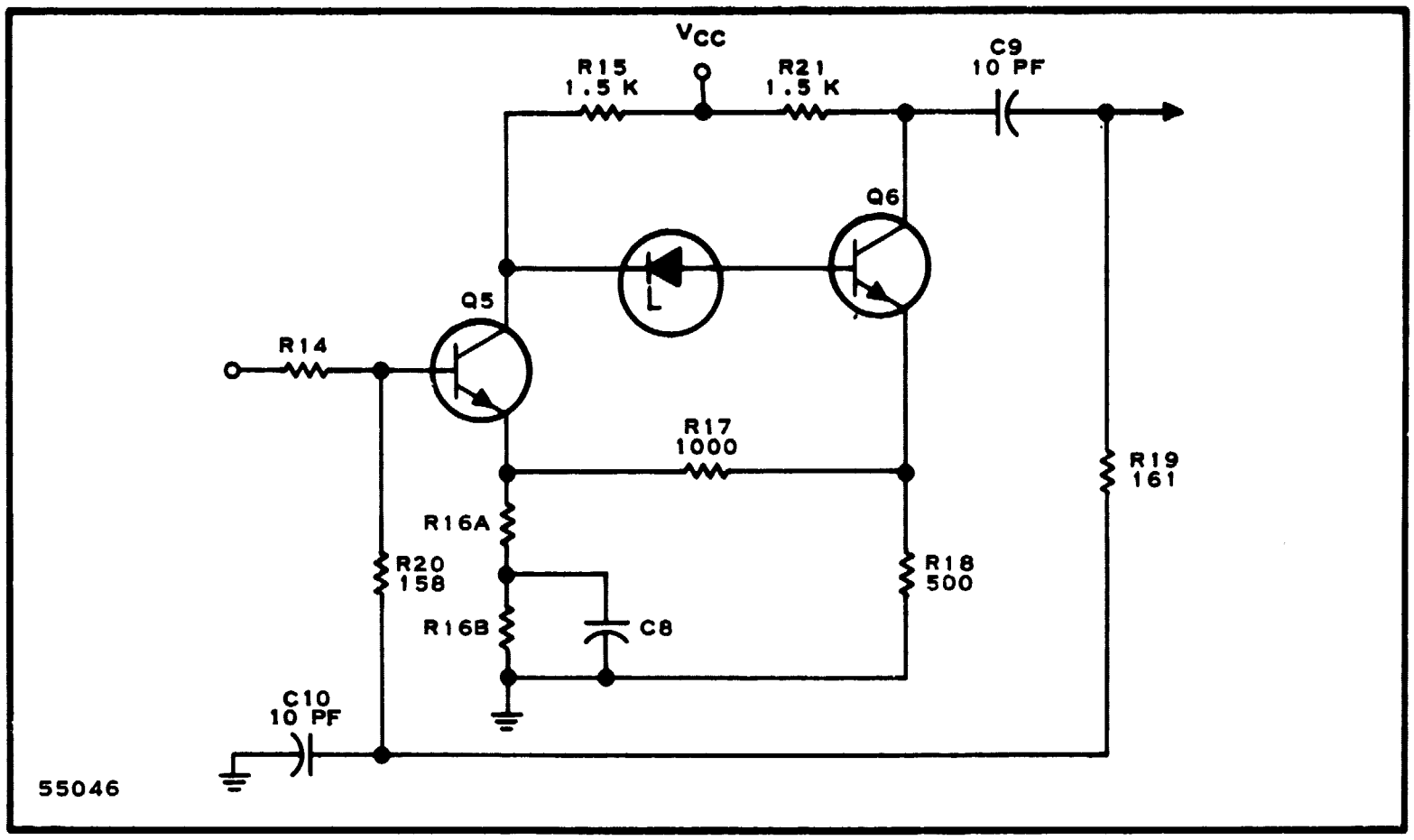

Figure 42. Feedback Amplifier, Schematic Diagram

The closed-loop gain at the resonance frequency is when $\frac{\omega}{\omega_1} = \frac{\omega_2}{\omega}$ is given from Equation 258 as

$$G_{CL} = \frac{A_5 A_6}{1 - A_5 A_6 \left[\frac{1}{3.02}\right]} \tag{261}$$

$$G_{CL} = \frac{3.02\, A_5 A_6}{3.02 - A_5 A_6} \tag{262}$$

It is seen that the feedback amplifier becomes unstable if $A_5 A_6$ equals or exceeds 3.02. Therefore, the open-loop voltage gain of the amplifier must be less than 3.02.

The voltage gain of the Q_6 is given

$$A_6 = \frac{R_{15}\, h_{fe\,2}}{R_{15} + R_{in}} \times \frac{R_{21}}{R_{in\,6}} \tag{263}$$

where

$$R_{in\,6} = (h_{ie})\,6 + (h_{fe})\,6\,\frac{R_{18}R_{17}}{R_{18} + R_{17}} \tag{264}$$

At 100 MHz, the parameters of the 2N2865 are

$$h_{ie} = 82 \text{ ohms}$$

$$h_{fe} = 5$$

Letting $R_{17} = 2\,R_{18}$, the input impedance of Q_6 in terms of its emitter resistance is

$$R_{in\,6} = 82 + 5 \cdot \frac{2}{3} R_{e2} = 82 + 3.33\,R_e \tag{265}$$

Biasing the second stage such that 2 volts is dropped across the emitter resistor when $I_e = 4$ milliamperes.

$$R_{18} = 500 \text{ ohms} \tag{266}$$

Then

$$R_{in\,6} = 82 + 3.33\,(500) = 1742 \text{ ohms} \tag{267}$$

For a 4-milliampere biasing current, the required collector resistor (R_{21}) for a voltage drop of 6 volts is 1.5 kilohms. Using a similar collector resistance in Q_5, the voltage gain of Q_6 is

$$A_6 = \left[\frac{(1.5\text{K} \quad 5)}{(1.5 + 1.74) \times 10^3}\right]\left(\frac{1.5 \times 10^3}{1.74 \times 10^3}\right) = 2 \tag{268}$$

The current gain of the Q_5, when degenerative feedback is used, is given

$$A_{I_5} = \frac{h_{fe_5} R_{15}}{R_{15} + h_{fe_5} \dfrac{R_{18} R_{17}}{R_{17} + R_{18}}} \tag{269}$$

Since $R_{17} = 2R_{18}$

$$A_{I_5} = \frac{h_{fe_5} R_{15}}{R_{15} + h_{fe_5} \frac{2}{3} R_{e18}} \tag{270}$$

For the 2N2865 transistor, $h_{fe_5} = 5.0$

$$A_{I_5} = \frac{(5)(1.5K)}{1.510 + 3.33\,(500)} \tag{271}$$

The voltage gain for Q_5 is given

$$A_5 = \frac{A_{I_5} R_L}{R_{in5}} = 2.37 \frac{R_2}{R_{in5}} \tag{272}$$

The load (R_L) seen by Q_5 is the parallel combination of R_{15} and the input resistance of Q_6

$$R_L = \frac{R_{15} R_{in6}}{R_{15} + R_{in6}} \tag{273}$$

where $R_{15} = 1.5$ kilohms, and R_{in_z} was given above as 1742 ohms. Therefore,

$$R_L = \frac{(1.5K)(1.74K)}{(1.5K + 1.74K)} = 805 \text{ ohms} \tag{274}$$

The input impedance of Q_5 is

$$R_{in_5} = h_{ie} + h_{fe} R_{16a} \tag{275}$$

where R_{16a} is the bypassed portion of R_{16}. For $R_{16a} = 250$ ohms

$$R_{in5} = 82 + 5(250) = 1332 \text{ ohms} \tag{276}$$

Therefore, the voltage gain of the Q_5 is

$$A_5 = 2.37 \times \frac{805 \text{ ohms}}{1.3 \text{ kilohms}} = 2.37 \times 0.618 = 1.46 \text{ volts} \tag{277}$$

The open loop voltage gain is then

$$G_{OL} = A_5 A_6 = (1.46)(2) = 2.92 \tag{278}$$

and from Equation 258, the closed-loop frequency response is

$$G_{CL} = \frac{A_5 A_6}{1 - \frac{A_5 A_6}{3.02 + j\frac{}{o} - \frac{o}{}}} \tag{279}$$

$$G_{CL} = \frac{A_1 A_2 \; 3.02 + j\frac{}{o} - \frac{o}{}}{3.02 - A_5 A_6 + j\frac{}{o} - \frac{o}{}} \tag{280}$$

where the nominal open-loop gain, $A_5 A_6$, is given by Equation 278 as

$$A_5 A_6 = 2.92 \tag{281}$$

Thus, the closed-loop gain at resonance is

$$G_{CL} = \frac{A_5 A_6 (3.02)}{3.02 - A_5 A_6} = 88.9 \tag{282}$$

$$G_{CL} = 20 \log 88.9 = 39.2 \text{ dB} \tag{283}$$

The bandwidth of the feedback bandpass amplifier is shown plotted in Figure 43 as it is determined by its closed-loop gain. The intermediate frequency passband response is seen to have poor selectivity. An improvement in response can be obtained by also using RC feedback networks in the untuned stages, Q_2, Q_3, Q_4. If each stage had been simply tuned, a 36-dB-per-octave roll-over could have been obtained. However, this would result in a much larger ceramic design. The best approach to obtaining good selectivity and small ceramic intermediate frequency amplifiers is still an unresolved problem.

b. Limiter

The clipping or limiting characteristic required in the receiver to remove unwanted amplitude variations from the input signal is achieved with a limiter. The limiter is shown schematically in Figure 44. The limiter network immediately follows the intermediate frequency amplifier, however, the limiter

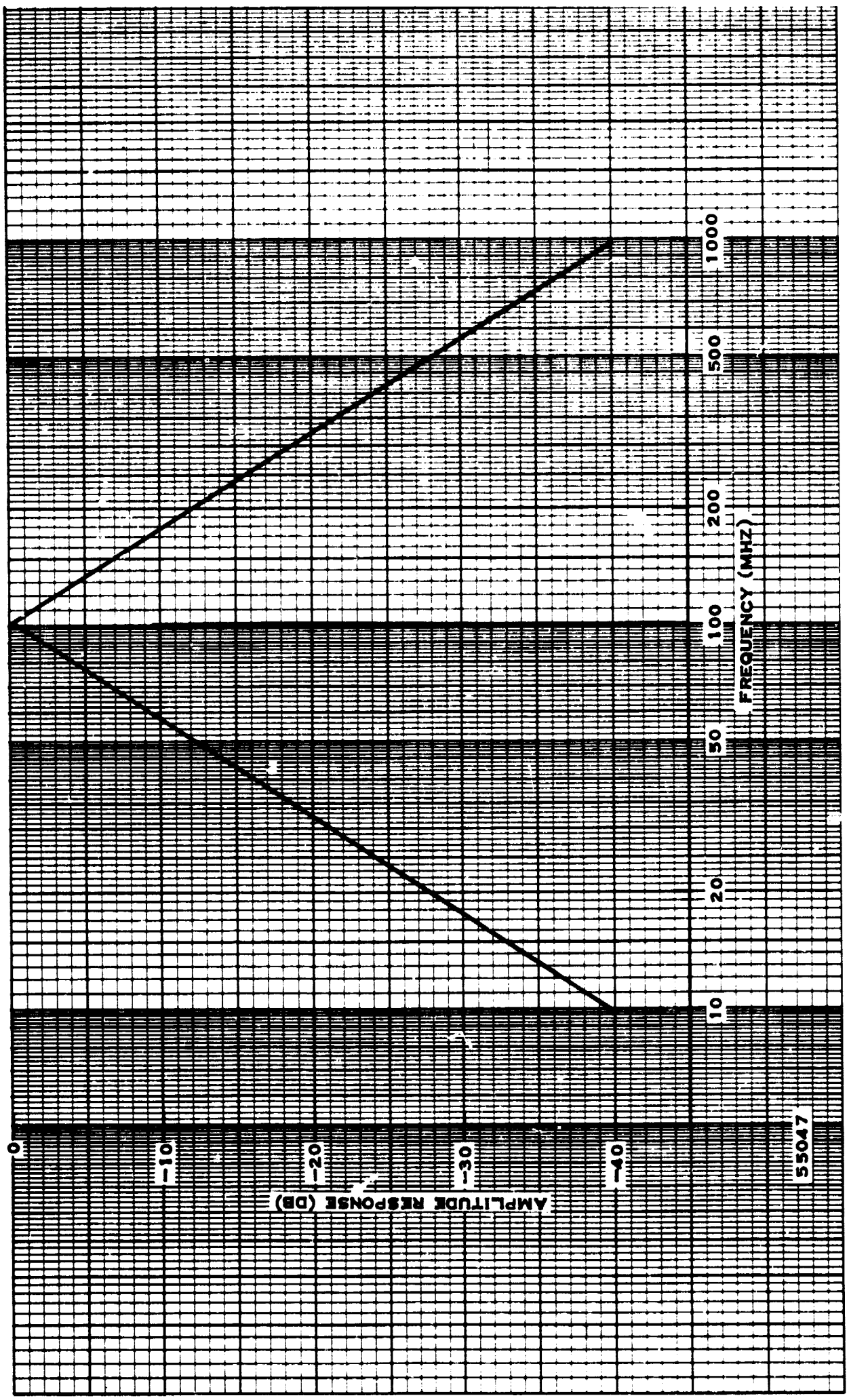

Figure 43. Intermediate Frequency Bandpass Response

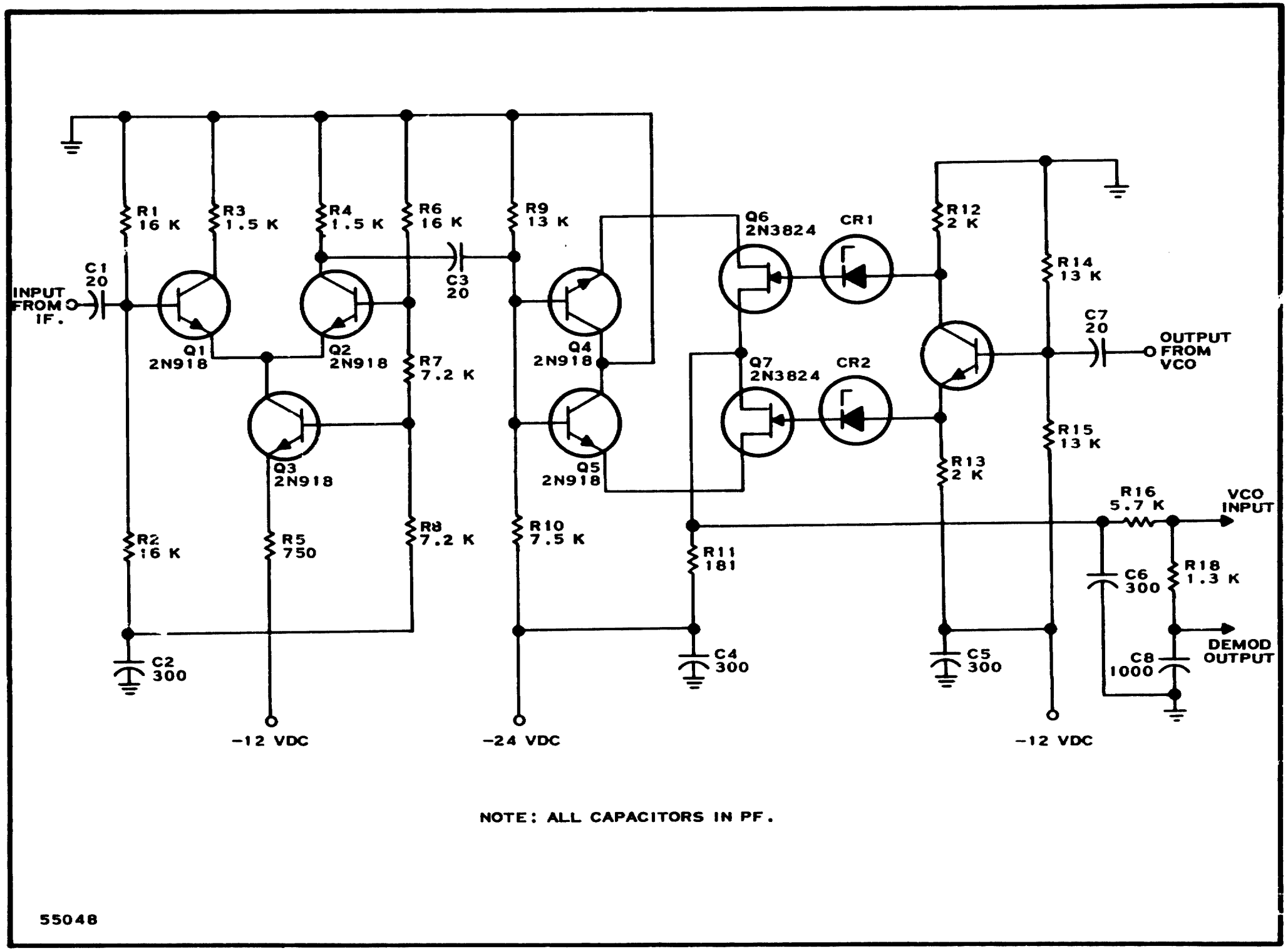

Figure 44. Receiver Limiter-Phase Detector, Schematic Diagram

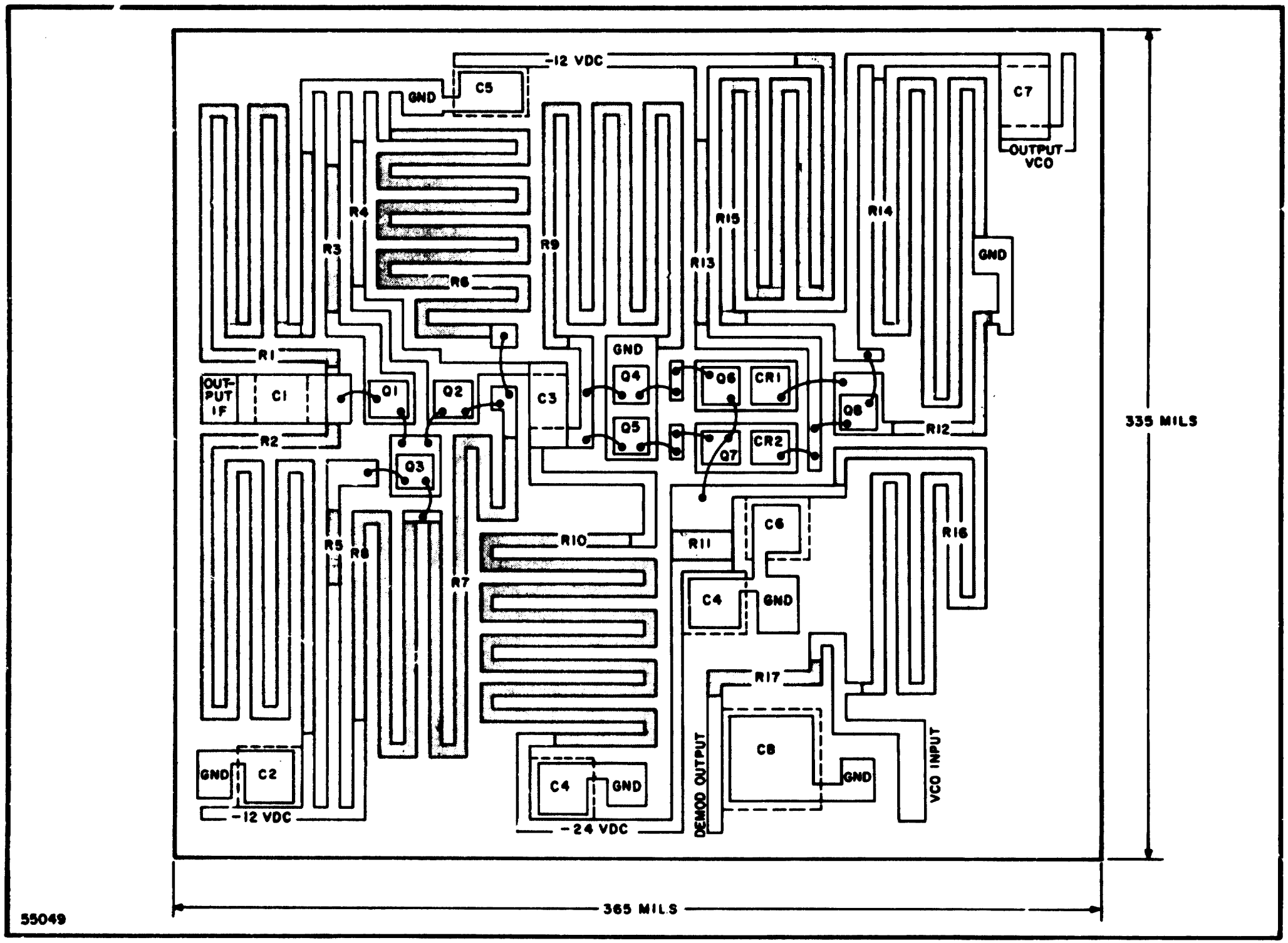

Figure 45. Receiver Limiter-Phase Detector, Ceramic Layout

is fabricated on the same substrate as the demodulator. The ceramic layout of the limiter is shown in Figure 45.

The limiter comprises three 2N918 silicon planar transistor chips which are 15 mils square. Transistors Q_1 and Q_2 are used in an emitter-coupled configuration. Transistor Q_3 is used as a common impedance shared by Q_1 and Q_2. For small-signal operation, the constant-current sink transistor (Q_3) is a large impedance, and the overall voltage gain of the network is

$$G_L = \frac{h_{fe}}{2\,(1 + hie/R_b)} R_L \tag{284}$$

where R_b is the parallel combination of the biasing resistors. Normally,

$$R_b >> hie \tag{285}$$

and the overall voltage gain is expressed,

$$G_L = \frac{h_{fe}}{2} R_L \tag{286}$$

Transistors Q_1 and Q_2 are biased using a single 12-Vdc supply with 2 mA of current flowing in each emitter. For a 3-volt drop across the respective collector resistors,

$$V_{CE_1} = V_{CE_2} = 3.0 \text{ volts} \tag{287}$$

and

$$R_{C_1} = R_{C_2} = 1.5 \text{ kilohms}$$

The small-signal current-transfer ratio h_{fe} of the 2N918 at 100 MHz is 6, therefore, the voltage gain of the limiter is,

$$G_L = (3.0)\,(1.5K) = 4.5 \times 10^3 \tag{288}$$

Approximately 6 volts is established at the emitter junction of Q_1 and Q_2 and the combined emitter current flowing through Q_3 is 4 mA. For V_{CE} = 3 volts and three volts dropped across R_E,

$$R_E = \frac{3.0 \text{ volts}}{4.0 \text{ mA}} = 750 \text{ ohms} \tag{289}$$

In thin-film technology, it is desirable to limit resistor values to less than 15 kilohms in order to control tolerance and to limit component size. Thus, to establish the proper bias voltage at the base of each of the emitter-coupled transistors, smaller biasing resistors are used as compared to those used in conventional design. The necessary biasing resistors for a single supply voltage may be determined,

$$R_b = \frac{V_{CC} - V_B}{I_B - I_2} \tag{290}$$

where

R_b = parallel combination of biasing resistors

I_B = base current of either Q_1 or Q_2

V_B = base bias voltage

I_2 = current flowing in R_2 to establish V_B

If $V_B = V_{CC/2}$, then $R_b = \frac{R}{2}$

where $R = R_1 = R_2$, then

$$R = \frac{2\left[V_{CC} - V_B\right]}{I_B - I_2} \tag{291}$$

$$R = 2V_{CC}\left[1 - 1/2\right]/\left(I_B + I_2\right) \tag{292}$$

The current (I_2) is sufficiently larger than the required base current (I_B) to ensure stability with temperature variations. Therefore,

$$I_2 = n I_B$$

where n is an integer.

$$R = \frac{V_{CC}}{I_B\left[1 + n\right]} \tag{293}$$

where $I_B = I_C/h_{FE}$

$$R = \frac{V_{CC} h_{FE}}{I_C\left[1 + n\right]} \tag{294}$$

and $I_C = aI_E + I_{CBO}$

$$R = \frac{V_{CC} h_{FE}}{\left[aI_E + I_{CBO}\right]\left[1 + n\right]} \tag{295}$$

where a is the low frequency current ratio.

At T = 25°C, I_{CBO} = 10 n A, and letting n = 10

$$R = (12)(30)/\left[0.98\left(2 \times 10^{-3}\right) + 10 \times 10^{-9}\right][11] = 16.4 \text{ kilohms} \tag{296}$$

Therefore, the base resistors necessary to establish 6.0 volts on the base of Q_1 or Q_2 are

$$R_1 = R_2 = 16 \text{ K}$$

The resistors required to establish 3.0 volts on the base of Q_3 are determined in similar fashion, where V_{CC} for this transistor is 6.0 volts. From Equation 295,

$$R = \frac{6(30)}{\left[0.98\left(4 \times 10^{-3}\right) + 10 \times 10^{-9}\right][1 + n]} \tag{297}$$

and for n = 5

$$R = 7.2 \text{ kilohms} \tag{298}$$

Hard limiting occurs when a signal swing of ±1.5 volts exists across R_{C2}. This corresponds to a rms signal of 1.06 volts. The voltage gain of the circuit is

$$G_L \cong \frac{h_{fe}}{2} R_{C1}$$

$$\sim 3.0\left(1.5 \times 10^{3}\right) \tag{299}$$

$$\sim 4.5 \times 10^{3}$$

The input signal required when 1.5 volts is developed across R_{C1} is then

$$e_{in} = \frac{e_o}{G_L} = \frac{0.707(1.5)}{4.5 \times 10^{2}} = \frac{1.06}{4.5 \times 10^{3}} = 0.235 \text{ volts.} \tag{300}$$

For a 50-ohm system, referenced to one millivolt the input power level required for limiting is

$$P = \frac{E^2}{50} \text{ watts}$$

$$P = \frac{\left(2.35 \times 10^{-4}\right)^2}{50} = \frac{5.53 \times 10^{-8}}{50} = 1.1 \times 10^{-9}\ \text{W} \qquad (301)$$

referenced to 1mW

$$P_{dBm} = 10 \log \frac{0.11 \times 10^{-6}\ \text{mW}}{1\text{mW}} \qquad (302)$$

$$P_{dBm} = -69.6\ \text{dBm}$$

5. Demodulator

Previously, a phase-locked demodulator following the first stage mixer was demonstrated to meet the system performance requirements. It was assumed that a demodulator could be constructed which would provide the desired demodulation properties at an operating frequency of 100 MHz. In this section, the feasibility of this concept is further explored by examining the design of the components making up a 100-MHz phase-locked demodulator.

The ceramic layout of the demodulator limiter-phase detector is shown in Figure 45. The demodulator is constructed on two separate substrates; one consisting entirely of a voltage-controlled oscillator (VCO); the other contains the amplitude limiter, phase detector, and low-pass loop filter.

The entire demodulator is designed using thin-film, hybrid techniques. However, it is entirely feasible that the complete demodulator could be made using monolithic processes.

a. The Phase Detector

The output of the limiter stage and the VCO output are multiplied in the phase detector shown in Figure 46. The output voltage from the phase detector is proportional to the instantaneous product of the two input signals and is supplied to the loop filter.

The phase detector performs as a synchronous detector producing sum and difference terms of the input quantities. This is shown in Figure 46, where an input signal is compared in phase with a reference signal of the same frequency. The output signal is proportional to the difference in phase between the two input signals and is given

$$V_d = K_d \sin \phi_{e(t)} \qquad (303)$$

The double frequency term is filtered by the following loop filter. For small phase errors,

$$\sin \phi_{e(t)} \sim \phi_{e(t)}. \qquad (304)$$

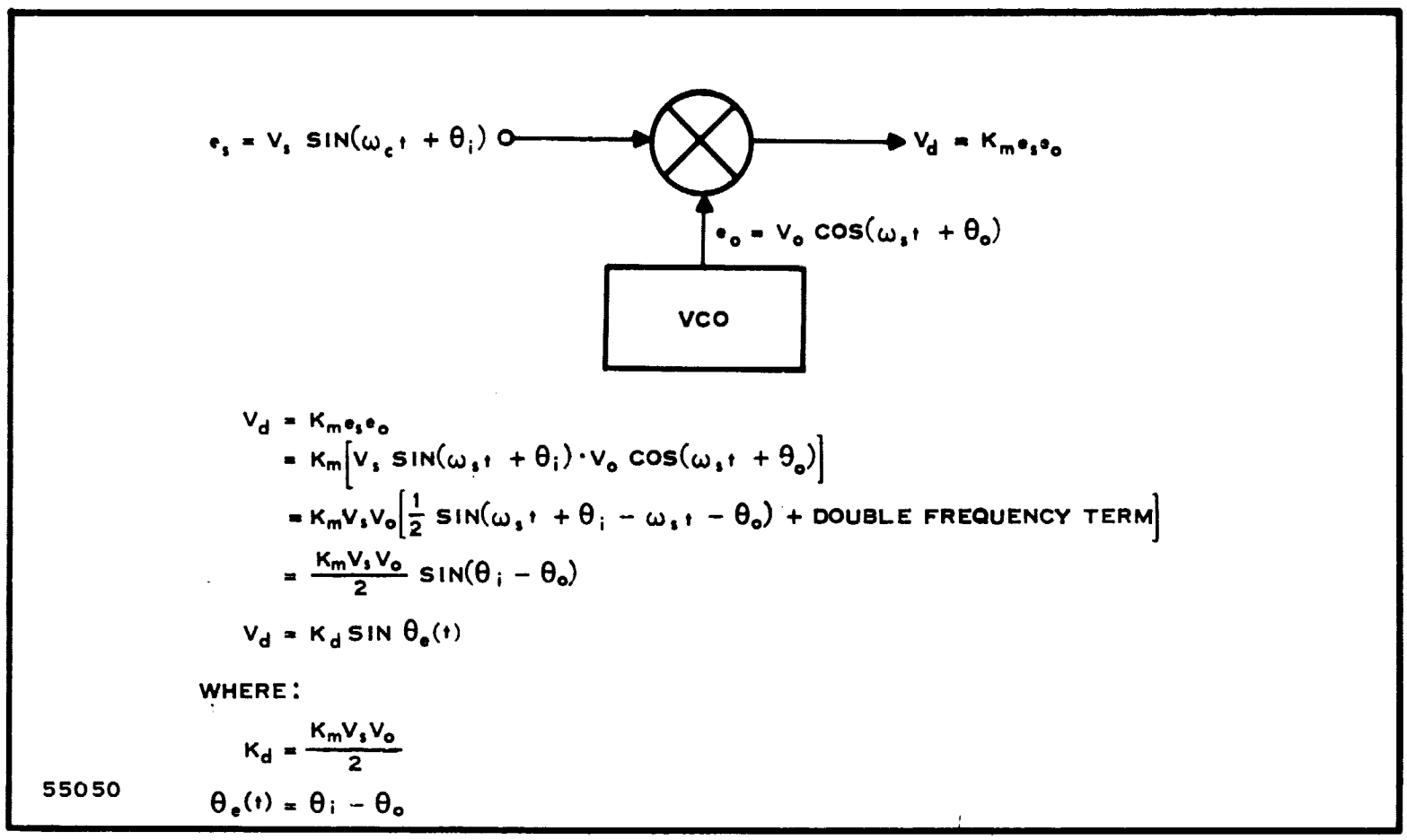

Figure 46. Block Diagram of the Phase Detector

In the case of a phase detector with a sinusoidal output characteristic, this relation is true for phase error less than 30 degrees. Since the phase detector is preceded by a limiter, the output characteristic is not sinusoidal and linearity holds for larger ranges of phase error. Under the assumption that the phase error is not excessive, the output voltage of a linearized phase detector is

$$V_d \sim K_d \phi_{e(t)} \tag{305}$$

where K_d is the gain sensitivity of the detector in volts/degree.

The phase detector uses two silicon N-channel junction FET's i' a balanced configuration. The near ideal square-law transfer characteristic of FET's minimizes distortion and cross modulation products. The input signal to the phase detector is supplied from a transistor that provides the necessary 180-degree phase relation between the gate junctions of the FET's.

Each FET is operated such that the gate-source voltage, V_{gs}, does not exceed the value of pinch-off voltage, V_p. Therefore, biasing the FET's must satisfy

$$|E_o| + |E_s| \leq \frac{V_p}{2} \tag{306}$$

where

$|E_o|$ = peak VCO voltage

$|E_s|$ = peak signal voltage

For the 2N3823 FET, $V_p = -5.6$ volts. The peak VCO signal is 3.0 volts, and the peak signal level out of the limiter is 1.5 volts at threshold.

The difference in the FET currents, i_{d1} and i_{d1}, flowing in the load resistance, R_L provides the output current

$$i_o = i_{d_1} - i_{d_1} = G_1 V_{d_1} - G_2 V_{d_2} \tag{307}$$

where G_1, G_2 describe the channel conductance

$$G_1 = G_2 = G_0 \left[1 - \left(\frac{V_{gs}}{V_p}\right)\right] \tag{308}$$

The value of conductance when the gate-source voltage (V_{gs}) is zero is given by G_0. The output current is then expressed

$$e_o = G_0 \left[1 - \frac{V_{gs1}}{V_p}\right] V_{d_1} - G_0 \left[1 - \frac{V_{gs2}}{V_p}\right] V_{d2} \tag{309}$$

where V_d is the signal supplied by the

The gate-source signal voltage is given

$$V_{gs1} = V_g - e_o \tag{310}$$

$$V_{gs2} = V_g + e_o \tag{311}$$

Thus,

$$i_o = G_0 \left[1 - \frac{(V_g - e_o)}{V_p}\right] e_s - G_0 \left[1 - \frac{(V_g + e_o)}{V_p}\right] e_s \tag{312}$$

$$i_o = \frac{2G_0 e_s e_o}{V_p} \quad .$$

The phase detector output is proportional to the product of the two input signals. The above expression assumes perfectly matched FET's, that is $G_{01} = G_{02}$. Actually a small direct offset current will be present in the output due to mismatched components.

The output voltage of the phase detector is given:

$$e_L = i_o R_L \tag{313}$$

The load resistance is determined by the biasing conditions, $V_{gs} = -1.5$ volts. The resistance required to establish this voltage when both FET's are biased with 4 mA is

$$R_L = \frac{V_{BB} - V_{gs}}{I_{D_1} + I_{D_2}} = \frac{(3.0 - 1.5) \times 10^3}{8} = 188 \text{ ohms} \tag{314}$$

The voltage, V_{BB}, is derived from the quiescent collector and emitter voltage of the single transistor providing the phase inversion to the separate FET gates. These voltages are 6.0 volts and Zener diodes are necessary to reduce the voltages to 3.0 volts.

The conductance G_0 of a 2N3832 FET is 5500 micromhos, and with Vp = 5.6 volts the output voltage of the phase detector is

$$e_L = \frac{2G_0}{V_p} e_s e_o R_L \tag{315}$$

$$= 2\left(5.5 \times 10^{-3}\right) e_s e_o (188) = 0.37\, e_s e_o$$

Thus, the output voltage is related to the product of the two input signals by the gain sensitivity constant,

$$K_d = 0.37 \text{ volts/degree} \tag{316}$$

or 21.2 volts/radian.

The output voltage of the phase detector is plotted in Figure 47 against various phase errors.

b. Loop Filter

A low-pass filter follows the phase detector to remove higher frequency terms contained in the error signal that is produced by the loop tracking of the input frequency. The error signal is a voltage proportional to the instantaneous frequency of the input signal, thus, it corresponds to the modulation on the input frequency. On this basis, the bandwidth of the loop

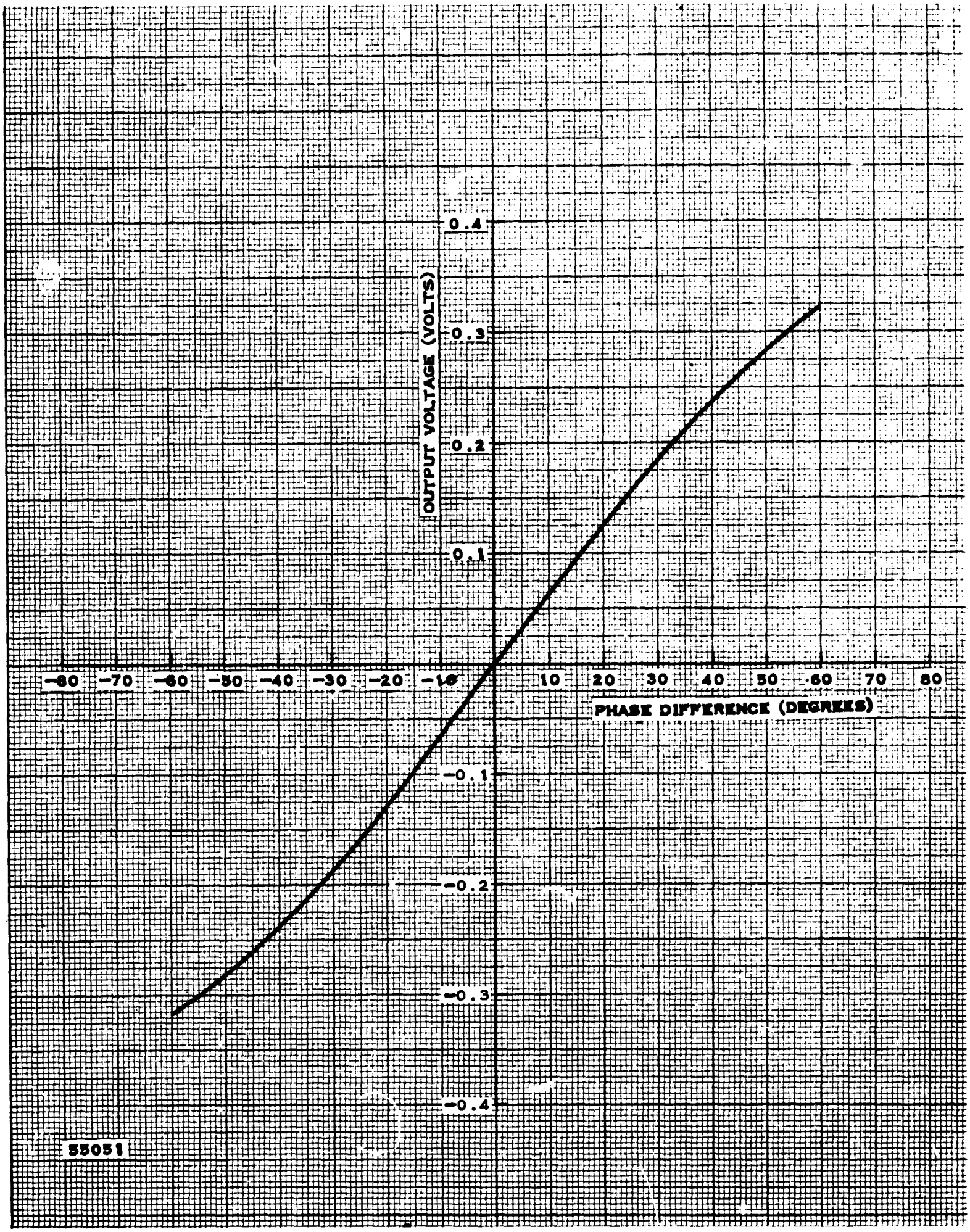

Figure 47. Phase Detector Output Versus Phase Error

filter must be wide enough to allow passage of the recovered information. As the loop filter must supply the error signal unaltered to the VCO in order to achieve proper tracking, its design is dictated by desired demodulator performance.

The best demodulator is a second-order loop with a transfer function given by:

$$H(s) = \frac{1 + \tau_2 s}{1 + \left(\tau_2 + \frac{1}{k_d K_v}\right)s + \frac{\tau_1 s^2}{k_d K_v}} \tag{317}$$

To realize this transfer characteristic, a lag-lead network is generally employed. A filter of this type and its closed-loop response are shown in Figure 48. The transfer function for this filter is

$$F(s) = \frac{1 + \tau_2 s}{1 + \tau_1 s} \tag{318}$$

and it is seen that the filter is specified by the loop time constants (τ_1 and τ_2) which in terms of the loop parameters are

$$\tau_1 = \frac{K_v}{\omega_n^2} \tag{319}$$

$$\tau_2 = \frac{2\xi}{\omega_n} \tag{320}$$

where

K_v = open loop gain

ω_n = natural resonant frequency of loop

ξ = damping ratio

After these time constants are defined from the desired demodulator performance, the filter components are determined. Since three elements need to be determined and only two equations given, one filter component may be arbitrarily selected. A reasonable value of capacitance which may be fabricated by thin-film techniques is 1000 picofarads.

In second-order loops, a constant or static phase error exists, and the frequency of the VCO lags behind the input frequency by the amount of this error. In servo terminology, this is the static "velocity" error,

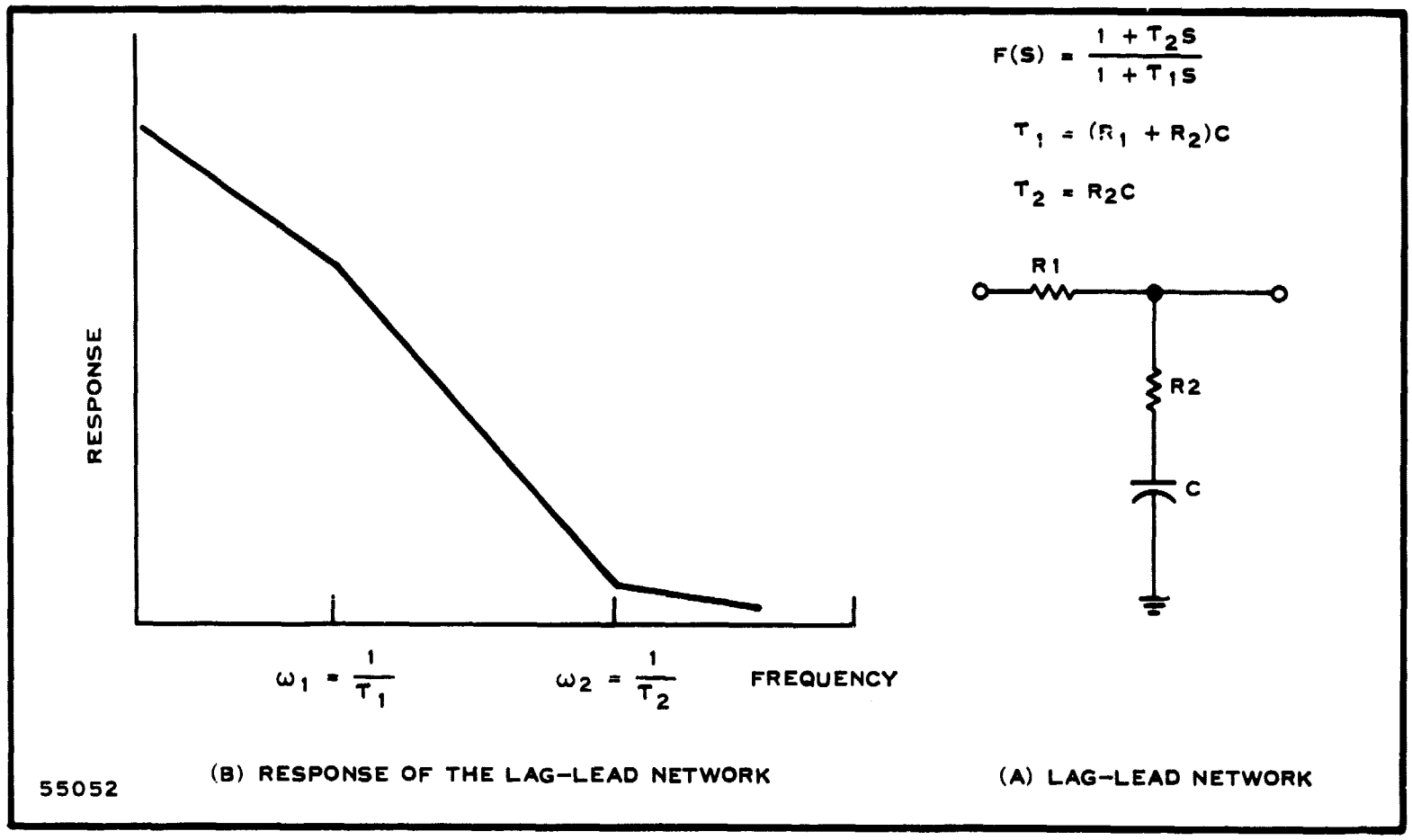

Figure 48. Loop Filter, Schematic Diagram and Response

and the threshold value of open loop gain required to permit tracking the input frequency within an allowable "velocity" or static phase error is given

$$K_V \geq \frac{\Delta\omega}{\sin \phi_e} \tag{321}$$

considering, the demodulator as a linear system,

$$K_V \geq \frac{\Delta\omega}{\phi_e} \tag{322}$$

where ϕe is the static phase error, and $\Delta\omega$ is the maximum radian frequency shift of the input signal. For a deviation ratio of 0.7, and a bit rate ($\mathcal{R}$) of 1.2 megabits/sec

$$D = \frac{f_U - f_L}{R} \tag{323}$$

where

f_U = upper frequency shift

f_L = lower frequency shift

$$\Delta\omega = 2\pi\Delta f = \frac{\pi DR}{2} = 2.64 \times 10^6 \text{ radians/sec} \qquad (324)$$

The maximum value of phase error is less than 90 degrees, if the loop is to remain in lock. However, to avoid distortion, the phase error should be within the linear range of the phase detector output characteristic. Since the phase detector is preceded by a limiter, its output characteristic is triangular and linearity holds for phase errors to 70 degrees.

In Figure 49, peak phase error due to sinusoidal FM is given as a function of the ratio of modulating frequency (ωm) to the loop natural frequency (ωn). The peak phase error occurs when these frequencies are equal. For a critically damped loop ($\zeta = 1$) which has the highest immunity to noise regarding loss of lock,

$$\phi e = 0.5 \frac{\Delta\omega}{\omega_n} \qquad (325)$$

whenever

$$\omega_m = \omega_n$$

The demodulator must recover a frequency of one-half the bit rate, thus ω_m is given

$$\omega_m = 2\pi R/2 \qquad (326)$$

and for a bit rate of 1.2 megabits per second.

$$\omega_m = \pi\,(1.2 \times 10^6) = 3.77 \times 10^6 \ \frac{\text{radians}}{\text{sec}} \qquad (327)$$

The 3-dB bandwidth of a critically-damped second-order loop is shown in Figure 19 to define a resonant frequency of

$$\omega_n = \frac{\omega_{3dB}}{2.48} \qquad (328)$$

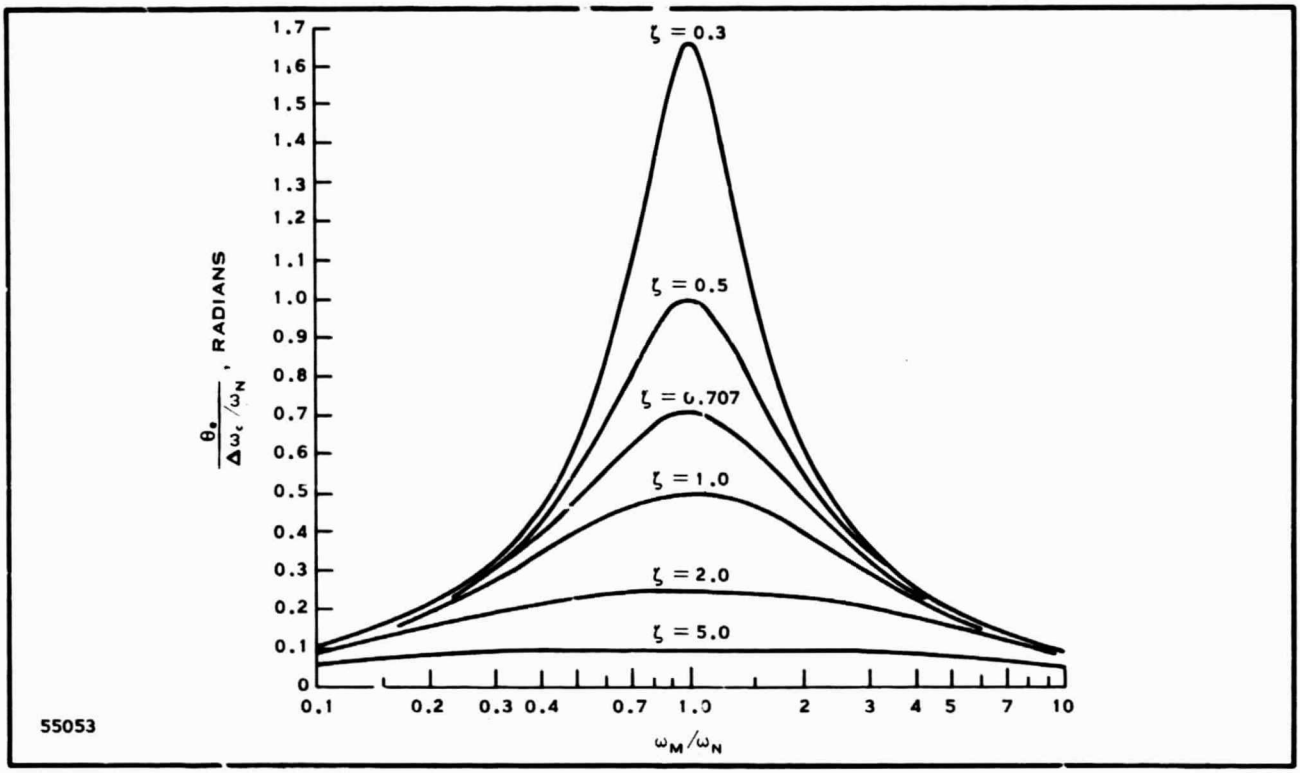

Figure 49. Maximum Steady-State Phase-Error with Respect to the Frequency Deviation $\Delta\omega_o$ Versus the Dimensionless Parameter ω_m/ω_n Due to Sinusoidal FM

and for

$$\omega_{3dB} = \omega_m \tag{329}$$

the loop natural resonant frequency becomes

$$\omega_n = \frac{3.77 \times 10^6}{2.48} = 1.52 \times 10^6 \frac{\text{radians}}{\text{sec}} \quad . \tag{330}$$

Therefore, the peak phase error as a result of modulation as obtained from Equation (325) is

$$\phi_e = \frac{0.5\,\Delta\omega}{\omega_n} = 0.873 \text{ radians} . \tag{331}$$

The open-loop gain required to ensure that the static phase error above is not exceeded is then:

$$K_v \geq \frac{\Delta\omega}{\phi_e}$$

$$\geq \frac{2.64 \times 10^6}{0.873} \quad (332)$$

$$K_v \geq 3.03 \times 10^6 \ \text{sec}^{-1}.$$

If the loop gain does not exceed this value, an amplifier will be required within the loop.

The open loop gain of the demodulator is determined by the separate gain sensitivities of the filter, VCO and phase detector as shown by

$$K_v = a\, K_{VCO}\, K_d\, F(o) \quad (333)$$

where

K_{VCO} = the gain constant of the VCO, $\frac{\text{radians}}{\text{volts}}$

K_d = the gain constant of the phase detector, $\frac{\text{volts}}{\text{radians}}$

$F(o)$ = the dc loss constant of the loop filter

a = the limiter suppression factor.

For the lag-lead filter, $F(s = 0) = 1$, and from Figure 50, it is seen that

$$K_{VCO} = \frac{280 \text{ kHz}}{\text{volt}} = 1.76 \times 10^6 \frac{\text{radians}}{\text{volts}} \quad (334)$$

and from Figure 47

$$K_d = 21 \text{ volts/radians}. \quad (335)$$

Therefore,

$$K_v = a\,(21)(1.76 \times 10^6) = a(3.7 \times 10^7 \ \text{sec}^{-1}) \quad (336)$$

The factor a accounts for the suppression of the input signal-to-noise ratio to the limiter, by the limiter. At threshold, the signal-to-noise ratio at the phase detector is degraded from the signal-to-noise ratio at the limiter input, by the suppression factor. This is due to the fact that the power delivered by the limiter is constant, and as the limiter's input signal-to-noise ratio falls below 10 dB, the noise level rises and the signal is suppressed. Thus, above threshold, the loop gain increases.

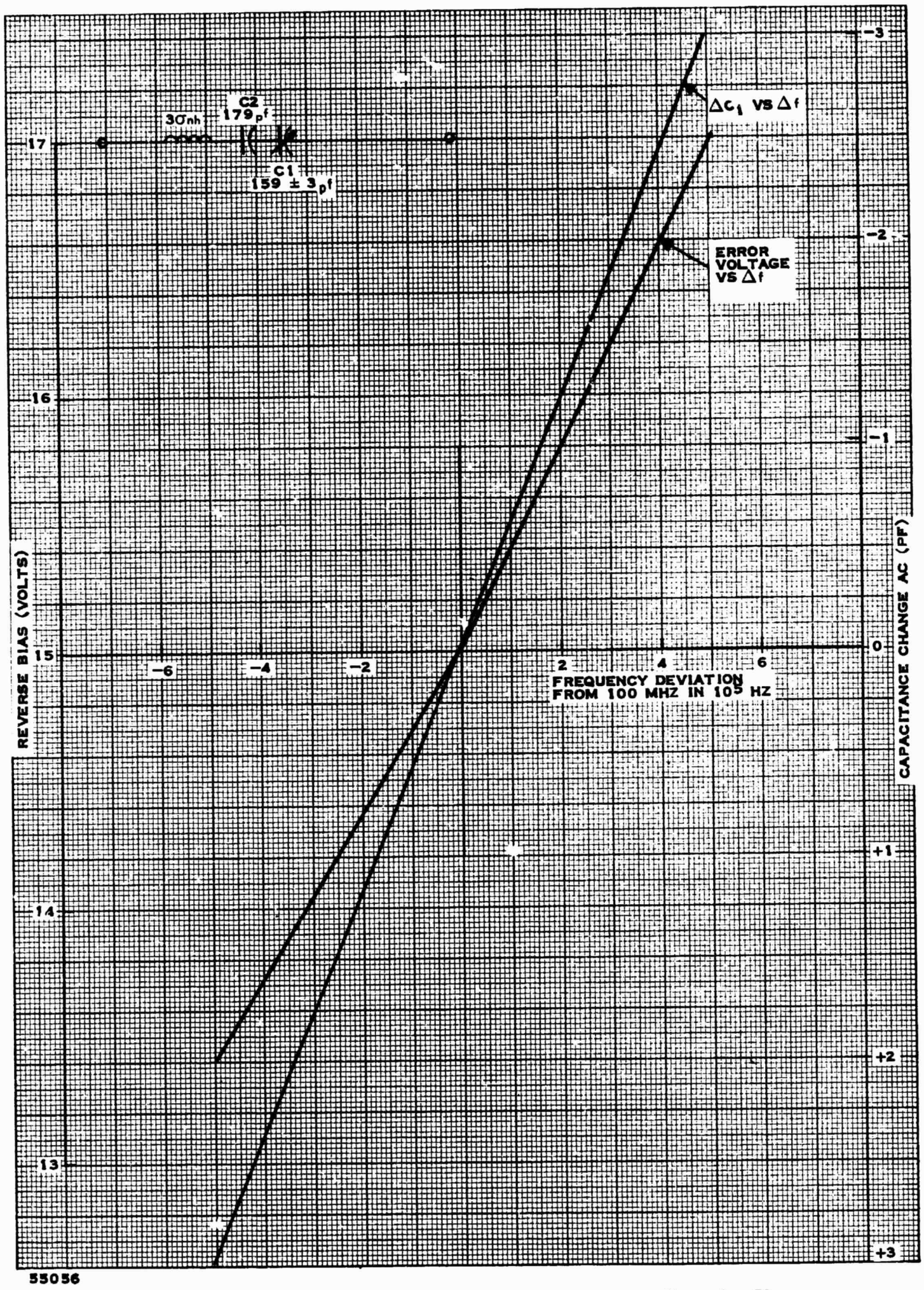

Figure 50. Frequency Deviation Versus ΔC and ΔV

The suppression factor is given:

$$a = \sqrt{\frac{(\overline{SNR})_i}{\frac{4}{\pi} + (SNR)_i}} \tag{337}$$

where $(SNR)_i$ is the threshold input signal-to-noise ratio before the limiter. For a 5 dB signal-to-noise threshold,

$$(SNR) = 0.313 \tag{338}$$

and

$$a = \sqrt{\frac{0.313}{\frac{4}{\pi} + 0.313}} = 0.44. \tag{339}$$

The existing open-loop gain at threshold is

$$K_v = 0.44\,(3.7 \times 10^7) = 1.63 \times 10^7\ \text{sec}^{-1}$$

$$K_v = 1.63 \times 10^7\ \text{sec}^{-1} \tag{340}$$

and since the loop gain requirement of Equation (332) is exceeded, a loop amplifier is not required, and a passive loop filter is sufficient to demodulate the input signal.

Since the demodulator parameters have been specified, the filter time constants are then given:

$$\tau_1 = \frac{K_v}{\omega_n{}^2} \tag{341}$$

$$\tau_1 = \frac{1.63 \times 10^7}{(1.52 \times 10^6)^2} = 7.05 \times 10^{-6}\ \text{sec} \tag{342}$$

and

$$\tau_2 = \frac{2\zeta}{\omega_n} \approx \frac{2}{1.52 \times 10^6} = 1.31 \times 10^{-6}. \tag{343}$$

The filter components are defined in Figure 48, and with C = 1000 pF, the required resistor values are:

$$R_2 = \frac{\tau_2}{C} = \frac{1.31 \times 10^{-6}}{1 \times 10^{-9}}\ 1.31\ \text{K ohms} \tag{344}$$

and

$$R_1 = \frac{\tau_1}{C} - R_2 = 5.74\ \text{K ohms}. \tag{345}$$

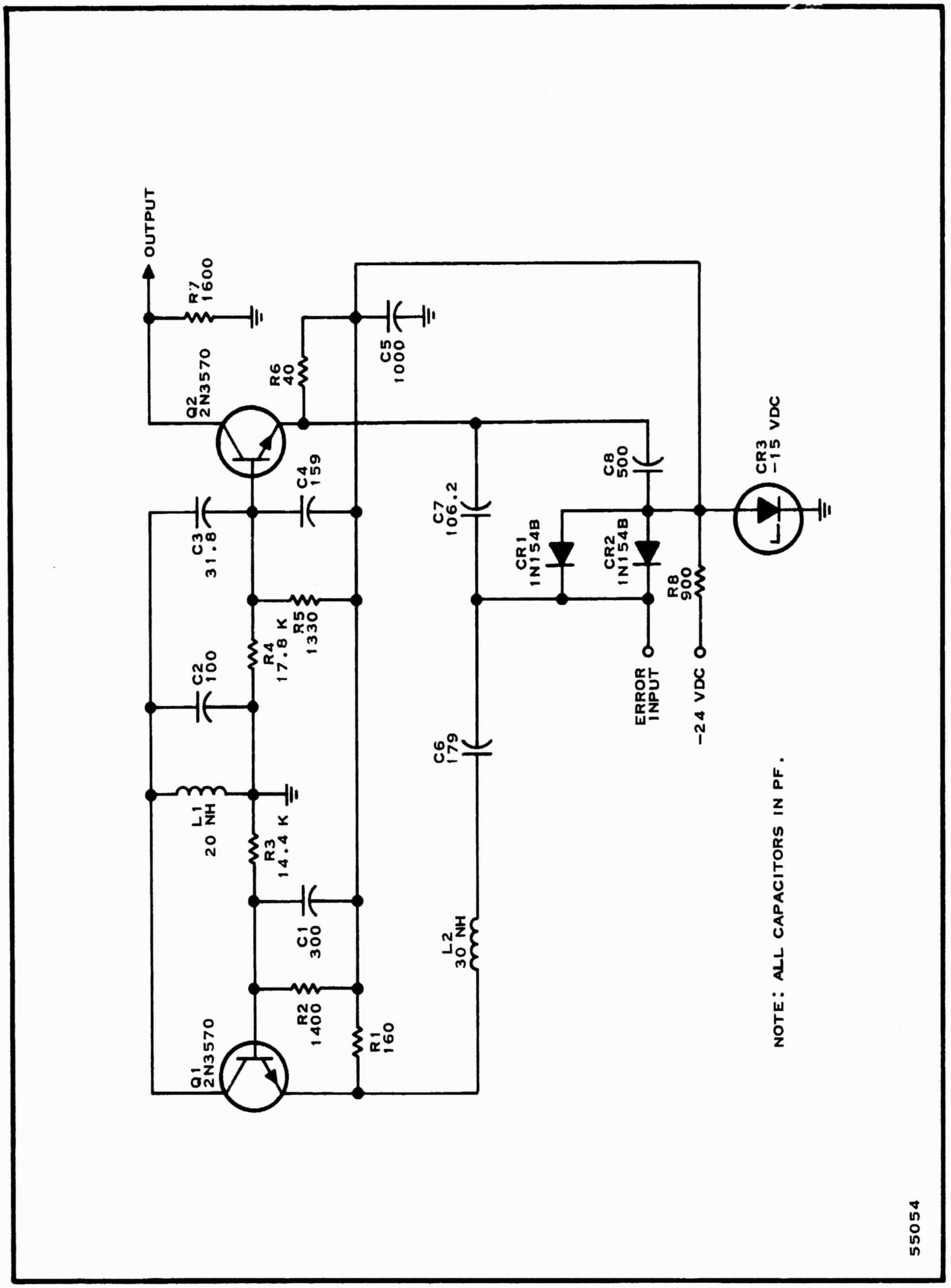

Figure 51. Receiver VCO, Schematic Diagram

c. Voltage Controlled Oscillator (VCO)

The VCO (Figure 51) is similar to the local oscillator (LO) except the crystal has been replaced with a voltage controlled series-resonant circuit composed of L_2, C_6, and C_7. Diodes CR1 and CR2 are varactors which provide variable capacitance in parallel with capacitor C7.

The first oscillator design approach was to vary the resonance of a crystal with a varactor. However, the analysis revealed that the frequency could be controlled over only 8 to 10 kHz. Using a crystal with a very low Q (5000 to 10, 000) would have extended the range to only 25 kHz. The frequency range needed to recover the modulation is 600 kHz so the crystal design was abandoned.

The component values of the series circuit which replaced the crystal were determined by analyzing the characteristics of an inductor (L_1) in series with two capacitors (C_1 and C_2). The design formulas are as follows:

$$C_T = \frac{C_1 C_2}{C_1 + C_2} \tag{346}$$

$$f_s = \frac{1}{2\pi\sqrt{LC_T}} \tag{347}$$

$$C_T = \frac{1}{4\pi^2 L f_s^2} \tag{348}$$

$$\frac{dC_T}{df} = \frac{-2f_s}{4\pi^2 L f_s^3} = \frac{-1}{2\pi^2 L f_s^3} . \tag{349}$$

For frequencies near resonance

$$\Delta C_T = \frac{-1}{2\pi^2 h f_s^3} \cdot \Delta f \tag{350}$$

also

$$\frac{dC_T}{dC_1} = \frac{(C_1 + C_2)C_2 - C_1 C_2}{(C_1 + C_2)^2} = \frac{C_2^2}{(C_1 + C_2)^2} \tag{351}$$

or

$$\Delta C_T = \frac{C_2^2}{(C_1 + C_2)^2} \cdot \Delta C_1 \tag{352}$$

and

$$\Delta C_1 = \frac{-1(C_1 + C_2)^2}{2\pi^2 L C_2^2 f_s^3} \cdot \Delta f . \tag{353}$$

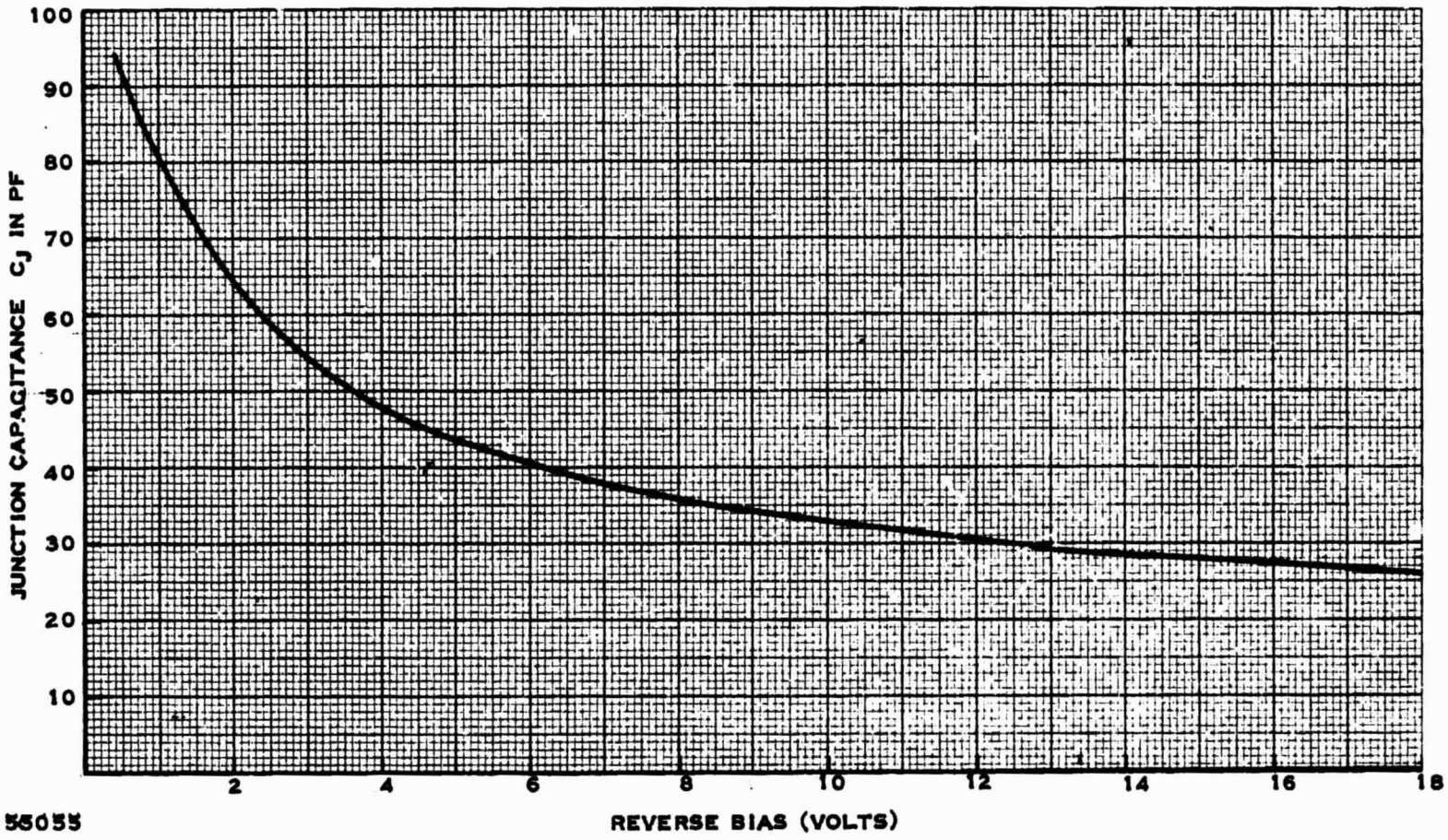

Figure 52. Plot of Varactor 1N1548

The following values may be determined.

$f_s = 10^8$ Hz (the intermediate frequency)

$L = 30 \times 10^{-9}$ h (chosen to be compatible with thin-film circuit design)

$\Delta f = \pm 6 \times 10^5$ Hz (sufficient bandwidth to recover the modulation)

$\Delta C_1 = \pm 3 \times 10^{-12}$ f (chosen from considerations to be explained later).

Therefore,

$$C_T = \frac{1}{4\pi^2 f_s^2 L} = 84.3 \times 10^{-12} \text{ farads} \qquad (354)$$

and from Equations (350) and (352)

$$\frac{C_2^2}{(C_1 + C_2)^2} = \frac{-1 \Delta f}{2\pi^2 L f_s^3 \Delta C_1} \qquad (355)$$

which after values are substituted is

$$\frac{C_2^2}{(C_1 + C_2)^2} = 0.281 \qquad (356)$$

and

$$C_2 = 1.128\, C_1$$

$$C_T = 84.3 \times 10^{-12} = \frac{1.128\, C_1^2}{2.128\, C_1} \tag{357}$$

$$C_1 = 159 \times 10^{-12} f \quad C_2 = 179 \times 10^{-12} \text{ farads.} \tag{358}$$

Resolve C_1 into a parallel combination of a constant capacitance and two variable capacitances (varactors) which fulfill the following requirements. Each varactor must provide a ±1.5 picofarad of capacitance variation in as linear a fashion as possible. This means that they must be biased with a large reverse voltage. (The C versus reverse voltage characteristic becomes more linear as reverse voltage increases.)

The junction capacitance of the varactor diode 1N1548 may be expressed as

$$C_j = \frac{125}{\left(1 + \frac{Y}{0.7}\right)^{1/2}} \tag{359}$$

where C_j is the junction capacitance at a reverse bias of V volts this equation is plotted in Figure 52. A change in reverse bias of 1.5 Vdc gives a ±1.5-picofarad change in capacitance. Putting two varactors in parallel makes the total capacitance change ±3.0 picofarads.

Equation (353) indicates that the frequency change Δf is linearly related to the change of capacitance. In Figure 50 the change in frequency, Δf, is plotted versus capacitance change, ΔC, and reverse bias.

The junction capacitance of each varactor at 15 Vdc reverse bias is 26.4 picofarads. From Equation 358, C_1 is equal to 159 picofarads. So the constant capacitor (C_1') must be

$$C_1' = 159 - 2\,(26.4) = 106.2 \text{ picofarads.} \tag{360}$$

Thus, the component values of the resonant circuitry has been determined as

$$C_6 = 179 \text{ pF} \tag{361}$$

$$C_1 = 106.2 \text{ pF} \tag{362}$$

$$L_2 = 30 \text{ nh.} \tag{363}$$

The rest of the circuit is identical in concept to the design of the local oscillator so a detailed design analysis will not be repeated here.

The ceramic layout is shown in Figure 53.

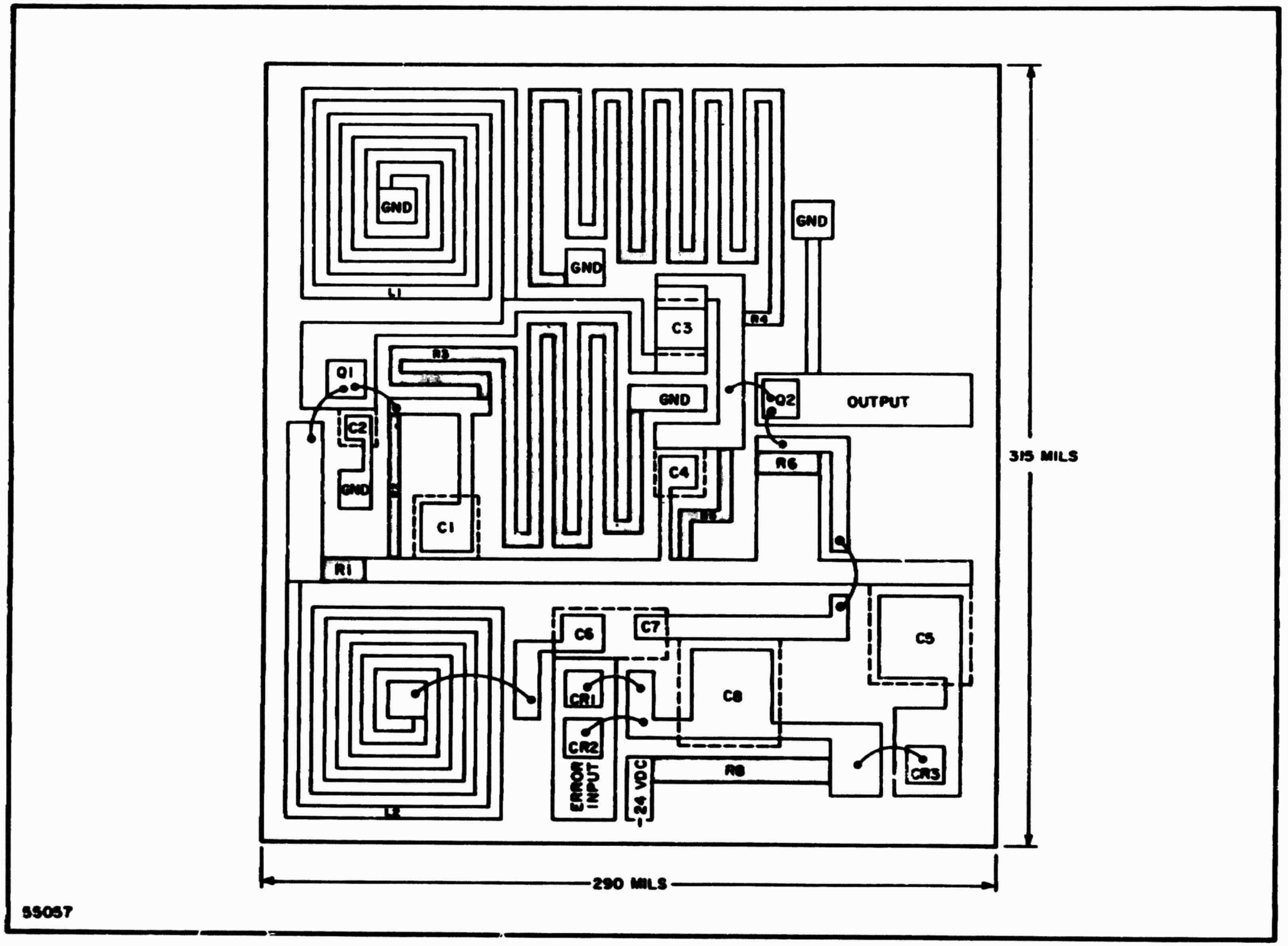

Figure 53. Receiver VCO Ceramic Layout

6. The Baseband Filter

To preserve the time relationship between coded pulses, use of a very flat time-delay filter in the baseband is desirable. The Bessel transfer function more nearly achieves a constant time delay than any other type. The general form of the Bessel transfer function is

$$T(s) = \frac{A}{s^2 + 3s + 3} \tag{364}$$

The circuit shown in Figure 54 has the following transfer function[20]

$$\left|\frac{E_2}{E_1}\right| = T(s) = \frac{\frac{1}{R_1 R_3}}{s^2 C_2 C_5 + sC\left(\frac{1}{R_1} + \frac{1}{R_3} + \frac{1}{R_4} + \frac{1}{R_3 R_4}\right)} \tag{365}$$

The Bessel function filter is derived by equating coefficients of Equations 364 and 365 and by specifying the gain (A). The need for temperature compensation is eliminated if substantial feedback is employed. Twenty- to forty-dB of feedback is provided if the gain is set at unity.

The Bessel function polynominal takes the form

$$T(s) = \frac{1}{1 - \frac{1}{3}\omega^2 + j\omega} \tag{366}$$

when S is replaced by $j\omega$ to represent the sinewave frequency response. This low-pass filter should have 3-dB attenuation at the cutoff frequency, $f_c = 6 \times 10^5$Hz.

Therefore

$$T(s) = \frac{1}{\left(1 - \frac{1}{3}u^2\right) + ju} = \frac{1}{1.414} \tag{367}$$

where

$$u = \frac{\omega}{\omega_m} \tag{368}$$

and ω_m is the angular velocity of the natural cutoff frequency.

Then

$$\frac{}{\sqrt{\left(1 - \frac{1}{3}u^2\right)^2 + u^2}} = 1.414 \tag{369}$$

solving for ω,

$$u = 1.36 \tag{370}$$

Therefore,

$$\frac{\omega_c}{\omega_m} = 1.36 \tag{371}$$

where ω_c is the angular velocity of the desired cutoff frequency.

$$\omega_c = 3.77 \times 10^6 \tag{372}$$

and

$$\omega_m = \frac{\omega_c}{1.36} = 2.77 \times 10^6 \tag{373}$$

The normalized values of the RC components are found by equating coefficients of the two transfer functions.

Let

$$\frac{1}{R_1} = G_1 \text{ etc.}$$

$$G_1 G_3 = 3 \text{ for unity gain in the passband} \tag{374}$$

$$G_3 G_4 = 3 \tag{375}$$

$$C_2 C_5 = 1 \tag{376}$$

$$C_5(G_1 + G_2 + G_3) = 3 \tag{377}$$

$$\text{Setting } G_1 = G_4 = 1 \tag{378}$$

$$\text{Yields } G_3 = 3 \tag{379}$$

$$C_5 = 3/5 \tag{380}$$

$$C_2 = 5/3 \tag{381}$$

$$R_1 = 1 \tag{382}$$

$$R_4 = 1 \tag{383}$$

$$R_3 = 1/3 \tag{384}$$

To scale the component values up in magnitude, it is necessary to multiply the R's and divide the C's by a scaling constant "b". To scale the transfer function to the proper frequency, the C's must be divided by a scaling factor "a," but the R's are not affected[21].

Choosing b = 1000 yields convenient values for R_1, R_3, and R_4.

$$R_1^* = R_1 b = 1000 \tag{385}$$

$$R_3^* = R_3 b = 333 \tag{386}$$

$$R_4^* = R_4 b = 1000 \tag{387}$$

Scaling factor "a" was established in Equation 373 as 2.77×10^6.

Therefore,

$$C^*_5 = \frac{1}{ab} C_5 = \frac{3}{5} \frac{1}{2.77 \times 10^6 \times 10^3} \tag{388}$$

$$C^*_5 = 216.5 \times 10^{-12} \text{ farads} \tag{389}$$

Likewise

$$C^*_2 = 602 \times 10^{-12} \text{ farads} \tag{390}$$

Substituting the scaled values into equation 364 and replacing S with $j\omega$ gives

$$\frac{E_2}{E_1} = \frac{1}{\left[\left(1 - 4.34u^2\right)\left(10^{-14}\right)\right] + j\omega\left[\left(3.61\right)\left(10^{-7}\right)\right]} \tag{391}$$

which has a magnitude-phase versus frequency relationship shown in Table 4 and Figure 54. The time delay is computed with the equation

$$t_d = \frac{1\theta 1}{360f} \tag{392}$$

*Indicates the scaled value of the component.

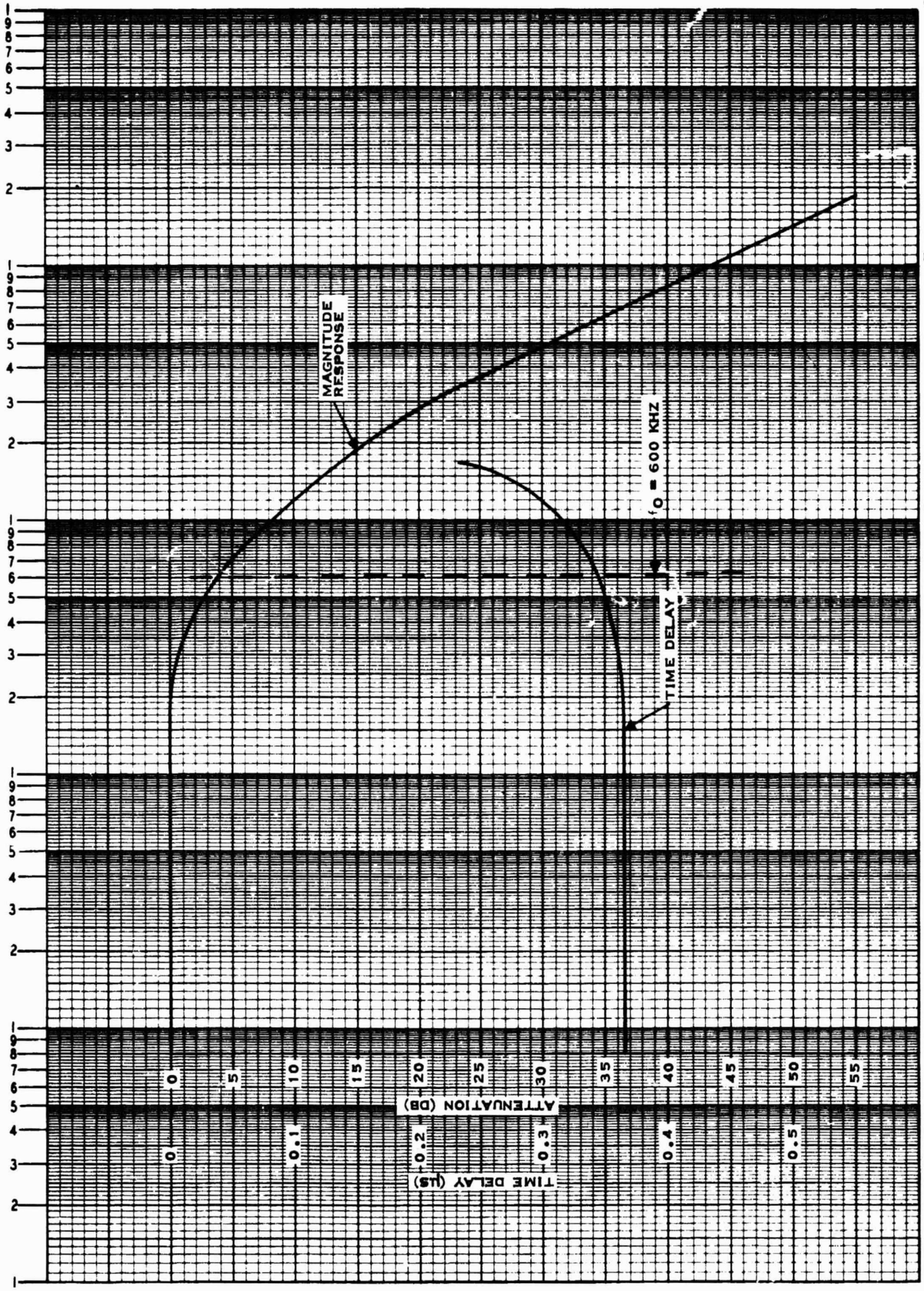

Figure 54. Response of the 600-kHz Baseband Low-Pass Filter

where ϕ is the phase shift of the transfer function. A plot of phase shift (ϕ) versus normalized frequency (ω/ω_c) is presented in Figure 55. The ceramic layout of the baseband filter is Figure 56 and the schematic diagram is Figure 57. A Texas Instruments Operational Amplifier, SN524A, has ample gain to provide more than 30 dB of feedback at 600 kHz. Because only a one-sided power supply is available it is necessary to create a floating ac ground. The bypass capacitor C1 presents 159 ohms to ground at 10 kHz. The circuitry associated with the operational amplifier is all thin-film, except C1 which is a chip capacitor.

Table 4. Magnitude-Phase Versus Frequency Response of the 600-kHz Baseband Maximumly Flat Time Delay Low-Pass Filter

f	ω	$\left\lvert\frac{E_2}{E_1}\right\rvert \angle\theta°$	dB	$\frac{\omega}{\omega_e}$	$t_d(\mu s)$
1.59×10^4	10^5	$1 \angle -2.1°$	0		0.367
1.59×10^5	10^6	$0.989 \angle -20.7°$	−0.1	0.265	0.365
3×10^5	1.88×10^6	$0.923 \angle -38.8°$	−0.8	0.50	0.360
6×10^5	3.77×10^6	$0.707 \angle -74.2°$	−3.0	1.0	0.344
1.59×10^6	10^7	$0.204 \angle -132.8°$	−13.8		0.232
1.59×10^7	10^8	$0.00231 \angle -175.2°$	−52.8		

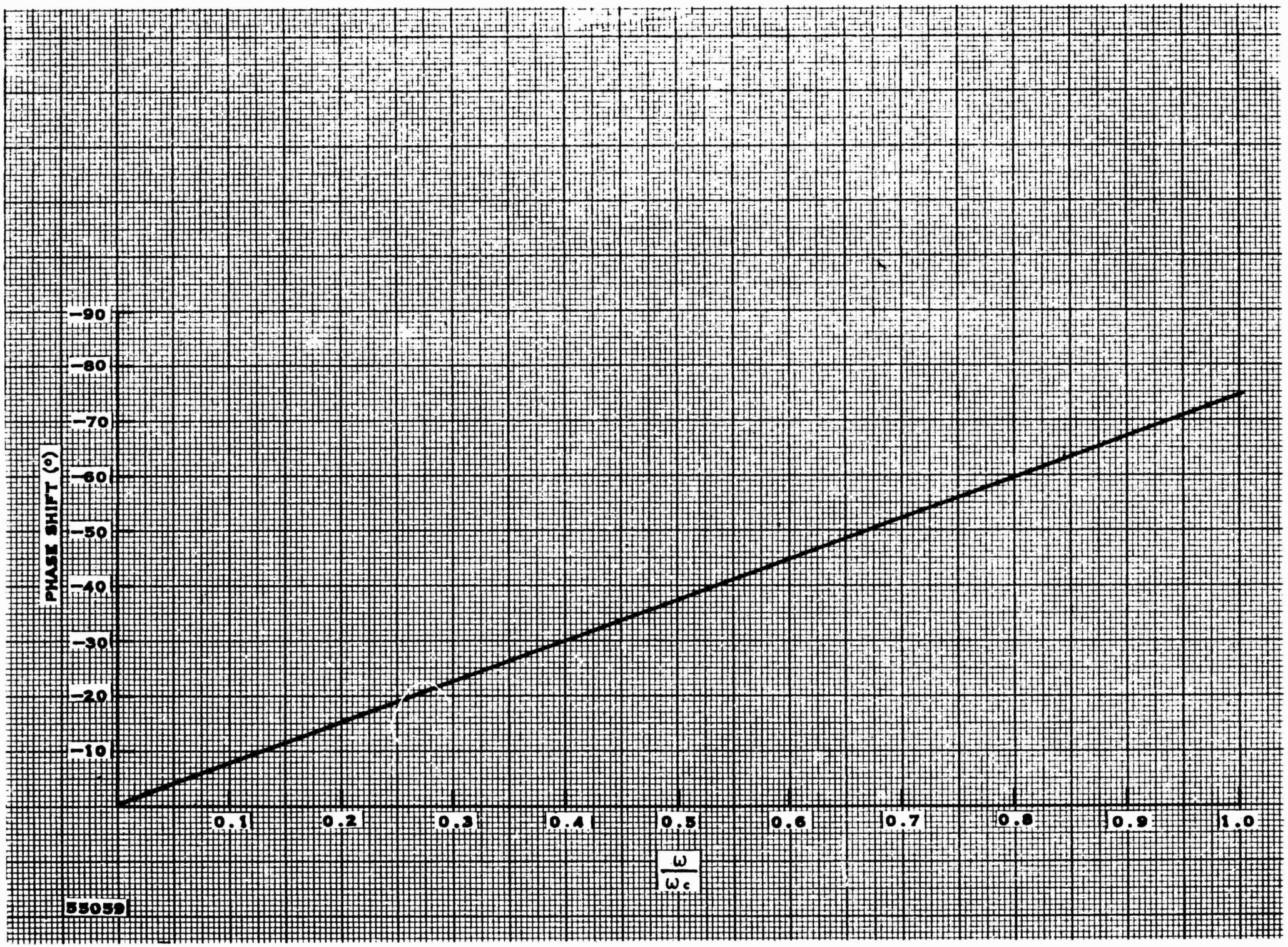

Figure 55. Phase Shift Versus Frequency of the Baseband Low-Pass Filter

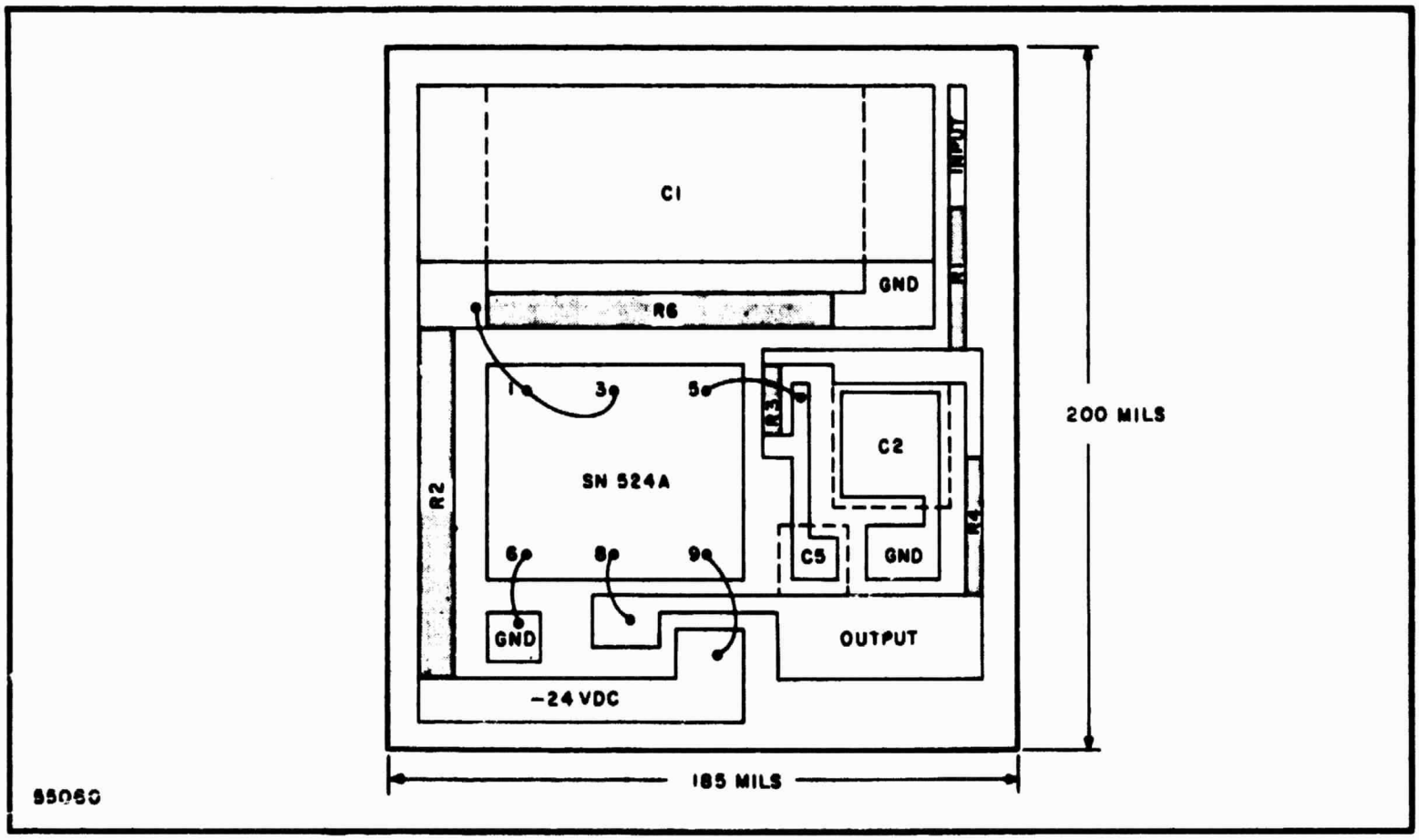

Figure 56. Baseband Filter, Ceramic Layout

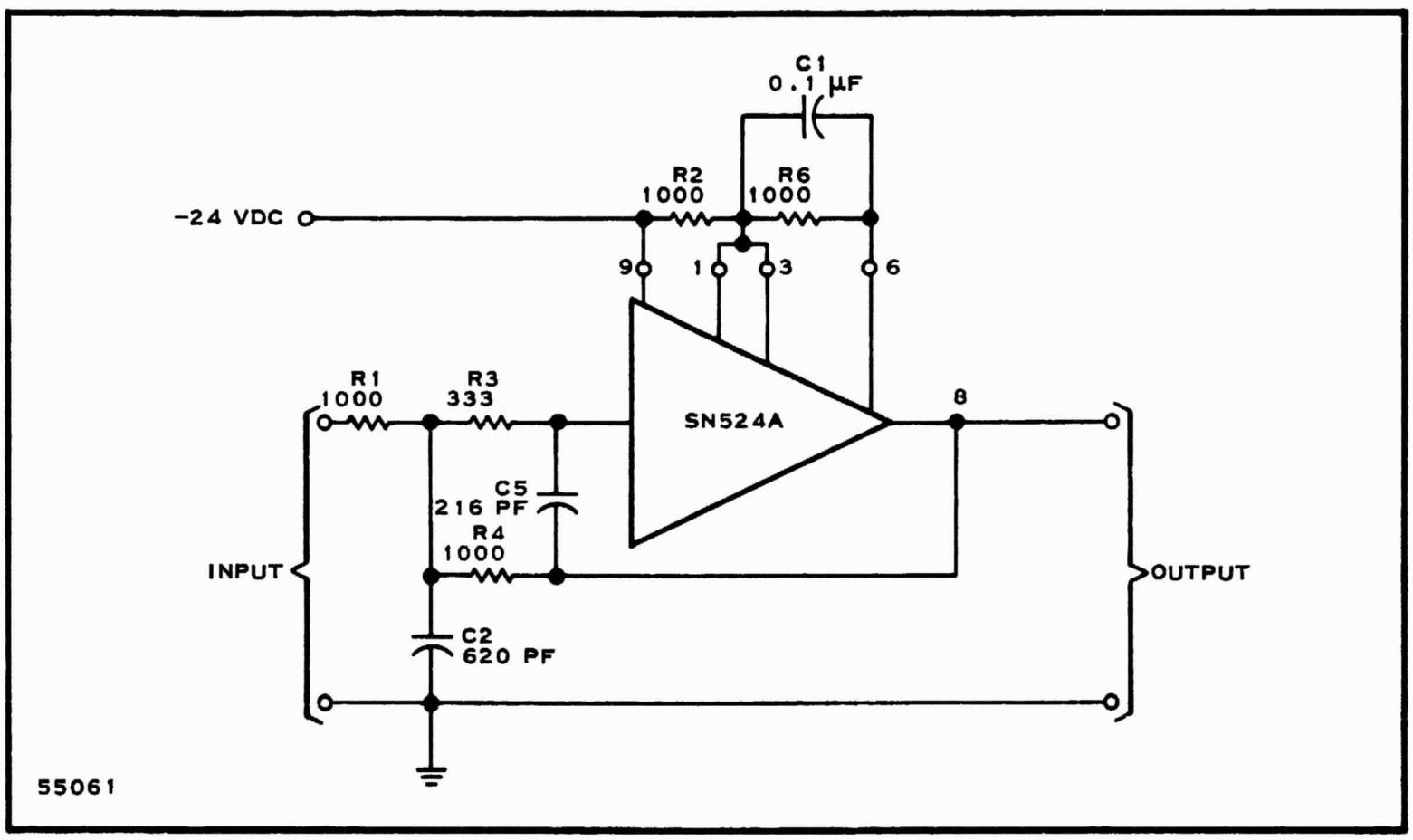

Figure 57. Baseband Filter, Schematic Diagram

SECTION IV

TRANSMITTER

A. GENERAL

The transmitter consists of a Voltage-Controlled Oscillator/Modulator assembly and a power amplifier chain. The minimum output power is one watt over a tunable-frequency band of 2200 to 2300 MHz.

The voltage-controlled oscillator (VCO) is a Colpitts oscillator network employing varactor tuning and was the first circuit fabricated under the present contract. The design of the VCO was reported in the Third Scientific Report and its breadboard development was discussed in the Fifth Scientific Report. In this reporting period, the VCO design was completed, and its ceramic development is outlined in this section.

The results obtained from device characterization during the last period permitted the design of the interstage matching networks used in the power amplifier assembly. The matching networks were developed for a ceramic substrate; the evaluation of these networks is included in this section.

After the dimensions of the VCO/modulator and power amplifier ceramic assemblies were determined, the packaging design of the transmitter was investigated. The volume of the completed transmitter was determined to be 0.5 cubic inches.

B. CERAMIC DEVELOPMENT OF THE VCO/MODULATOR ASSEMBLY

1. VCO Ceramic Design

In the fabrication of the voltage-controlled oscillator, thin-film capacitors were not used. Consequently, only the following three masks were required:

A Tantalum-etch mask

An anodization mask

A metalization, or plating, mask.

Four VCO circuits at a time were fabricated on a 2-inch by 2-inch by 20-mil glazed ceramic substrate. The major steps in the fabrication process include:

Sputtering a uniform layer of tantalum over the entire surface

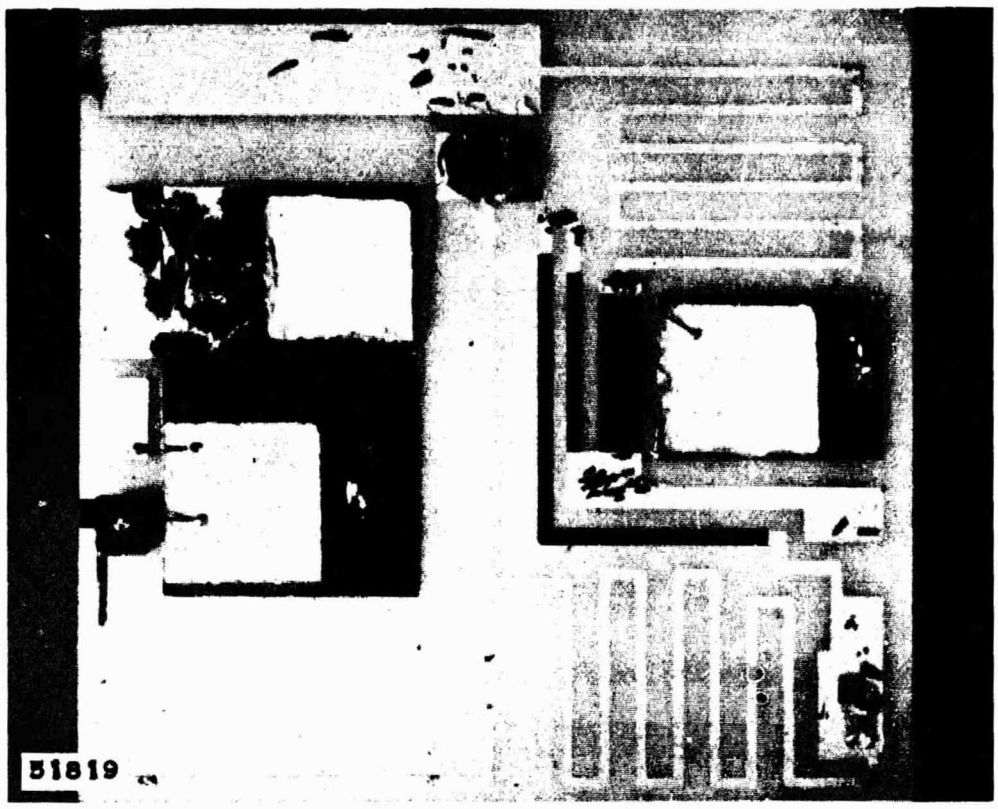

Figure 58. VCO Ceramic Layout

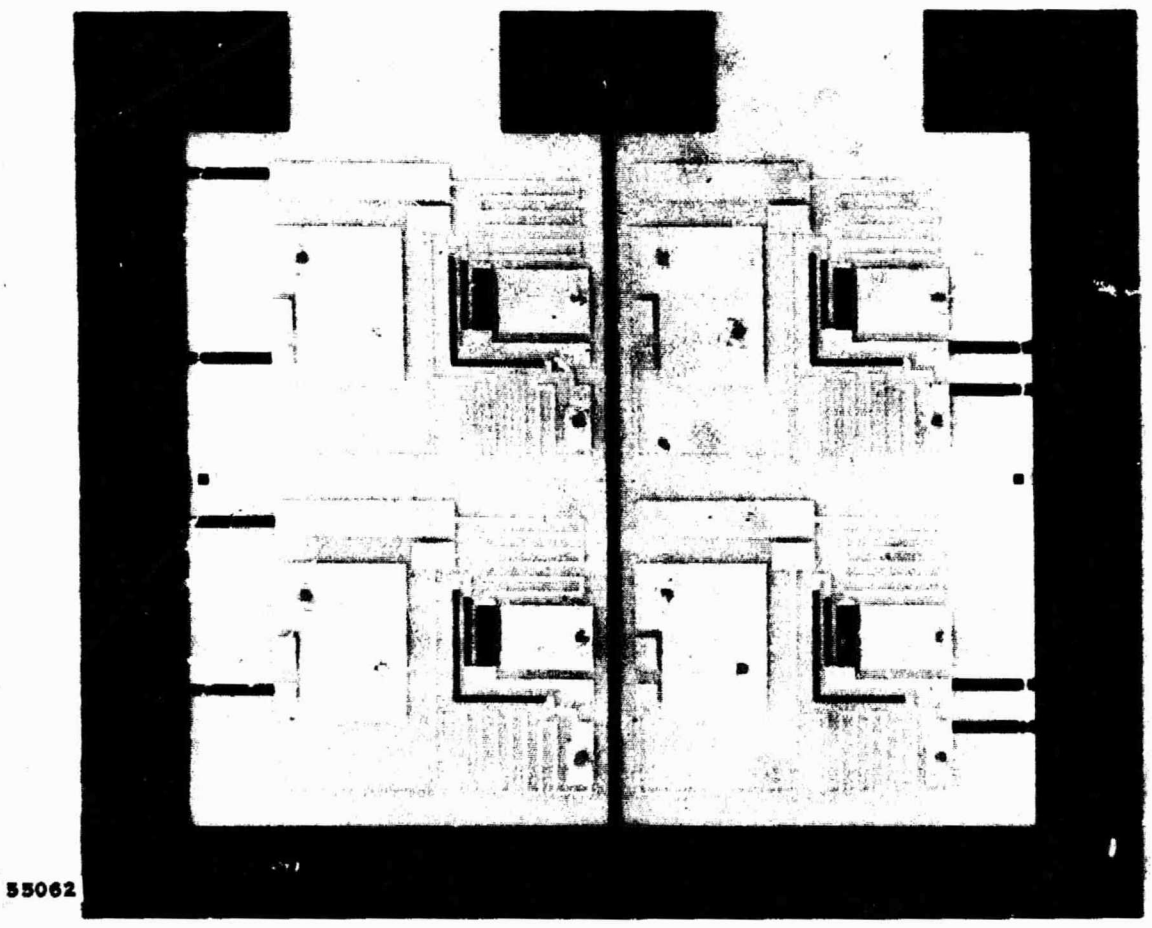

Figure 59. VCO Ceramic Substrate

Applying photo-resist—exposing, using the anodization mask; developing the desired pattern; then, etching the excess tantalum away

Applying photo-resist—exposing, using the anodization mask; developing the desired pattern; then, anodizing the previously deposited tantalum to the desired resistance values.

Applying photo-resist—exposing, using the metalization mask; developing the desired pattern; then, evaporating a thin layer of chrome-gold on the pattern side of the substrate

Plating a thick layer of gold over the chrome-gold

Drilling holes for ground connections, using an air-abrasive drill

Welding gold-mesh tabs over the holes

Evaporating chrome-gold on the ground-plane side of the substrate and plating a layer of gold over the chrome-gold

Cutting the circuits to the desired size

Attaching discrete components such as transistors diodes, and chip-capacitors

Testing.

Figure 58 is a photograph of a circuit which has been processed. Tantalum resistivity of 20 ohms per square was used for the three resistors in the circuit.

Several substrates (four circuits each) (Figure 59), were processed during the reporting period and the best circuits obtained were selected for final processing, cutting to size and attaching components.

The results obtained with the first circuits fabricated indicated that scaling from the Teflon breadboard to ceramic is not strictly in relation to the ratio of the dielectric constants of the two materials. The output frequency was higher than anticipated, the output power was considerably lower than anticipated and the best output-tap location was not at the predicted point. Figure 60 shows the output power versus frequency for one of the circuits.

In order to determine why the frequency was higher and the power was lower than expected; an emitter tab, a collector line, and a quarter-wavelength line were measured. The results of these measurements are shown in Table 5.

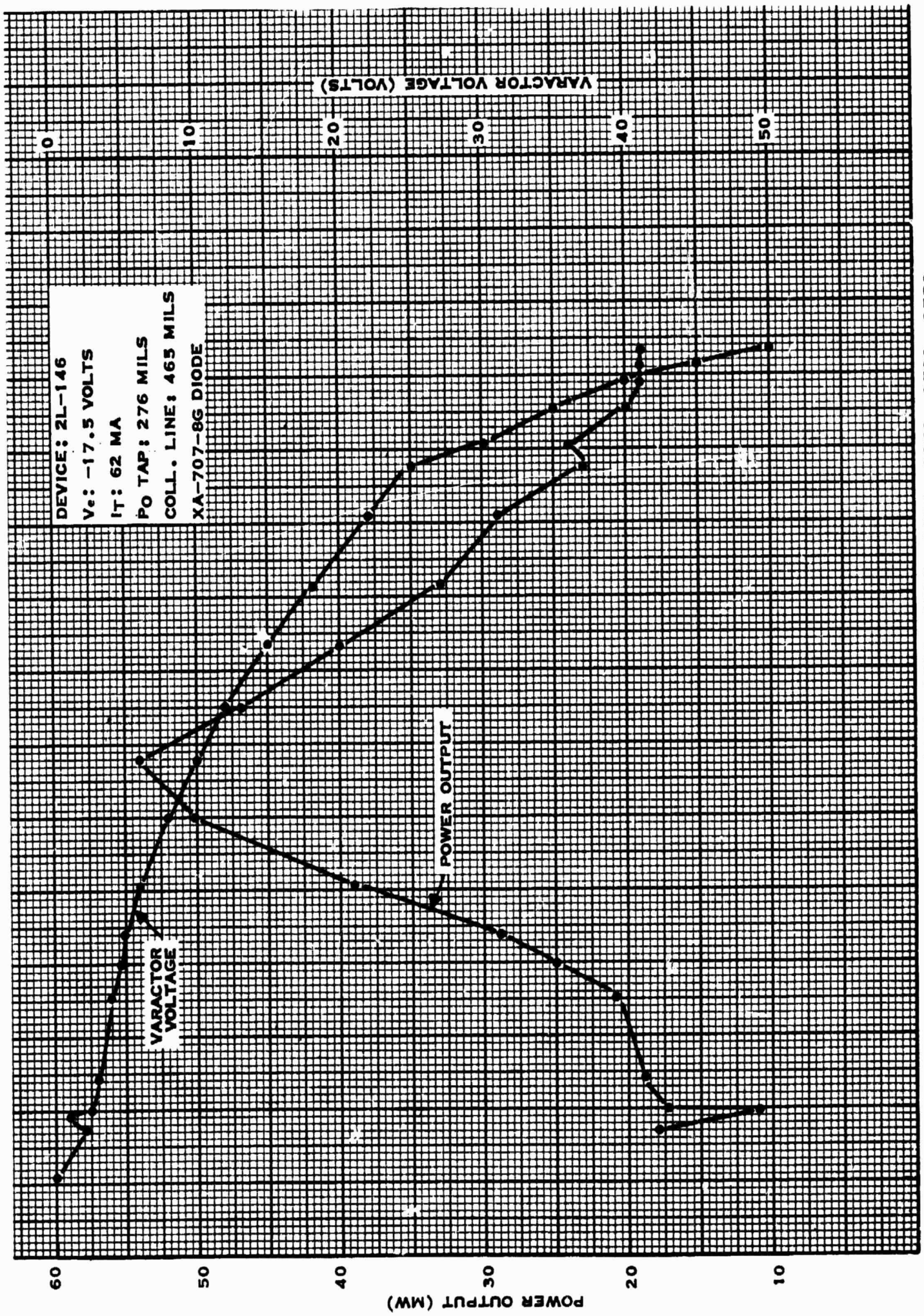

Figure 60. Ceramic VCO Performance (Power Output Tap 276 Mils)

Table 5. Teflon and Ceramic Data

Item	Frequency MHz	Ceramic Δλ	Teflon Δλ
λ/4 Lines	2250	0.263	0.25
Emitter Tab	2250	0.351	0.367
Collector Line	2250	0.208	0.224

Since the quarter-wavelength lines measured 0.263λ, it is clearly seen that they are 0.013λ or 29.9 mils too long. The excess length of the quarter-wavelength lines does not pose a problem since their actual length was varied on the Teflon circuit with no appreciable degradation of the circuit.

To determine the required emitter capacitance for maximum output power in the band, the capacitance of the Teflon circuit was measured and found to be 1.285 pF.

The corresponding length of the emitter on ceramic is determined by:

$$\ell = VZC$$

$$= \frac{3 \times 10^{10}}{2.55} \times 1.285 \times 10^{-12} \times 35.5 \qquad (386)$$

$$= 53.6 \times 10^{-2} \text{ meters}$$

$$\ell = 211 \text{ mils.}$$

Therefore, the emitter tab must be lengthened 42 mils. In order to lengthen the tab and make some measurements, a piece of ceramic was added which would yield the required emitter capacitance. Figures 61 and 62 show the results for two different power output tap points. The power output ranged from 70 to 80 mW across the band on both circuits.

The results showed that by extending only the emitter tab, satisfactory operation could be achieved. The output power was still less than expected and in order to achieve better results a new circuit was built.

The circuit contained several changes, leaving a larger border of ceramic around the circuitry, lengthening the emitter tab slightly and relocating the base-grounding point. The results of these changes produced a power output versus frequency response as shown in Figure 63. The inband loss was 0.84 dB for a power range of 102 to 124 mW.

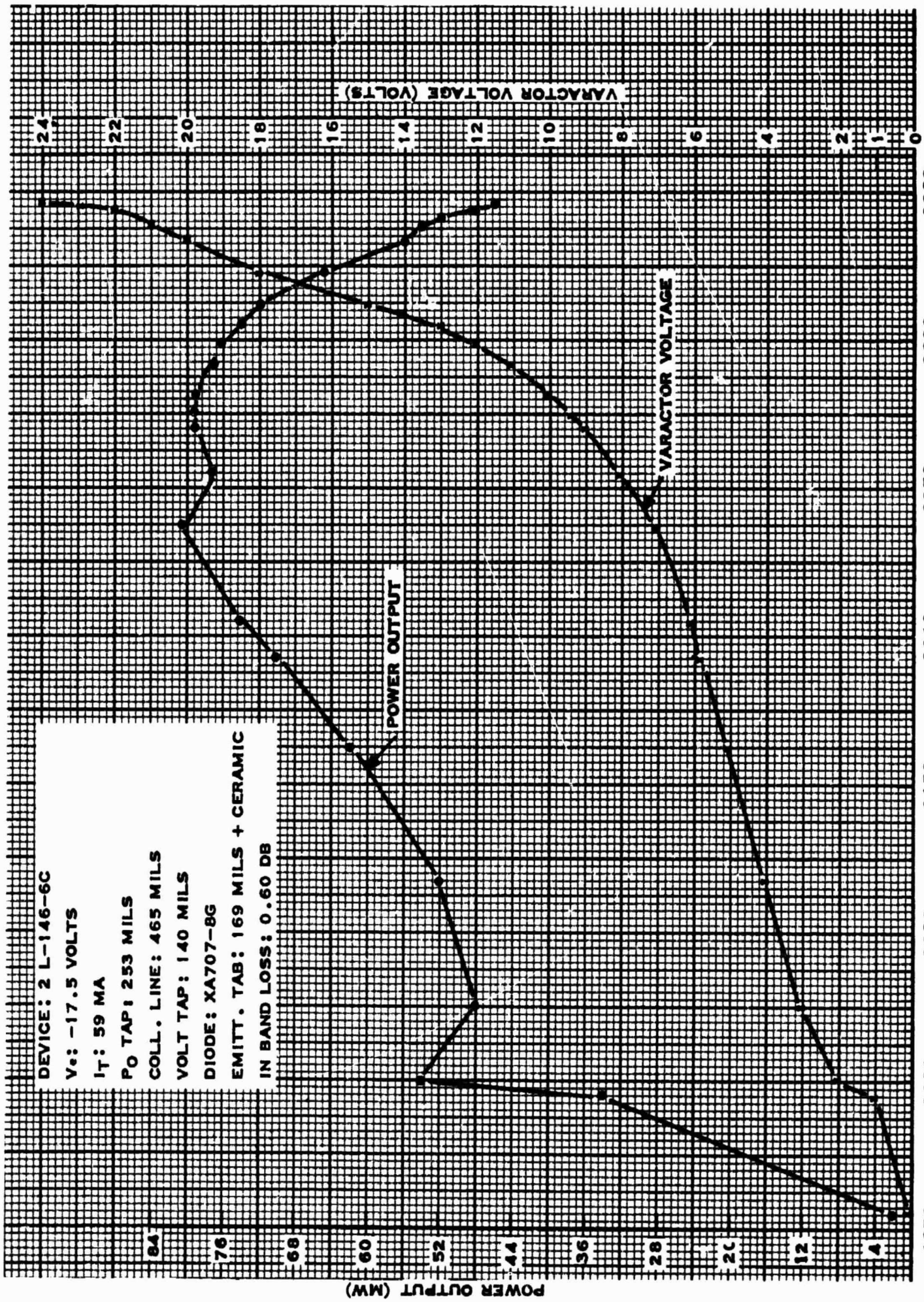

Figure 61. Ceramic VCO Performance (Power Output Tap 253 mils)

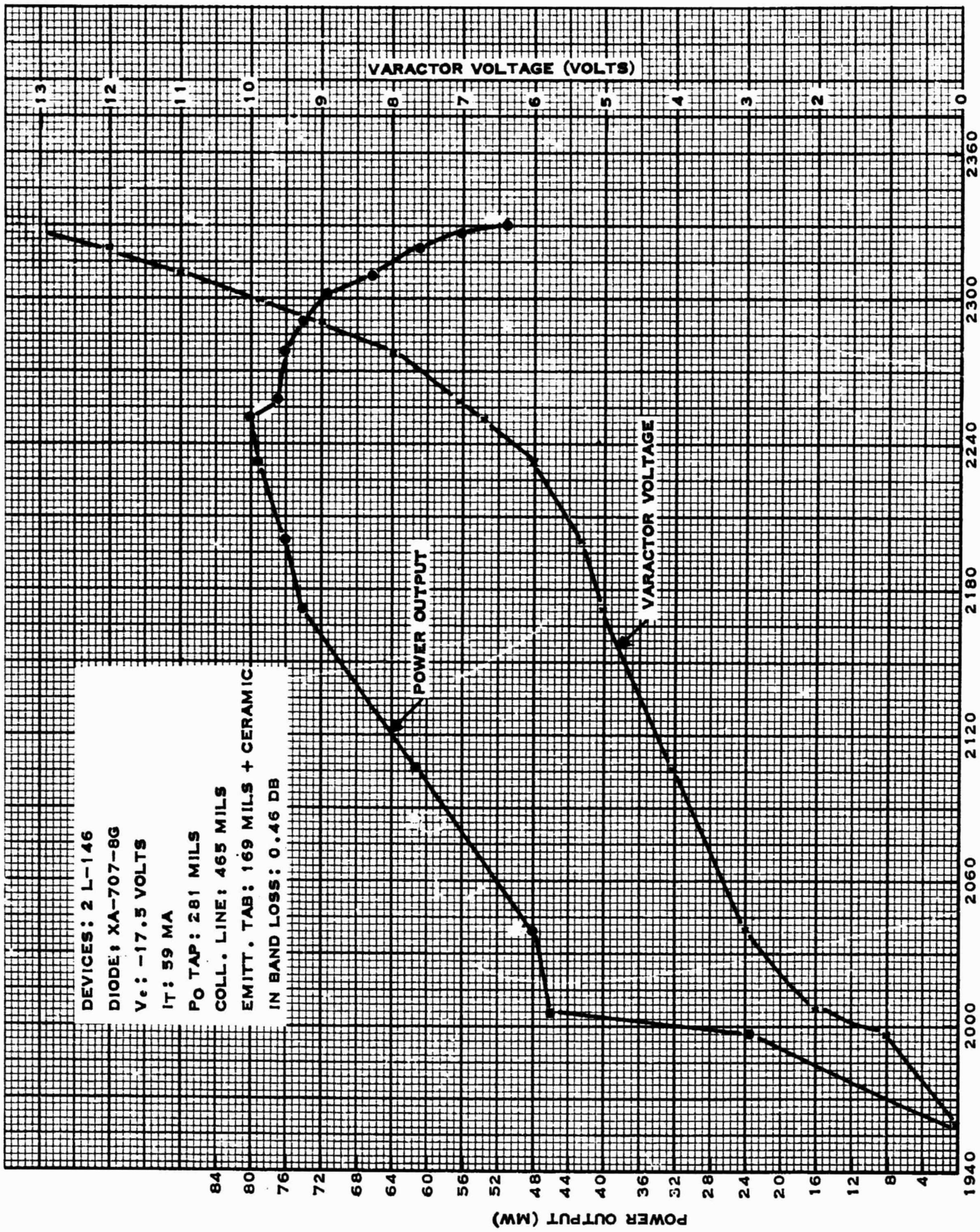

Figure 62. Ceramic VCO Performance (Power Output Tap 281 mils)

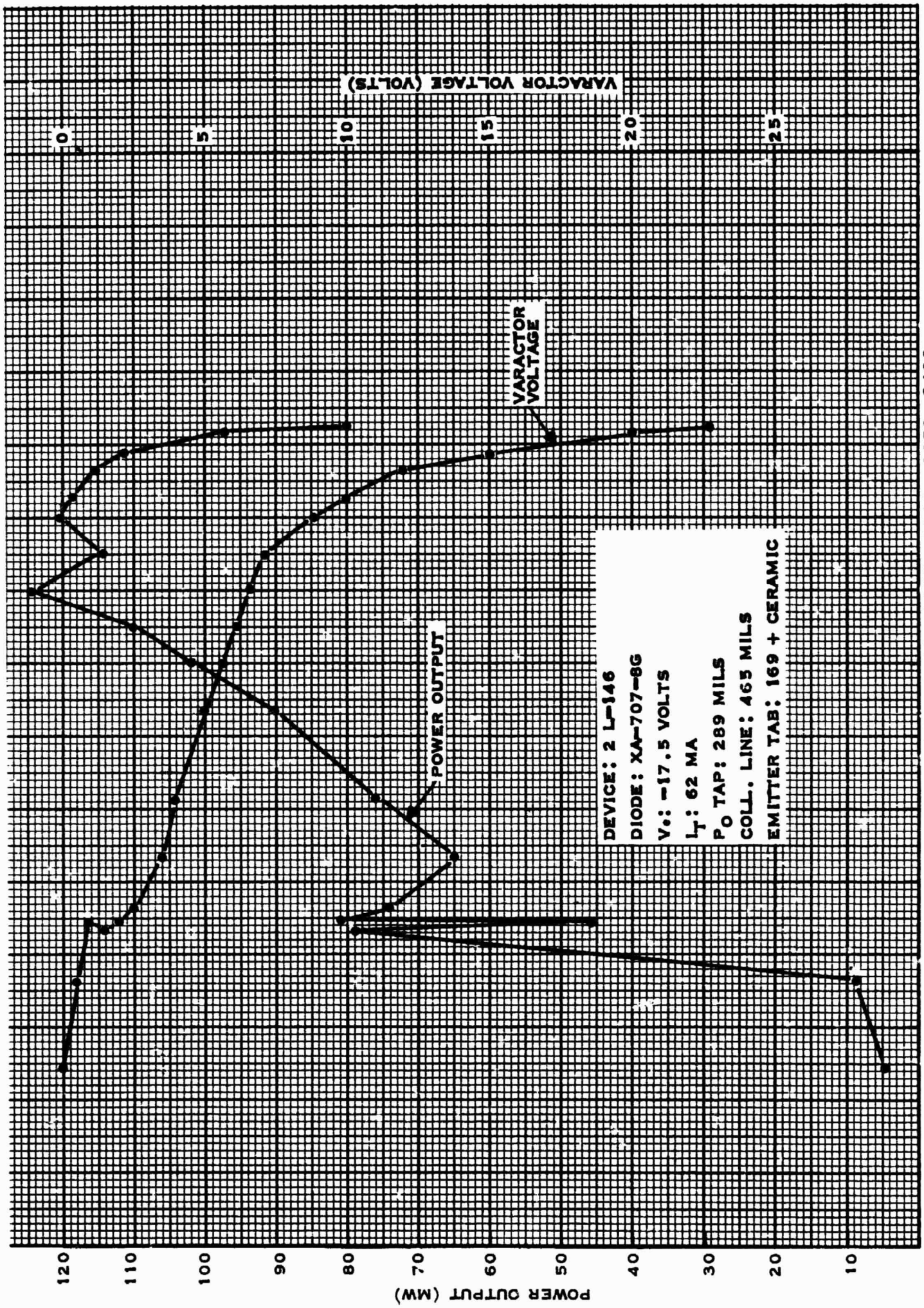

Figure 63. Ceramic VCO Performance (Power Output Tap 289 mils)

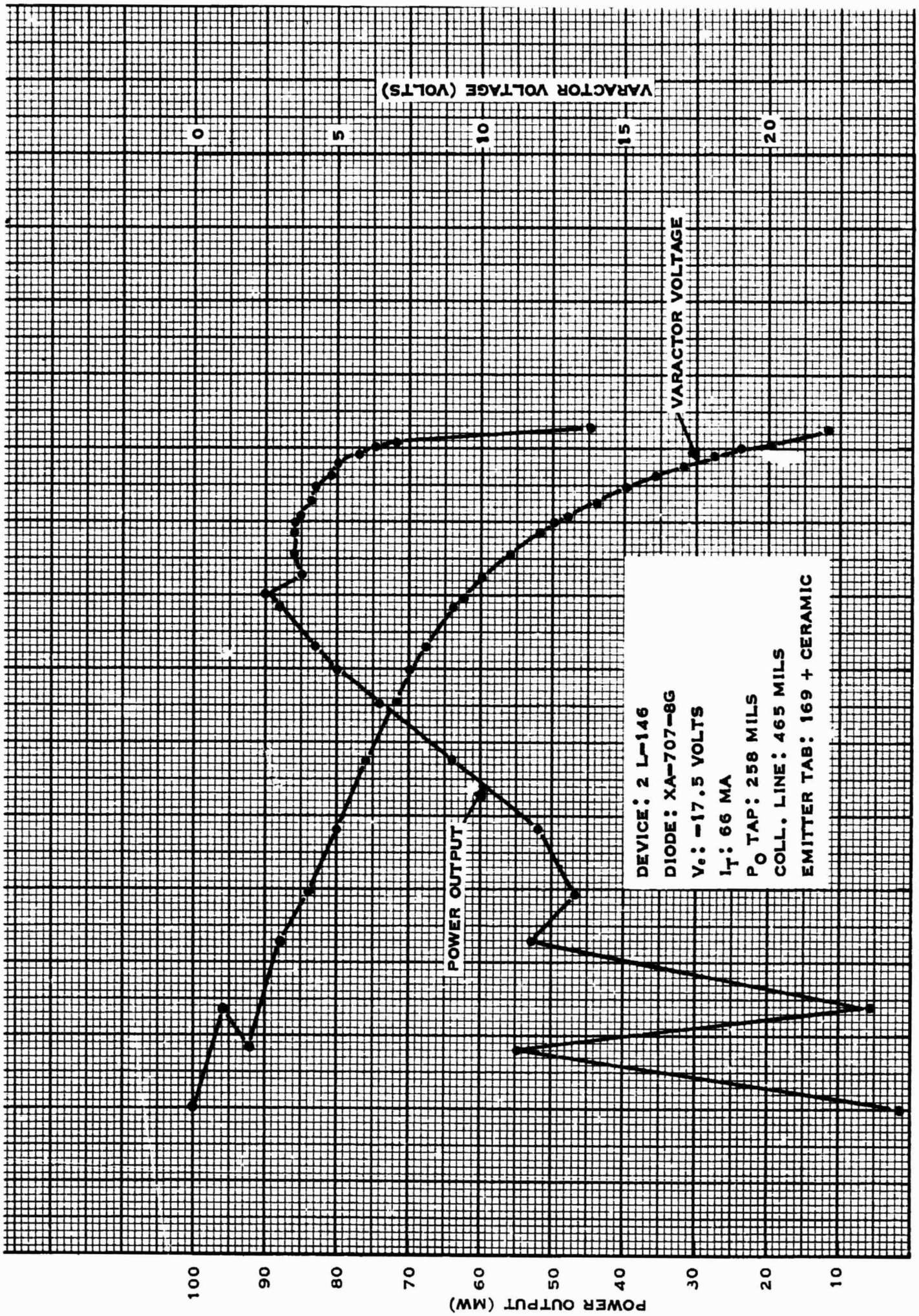

Figure 64. Ceramic VCO Performance (Power Output Tap 258 mils)

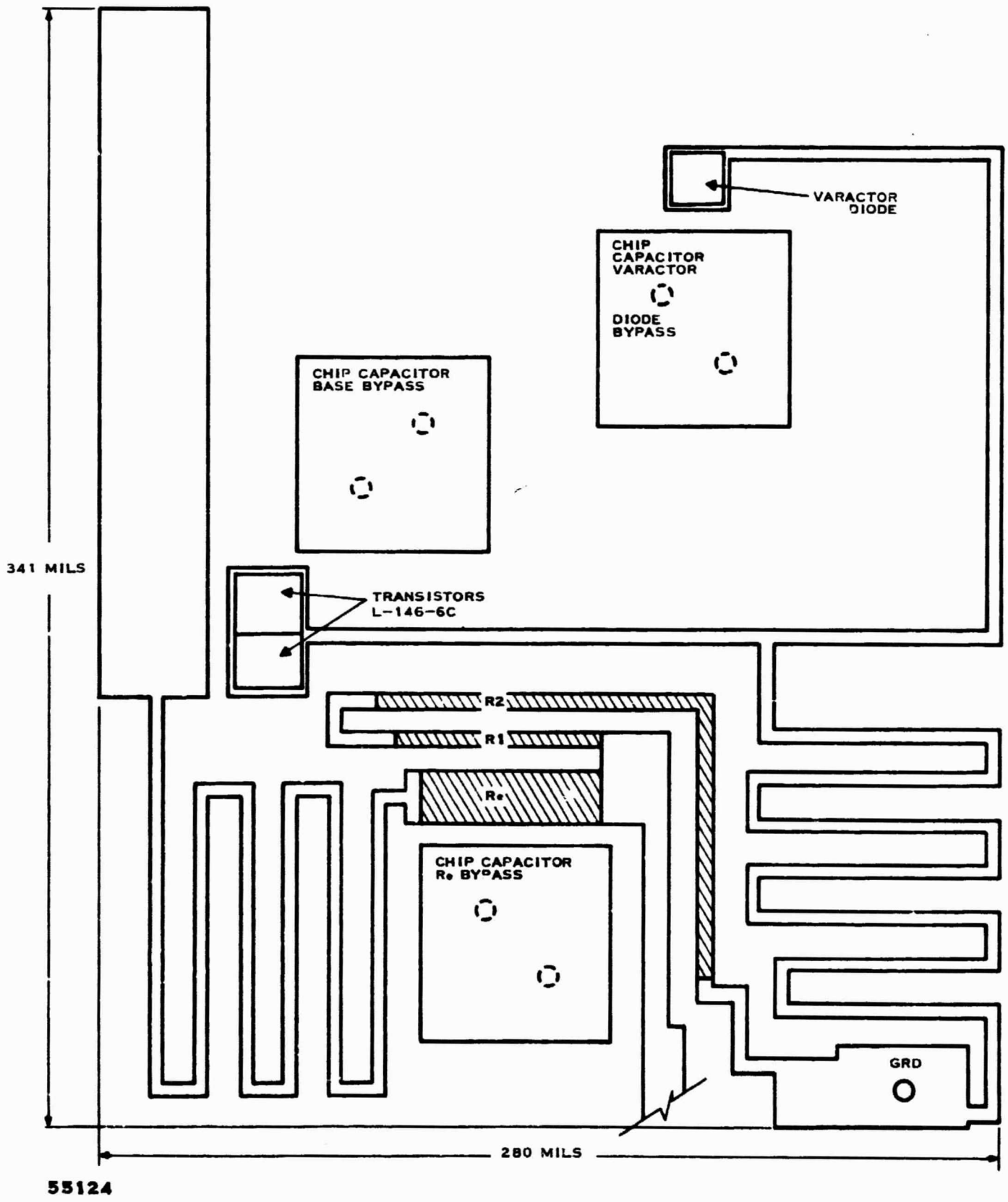

Figure 65. Final Ceramic Layout

In order to determine the reproducibility of the circuit another oscillator was built with the results shown in Figure 64. The power output ranged from 80 to 90 mW for an inband loss of 0.50 dB. Figure 65 is the final ceramic layout for the VCO.

2. Modulator

The final modulator circuit is basically the same as that reported in the Fifth Scientific Report. It has five elements, four resistors and one capacitor, as shown in Figure 66. For a constant 1 V rms input, the output varied from 15.2 mV to 16.1 mV over the modulation frequency range as shown in Figure 67. The modulator ceramic layout is shown in Figure 68 which utilizes 200 ohms per square and measures 230 by 206 mils.

The complete VCO modulator circuit is shown in Figure 69 and measures 625 by 286 mils.

C. POWER AMPLIFIER

1. Ceramic Development

At the beginning of this report period, the power amplifier network had been designed for operation on Teflon-fiberglass and was in the early stages of having the first matching network checked. However, at this time, in order to reduce development time, the decision was made to perform all breadboarding activities on ceramic substrates. The use of ceramic breadboards will allow the breadboard configuration and the final configuration to be very nearly the same. Because the breadboard and final circuits are now on the same substrates, in the same environment, the effects of coupling can be considered in the breadboard design and analysis.

As a first design for a ceramic layout, the Teflon-fiberglass design was scaled to ceramic. In scaling microstrip circuitry from one dielectric to another, the characteristic impedances of the various elements in the matching networks remain the same; thus, the proper strip widths are determined from a graph which gives the variation in the characteristic impedance (Z_o) for variations in the strip width and for a constant dielectric thickness (W). The electrical lengths also remain the same, and the physical length can be determined by multiplying the element length on Teflon-fiberglass by the ratio of the slowing factor of Teflon-fiberglass to the slowing factor of ceramic. The slowing factor for Teflon-fiberglass varies from 1.47 to 1.38 over the range of Z_o (30 to 100 ohms); the slowing factor for ceramic varies from 2.62 to 2.27 over the same Z_o range. As a result, during scaling, an element with a lower Z_o will be shortened more than an element with a higher Z_o. The direct scaling from Teflon-fiberglass resulted in a size reduction from 6.588 by 1.391 inches to 2.240 by 0.684 inches which corresponds to an area reduction of approximately 83 percent. In both cases three ground plane spacings were maintained between parallel elements in order to keep coupling at a minimum.

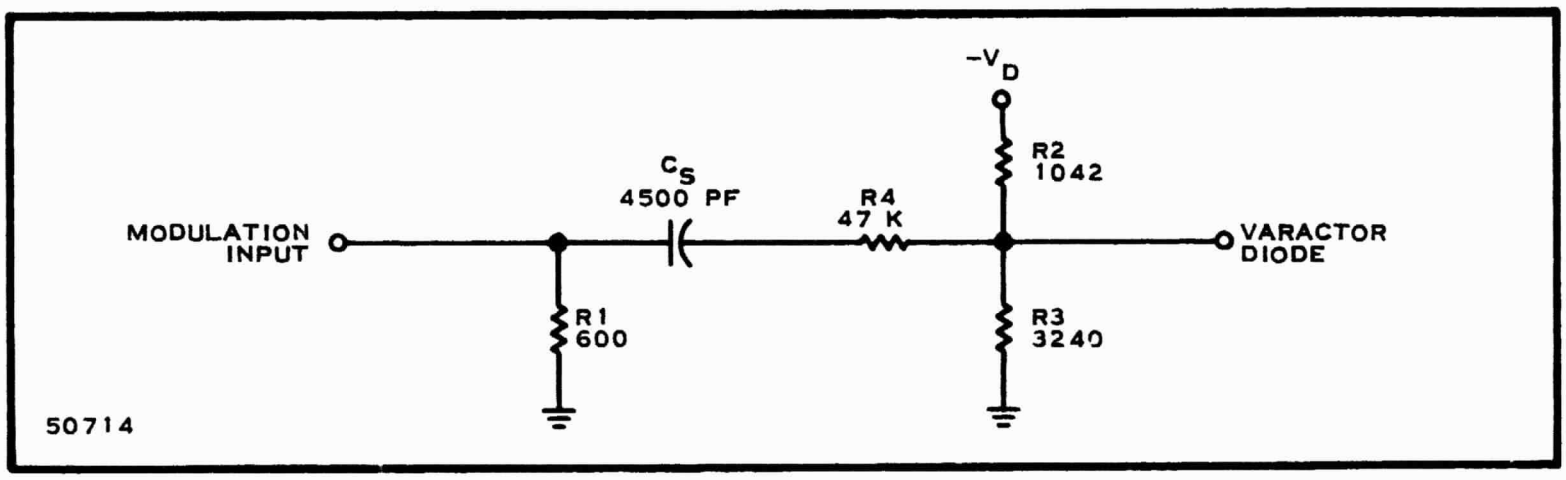

Figure 66. Final Modulator Schematic

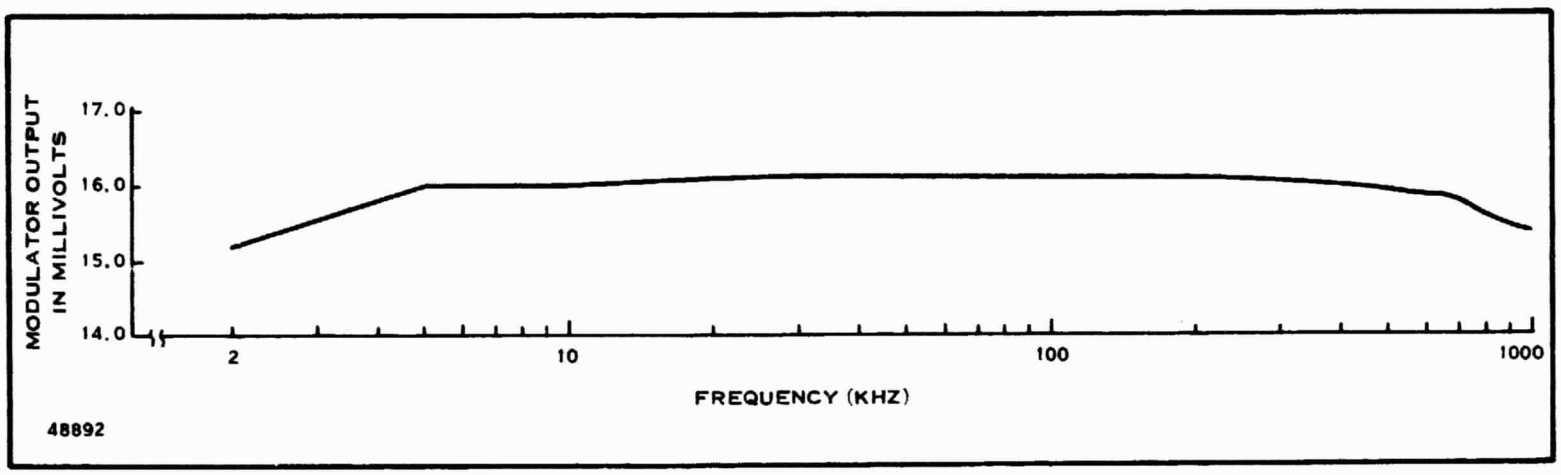

Figure 67. Final Modulator Response

Even though the scaling from Teflon-fiberglass to ceramic resulted in a considerable size reduction the size apparently could be further reduced by limiting the range of Z_o from 50 to 100 ohms. Since the narrower the line, the easier it is to meander, the reduction in maximum strip width from 0.056 inch (30 ohms) to 0.021 inch (50 ohms) will allow more meandering, resulting in a reduced circuit area. Since the computer program used in designing the matching networks can be programmed directly for 0.020 inch glazed ceramic, a new set of matching networks was designed with the Z_o range limited to 50 to 100 ohms. The results of that program are shown in Figures 70 through 74.

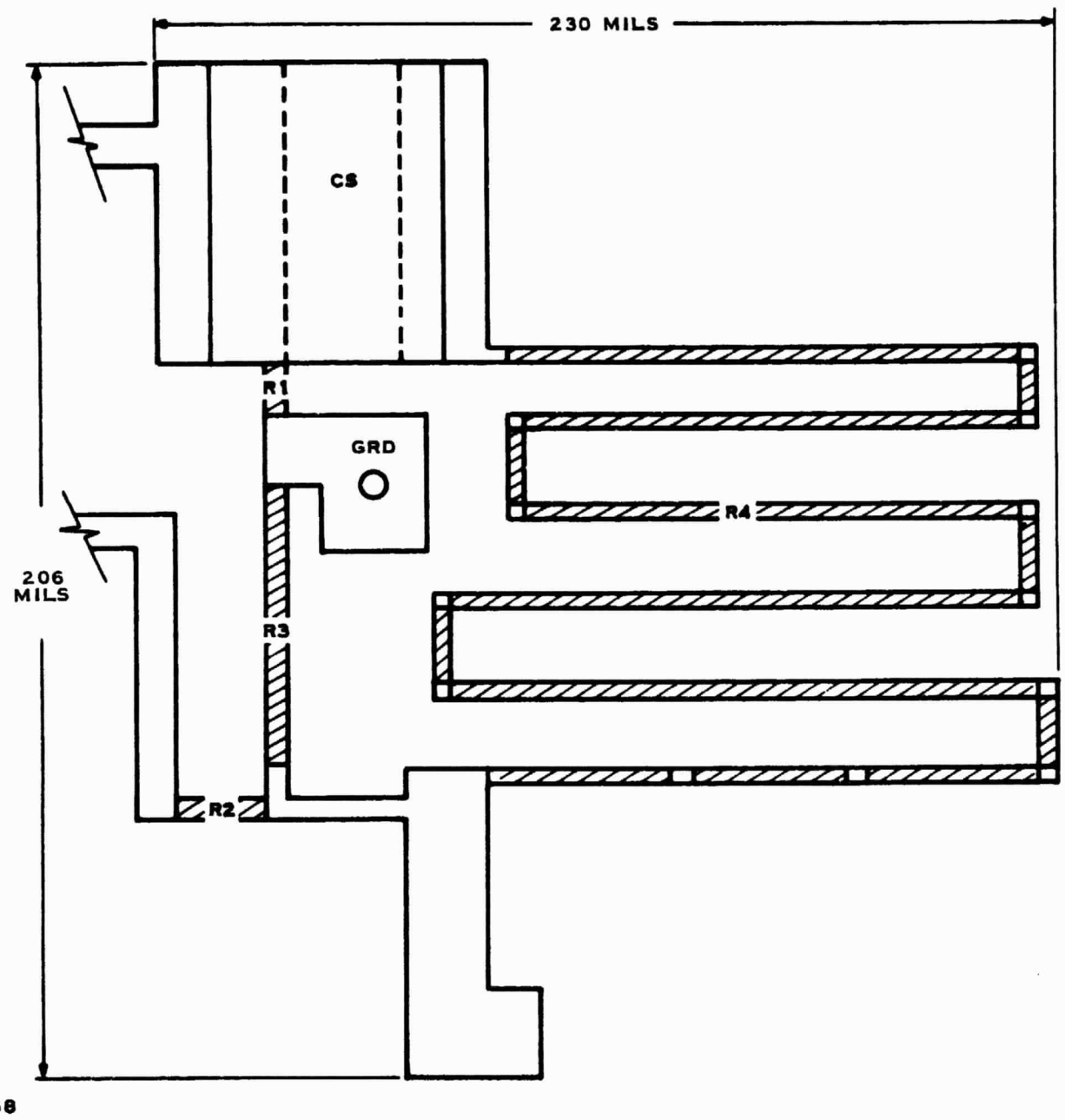

Figure 68. Modulator, Ceramic Layout

The new matching networks were incorporated into the design. Shorted stubs were used, where practical, in the output networks to form the dc return. When shorted stubs were not practical, quarter-wavelength shorted lines were used. For the input networks, quarter-wavelength shorted lines were necessary in all cases for the dc input. Since the power amplifier circuitry employs a parallel path approach after the buffer amplifier, only one-half the parallel path was included in the breadboard layout. In the final layout, the parallel paths will be separated by a minimum of five ground-plane spacings which will minimize any coupling between paths. Four ground-plane spacings are generally considered sufficient to reduce any potential side coupling to a negligible amount.

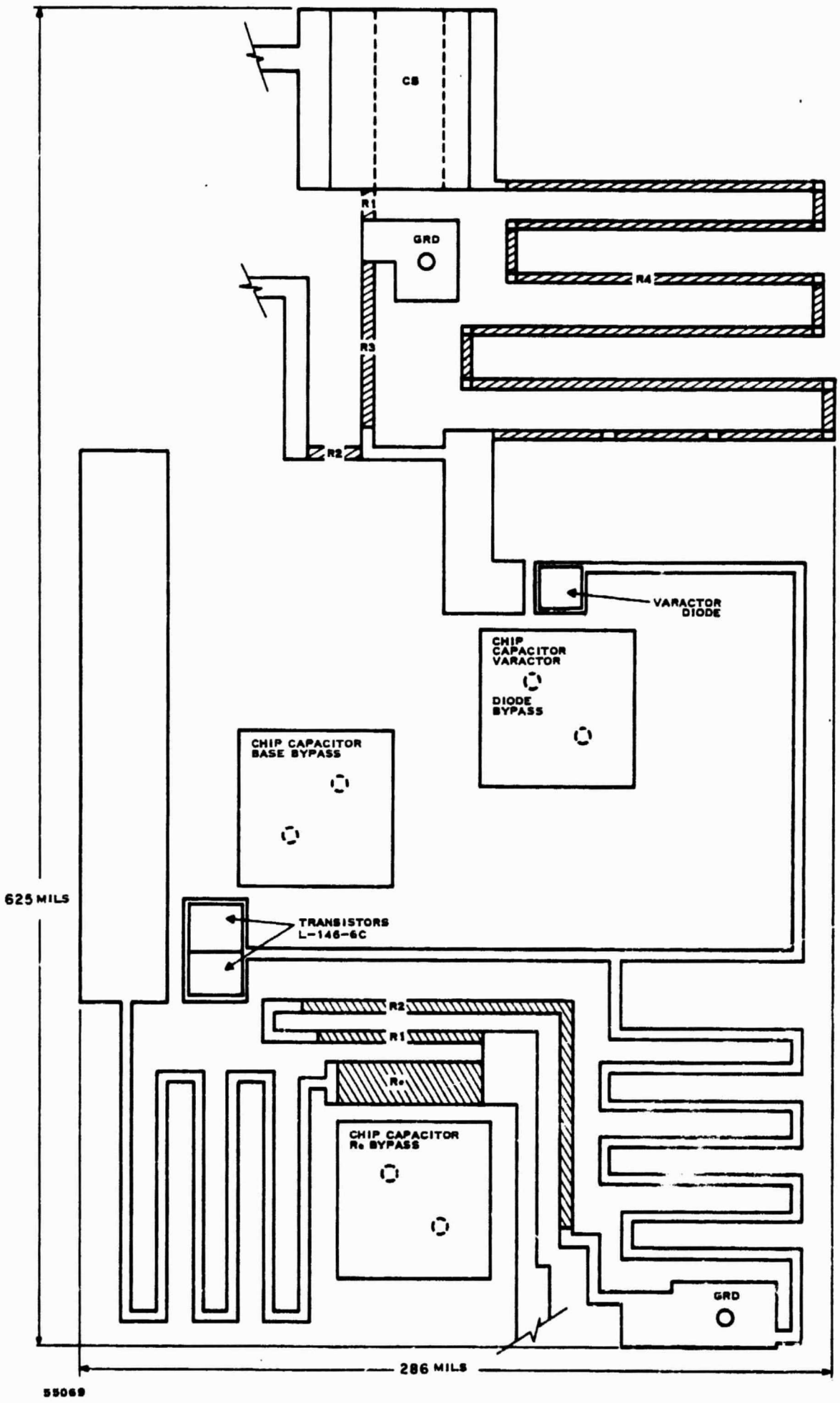

Figure 69. Final Modulator Schematic

FREQUENCY GHZ	POWER LOSS DB
2.100	100.000
2.110	100.000
2.120	100.000
2.130	100.000
2.140	100.000
2.150	100.000
2.160	100.000
2.170	100.000
2.180	2.427
2.190	0.305
2.200	0.013
2.210	0.033
2.220	0.087
2.230	0.141
2.240	0.169
2.250	0.122
2.260	0.072
2.270	0.039
2.280	0.025
2.290	0.107
2.300	0.507
2.310	1.735
2.320	7.123
2.330	100.000
2.340	100.000
2.350	100.000
2.360	100.000
2.370	100.000
2.380	100.000
2.390	100.000
2.400	100.000

ELEMENT	TYPE	WIDTH	LENGTH
1	FAT SERIES SECTION	21.8	146.1
2	OPEN STUB	21.8	414.4
3	GENERAL SERIES SECTION	15.8	64.5

55070

Figure 70. Matching Network Response (50 ohms to Input of L-158C, Class A)

FREQUENCY GHZ	POWER LOSS DB
2.100	1.447
2.110	0.974
2.120	0.633
2.130	0.395
2.140	0.233
2.150	0.127
2.160	0.062
2.170	0.025
2.180	0.007
2.190	0.001
2.200	0.001
2.210	0.003
2.220	0.006
2.230	0.008
2.240	0.008
2.250	0.005
2.260	0.002
2.270	0.000
2.280	0.002
2.290	0.012
2.300	0.037
2.310	0.084
2.320	0.164
2.330	0.282
2.340	0.486
2.350	0.770
2.360	1.174
2.370	1.736
2.380	2.507
2.390	3.558
2.400	5.012

ELEMENT	TYPE	WIDTH	LENGTH
1	GENERAL SERIES SECTION	3.6	156.9
2	FAT SERIES SECTION	3.7	144.9
3	SHORTED STUB	3.7	141.9
4	GENERAL SERIES SECTION	8.3	85.4

SS071

Figure 71. Matching Network Response (Output of L-158C to Input of Power Divider)

FREQUENCY GHZ	POWER LOSS DB
2.100	1.458
2.110	1.242
2.120	1.044
2.130	0.866
2.140	0.709
2.150	0.572
2.160	0.455
2.170	0.356
2.180	0.274
2.190	0.207
2.200	0.152
2.210	0.107
2.220	0.070
2.230	0.041
2.240	0.019
2.250	0.005
2.260	0.000
2.270	0.008
2.280	0.033
2.290	0.079
2.300	0.154
2.310	0.261
2.320	0.409
2.330	0.602
2.340	0.844
2.350	1.140
2.360	1.491
2.370	1.897
2.380	2.356
2.390	2.865
2.400	3.421

	ELEMENT	TYPE	WIDTH	LENGTH
55072	1	FAT SERIES SECTION	12.2	61.0
	2	OPEN STUB	21.8	429.4
	3	GENERAL SERIES SECTION	4.7	62.7

Figure 72. Matching Network Response (Output of Power Divider to Input of L-158C, Class C)

FREQUENCY GHZ	POWER LOSS DB
2.100	3.208
2.110	3.141
2.120	2.443
2.130	1.830
2.140	1.312
2.150	0.892
2.160	0.568
2.170	0.332
2.180	0.172
2.190	0.074
2.200	0.023
2.210	0.004
2.220	0.000
2.230	0.007
2.240	0.012
2.250	0.011
2.260	0.007
2.270	0.002
2.280	0.002
2.290	0.009
2.300	0.017
2.310	0.026
2.320	0.021
2.330	0.013
2.340	0.035
2.350	0.101
2.360	0.229
2.370	1.555
2.380	3.135
2.390	5.293
2.400	7.654

ELEMENT	TYPE	WIDTH	LENGTH
1	FAT SERIES SECTION	3.7	370.2
2	OPEN STUB	15.0	486.2
3	GENERAL SERIES SECTION	11.7	61.2

55073

Figure 73. Matching Network Response (Output of L-158C to Input of L-158A)

FREQUENCY GHZ	POWER LOSS DB
2.100	100.000
2.110	100.000
2.120	100.000
2.130	100.000
2.140	100.000
2.150	3.394
2.160	1.485
2.170	0.726
2.180	0.360
2.190	0.172
2.200	0.075
2.210	0.028
2.220	0.007
2.230	0.001
2.240	0.003
2.250	0.007
2.260	0.010
2.270	0.013
2.280	0.014
2.290	0.014
2.300	0.015
2.310	0.019
2.320	0.034
2.330	0.066
2.340	0.131
2.350	0.256
2.360	0.491
2.370	0.942
2.380	1.881
2.390	4.368
2.400	100.000

ELEMENT	TYPE	WIDTH	LENGTH
1	FAT SERIES SECTION	3.6	73.0
2	SHORTED STUB	4.9	102.0
3	GENERAL SERIES SECTION	5.1	62.7

55074

Figure 74. Matching Network Response (L-158A Output to Input of Power Combiner)

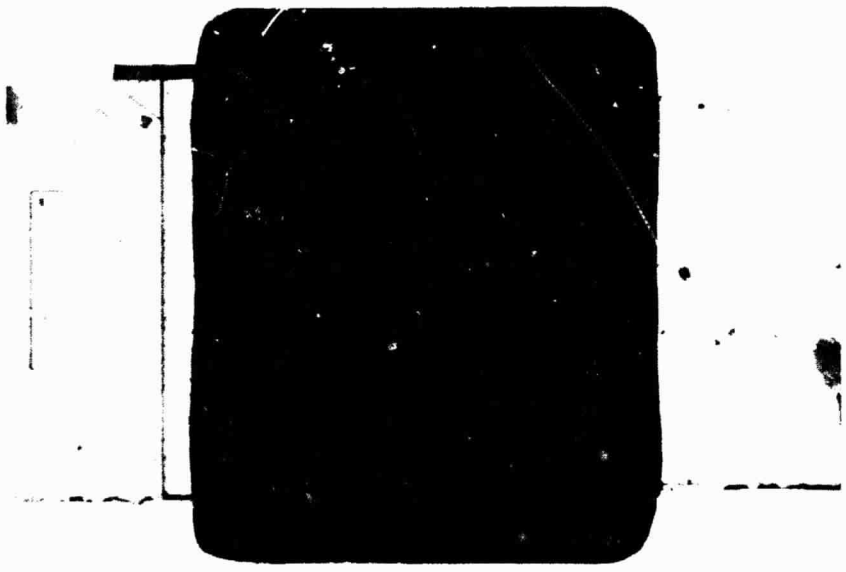

55075

Figure 75. Eighty pF Beam Lead Capacitor

The breadboard layout does not include any thin-film resistors or capacitors. Chip and/or beam-lead capacitors will be used where necessary. The chip capacitors are 0.060 by 0.060 by 0.010 inch. The beam-lead capacitors have been developed at Texas Instruments and several types were fabricated including an MOS capacitor, a metal–SiO_2–metal capacitor, and a tantalum oxide version. For our particular application, that of rf bypassing and/or dc blocking, the tantalum oxide version is necessary. The capacitance values used are 80 and 110 pF (Figures 75 and 86). The capacitors are approximately 0.037 by 0.021 by 0.015 inch. A one-mil gap between the leads separates the capacitor plates. Since the Class C amplifiers use NPN transistors operating in a common-base configuration and are supplied by a negative voltage, the transistor bases must be well rf bypassed, to ground through a minimum distance. For this reason, the chip capacitors will be used for base bypassing. The path through the chip capacitor is approximately 10 mils whereas the path through the beam-lead capacitor is roughly double this value. The beam-lead capacitors will be used for dc blocking between stages, where they can be inserted in series with the circuitry and form a section of a series element, and for bypassing the -24-Vdc supply lines. In order to provide a ground area for one plate of the bypass capacitors, holes (approximately 10 mils in diameter) must be drilled in the ceramic substrate and then plated through during the plating of the main ground-plane, thus, joining the small ground areas on the circuit side to the larger main ground-plane. In order to keep the attenuation due to conductor loss small, the conductors are plated to a thickness between 250 and 300 microinches which corresponds to a minimum of five skin depths in gold at 2.25 GHz.

In order to provide adequate heat transfer from the transistors so that a 1-watt output can be realized, the glaze must be removed from the substrate in the area of the transistors. The bottom window area that is left, once the glaze is removed, is then plated and the transistors are mounted on the resulting pad. A finished amplified breadboard substrate is shown in Figure 77. The new amplifier configuration measures 1.600 by 0.720 inches which is a 25-percent reduction of the scaled configuration. The bias and emitter resistors will be connected to the circuit externally through micro-manipulators so their values can be optimized during circuit operation. The isolation resistors in the power divider/combiner are 1/10 watt and are attached to the metalization by a conductive epoxy.

2. Measurement of Networks

As a means of adapting from the coaxial-type measuring equipment to the microstrip circuitry, several microstrip-to-coax adapters were fabricated. These adapters (Figure 78) were tested and proven to be adequate. Across the frequency band of interest (2.20 to 2.30 GHz) their insertion loss is typically 0.1 dB or less and their VSWR is typically 1.03 or less.

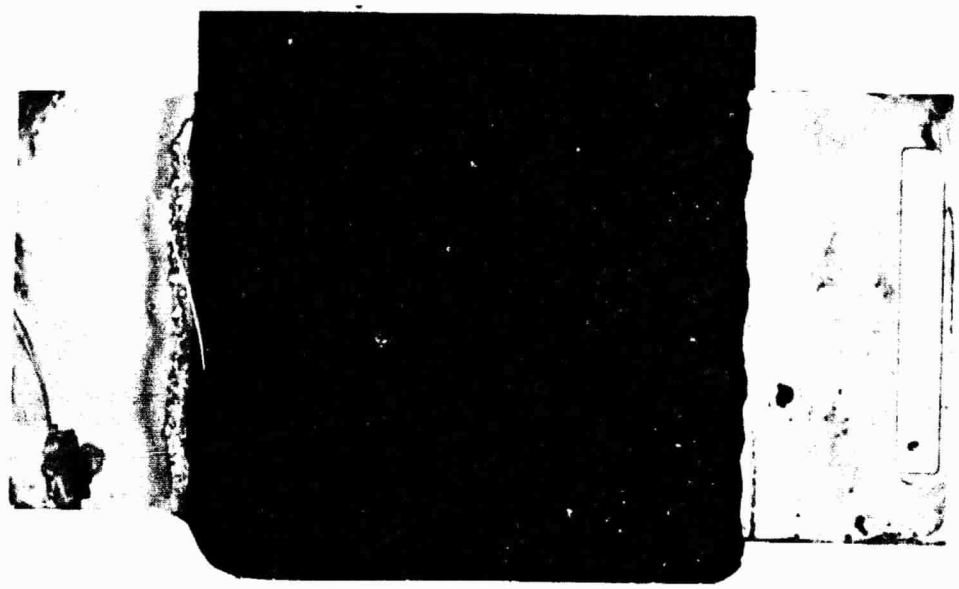

55076

Figure 76. One Hundred pF Beam Lead Capacitor

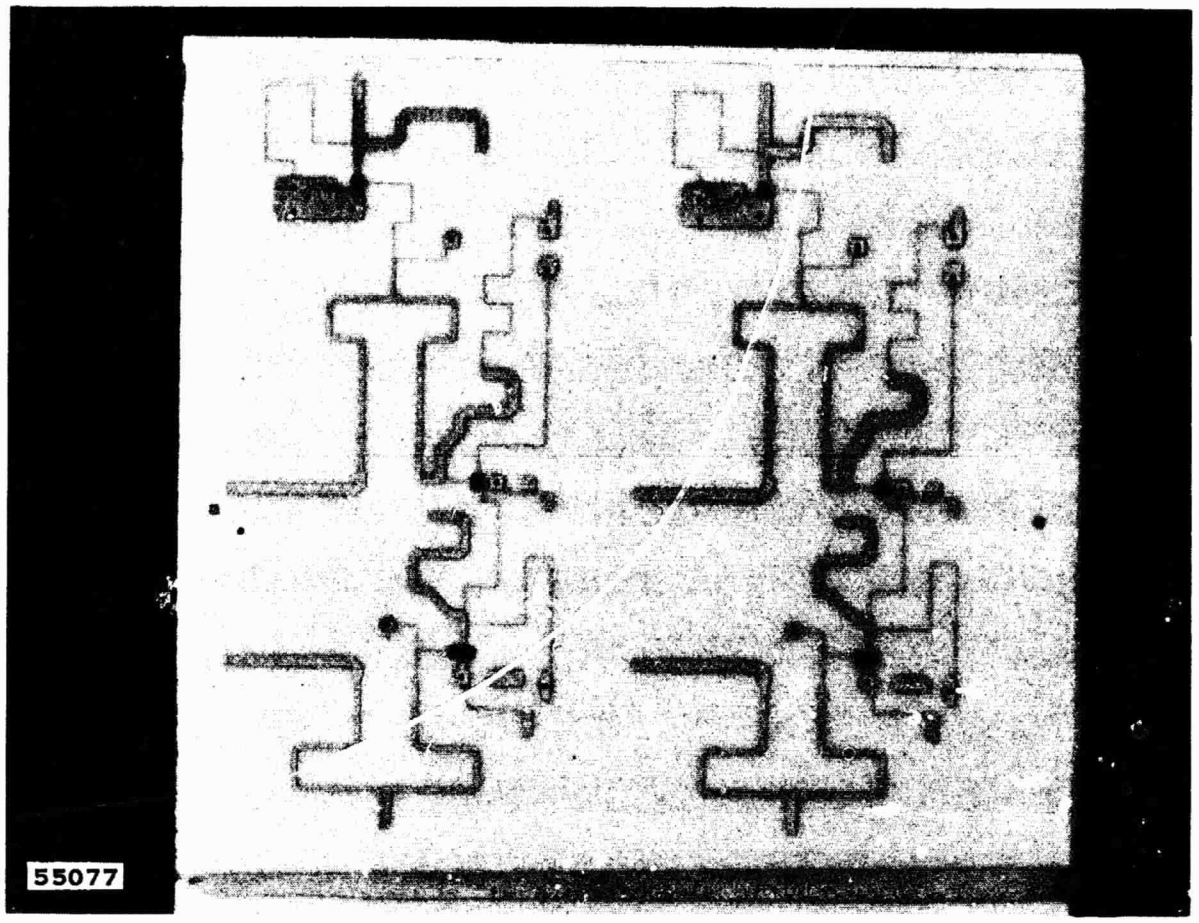

Figure 77. Power Amplifier on Ceramic Substrate

As an initial step in verifying the matching networks prior to mounting transistors on them, one network, the Class A output to the power divider input (Figure 79A) was cut out of the main substrate and checked. Checking the network was performed by terminating the port which connects to the power divider in 50 ohms and measuring the input impedance at the input port, using slotted line techniques. The results of this test along with the desired results (that is, data used in matching program) are shown on the Smith chart of Figure 80. The small difference between the measured and desired points can be attributed to the attenuation of the reflection coefficient by the microstrip-to-coax adapters and the inability to define the exact point where the transition from coax to microstrip occurs. From the results of the foregoing test, the network appears to be close enough to its design value to warrant its use in an active circuit.

The second circuit checked was the power divider/combiner (Figure 79B). The results of that test are shown in Table 6.

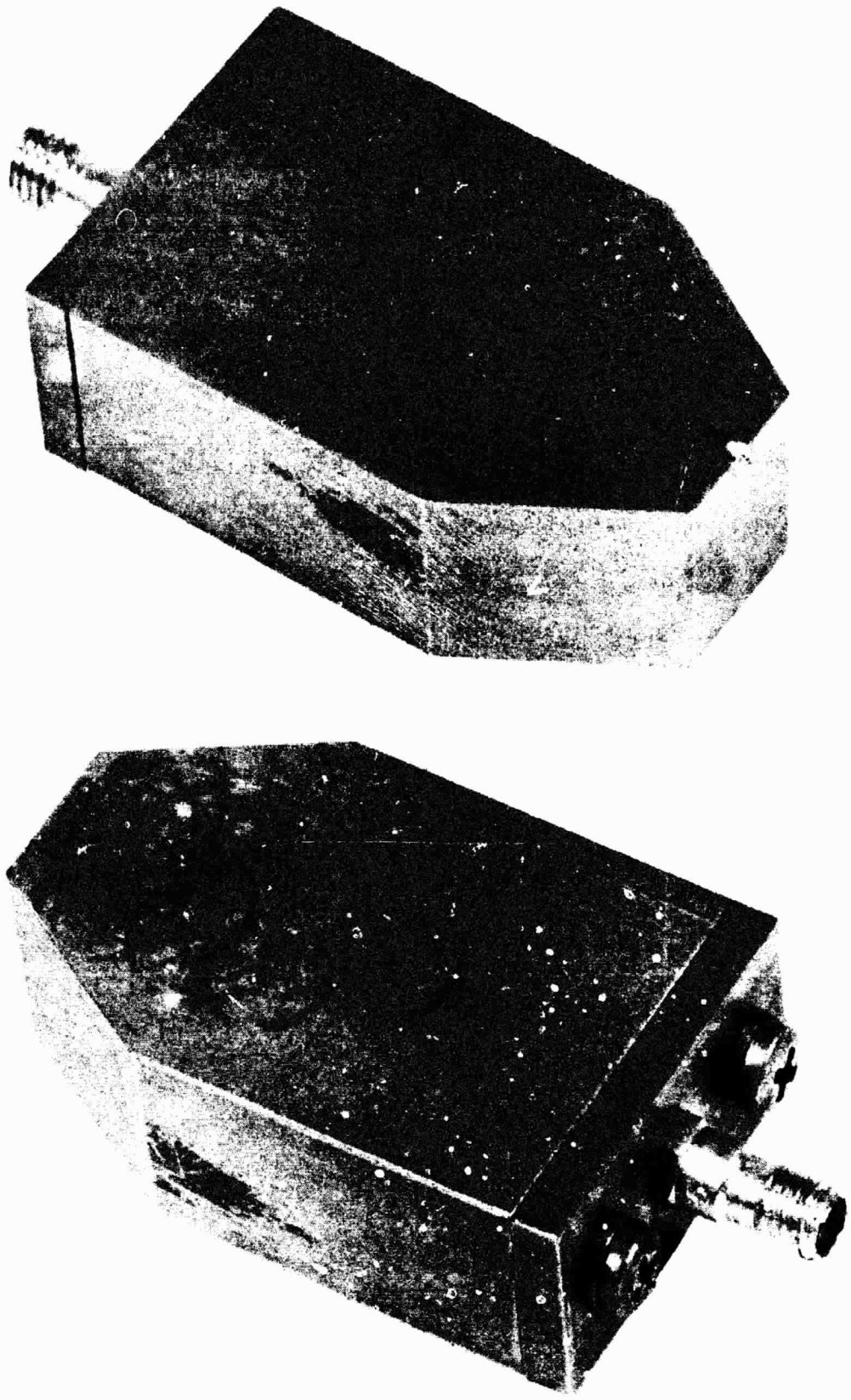

55078

Figure 78. Coaxial to Microstrip Adapter

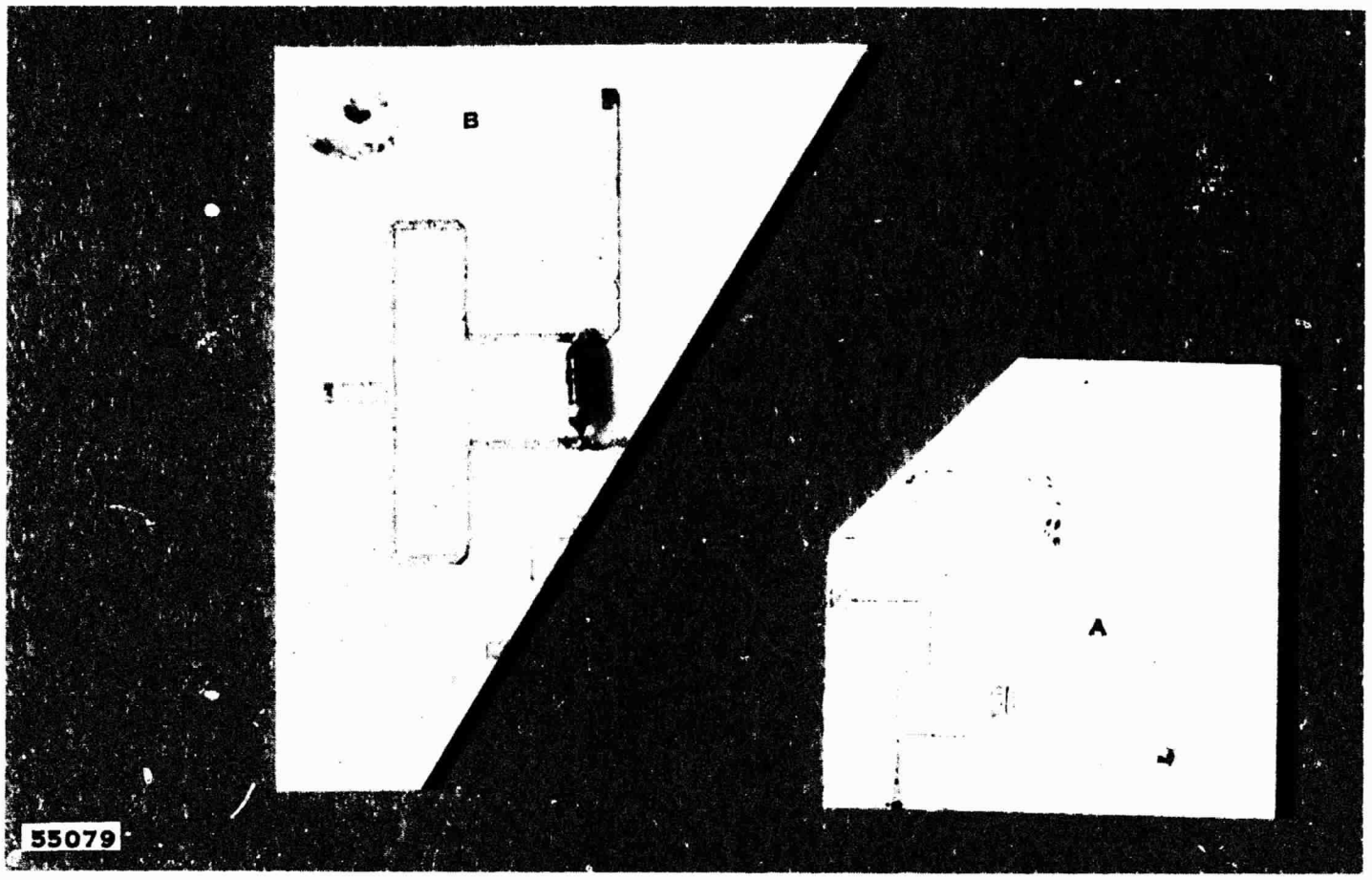

Figure 79. Ceramic Evaluation Circuits

Table 6. Ceramic Power Divider/Combiner

Frequency GHz	VSWR Port A	VSWR Port B	VSWR Port C	Isolation Between Ports B&C dB	Insertion Loss Port C to A dB	Insertion Loss Port B to A dB
2.20	1.14	1.10	1.06	16.6	0.10	0.10
2.25	1.14	1.11	1.05	17.1	0.15	0.22
2.30	1.14	1.12	1.05	17.5	0.11	0.18

As can be seen from Table 6, the VSWR looking into each port showed a substantial decrease on the ceramic divider/combiner as compared to the divider/combiner on Teflon-fiberglass (reference Table XIII, Power Divider No. 2 Test Data, p. 80, Scientific Report No. 5). The decrease in isolation of the ceramic divider/combiner as compared to the Teflon-fiberglass divider/combiner is due to the 10 percent, 1/10 watt isolation resistor used on the ceramic breadboard version.

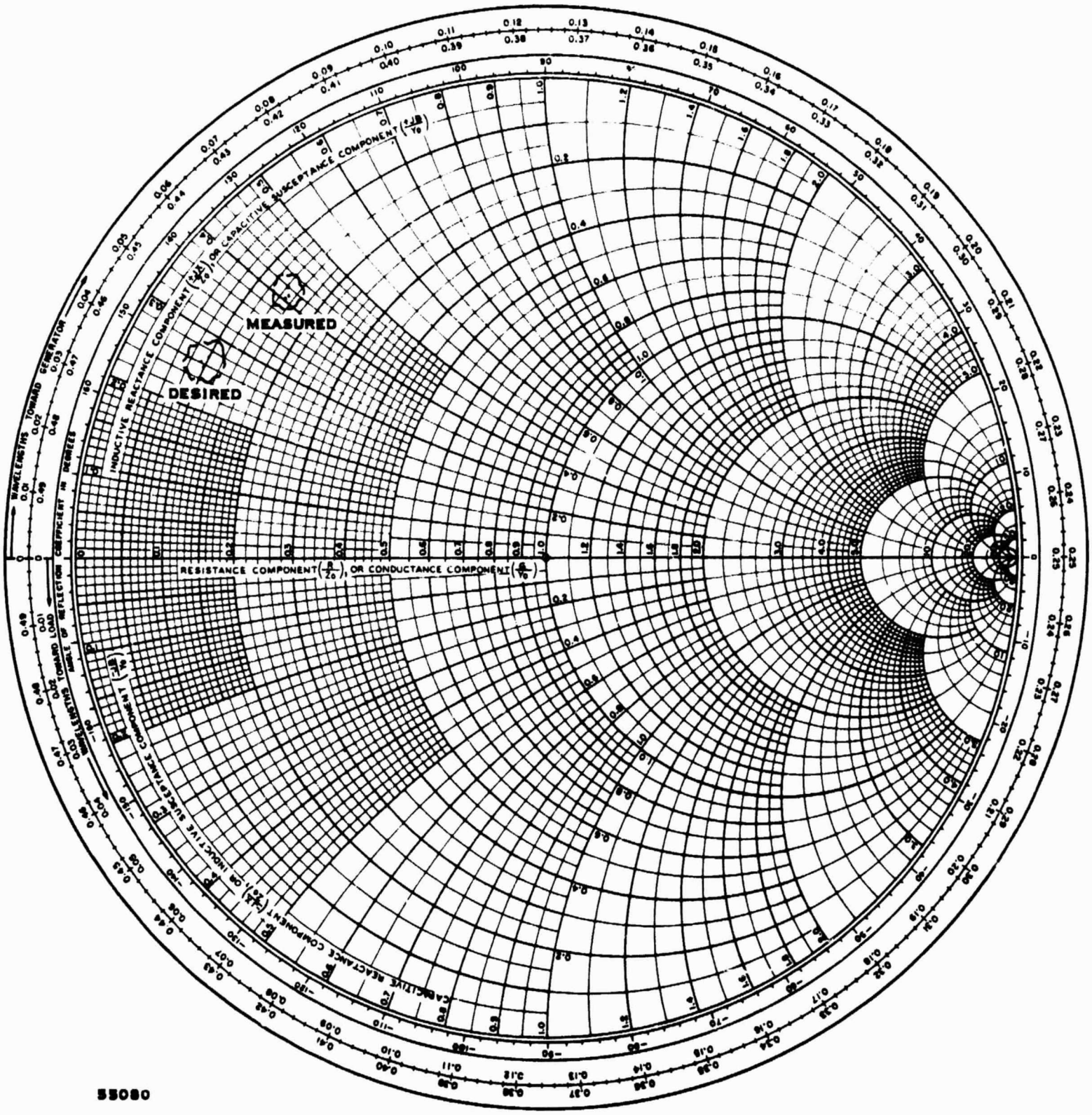

Figure 80. Measurement of the Output Matching Network of the Buffer Amplifier

3. Buffer Amplifier

The first stage of the power amplifier to be breadboarded on ceramic was the buffer amplifier which is used between the VCO output and the driver stages. It is operated class A to ensure a reasonably constant load to the VCO.

The amplifier was tested as a separate circuit with varying results. Initially, the circuit was unstable and the instability could not be corrected by tuning (using stub tuners) at either the input or the output. The instability was eliminated by shortening grounding paths; however, the gain of the stage was only 3 dB.

To achieve higher gain, the matching networks were modified with ceramic chips. This allows the circuit to be tuned, and indicates areas where modifications are necessary. Having determined the critical areas a conductive epoxy is painted on the circuit and then trimmed to produce maximum output power and minimum reflected input power. The final layout is shown in Figure 81.

As an example, Table 7 represents data taken on a circuit with and without tuning elements.

Table 7. Class "A" Output Data

Frequency MHz	Without Ceramic Chips				With Ceramic Chips		
	P_o mW	P_r mW	Gain dB	P_{in} mW	P_o mW	P_r mW	Gain dB
2200	76	8.5	4.0	30	172	5.6	7.6
2250	80	10	4.2	30	149	3.5	6.9
2300	71	1.3	3.7	30	125	3.3	6.2
2200	100	12.3	2.2	60	211	7.7	5.4
2250	107	14	2.5	60	214	5.1	5.5
2300	100	17	2.2	60	192	6.4	5.1

NOTE: amplifier current 64 mA, voltage -24 volts.

The data in Table 7 shows that the addition of ceramic chips increases the power output, but the gain is low by several dB from the characterized data.

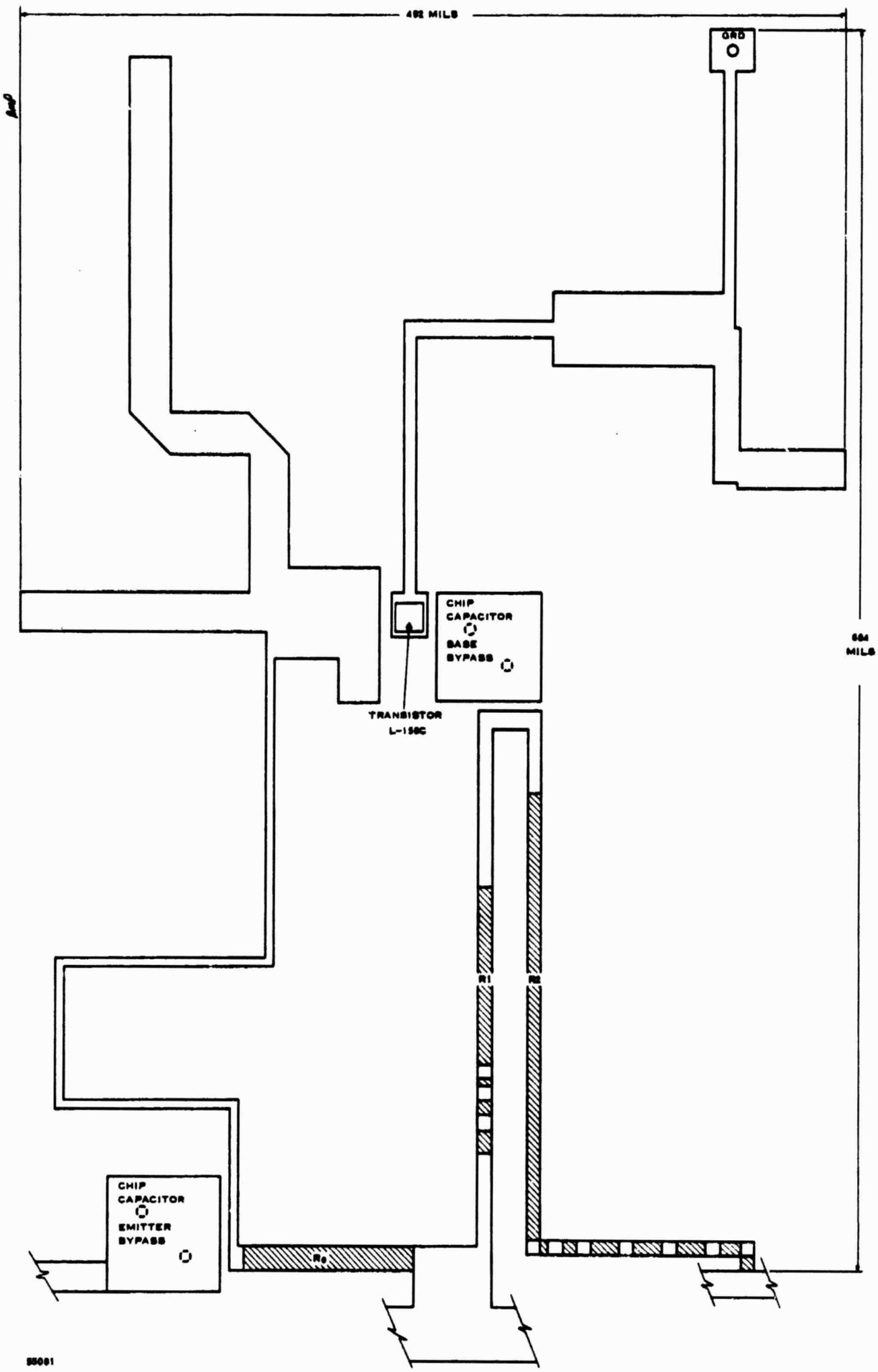

Figure 81. Buffer Amplifier Ceramic Layout

In order to achieve the desired output power, the input power and the amplifier current were increased and the results of Table 8 were obtained.

Table 8. Class A Output Data With Ceramic and Epoxy

Frequency MHz	P_{in} mW	P_o mW	P_r mW	Gain dB	I_T mA	P_{in} mW	P_o mW	P_r mW	Gain dB
2200	90	250	11.6	4.4	64	80	242	10.6	4.8
2250	90	246	7.7	4.3	64	80	239	7.0	4.7
2300	90	226	9.8	4.0	64	80	218	8.6	4.3
2200	90	257	11.0	4.5	67	80	251	10.2	5.0
2250	90	252	7.4	4.4	67	80	245	6.8	4.8
2300	90	230	9.9	4.1	67	80	221	8.6	4.4

The data in Table 8 indicates that with an input of 80 mW or greater the desired output of 250 mW can be obtained. Since the VCO has the capability of producing this amount of power, it would be beneficial to mate the two circuits.

D. MATING OF THE VCO AND BUFFER-AMPLIFIER

The mating of the VCO and Buffer-Amplifier was accomplished as shown in Figures 82 and 83. The first attempt was unsuccessful due to the nonoptimum matching network which caused instability.

The addition of an attenuator between the two circuits gave sufficient isolation for the circuits to function properly but the output power was lower than expected.

Several new circuits were fabricated with the matching networks being modified. The first results obtained are shown in Figure 84. The power output ranged from 180 to 160 mW for an inband loss of 0.5 dB.

In order to achieve the required output, 250 mW, additional ceramic and epoxy were added. The results (Figure 85) show that the output power ranged from 175 to 213 mW, a considerable increase from previous results, and the inband loss was 0.84 dB. To achieve still better results, the area of heat dissipation was investigated. By placing dry ice on the bottom side of the test stand, the output power increased 14 mW to 227 mW, at 2286 MHz, indicating the need for good heatsinking. Figure 86 shows the final VCO-buffer-amplifier layout.

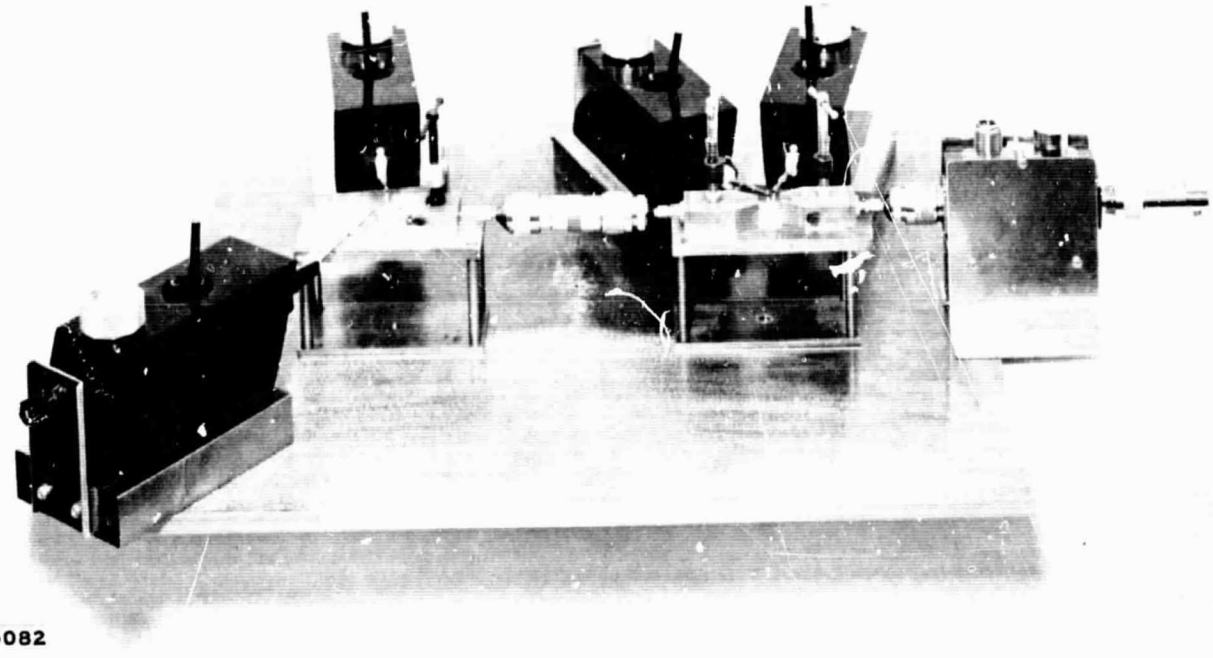

Figure 82. Test Setup of VCO and B ffer Amplifier

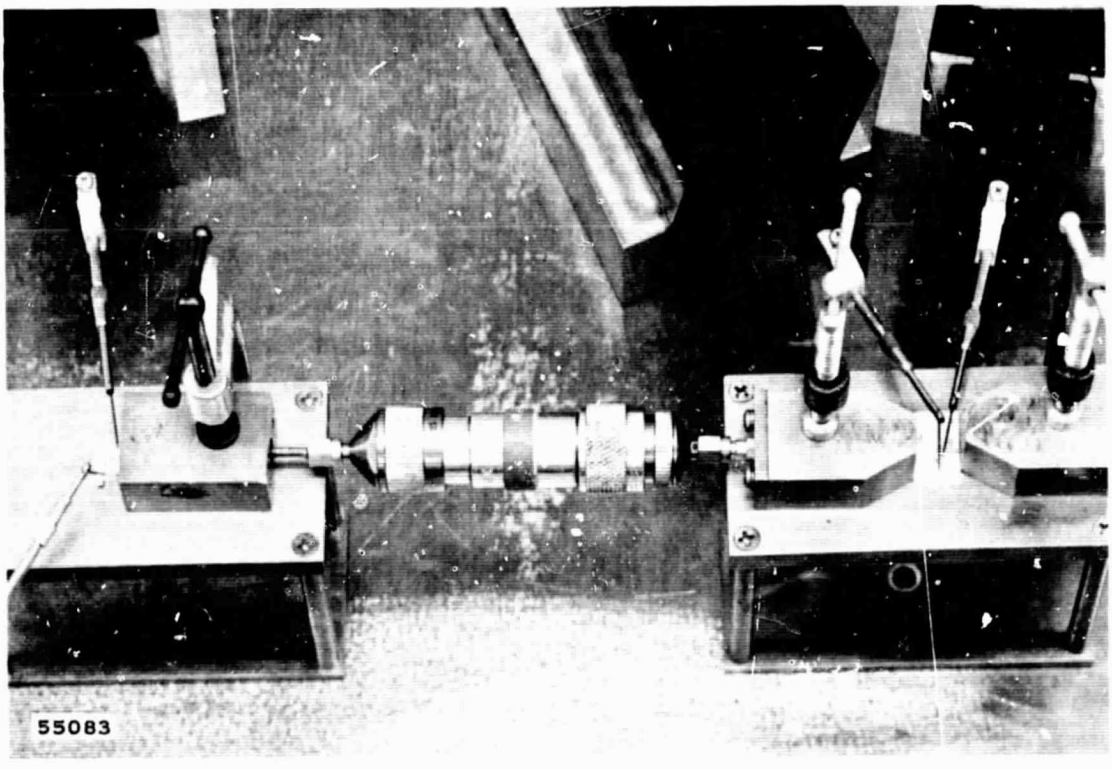

Figure 83. Test Setup of VCO and Buffer Amplifier, Detail View

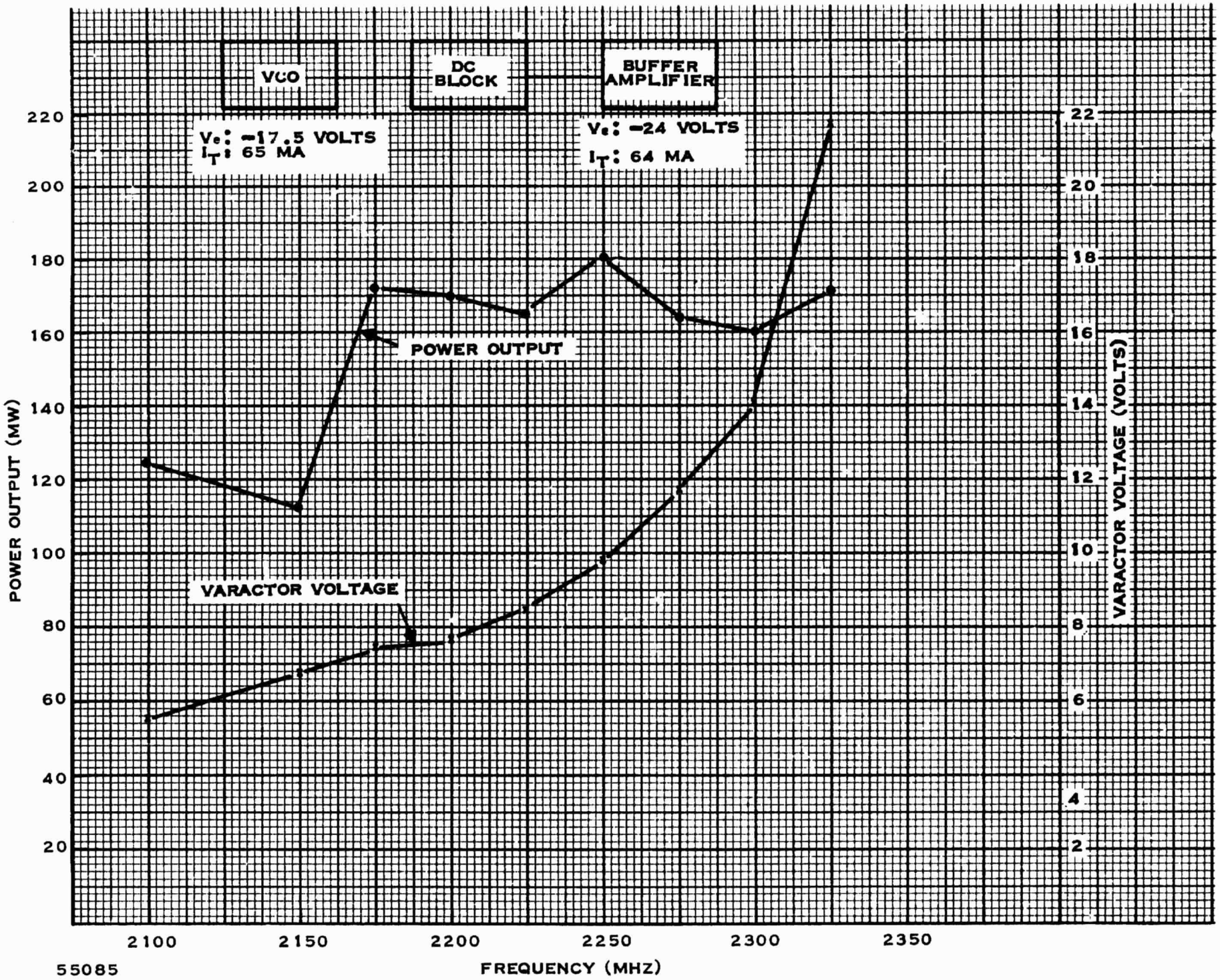

Figure 84. Ceramic VCO-Buffer-Amplifier Performance

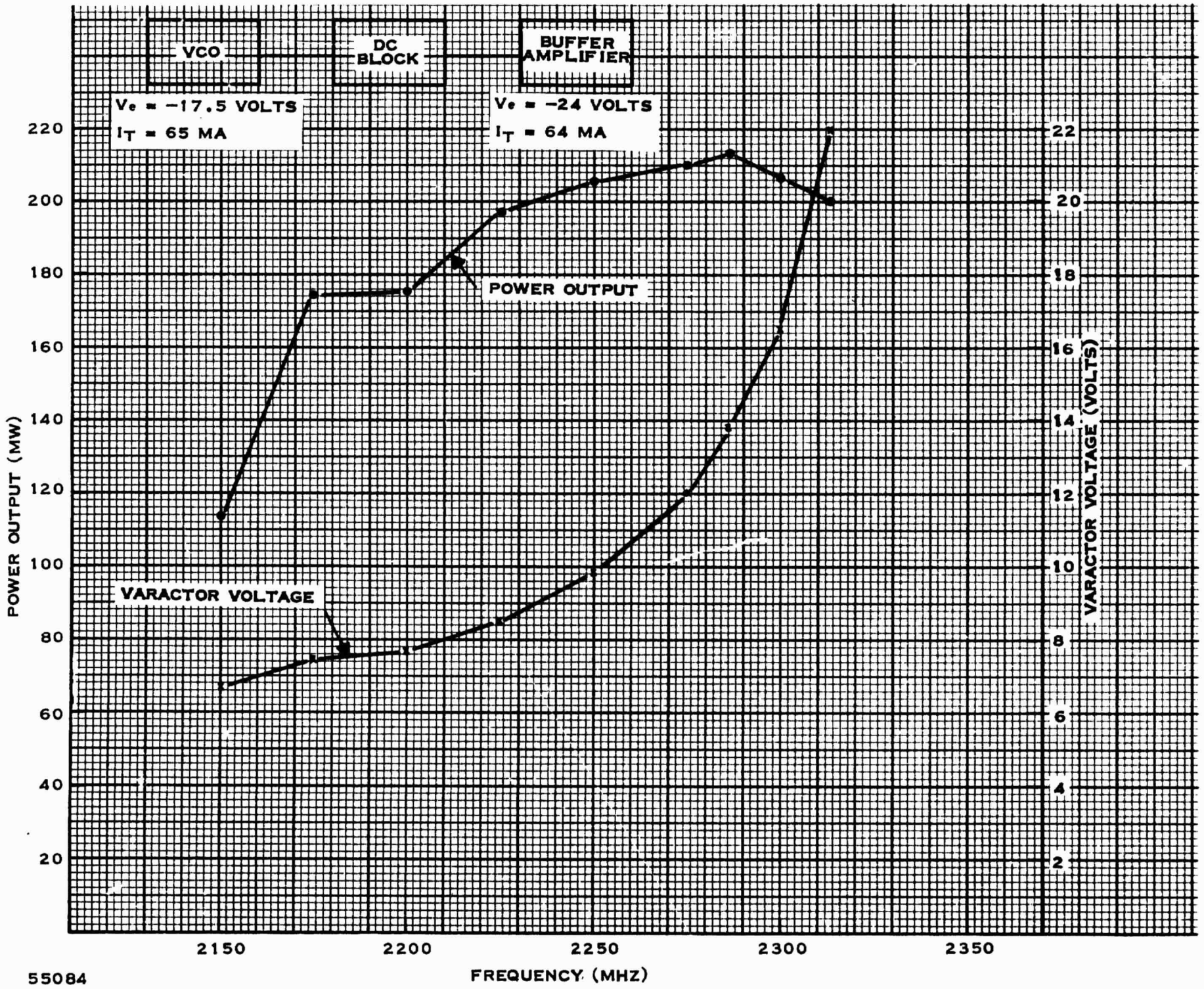

Figure 85. Ceramic VCO-Buffer Amplifier Performance (Additional Ceramic)

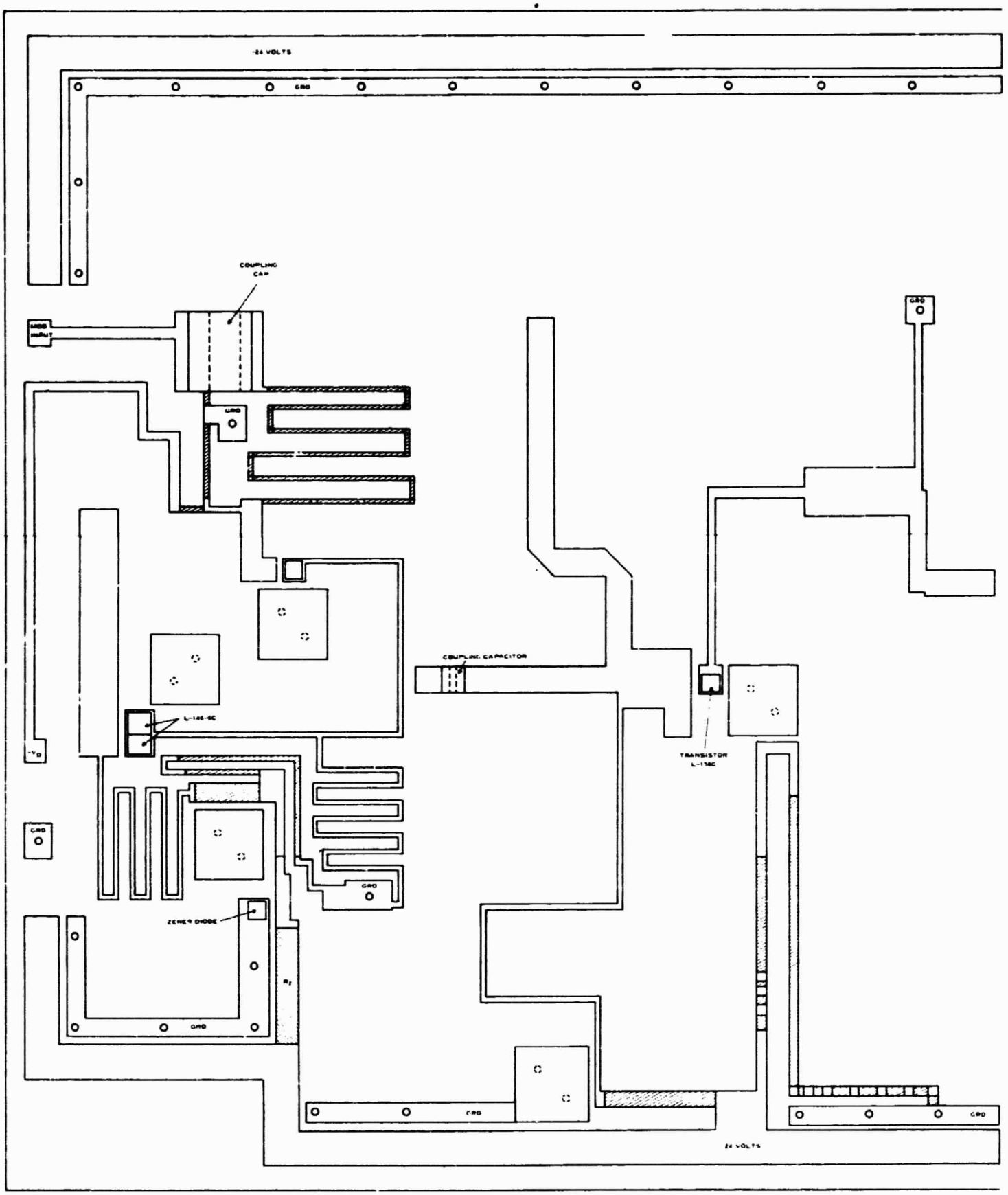

Figure 86. VCO-Buffer-Amplifier, Ceramic Layout

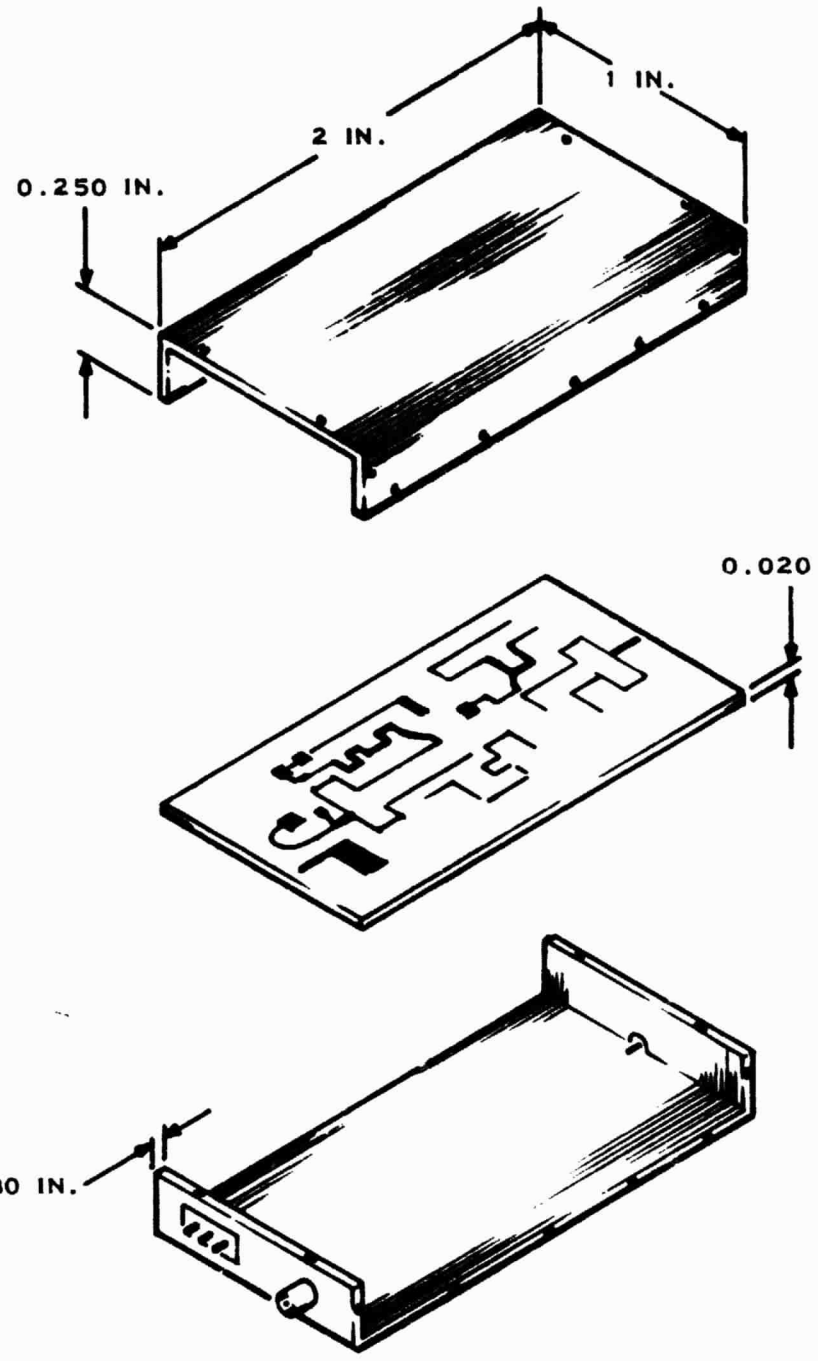

Figure 87. Transmitter Package

E. PACKAGING

Proceeding on the assumption that the final ceramic design would occupy an area equal to, or less than, the combined areas of the individual VCO/modulator and power-amplifier substrates, a package to house the transmitter was designed. A sketch of the proposed package is shown in Figure 87. The housing will measure approximately 2.000 by 1.000 by 0.250 inches. The base of the housing is in the form of a channel with 0.080-inch thick walls and base. The channel shape was selected because it facilitates the mounting of the substrates. A sheet metal cover 0.020 inch thick will be attached to the channel to protect the ceramic substrates and their circuitry.

The housing will have three connectors mounted on its end walls. Two of the connectors are modified Selectro hermetically sealed 50-ohm connectors with an outside diameter of 0.145 inch. These two connectors will be used for the modulation input and the power-output ports. The third connector is a special Texas Instruments-made, three-pin ceramic connector. The three pins will be used for the supply voltage, ground, and varactor bias inputs. The power connector measures 0.250 by 0.100 by 0.045 inch.

The three connectors and the ceramic substrates will be attached to the channel using a gold-base alloy. Since the alloying process used in mounting the connectors and substrates requires relatively high temperatures (200° to 300°C), a material with a thermal coefficient of expansion close to that of the ceramic (6.4 by 10^{-6} inch/inch/°C) will be required to keep internal stresses from being setup. The material will also require adequate thermal conductivity so it will provide a good heatsink for the transistors. To satisfy the expansion requirements the housing material will be Kovar (thermal) coefficient of expansion = 6.2 by 10^{-6} inch/inch/°C. Adequate thermal conductivity will be provided by gold plating the Kovar channel.

SECTION V

CONCLUSION

In this reporting period, a receiver system was developed from a conception to implementation in thin-film hybrid circuitry. The prime goal in the development was to achieve the lowest possible noise figure using present high-frequency components applicable to microelectronic integration. Low-noise receivers permit obtainment of lower receiver sensitivity. The receiver developed in this period did not meet the sensitivity requirement initially desired, primarily because of a tradeoff to develop a receiver with a high-information handling capability. The receiver was developed for a 600-kHz baseband capacity. If the information capacity were reduced, the receiver would meet the sensitivity requirement.

The receiver requires the use of a 2200- to 2300-MHz preselector which was not designed in this period. The design of this filter will be reported at the next reporting period.

The thin-film development of the VCO/modulator circuits and the transfer of the power amplifier circuits to a ceramic substrate were accomplished in this reporting period. The VCO/modulator network was finalized using thin-film techniques and a ceramic substrate.

The package design for the final transmitter assembly was completed and reported. In the next phase of the study, the performance of the completed transmitter will be evaluated in accordance with the test plan submitted in Scientific Report No. 5.

SECTION VI

PROGRAM PERSONNEL

Name	Title
Ben S. Skinner, Jr.	Project Engineer
Louis I. Farber	Senior Engineer
James C. Pinac	Engineer
Charles T. Johnston	Engineer
Eldon L. Gordon	Engineer
Wayne J. Harrison	Technician

APPENDIX

The current and voltage of a Schottky barrier diode are related by the exponential equation.

$$i = i_o(\epsilon^{\alpha V} - 1) \qquad \text{(A-1)}$$

where

i_o = the saturation current

$\alpha = \frac{q}{kT} = 40 \text{ volts}^{-1}$ at 25°C

$V = V_o \cos \omega_o t$

where V is the local oscillator voltage applied to the diode. The bias voltage is assumed to be zero. The VI characteristics expressed in the above equation plotted on logarithmic coordinates may be approximated over a large portion of the current range by a straight line given by:

$$i = Kv^x \qquad v > 0 \qquad \text{(A-2)}$$

where

K = constant of proportionally

x = nearly constant slope VI characteristics plotted on logarithmic coordinates

$x = \frac{\log i_2/i_1}{\log v_2/v_1}$, where $i_2 > i_1$; $v_2 > v_1$.

The log-log plot of a typical Gallium-Arsenide diode was shown in Figure 25, and the slope, x , is seen to be

$$x = \frac{(1 - 0.1)}{(0.68 - 0.61)} \text{ mA/volts} \qquad \text{(A-3)}$$

$$x \cong 13 .$$

The proportionality constant is determined from Equation (A-2). In Figure 25 for a current of 1×10^{-5} amperes, V = 0.68, thus

$$K = \frac{i}{V^{13}} \qquad \text{(A-4)}$$

$$= \frac{1 \times 10^{-5}}{(0.68)^{13}}$$

$$= 1.48 \times 10^{-3}.$$

The rectified current (I_a) of the diode has been shown by Strum[12] to be expressed in terms of the slope of the diode VI characteristics and peak LO voltage as given by

$$I_a = \frac{K V_o{}^x}{2\pi} \left[\frac{\sqrt{\pi} \left(\frac{x-1}{2} ! \right)}{\left(\frac{x}{2} ! \right)} \right] \tag{A-5}$$

and for $x = 13$

$$\frac{x-1}{2} ! = 6 ! \tag{A-6}$$

$$\frac{x}{2} ! = \frac{13}{2} !$$

Utilizing the fractional expression for the factorial[23]

$$\left(n + \frac{1}{2} \right) ! = \sqrt{\pi} \; \frac{1.3.5 \ldots (2n+1)}{2^{n+1}} \; . \tag{A-7}$$

Equation (A-5) may be written

$$I_a = \frac{K V_o{}^{13}}{2\pi} \left[\frac{(1.77)(720)}{(1.87 \times 10^3)} \right] \tag{A-8}$$

$$I_a = 0.108 \; K V_o{}^{13} \; .$$

And, since $K = 1.48 \times 10^{-3}$, the peak LO voltage for a 4-mA current is then

$$V_o = \left[\frac{(4 \times 10^{-3})}{(0.108)(1.48 \times 10^{-3})} \right]^{0.077} \tag{A-9}$$

$$V_o = (25)^{0.077}$$

$$V_o = 1.281 \text{ volts.}$$

The instantaneous small-signal conductance (g) of a mixer, when a low-level signal is applied to a mixer driven by a periodic LO signal, may be expressed

$$g = K \times V^{x-1} \quad . \tag{A-10}$$

When the LO voltage is periodic, the instantaneous conductance may be written

$$g = K \times V^{x-1} \cos^{x-1} \omega_o t \qquad \left(-\frac{\pi}{2} < \omega_o t < \frac{\pi}{2}\right) \tag{A-11}$$

Strum[12] has shown that the time-average conductance of this expression is

$$g_o = \frac{K \times V_o{}^{x-1}}{2\pi} \left[\frac{\sqrt{\pi}\ \ \frac{x-2}{2}!}{\frac{x-1}{2}!}\right] \quad . \tag{A-12}$$

The factorials expanded by Equation (A-7) when $x = 13$ are given

$$\frac{x-2}{2}! = \frac{11}{2}! = 289 \tag{A-13}$$

$$\frac{x-1}{2}! = 6! = 720 \ .$$

Therefore,

$$g_o = \frac{(1.48 \times 10^{-3})(13)V_o{}^{12}}{6.28} \left[\frac{(1.77)(289)}{720}\right] \tag{A-14}$$

$$g_o = 2.17 \times 10^{-3}\ V_o{}^{12} \ .$$

From Equation (A-9), $V_o = 1.281$ volts, thus

$$V_o{}^{12} = (1.281)^{12} \tag{A-15}$$

$$= 19.5 \text{ volts.}$$

Substituting into Equation (A-14),

$$g_o = (2.19 \times 10^{-3})(1.95 \times 10^{1}) \tag{A-16}$$

$$g_o = 4.27 \times 10^{-2} \text{ mhos.}$$

It has been shown[22] that a mixer can be represented as a three-port network with conductance at the signal, image and IF terminals. The conductance at these terminals may be expressed as Fourier components derived from the instantaneous conductance, g, when the mixer is driven by a sinusoidal LO voltage. The harmonic components are given by the Fourier series:

$$g = g_o + \sum_{n=1}^{\infty} g_n \cos n\omega_o t \qquad \text{(A-17)}$$

where g_o is the time average of g and g_n is the amplitude of the n^{th} harmonic component of the periodic conductance. Strum[12] has analyzed mixer conversion loss for different image terminations when these conductance elements are normalized with respect to g_o. The conversion loss derived by Strum for an open-circuit image termination in terms of these normalized conductances is

$$L_c = \left[1 + \sqrt{\frac{1 + \gamma_{2n} - 2\gamma_n{}^2}{(1 - \gamma_n{}^2)(1 - \gamma_{2n})}} \right]^2 \left[\frac{(1 - \gamma_n{}^2)(1 + \gamma_{2n})}{\gamma_n{}^2(1 - \gamma_{2n})} \right] \qquad \text{(A-18)}$$

where

$$\gamma_n = \frac{g_{cn}}{g_o} \quad . \qquad \text{(A-19)}$$

The first harmonic conductance element normalized to g_o is given

$$\gamma_n = \frac{\left(\frac{x-1}{2}!\right)^2}{\frac{x}{2}!\,\frac{x-2}{2}!} \quad . \qquad \text{(A-20)}$$

For $x = 13$, and from Equation (A-7)

$$\left(\frac{x-1}{2}!\right)^2 = (6!)^2 = 5.18 \times 10^5 \qquad \text{(A-21)}$$

$$\frac{x}{2}! = \frac{13}{2}! = 1.87 \times 10^3$$

$$\frac{x-2}{2}! = \frac{11}{2}! = 289 \; .$$

And Equation (A-20) becomes

$$\gamma_n = \frac{5.18 \times 10^5}{(1.87 \times 10^3)(289)} \qquad \text{(A-22)}$$

$$\gamma_n = 0.96 .$$

The second harmonic conductance element, g_{c2}, normalized with respect to g_o is given

$$\gamma_{2n} = \frac{\left(\frac{x-1}{2}!\right)^2}{\left(\frac{x+1}{2}!\right)\left(\frac{x-3}{2}!\right)} \qquad \text{(A-23)}$$

and

$$\frac{x+1}{2}! = 7! = 5.04 \times 10^3 \qquad \text{(A-24)}$$

$$\frac{x-3}{2}! = \frac{10}{2}! = 1.2 \times 10^2$$

then

$$\gamma_{2n} = \frac{5.18 \times 10^5}{(5.04 \times 10^3)(1.2 \times 10^3)} \qquad \text{(A-25)}$$

$$= 0.855 .$$

Substituting the normalized conductance terms into Equation (A-18) gives the conversion loss of a gallium-arsenide diode with the forward characteristics shown in Figure 25.

$$L_c = \left[1 + \sqrt{\frac{1 + \gamma_{2n} - 2(\gamma_{in})^2}{(1 - \gamma_n^2)(1 + \gamma_{2n})}}\right]^2 \left[\frac{(1 - \gamma_n^2)(1 + \gamma_{2n})}{\gamma_n^2(1 - \gamma_{2n})}\right] \qquad \text{(A-26)}$$

$$= \left[1 + \sqrt{\frac{1 + (0.855) - 2(0.96)^2}{[1 - (0.96)^2][1 + 0.855]}}\right]^2 \left[\frac{[1 - (0.96)^2][1 + (0.855)]}{(0.96)^2[1 - (0.855)]}\right]$$

$$= \left[1 + \sqrt{\frac{0.011}{0.145}}\right]^2 \left[\frac{0.145}{0.134}\right]$$

$$= (1.63)(1.08)$$

$$L_c = 1.75$$

or

$$L_c = 2.45 \text{ dB.}$$

REFERENCES

1. D.D. McRae, "Considerations of RF Parameters for PCM Telemetry Systems," IRE Transactions on Space Electronics and Telemetry, Volume 1 SET-5, June 1959, pp. 61-65.

2. Joseph F.A. Ormsby, "PCM/FM Telemetry Signal Analysis and Bandwidth Effects," IRE Transactions on Space Electronics and Telemetry, SET-6, Sept-Dec 1960, pp. 130-138.

3. John J. Downing, Modulation Systems and Noise, Prentice-Hall, Englewood Cliffs, N. J., 1964, p. 173.

4. Robert C. Tausworthe, JPL Technical Report No. 32-819, Theory and Practical Design of Phase-Locked Receivers, Vol. I, Feb. 15, 1966.

5. W.B. Davenport, Jr., and W.L. Root, An Introduction to the Theory of Random Signals and Noise, McGraw-Hill, New York, N.Y., 1958.

6. Mischa Schwartz, Information Transmissions, Modulation and Noise, McGraw-Hill, New York, N.Y., 1959.

7. S.O. Rice, "Mathematical Analysis of Random Noise," Bell System Technical Journal, Vol. 23, July 1944, pp. 282-222; Vol. 24, Jan. 1945, pp. 96-157.

8. F.M. Reza, An Introduction to Information Theory, McGraw-Hill, New York, N.Y., 1961.

9. S.O. Rice, "Noise in FM Receivers," Chapter 25 in Proceedings, Symposium on Time Series Analysis, M. Rosenblat (ed.), John Wiley and Sons, Inc., New York, N.Y., 1963, pp. 375-424.

10. J.H. Crow, PCM Signal-to-Noise Performance, Proc. National Telemetering Conference, Session 5, Vol. 1, May 23-25, 1962, Washington, D.C.

11. Robert P. Rafuse and Joze Vugrinec, Very Low Noise PN Junction Microwave Mixers, Massachusetts Institute of Technology Report for Electronic Research Center, NASA, Cambridge, Mass., Grant NSG-419 and Grant NGR 22-009-163.

12. P.D. Strum, "Some Aspects of Crystal Mixer Performance," Proceedings IRE, Vol. 41, July 1953.

13. M.R. Barber, "Noise Figure and Conversion Loss of the Schottky Barrier Mixer Diode," IEEE Transactions, Vol. MTT-15, No. 11, Nov. 1967.

14. R.E. Heitzman, "A Study of the Threshold Power Requirements of FMFB Receivers," IRE Transactions, Vol. SET-8, No. 4, Dec. 1962.

15. F.M. Gardner, Steven S. Kent and R.D. Dasenbrock, Theory of Phaselock Techniques, Resdel Engineering Corp. NASA Sponsored Course Textbook.

16. J.J. Spilker, Jr., "Threshold Comparison of Phase-Lock, Frequency-Lock, and Maximum-Likelihood Type of FM Discriminators," IRE WESCON.

17. B.D. Martin, "The Pioneer IV Lunar Probe; a Minimum-Power FM/FM System Design," Technical Report No. 32-215, Jet Propulsion Laboratory, Pasadena, California, March 1962.

18. G.L. Matthaei, L. Young, and E.M.T. Jones, Microwave Filters, Impedance-Matching Networks, and Coupling Structures, McGraw-Hill, New York, N.Y., 1964.

19. Hewlett-Packard Associates, Step Recovery Diode Frequency Multiplier Design, Application Note 913.

20. Burr-Brown Research Corporation, Handbook of Operational Amplifier Active R-C Networks, Burr-Brown Research Corporation, 1966, pp. 29-31, 74.

21. M.E. Van Valkenburg, Modern Network Synthesis, John Wiley and Sons, Inc., New York, N.Y., 1965, pp. 48-53.

22. L.C. Peterson and F.B. Llewellyn, "The Performance and Measurement of Mixers in Terms of Linear-Network Theory," Proceedings of the IRE, Vol. 33, No. 7, July 1945, p. 458.